UNIVERSITÀ
DEGLI STUDI
DI TRIESTE

UNIVERSITÀ DEGLI STUDI DI TRIESTE

XXXVIII CICLO DEL DOTTORATO DI RICERCA IN

**EARTH SCIENCE, FLUID-DYNAMICS AND MATHEMATICS.
INTERACTIONS AND METHODS**

The fellowship was funded 50% by Istituto Nazionale di Oceanografia e di Geofisica Sperimentale – OGS

OBSERVATIONAL EVIDENCE FOR CLIMATE CHANGE IN THE SOUTHERN ADRIATIC FROM PHYSICAL PROCESSES AT THE BASIN SCALE, SUB-MESOSCALE, AND MICROSCALE

Settore scientifico-disciplinare: **GEO12**

DOTTORANDO
JULIEN LE MEUR

COORDINATORE
PROF. STEFANO MASET

SUPERVISORE DI TESI
DR. VANESSA CARDIN

CO-SUPERVISORE DI TESI
DR. ACHIM WIRTH

CO-SUPERVISORE DI TESI
DR. STEFANO SALON

ANNO ACCADEMICO 2024/2025

Acknowledgments

Firstly, I would like to express my gratitude to my supervisors, Vanessa, Achim, and Stefano for their help in completing my research project. Thanks to them and our constructive discussions, I was able to develop my scientific knowledge, acquire rigour in the writing process, and explore the world of research more deeply. I am very grateful to Dr Louis Gostiaux and Dr Alejandro Orfila, who kindly accepted to review this thesis and provided essential comments to improve its quality. I would now like to thank the PHYS, ECHO, TECDEV, and CTMO research groups at the National Institute of Oceanography and Applied Geophysics (OGS) for providing insightful feedback and discussions on my work and on science in general. I want to thank the OGS Argo team for giving me support and precious advices during my journey. I would also like to thank all the co-authors with whom I had the privilege to work during my PhD. I would like to express my deep thanks to the LEGI laboratory (Grenoble, France) for their hospitality during my stay, and to Achim for his support, not only in science but also in my life in Grenoble.

I would like to thank all scientists, technicians, engineers, and crew members from RV Explora, RV Laura Bassi, and RV Gaia Blu, as well as their captains, for their commitment to data collection during oceanographic cruises at the EMSO-E2M3A, EMSO-BB, EMSO-FF, D1200 moorings, and at the Vida Buoy. I also thank OGS and CNR-ISP for producing data at the EMSO South Adriatic Regional Facility, an EMSO IT Joint Research Unit and EMSO-ERIC Site. I am grateful to the scientists from ECMWF, ARGO, and the EU Copernicus Marine Service for providing marine in-situ, modelled, and reanalysed data. I thank the National Recovery and Resilience Plan of the Italian Ministry of University and Research, funded by the EU, and OGS for financing this PhD scholarship. Finally, I acknowledge the creators of ChatGPT, which was used for text refinement of the Extended Abstract, Sections 1.2 and 1.3.

I would like to thank my friends at OGS, who made my PhD journey more enjoyable. I value these people, their open-mindedness, and their help towards a French student arriving at the edge of Italy. I would like to give special thanks to my long-time office partners, Sofia, Carlotta, and Davide, for bringing such energy, smiles, and a positive attitude. I also wish to thank the students from LEGI for welcoming me and for the great time spent together. I am truly grateful to my long-time friends in France, especially Tugdual, Nicolas, Corentin, Paul, and Mélina, for the support they gave me throughout my PhD thesis.

I want to thank my parents, Huguette and Jacques, and my sisters, Marie and Florence, who were always there for me, believing in my ability to conduct my research and follow the path of a PhD student. I especially want to thank my brother, Sébastien, without whom I would not be where I am now. More than a brother, he took on the role of mentor, and see, Sébastien, *je me suis accroché et j'y suis arrivé.*

Carlotta, the moments with you during this journey have been by far the most beautiful, and I cannot express how much your support has meant to me. CaJu forever.

Extended Abstract

Introduction

The Adriatic Sea is a semi-enclosed basin of the Mediterranean Sea whose water masses are strongly influenced by physical and biogeochemical processes acting across temporal and spatial scales, from basin scale dynamics to submesoscale and microscale. The smaller spatial scale of the Adriatic basin compared to the oceans and its shorter time scale of response to atmospheric forcing make it a natural laboratory for the study of climate change. It plays an important role in the thermohaline circulation of the Mediterranean, as the Adriatic Deep Water (AdDW) is the main source of the Eastern Mediterranean Deep Water (EMDW), one of the two densest water masses there. In addition, the southern Adriatic forms a dynamic interface where the incoming salty and warm water masses meet the colder and fresher Adriatic water masses. The southern Adriatic is therefore a hotspot for thermohaline circulation in the Mediterranean and for climate change.

Physical and biogeochemical processes occurring at the basin scale, submesoscale and microscale can be analysed independently, but are also interconnected. The aim of this thesis and its novelty is to observe how physical processes at different scales influence and modulate the variability in the South Adriatic Pit (SAP) area using the longest time series of in-situ temperature, salinity, dissolved oxygen and velocities. Firstly, at the basin scale over the last century to observe long term changes, then through a study of gravity currents and their characteristics, and finally through a study of double diffusion regime changes in the SAP.

More precisely, the main questions driving this research are: How is the SAP responding to the combined effects of global warming and increasing salinisation of the Adriatic Sea? Considering that the renewal of the deep SAP water masses depends primarily on the North Adriatic Dense Water (NAdDW), have the driving forces and the periodicity or timescale of the associated gravity currents changed? And finally, what are the mechanisms behind the recent changes in the double-diffusive regime in the SAP, and what consequences do they have for the transformation of water masses and circulation in the Mediterranean?

Methods

This study is based on a combination of measured, modelled, and reanalysed data. The measured data include long-term hydrographic records from oceanographic cruises, mooring observations at EMSO-E2M3A (center of the SAP), EMSO-BB (in Bari canyon) and EMSO-FF (North of Bari canyon), oceanographic buoys and Argo floats in SAP. The main dataset used in this study, from EMSO-E2M3A, is the longest available time series of hydrographic variables in the Adriatic Sea, spanning from 2006 to present, coupled

with cruise measurements collected from the late 20^{th} century up to the present day. This dataset was corrected considering a primary quality control based on (Cardin et al., 2014b) and a secondary quality control considering the cruise repeated robust measurements to correct for offsets and drifts of the different sensors. This dataset allows the assessment of a basin-scale variability and long-term changes in temperature and salinity. The three moorings deployed in the SAP enabled continuous high-frequency observations of the water column and aimed to resolve the processes at a finer temporal scale. These were complemented by modelling and reanalysed data, mainly from the Copernicus Marine Service, to investigate the processes on the Adriatic scale and observe the performance of the models.

The methodological approach is consistent with the multiscale structure explored in this thesis. Changes at the basin scale were analysed by combining the long time series of moorings and cruise measurements with the heat fluxes derived from the atmospheric reanalysis ERA5 to detect long-term trends and anomalies in the water mass properties (Terzić, Cardin, Le Meur et al., 2025). Submesoscale variability was investigated from studying the intermittent gravity currents recorded by moorings in the SAP, coupling the results with atmospheric and oceanic reanalyses. This allowed for the characterisation of the frequency, time scale, drivers of gravity currents and their links to the formation of dense water in the northern Adriatic (Le Meur et al., 2025). Finally, double diffusive regimes were studied computing the Turner angle from the long-term time series of mooring data, with particular attention to the exceptional salinity anomaly of 2017 and its relationship with the tipping of the double diffusive regime (Amorim, Le Meur et al., 2024).

Taken together, this integrated observational framework provides a multiscale perspective that links climate-driven variability in the basin with submesoscale and microscale processes that characterise the dynamics of the SAP.

Results and Discussion

Over the last two decades, the SAP has undergone significant thermohaline changes, highlighting its role as a hotspot for climate change in the Mediterranean. Observations show a persistent increase in temperature, salinity (spiciness) throughout the water column. The strongest trends were observed in the intermediate to deep layers (350 to 900 dbar), while the most moderate warming is observed in the upper layer. These differences in the dynamics within the water column can be explained by the topography of the SAP and the different water masses involved in its dynamics. Over the last ten years, a two to four times higher increase in temperature and salinity has been observed in the deep SAP compared to the rest of the Mediterranean (0.2 °C and 0.4 to 0.8). These results indicate that changes assumed to occur on a centennial scale for the Mediterranean can occur within one or two decades in the SAP, illustrating the *"climate change hotspot"* definition for the SAP.

The deep layers also show the strongest negative trends in the potential density anomaly (PDA), in line with the vision of a shift towards a two-layer structure in the SAP, especially after the exceptional salt inflow in January 2017, which increased stability at depth below 900 dbar and reduced it above 900 dbar. On a broader spatial scale, the warming trends in the SAP are stronger than in the Ionian Sea, emphasising the importance of locally driven processes.

The ventilation of the deep SAP is determined by the interplay of small-scale mixing

and intermittent gravity currents originating from the northern Adriatic Sea. Between 2007 and 2023, only four major events reaching the seafloor were identified based on six detection criteria (2012, 2017, 2018, 2022). These criteria include simultaneous fluctuations in PDA and dissolved oxygen at the three moorings in the SAP (EMSO-E2M3A, EMSO-BB and EMSO-FF), small density differences between EMSO-BB and EMSO-FF, sufficient PDA of the cascading water, coherence with the PDA of the formed NAdDW and T/S diagrams confirming mixing between the resident and inflowing water. The gravity current events showed variability in both, drivers and inflow pathways: while temperature dominated in 2012, salinity became the main driver in 2017 and 2022, and both acted together in 2018. The main inflow pathways also varied from EMSO-FF in 2012, 2018 and 2022 to EMSO-BB in 2017. It was also found that the timescales of these events indicate that the NAdDW pulses occur between late winter and spring, with typical travel times of about two months from the generation region to EMSO-E2M3A and two weeks from EMSO-BB and EMSO-FF to EMSO-E2M3A. Our results indicate that 2017 marks a turning point in the supply of dense water to the deep SAP, with evidence suggesting a transition toward more salinity-driven gravity current dynamics.

At the microscale, salt fingering proved to be the dominant double diffusion regime, controlled by the intrusion of saline water from the Ionian Basin. Between 2014 and 2016, the increasing stratification above 400 dbar and at 800 dbar reduces the favourable double diffusive mixing between the upper layer and the deep SAP. It was also observed that after the winter of 2014/2015, the upper layer shifted from a regime of salt fingering to a doubly stably stratified regime, reducing the potential active salt fingering and consequently the vertical double diffusive mixing. In addition, the salt inflow in January 2017 triggered deep convection up to 750 dbar, which enhanced the salt fingering above 900 dbar. The increase in the salt fingering regime after this extreme event is of great importance as it can change the entire thermohaline circulation of the region. In particular, salt fingering competes with gravity currents: The latter enhance stratification at depth and the former increase vertical exchange, leading to involved mixing regimes in the deep SAP after 2017.

Conclusion

The analysis of the SAP from the basin scale to the microscale reveals interacting processes that together determine its thermohaline evolution. Warming and salinisation at the basin scale influence the stratification of the water column, which in turn modulates the properties and pathways of cascading gravity currents and the dominance of salt fingering over other double diffusive regimes. The exceptional salinity input into the Adriatic Sea in 2017 marked a turning point: gravity currents became more salinity-driven and the salt fingering was enhanced throughout the water column. At the same time, the gravity currents transported heat and salt into the deep SAP, increasing stability and partially decoupling the deep water from the overlying intermediate and upper layers.

This relative decoupling from the deep to the rest of the water column is the result of physical processes at different scales influencing and modulating variability: basin-scale salinity intrusions, submesoscale gravity currents and microscale double diffusion, which together control vertical stability and transport. These results emphasise the role of the Adriatic Sea both as a producer of dense Mediterranean water and as a hotspot for accelerated climate change, where centennial changes of the Mediterranean may occur within a few decades in the SAP.

Contents

Acronyms

α	Coefficient of thermal expansion
ADCP	Acoustic Doppler Current Profiler
AdDW	Adriatic Dense Water
ADV	Acoustic Doppler Velocimeter
AW	Atlantic Water
β	Coefficient of salt contraction
BiOS	Bimodal Oscillating System
CDW	Cretan Deep Water
CIW	Cretan Intermediate Water
CT	Conservative Temperature
CTD	Conductivity Temperature Depth
dSAP	deep South Adriatic Pit
DC	Diffusive Convection
DS	Doubly Stable
DWF	Deep Water Formation
DWOC	Deep Water of the Otranto Channel
EMDW	Eastern Mediterranean Deep Water
E2M3A	Eastern Mediterranean Multiparametric Moored Array
EAC	Eastern Adriatic Current
EMT	Eastern Mediterranean Transient
f	Coriolis frequency
ISW	Ionian Surface Water
κ_S	Salt diffusivity coefficient
κ_T	Heat diffusivity coefficient
LIW	Levantine Intermediate Water
LSW	Levantine Surface Water
MAP	Middle Adriatic Pit
MAW	Modified Atlantic Water
MLD	Mixed Layer Depth
MOW	Mediterranean Outflow Water
η_X	Temporal variability of a variable X based on a centered sliding mean
N	Brunt–Väisälä frequency
NAdDW	North Adriatic Dense Water

NIG	North Ionian Gyre
PAR	Photosynthetically Active Radiation
PDA	Potential Density Anomaly
PDF	Probability Density Function
Q_{LF}	Latent heat flux
Q_{LW}	Latent wave radiation
Q_{SF}	Sensible heat flux
Q_{SW}	Short wave radiation
Q_{TOT}	Total heat flux
R	Mixing ratio coefficient
R_o	Rossby number
RV	Relative Vorticity
S	Salinity
SA	Absolute Salinity
SAP	South Adriatic Pit
SF	Salt Fingering
θ	Potential Temperature
T	Temperature
Tu	Turner angle
TV	Test Value coefficient
VL	Vector Length
WAC	Western Adriatic Current
WMDW	Western Mediterranean Deep Water
WMT	Western Mediterranean Transient

Introduction

0.1 Aims of the study

Oceans constitute key areas for 1.4 billion humans (Bindoff et al., 2019). Therefore, all aspects that may influence the changes currently observed due to global warming must be studied carefully. The consequences of the global warming on the ocean are multiple: sea level rise due to thermal expansion and melting of ice sheets and permafrost, affecting hundreds of millions of people (Li et al., 2009; Hinkel et al., 2014; IPCC, 2022); increased salinity and temperature of oceans; acidification of the ocean due to higher quantities of CO_2 absorbed from the atmosphere; and the disappearance of fauna and flora. All these elements justify rigorous studies of oceans, either through modelling or in-situ observation using multiple types of platforms, to further our understanding of the processes involved, enable prediction, and estimate the response to anthropogenic forcing.

In this thesis, we focus on the Mediterranean Sea and more specifically on one of its sub-basins, the Adriatic Sea, which can be considered a laboratory for climate change impacts because its smaller size results in a shorter time scale of response to changing atmospheric forcing. The Adriatic Sea is a key area for the thermohaline circulation of the Mediterranean Sea and is an important area where the Adriatic Deep Water (AdDW) originates. This water mass is the main source of the Eastern Mediterranean Deep Water (EMDW), which, together with the Western Mediterranean Deep Water (WMDW), formed in the Gulf of Lions, constitutes one of the two densest water masses in the Mediterranean Sea. This dense water exits the Mediterranean through the Strait of Gibraltar and leaves its imprint in the Atlantic Ocean, slightly influencing the Atlantic Meridional Overturning Circulation (AMOC) (Rahmstorf, 1998).

The South Adriatic is a dynamic area, at the interface between water masses entering and leaving the Adriatic Sea. There, physical processes act from the basin scale to the microscale. How is the South Adriatic Pit (SAP) responding across scales to climate change? To address this general point, this thesis will aim to answer the following questions:

- How does the SAP react to the effects of global warming and the increasing salinisation of the Adriatic Sea?
- As the deep SAP water masses are mainly renewed by the North Adriatic Dense Water (NAdDW), have there been changes in its drivers, in the periodicity or timescales of the associated gravity currents?
- What are the mechanisms and consequences for the recent changes in the double diffusive regime in the SAP?

In the following sections of this introduction, I will first describe the Adriatic Sea, its dynamics, and its connection to the Mediterranean Sea (section 0.2). I will then introduce the key physical processes occurring in the Adriatic Sea: convection (section 0.3.1), gravity currents (section 0.3.2), salt fingering (section 0.3.3), boundary currents (section 0.3.4), and eddies (section 0.3.5).

This thesis is divided into four parts. The first part deals with the post-processing of mooring data using standard quality control, followed by a second quality control based on measurements collected during cruises (part I). The remaining three parts are based on the three publications that form the basis of this thesis. They address the research questions step by step by downscaling the impact of climate change in the SAP. Part II examines variability at the basin scale and analyses long-term changes in water masses in the SAP (Terzić, Cardin, Le Meur et al., 2025). Part III focuses on submesoscale gravity currents

occurring in the deep SAP and explores their connection with the physical dynamics of the North Adriatic, as well as their characteristic time scales (Le Meur et al., 2025). Part IV investigates microscale processes, particularly changes in the double diffusive regime in the SAP in 2017 and the resulting possible tipping point (Amorim, Le Meur et al., 2024). Finally, the thesis concludes with the main results obtained in the different parts and addresses perspectives on the key questions formulated.

0.2 The Adriatic sea

0.2.1 Brief presentation of the Mediterranean Sea dynamics

The Mediterranean Sea (fig. 1), is a semi-enclosed basin with a mean depth of around 1500 m. It is composed by the Adriatic, Tyrrhenian, Ionian, Levantine, Aegean, Liguro-Provencal, Balearic and Alboran, sub-basins, each one having their own characteristics and dynamics. It covers an area of 2.5 million m^2, which is small compared to the oceans (representing 0.7% and 0.3% of the surface and volume of the world oceans respectively, according to Bethoux et al. (1999)), but has been intensively studied because many of the physical processes occurring in the world's oceans are also present there (Robinson and Golnaraghi, 1994). In addition, smaller basins of the world's oceans (such as the Mediterranean Sea, Red Sea, Persian Gulf, and Baltic Sea) produce water masses with extreme properties and transport them into the larger oceans, where they influence the dynamics. The Mediterranean Sea also offers the advantage that physical processes occur on shorter timescales (the water mass renewal and the circulation occur over decades, while in the oceans these processes take centuries, according to Bethoux et al. (1999)) and on smaller spatial scales, which allows an easier monitoring of water masses. In this sense, the Mediterranean Sea acts as a laboratory to study the influence of climate change, and the evolution of the global ocean (Lejeusne et al., 2010) as well as the associated processes. For instance, the high-salinity Mediterranean Outflow Water (MOW) (de Pascual-Collar et al., 2019), which exits the Mediterranean Sea through the Strait of Gibraltar and flows into the Atlantic Ocean, slightly affects the overturning circulation in the North Atlantic (Rahmstorf, 1998; Artale et al., 2002; Ivanovic et al., 2014). Moreover, it has recently been shown that the Mediterranean Sea is one of the main climate hotspots (Giorgi, 2006), and numerous authors have noted the increasing temperature (Romanou et al., 2010; Skliris et al., 2012; Rivetti et al., 2017; Pisano et al., 2020) and salinisation (Skliris et al. (2018) for the whole Mediterranean, Ozer et al. (2017) in the south-east Mediterranean Sea, and Vargas-Yáñez et al. (2017) near the Spanish coast).

The general cyclonic circulation of the Mediterranean Sea (see fig. 1) is driven by water exchanges at the Strait of Gibraltar, by air-sea exchanges of heat, momentum and freshwater, by river inputs, and by exchanges with the Black Sea. Chiggiato et al. (2023) provides an overview of the Mediterranean Sea circulation: the fresher Atlantic Water (AW) enters the Mediterranean Sea through the Strait of Gibraltar, is transformed into Modified Atlantic Water (MAW) due to increased salinity and heat content in the Alboran Sea, and subsequently follows the African coast. When it reaches the Sardinian Channel, it splits in two, one branch enters the Tyrrhenian Sea, the other continues to the Eastern Mediterranean through the Sicily Channel. In both, the Western and the Eastern Mediterranean, the MAW is modified due to air-sea interactions and mixing with surroundings water masses, but it can still be recognised at the surface by its salinity minimum. After arriving in the far Eastern Mediterranean, the MAW is transformed into

saltier water masses during winter (due to strong dry winds inducing evaporation), namely the Levantine Surface/Intermediate Water (LSW and LIW) and the Cretan Intermediate Water (CIW). After its formation, the intermediate water is embedded in the cyclonic circulation and flows westwards: part of it enters the Adriatic Sea and influences its dynamics, particularly by being an important driver for the formation of the AdDW, which makes the largest contribution to the EMDW and thus regulates the thermohaline circulation in the Mediterranean Sea. Part of the LSW is also transformed into Ionian Surface Water (ISW) and enters the Adriatic Sea. LIW and ISW enter the Adriatic especially during the cyclonic phase of the North Ionian Gyre (NIG). The remaining LIW passes through the channels of Sicily or Sardinia. This intermediate water progressively mixes with surrounding water masses, becoming fresher, colder and less oxygenated (Schroeder et al., 2020). After passing through the Sicily or Sardinian channel, it arrives in the western part of the Mediterranean Sea, becomes a driver of Deep Water Formation (DWF) in the Gulf of Lions (source of WMDW), and outflows at depth through the Strait of Gibraltar into the Atlantic Ocean.

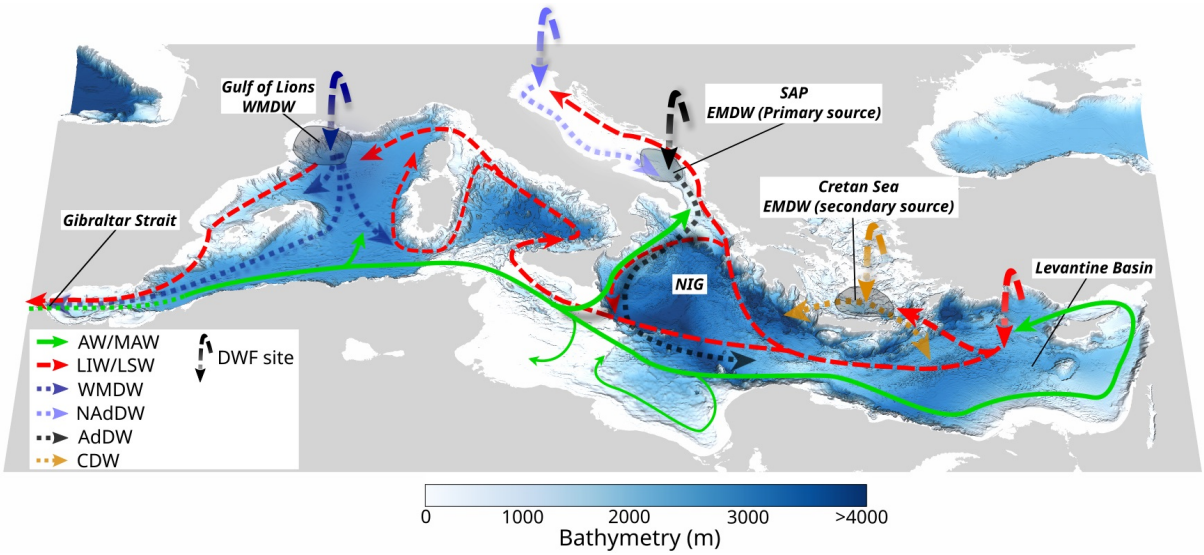

Figure 1: Bathymetric map of the Mediterranean Sea with the main water masses and main circulation patterns

0.2.2 Physical dynamics of the Adriatic Sea

The Adriatic Sea is a semi-enclosed basin bordered by Italy, Slovenia, Croatia, Montenegro, and Albania (fig. 2). It is relatively small, measuring only 800 km in length and 200 km in width, and is connected to the Ionian Sea by the Otranto Strait (780 m deep and 72 km wide), see fig. 2. It can be divided into three sub-basins, each with distinct characteristics:

- The North Adriatic, which is less than 50 m deep.
- The Middle Adriatic, with the Jakuba Pit, has a maximum depth of 270 m.
- The South Adriatic, with depths up to 1200 m in the South Adriatic Pit (SAP).

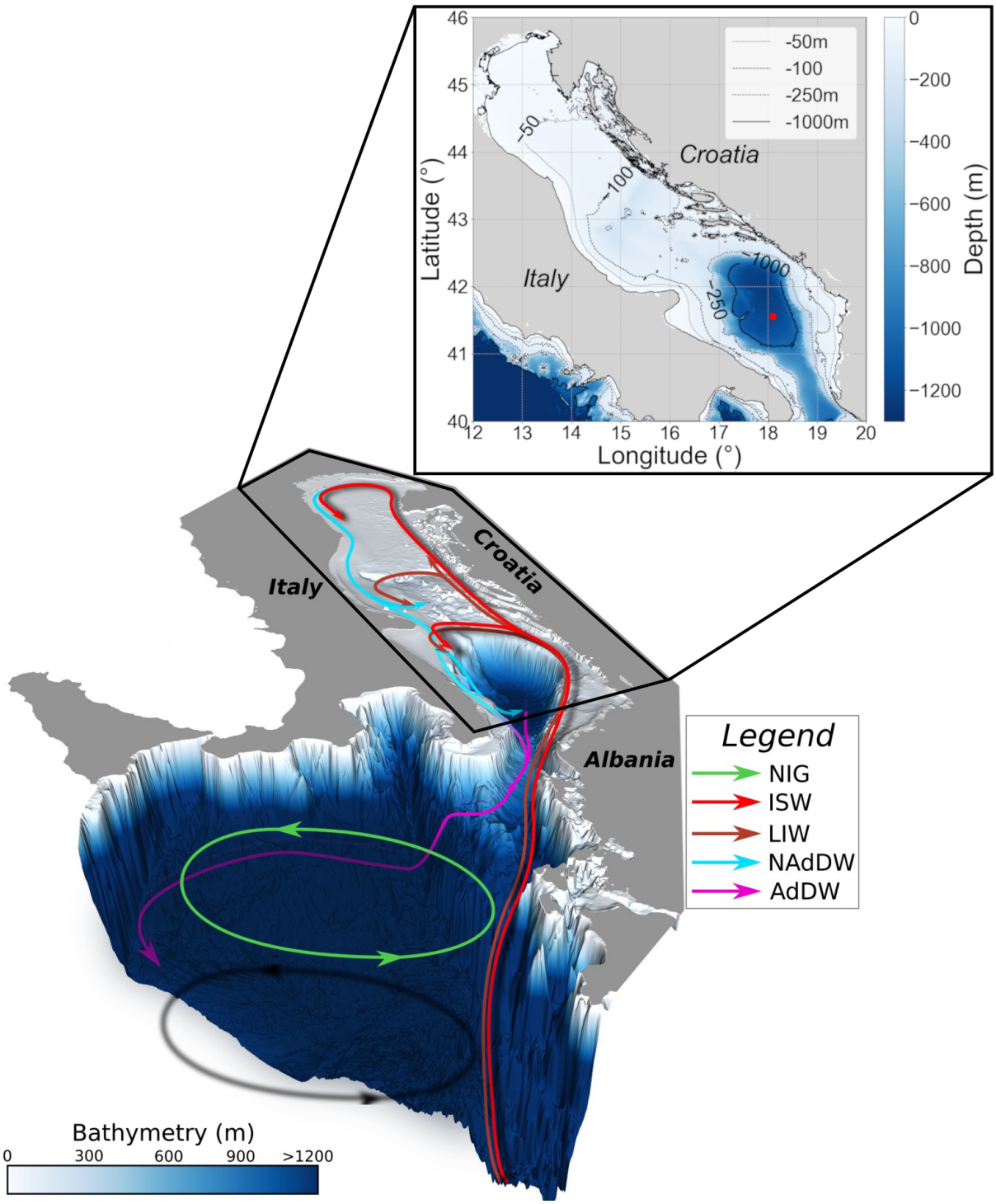

Figure 2: Bathymetric map of the system Adriatic-Ionian Seas with the main water masses and circulation patterns in a situation of cyclonic phase of the North Ionian Gyre and zoom on the Adriatic Sea (top right). The red dot placed at the center of the SAP on the top right figure corresponds to the location of the mooring EMSO-ERIC E2M3A.

After entering the Adriatic Sea at the eastern part of the Otranto Strait, surface and intermediate waters become embedded in a basin-scale cyclonic circulation and are redistributed into the three sub-basins. Each of these sub-basins has a dominant cyclonic circulation. The Adriatic Sea displays seasonal patterns of heat fluxes, river runoff and

nutrient loading, freshwater input and exchanges with the Mediterranean Sea, wind field, and vertical structure of the water column. The Adriatic is a dilution basin (there is an annual gain in the freshwater balance, Artegiani et al. (1997)) and, on average, it loses heat. These fluxes are compensated by the inflow of warm and salty LIW/ISW.

The thermohaline circulation, the vertical structure of water masses, and the exchanges of water masses with the Ionian are driven by density gradients. These density gradients result from buoyancy gain through heating, precipitation, and river runoff, or loss through cooling and evaporation. The Adriatic Sea exhibits both estuarine (fig. 3a) and inverse-estuarine (fig. 3b) thermohaline circulation (Cushman-Roisin et al., 2001; Valle-Levinson, 2022). In the north, the Po River's discharge of fresh water creates a higher sea level, which induces a barotropic pressure gradient directed out of the basin. To satisfy geostrophy, surface water is displaced against the eastern coast of Italy, creating a sea level rise. The resulting Western Adriatic Current (WAC) flows southward. The WAC is balanced by the inflow of saltier water masses (LIW and ISW), accounting for the estuarine-like circulation of the Adriatic Sea (Hopkins et al., 1999). Conversely, the generation of dense water in DWF sites (in the North Adriatic with the generation of the NAdDW and in the South Adriatic) creates a baroclinic pressure gradient directed outward from the basin, as the surrounding water is less dense. Here, the geostrophic response is a convergence of the dense water mass, against the eastern Italian boundary, which then flows southward as a bottom boundary current (Deep Water of the Otranto Channel - DWOC) (section 0.3.2). The outgoing DWOC and the remainder of the Ionian constitute the inverse estuarine thermohaline circulation. This double thermohaline circulation is possible because only a small fraction of the fresh water mixes with the interior. Therefore, the surface buoyancy gain does not prevent the formation of dense water during winter in the northern Adriatic.

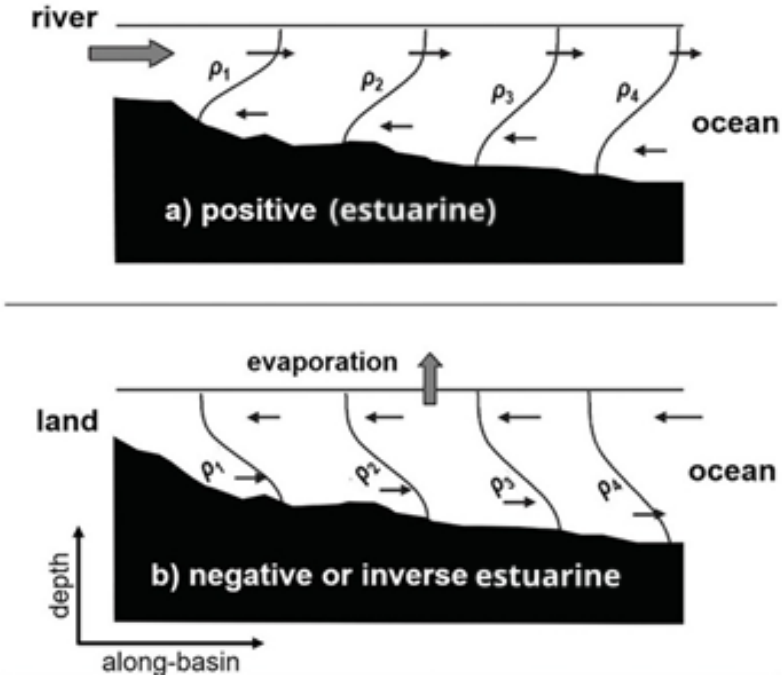

Figure 3: Classification of semi enclosed basin based on the water balance, modified from Valle-Levinson (2022). **a** represents the estuarine circulation and **b** the inverse estuarine circulation

The transport of water on the western side of the Adriatic through the estuarine and inverse estuarine circulation creates a pressure gradient with the Ionian Sea, which induces the flow of water masses originating from the Ionian Sea through the Otranto Channel along the eastern side of the Adriatic (Eastern Adriatic Current - EAC). This current, which is wider than the WAC, is composed of ISW near the surface and LIW centred at around 300 m depth in the Strait of Otranto. These two water masses, which are saltier and warmer compared to Adriatic water masses, compensate in winter for the buoyancy loss due to heat loss. The path of the EAC differs between winter, when it reaches the North Adriatic, and summer, when it is restricted to the South and Middle Adriatic. Furthermore, during the warmest months, the waters on the western side appear to be warmer than those on the eastern side, and the reverse occurs during the coldest months. During winter especially, the strong, cold, and dry north-eastern Bora wind generates strong shear at the surface, causing upwelling on the eastern side of the Adriatic, a weakening of the EAC (and thus of LIW inflow), and a strengthening of the WAC.

The Adriatic Sea is influenced by two main winds: the Bora and the Scirocco. The Bora is a cold, dry north-easterly wind that generates strong air-sea heat fluxes and evaporation, especially in the North Adriatic, and causes upwelling along the eastern coast of the Adriatic. The Scirocco is a humid, warm south-easterly wind that can reverse the WAC and, which is a major factor in floods in Venice. The Bora is one of the main drivers of the strong heat fluxes, on the continental shelf in the North Adriatic and in the open-sea in the SAP (section 0.3.1). These areas are crucial, as DWF links the surface layer, which is forced by the atmosphere, to the deep layers. The outflowing AdDW into the Ionian consists of the dense water formed in these sites and is the main component of the EMDW. This explains why studying the Adriatic Sea is of primary importance in the context of climate change.

The contribution of the Adriatic to the EMDW is not independent from the rest of the Mediterranean Sea. The Ionian Sea influences this contribution by transporting more or less LIW/ISW into the Adriatic. In particular, the NIG, which undergoes a nearly decadal bimodal oscillation (Bimodal Oscillation System - BiOS), plays a key role. A concise explanation of this process is given by (Gačić et al., 2010; Civitarese et al., 2023): the cyclonic (phase A) mode of the NIG brings salty LIW and ISW, while the anticyclonic mode (phase B) brings fresher MAW into the Adriatic Sea. The inflow of LIW/ISW or MAW therefore leads to the generation of denser or less dense AdDW, which subsequently spreads into the Ionian basin, representing a feedback mechanism. More precisely:

Phase A. The cyclonic NIG supplies salty LIW and ISW to the Adriatic, enhancing the formation of high-density AdDW. The outflow of this dense water mass into the deep Ionian Sea causes a shallowing of isopycnals, meaning the water column tends to compress and its height decreases. To satisfy the principle of conservation of potential vorticity, defined as $q = \frac{f+\zeta}{H}$, where f is the Coriolis frequency, ζ is the relative vorticity, and H is the height of the water column, the compression of the water column is balanced by a decrease in ζ (f is nearly constant). This results in a weakening of the cyclonic vorticity of the NIG. After roughly a decade, the system shifts towards its anticyclonic phase.

Phase B. After a period of weakening of its cyclonic mode, the NIG shifts into its anticyclonic phase, favouring fresher MAW to enter the South Adriatic. This results in the formation of less dense AdDW, which, after flowing into the deep Ionian Sea, deepens the isopycnals and stretches the water column. This stretching of the water column

is balanced by an increase in ζ, that is, a decrease in anticyclonicity. Eventually, the system is able to shift back to the cyclonic phase, completing the BiOS oscillation.

Apart from the BiOS mechanism, the Eastern Mediterranean experienced a shift in the main water masses contribution in the late 1980s to mid-1990s, known as the Eastern Mediterranean Transient (EMT), during which the Aegean Sea became the most important contributor to the EMDW. The EMT can be schematized in the following phases (Li and Tanhua (2020); fig. 4):

1. Before the EMT, the cold and low-salinity AdDW predominated in the generation of the EMDW.
2. During the EMT, a shift occurred and the Cretan Deep Water (CDW) became dominant over the AdDW.
3. Progressively, the amount of CDW produced decreased, leading to a higher predominance of AdDW. This is the Western Mediterranean Transition (WMT).
4. After the EMT, in the late 2010s, the AdDW are the dominant source of EMDW but are weakened compared to the situation pre-EMT.

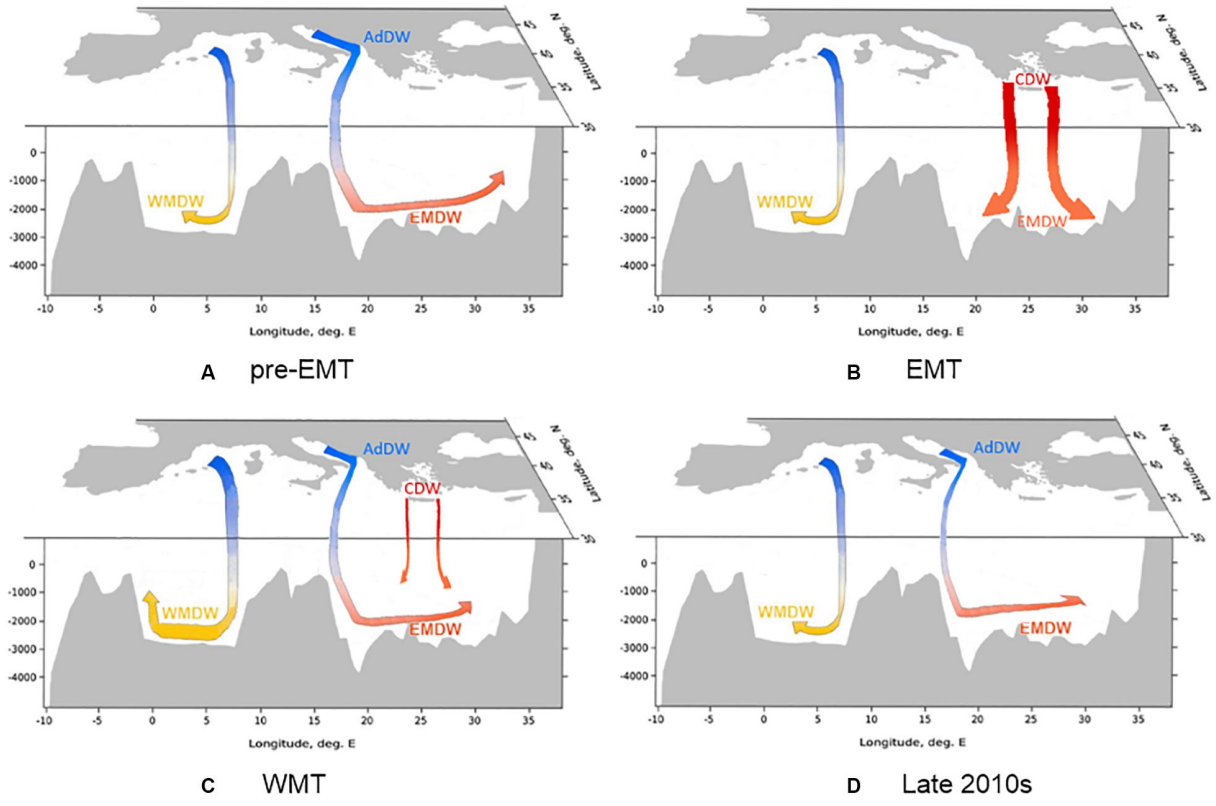

Figure 4: Visual representation of the water masses involved in the generation of EMDW before, during, and after the EMT. From Li and Tanhua (2020)

0.3 Processes

In the ocean, a water column is usually layered with water masses of increasing density with depth, a phenomenon known as stratification. Away from the boundaries, the modi-

fication of this stratification occurs through vertical and horizontal mixing processes and advection. These processes are essential for the redistribution of heat, salt, carbon and nutrients, and ultimately regulate the large-scale circulation and climate. Among them, deep convection in the DWF areas, gravity currents, salt fingering, boundary currents and eddies occur in the South Adriatic, all contributing to the renewal of water masses in the SAP.

0.3.1 Convection

When the stratification is stable, the squared Brunt–Väisälä frequency ($N^2 = -\frac{g}{\rho_0}\frac{d\rho}{dz}$) is positive ($N^2 > 0$), indicating a restoring force to vertical displacement. If $N^2 < 0$, the water column is statically unstable and convection can occur.

In the latter case, in the DWF areas, convection occurs; that is, vertical exchange between surface water and deeper waters takes place, and surface water can sink to great depths. DWF areas are often characterised by cyclonic circulation, reduced stratification near the surface and a significant surface buoyancy loss during winter. All these factors create favourable conditions for deep convection.

The open ocean convection process is divided into three phases:

1. Preconditioning at the basin scale
2. Convective mixing through localised vertical plumes
3. Lateral mixing and restratification through mesoscale and submesoscale processes

During preconditioning, the general cyclonic circulation domes the isopycnals and brings weakly stratified water to the surface at the interior of the eddy. This reduces the vertical stratification near the surface. The remaining stratification is then gradually eroded by the loss of buoyancy at the surface due to cooling and evaporation driven by air-sea interaction (Marshall and Schott, 1999).

When the surface water is denser than the underlying water masses, localised convective plumes develop ($<$ 1km), which are characterised by vertical velocities of up to 10 $\mathrm{cm\,s^{-1}}$ (Schott and Leaman, 1991). Convection on large scales cannot take place due to geostrophic equilibrium, which opposes vertical movement. The downwelling water in the plume results in upwelling in between. The vertical motion in the plumes is driven by the conversion of the available potential energy into kinetic energy, which is roughly given by $w^2 \approx \frac{1}{3}\Delta b \Delta z$, where Δb is the buoyancy difference and Δz the vertical depth of the plume (Marshall and Schott, 1999).

When plumes sink, they entrain the surrounding water and expand laterally. If the convection is deep and persists over time scales comparable to f^{-1} (the inverse Coriolis frequency), the Earth's rotation influences the dynamics. The plumes begin to behave like Taylor columns, which resist lateral expansion at depth and develop into anticyclonic conical eddies. These structures exhibit cyclonic vorticity near the surface and anticyclonic vorticity at greater depth. On the plume scale, upwelling and downwelling almost balance each other, resulting in negligible net vertical transport, while on the patch scale, a net downward transport is observed (Marshall and Schott, 1999).

Horizontal density gradients develop in the mixed layer due to heterogeneous surface forcing and asymmetries in plume strength. In addition, convection dynamics are further complicated by horizontal shear, fronts and mesoscale eddies. The multiplication of plumes in the DWF region contributes to the homogenisation of the mixed patch. When

convection intensifies, a strong rim current forms around the convective region at the surface. This current restricts the convecting water and limits lateral exchange with the surrounding stratified water. If the rim current is strong enough, it can become baroclinically unstable, creating meanders and eventually break up the patch and allow lateral exchange. The patch then disintegrates into cone-shaped structures on the scale of the first baroclinic Rossby deformation radius (Maxworthy and Narimousa, 1994). Under strong rotational influence, the baroclinic instabilities caused by horizontal density gradients lead to the formation of geostrophic eddies that transport convected water laterally and entrain the surrounding stratified fluid. These baroclinic eddies redistribute potential vorticity and drive lateral spreading and restratification on time scales of weeks to months (Marshall and Schott, 1999).

There are two important DWF sites in the Adriatic. The first is in the northern Adriatic, a shallow continental shelf area (less than 50 m deep) exposed to the strong, cold, and dry Bora winds (fig. 2). This region is characterised by a cyclonic sub-basin circulation driven by density differences between the EAC and WAC. The shallow depth favours strong preconditioning, supported by the Bora winds and the inflow of ISW from the south. During intense Bora events, increased evaporation and surface cooling cause the entire water column to cool and dense surface water to form. The freshwater inflow from the Po River remains limited near the coast and does not significantly increase buoyancy in the central basin. The dense water formed, known as NAdDW, is considered one of the densest water masses in the Mediterranean (Cushman-Roisin et al., 2001). After its formation, it flows southward as a gravity current along the western Adriatic shelf, partially filling the Middle and South Adriatic Pits (MAP and SAP) or exiting the Adriatic Sea through the Strait of Otranto (section 0.3.2). The second DWF site is located in the open sea of the SAP, which also exhibits cyclonic circulation (fig. 2). There, the salty LIW/ISW contribute to preconditioning by weakening the stratification, and Bora events trigger convection. After such events, the resulting dense water can flow from the Adriatic through the Strait of Otranto into the Ionian Sea. A major difference between these DWF sites lies in the depth of vertical mixing: in the north, the shallow depth allows mixing of the entire water column, while in the south, convection rarely reaches the bottom of the SAP (Gačić et al., 2002; Cardin et al., 2011; Bensi et al., 2014). The deep SAP is ventilated intermittently by gravity currents that transport NAdDW (section 0.3.2, chapter 3).

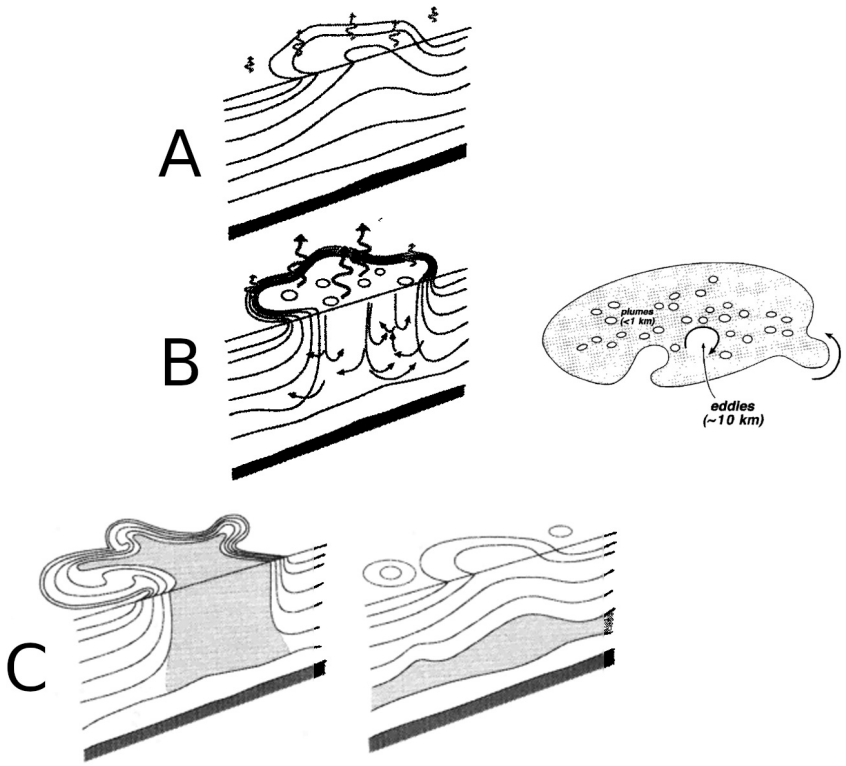

Figure 5: Schematic diagram of the phases of open ocean deep convection, from (Marshall and Schott, 1999). **A** Preconditioning; **B** Deep convection, with a representation on the right showing the formation of the mixed patch with plumes and eddies; **C** Restratification, resulting in lateral exchange and spreading. The mixed fluid is shown shaded.

0.3.2 Gravity currents

In areas where deep convection does not reach the bottom of the water column, such as the SAP (Gačić et al., 2002; Cardin and Gačić, 2003; Cardin et al., 2011; Bensi et al., 2014), gravity currents play a key role in ventilating intermediate and deep waters. These currents transport cold and/or salty water masses from coastal areas into the deep sea, renewing the content of heat, salt, oxygen, and nutrients, or even forming new water masses through turbulent mixing.

Gravity currents are driven by horizontal density gradients resulting from differences in temperature, salinity or suspended matter (Benjamin, 1968). These gradients generate buoyancy forces that set the fluid in motion (Huppert, 2006; Wirth, 2009). Oceanic gravity currents can be up to 20 km wide and 200 m thick. Their initial shape, structure and velocity depend on generation mechanisms, topography and the density ratio between the dense source water and the surrounding water mass. Depending on the density structure of the surrounding water, they can spread along the bottom (dense gravity current), the case considered here, in intermediate layers (intruding gravity current) or at the surface (buoyant gravity current). In the first case, the topography of the seafloor plays an important role in shaping their trajectory.

Gravity currents are generally categorised as either compositional or particle-driven. Compositional gravity currents are driven by temperature and dissolved components such as salt. Since the mass of these solutes is conserved away from the surface, these scalars

are considered conservative. In such flows, changes in density over time are mainly due to the entrainment of ambient water with different properties (dos Santos Nogueira, 2014).

When the time scale of the current exceeds that of planetary rotation, the Coriolis force becomes significant and the current undergoes geostrophic adjustment. This adjustment restructures the flow into two dynamically distinct regions: the central, geostrophically balanced vein, and a surrounding friction layer (fig. 6) in which turbulence, shear, and non-linearity dominate (Wåhlin and Walin, 2001; Wirth, 2009; Negretti et al., 2021; Ungarish, 2022). The friction layer is partly fed by lateral and vertical exchange with the vein. In this context, downslope transport is no longer purely determined by gravity, but is regulated by near-slope Ekman dynamics and Ekman drainage resulting from the frictional effects of the upper layer (Shapiro and Hill, 1997). As a result, the core of the current is deflected laterally (to the right in the northern hemisphere) and tends to align along topographic contours instead of plunging directly downwards.

Although the development of a gravity current in idealised, non-rotating systems is described by three phases (slumping, inertial, and viscous), which are determined by the balance between buoyancy, inertia, and viscous forces (Huppert and Simpson, 1980; Simpson, 1997), this classification becomes less clear in rotating flows. In the idealised case, the slumping phase begins with the release of dense fluid and is characterised by acceleration to an almost constant velocity. This is followed by the inertial phase, in which the flow slows down and thins through entrainment and spreading. Finally, in the viscous phase, friction dominates and the current slows down further (Huppert, 1982; dos Santos Nogueira, 2014). In rotating systems, however, the transition between these phases is modified or completely suppressed by Coriolis forces, and the dynamics are better described by geostrophic adjustment, Ekman transport, and the development of boundary layers.

Mixing in gravity currents with the surrounding water occurs mainly at the upper interface, where shear and entrainment generate turbulence. Within the gravity current, mixing also arises from friction with the sloping topography, which increases diapycnal diffusivity (Legg et al., 2009). The interface between the gravity current and the surrounding water is turbulent and often contains Kelvin–Helmholtz instabilities, as well as lobes and clefts (Allen, 1971; Middleton, 1993; Princevac et al., 2005; Lee, 2010).

An analysis of gravity current dynamics in the Adriatic Sea and its influence on the deep SAP dynamics is provided in chapter 3.

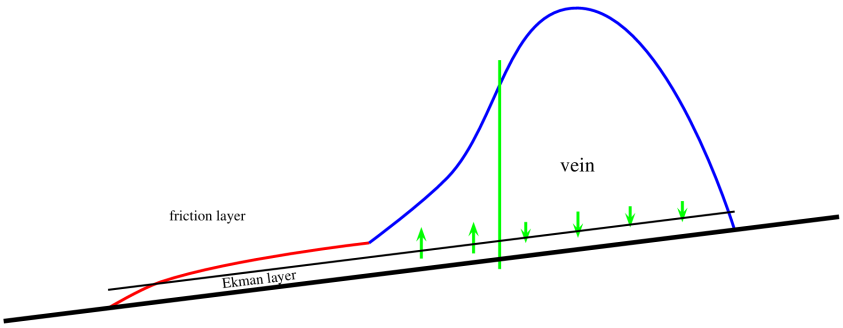

Figure 6: Schematic representation from Wirth (2009) of a cross-section through a gravity current on an inclined plane. The gravity current is shown in a rotating system, with the vein and the friction layer highlighted. The green arrows indicate the direction of the vertical velocities.

0.3.3 Salt fingering

In seawater, the molecular diffusivity of heat (κ_T) is about 100 times greater than that of salt (κ_S) (Stern, 1960; Marshall and Schott, 1999; Talley et al., 2011). This significant difference in diffusivities can result in double-diffusive convection, i.e. instabilities that occur when vertical temperature and salt gradients have opposing effects on the density (Marshall and Schott, 1999). In such regimes, the system may remain stably stratified with respect to the mean density, but still become unstable due to the differing diffusivities of heat and salt. Depending on the water mass distributions, two types of instability arise: the diffusive regime and the salt-fingering regime (Stern, 1960; Schmitt, 1994). Following the pioneering work of Stern (1960), Veronis (1965) demonstrated that the system can exhibit oscillatory instability, which enhanced the theoretical understanding of double-diffusive convection beyond steady convection.

In the diffusive regime, a cooler and fresher water mass lies above a warmer and saltier one. In this situation, the upward diffusion is more effective for heat than for salt, which increases the vertical heat flux while the effect on salinity is limited. This has a stabilising effect on the stratification (Marshall and Schott, 1999).

The salt-fingering regime occurs when warm, salty water overlies colder, fresher water. This happens, for example, when Mediterranean water enters the Atlantic Ocean (Talley et al., 2011) or in the Adriatic Sea due to the entrance of warm and salty LIW (see chapter 4). In this case, a small water parcel that is displaced downwards loses heat faster than salt due to the different diffusivities of heat and salt. As a result, the parcel becomes denser than its surroundings and continues to sink. To conserve mass, an upward displacement of another water parcel balances the sinking. This process produces vertical structures called *"salt fingers"* (Stern, 1960; Talley et al., 2011; Yano, 2023) (fig. 7). Despite the overall stable density gradient, the decrease in mean salinity with depth provides the energy source for persistent convective motions (Stern, 1960). Salt fingering occurs on a centimetre to metre scale, but is still able to mix the internal layers of the water column effectively. This scale is still too small to be explicitly resolved in numerical models of ocean dynamics, although it can be of great importance for heat and salt transport and mixing.

On a large scale, double-diffusive processes contribute significantly to the structuring of ocean stratification through the formation of layered staircases and increased vertical exchange. This triggers the transformation of water masses and the transport of nutrients. Although acting on small spatial scales, their effects can influence large-scale ocean circulation and thermohaline dynamics (Stern, 1960; Yano, 2023).

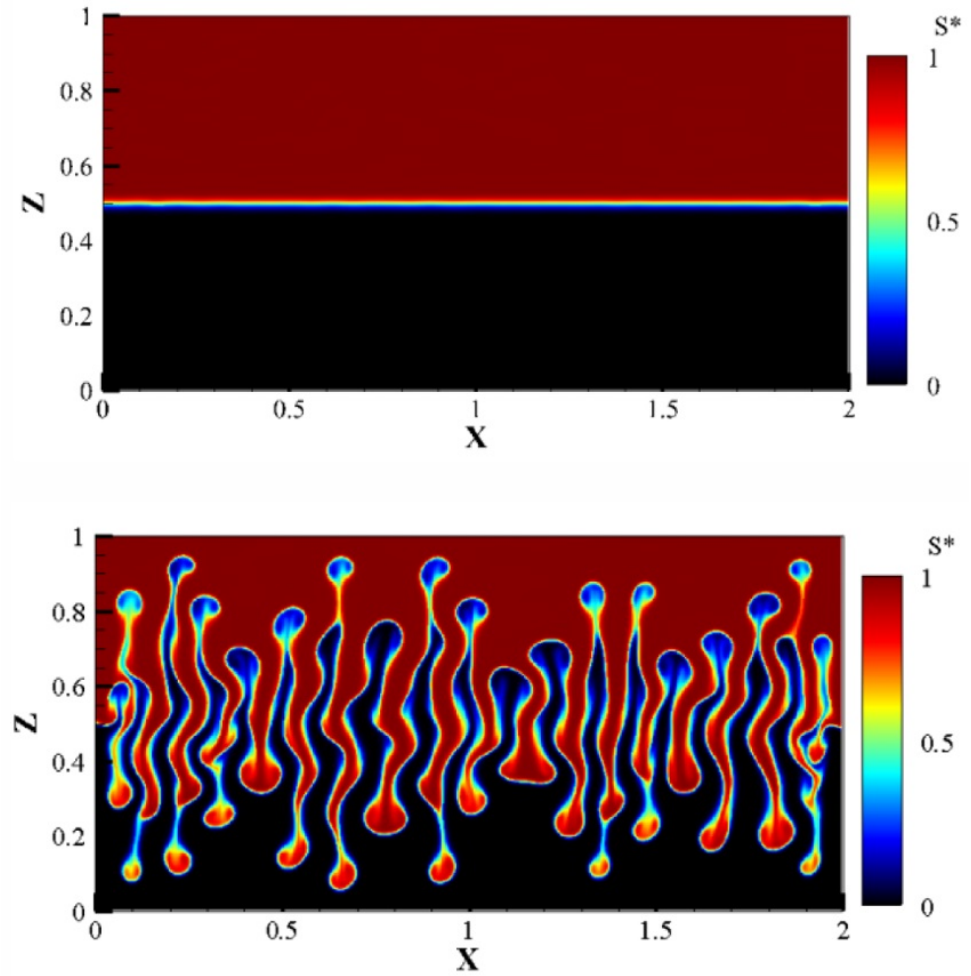

Figure 7: Visualisation of salt fingers via a numerical modelling by Ouzani and Khelladi (2023). The top figure is the initial state with a warm and salty ($S^* = 1$) water mass overlying a cold and fresh water mass. The bottom figure is the situation after few hours.

0.3.4 Boundary currents

In the Adriatic Sea, as in other marginal seas and the global ocean, boundary currents are key processes for redistributing the thermohaline properties of water masses, and thus for large-scale circulation. These are continuous, narrow currents that develop along the flanks of basins. In semi-enclosed seas such as the Adriatic, the geometry and atmospheric influences have a greater impact on the stratification of the water column than in the open ocean, which in turn affects the structure, strength, and mixing of the boundary currents. Boundary currents are influenced by geostrophic balance, which controls lateral pressure gradients along basin margins; conservation of potential vorticity, which influences curvature, width, and meandering; buoyancy forcing, which influences vertical structure and stratification; and topographic control, which determines the path of currents along topography (Pedlosky, 1996; Vallis, 2017).

In rotating fluids, the balance between the horizontal pressure gradient and the Coriolis force leads to the development of geostrophic currents. When the upper layers in a semi-enclosed basin are influenced by surface forcing, whether by wind stress (Bora in the Adriatic), buoyancy flux from warming, cooling, or freshwater input by rivers (such as

the Po in the northern Adriatic), the sea interior responds with a broad, basin-scale circulation that reflects the integrated effect of surface forcing. Boundary currents form along the edges of the basin as a result of the maintenance of potential vorticity and horizontal density gradients (buoyancy) throughout the basin. Within these boundary currents, frictional effects and eddies generated by baroclinic instabilities together act to disperse excess vorticity and regulate the transport of heat and salt (Stommel, 1948; Munk, 1950; Spall, 2004).

Spall (2004) showed that when there is a net buoyancy loss at the surface, either through cooling or evaporation, the boundary currents generated in a semi-enclosed basin contribute directly to the formation of dense water and mediate the thermohaline balance. In seas connected to a larger basin by a strait (such as the Adriatic Sea with the Strait of Otranto), the net buoyancy loss at the surface must be compensated by the inflow of water masses through the strait (LIW and ISW in the Adriatic), typically by cyclonic boundary currents. Along this type of current, the water temperature continuously decreases, resulting in the outflowing water being denser than the inflowing water (fig. 8). Through this process, the heat loss (and thus the buoyancy loss) is compensated. More precisely, if the temperature gradient between the interior of the basin and the boundary current region is strong enough, eddies that detach from the boundary current bring warm water into the interior to compensate for the heat loss there (Marshall and Schott, 1999; Spall, 2004). Spall (2004) showed that baroclinic instabilities interacting with the topography of the basin are the key processes controlling the transformation of water masses. Furthermore, when the seafloor is nearly flat, the boundary current can be completely eroded by eddies before it completes a full rotation of the basin.

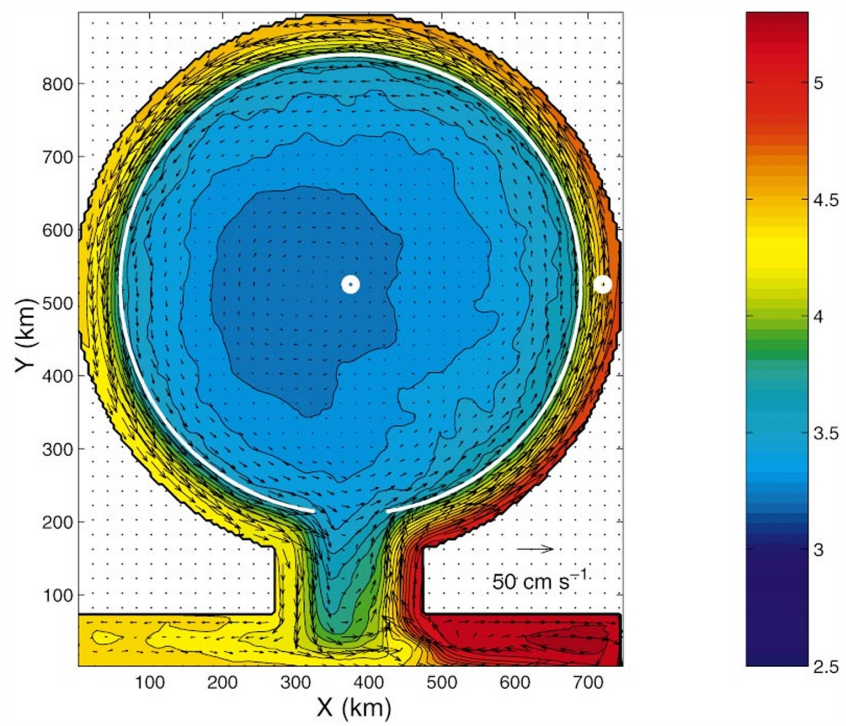

Figure 8: Result from a model of an idealised semi-enclosed basin from Spall (2004). The colours indicate the temperature of the upper layer averaged over four grid points, while the arrows show the corresponding horizontal velocities averaged over the same grid points.

In the Adriatic, this general mechanism is consistent with the inverse estuarine circulation, which is primarily driven by a net buoyancy loss in years when river discharge does not exert a stronger influence than surface heat losses. On average, there is a small annual net buoyancy loss in the Adriatic (Verri et al., 2024). Additionally, the seasonal and interannual variability of stratification affects the baroclinic and barotropic components of the boundary currents, while the topography of the Adriatic Sea, with its continental slopes and sills, controls the flow and generates recirculation gyres in the sub-basins (Cushman-Roisin and Beckers, 2011).

Instabilities in boundary currents enable the redistribution of heat and salt, mediate the exchange between the boundaries and the interior, and link local DWF with the larger-scale circulation. Their variability reflects the combined effects of wind, buoyancy, and basin geometry, and emphasises the central role of boundary currents in controlling thermohaline structure and water mass transformation in marginal seas (Spall, 2004; Verri et al., 2024).

0.3.5 Mesoscale and submesoscale eddies

Eddies are rotating, vertically extended coherent structures that occur at the mesoscale (10–100 km), where they maintain their coherence for weeks to months, and at the submesoscale (less than 10 km), where they last only days. They can be characterised by the Rossby number, which is defined as follows

$$R_o = \frac{U}{fL} \tag{1}$$

with U the fluid velocity, f the Coriolis frequency and L the horizontal length scale. At the mesoscale, eddies typically have $R_o \ll 1$ and are close to geostrophic balance, while at the submesoscale $R_o \approx 1$ so that the Coriolis force no longer dominates the momentum balance, allowing ageostrophic motions and vertical velocities significantly larger than those caused by Ekman pumping (Lapeyre et al., 2006; Trotta et al., 2017; Taylor and Thompson, 2023). Eddies play a crucial role in the oceans as they contribute to the redistribution of heat, salt, nutrients, and momentum between the atmosphere-ocean interface, the mixed layer and the ocean interior (Williams and Follows, 1998; Lapeyre and Patrice, 2006; Capet et al., 2008; Lévy et al., 2012). Eddies are also capable of pulling fluid away from its original location and transporting it across ocean basins (Early et al., 2011).

Several processes can generate eddies at the mesoscale and submesoscale (fig. 9). At the mesoscale, eddy formation is primarily associated with baroclinic instability, in which horizontal density gradients tilt the stratified layers, allowing small perturbations to grow and convert potential energy into kinetic eddy energy. This mechanism is particularly important at the interfaces of fronts and during convection events (Marshall and Schott, 1999). In addition, barotropic instability can convert kinetic energy from the mean flow into eddies that propagate through the water column. Where straits are present and dense water flows along the continental slope, eddies are generated by stretching of the water column and the associated increase in potential vorticity (Spall and Price, 1998).

At the mesoscale, eddies can be associated with the process of convection. In this case, strong vertical and horizontal density gradients in convective areas lead to baroclinic instabilities, and the resulting eddies play a key role in the lateral exchange of water masses and restratification of the water column (Marshall and Schott, 1999). Mesoscale eddies

can also be associated with boundary currents, again through baroclinic instability. These currents generate strong horizontal density gradients that provide the potential energy necessary for eddy formation. Boundary currents and the eddies they generate are crucial for the transport of heat, salt, and nutrients.

On smaller scales, submesoscale eddies form through processes such as frontogenesis and baroclinic instabilities in the mixed layer. Frontogenesis refers to the intensification of horizontal density gradients, typically driven by mesoscale straining. This intensification disturbs the geostrophic balance and generates a secondary ageostrophic circulation, which tilts the isopycnals back towards the horizontal and generates vertical motions. The combination of horizontal straining and vertical motions leads to coherent vortices along fronts and filaments. Along with baroclinic instabilities in the mixing layer, these mechanisms supply energy to the submesoscale range, strongly influencing turbulence in the upper ocean and contributing to rapid restratification of the mixed layer (Lapeyre et al., 2006; Capet et al., 2008; Taylor and Thompson, 2023).

In the Adriatic, eddies have been observed throughout the basin, including the southern Adriatic (Bensi et al., 2013; Hariri, 2020). They have also been studied in the Gulf of Taranto (Ursella et al., 2011; Trotta et al., 2017). Generally, eddies form in the cores of gyres in the southern, middle, and northern Adriatic and slow down the movement of particles within the basin (Hariri, 2020). In the Adriatic Sea, eddies are also generated by boundary currents along the eastern (EAC) and western (WAC) flanks of the basin, which are influenced by strong inflows from the Ionian Sea and Po River discharge (Hariri, 2020). The Strait of Otranto is also an important site of eddy formation, where eddies contribute to the exchange between the shelf and the open sea and play a role in the outflow of AdDW through entrainment processes (Ursella et al., 2011). Overall, the interplay between baroclinic instability generated in convective patches or frontal areas, topographic control of the pit, and exchange dynamics at the Strait of Otranto makes the South Adriatic a natural laboratory for the study of eddy generation across scales.

The characteristics of the eddies also vary along the basin margins. Along the Italian coast, periodic meanders and eddies are observed, developing more strongly during calm periods, which indicates baroclinic instability in a relatively undisturbed form. In contrast, the Croatian coast is dominated by jets and filaments with varying speed and penetration, but whose locations are relatively fixed. Simulations confirm this contrast and show a predominance of jets and cold filaments on the Croatian side and of meanders and eddies on the Italian side, both accompanied by well-defined fronts (Cushman-Roisin et al., 2007). In the northern Adriatic, the inflow of freshwater creates a frontal zone that leads to baroclinic instability and the formation of filaments and eddies (Korotenko, 2007).

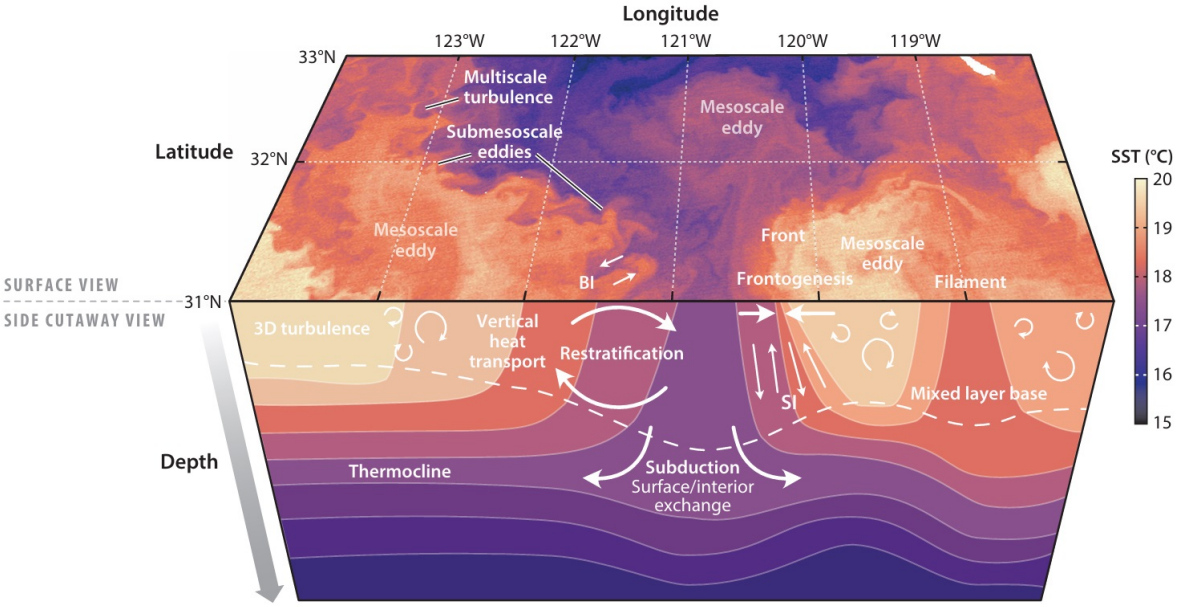

Figure 9: From Taylor and Thompson (2023), Sea surface temperature (SST) from satellite measurements on the western coast of the United States of America. Hypothetical temperature contours illustrate various processes, including submesoscale baroclinic instability and symmetric instability.

Part I

Post-processing of observations

EMSO-ERIC E2M3A mooring

The E2M3A mooring is part of the European Multidisciplinary Seafloor and Water Column Observatory – European Research Infrastructure Consortium (EMSO-ERIC) network (`https://emso.eu/`). This infrastructure brings together multidisciplinary marine research institutes to observe and understand oceanic processes and their impact on the Earth system. EMSO-ERIC consists of 14 observatories and provides long-term, high-quality data to a wide range of users, including scientists, industry, institutions, and policy makers. The network addresses important marine challenges such as climate variability, ecosystem protection, and geohazards.

The EMSO-ERIC E2M3A Regional Facility (referred to as E2M3A hereafter) ([1]) is located in the centre of the SAP, a key site for deep convection processes (section 0.3.1). It is the only observatory of its kind in the Adriatic Sea and provides the longest continuous time series of thermohaline variables with hourly temporal resolution (since 2006). The regional facility consists of two complementary mooring lines (E2M3A-B and E2M3A-M) used to observe physical and biogeochemical processes at the surface, in the subsurface, intermediate and in deep layers. Together, the mooring lines provide a complete overview of the coupled atmosphere-ocean system in the SAP. Furthermore, instruments on these mooring lines provide continuous, high-frequency observations of physical and biogeochemical processes, which are crucial for understanding physical dynamics in the SAP. The first mooring line (or E2M3A-B) is designed to observe air-sea interactions in the upper layer of the water column with a surface buoy equipped with a meteorological station, radiometers, and sensors for temperature, salinity, oxygen, pCO_2, and pH, with data transmitted in real time. The second mooring line (E2M3A-M) is a deep mooring line designed to monitor the physical variability of the water column from the surface to the deepest layers (fig. I-Intro.1). It consists of a series of sensors distributed throughout the water column from the surface to the seabed, which are listed below:

- Eight CTD (Conductivity Temperature Depth) SBE37-ODO and one CTD SBE37 strategically placed at approximately 150, 350, 450, 550, 750, 900, 1000, 1100, and 1200 dbar, providing high-resolution measurements of temperature, salinity, and dissolved oxygen. These instruments enable the monitoring of the thermohaline variability of the water masses in the SAP. In particular, they allow observation of the LIW (usually between 300 dbar and 600 dbar) and the inflow of the NAdDW (from 700 dbar to the bottom of the SAP).

- Three ADCPs (Acoustic Doppler Current Profilers) are deployed: an upward-looking RDI WHS 150 kHz and two downward-looking Nortek (Signature 55 kHz and Signature 100 kHz), which provide measurements of the three velocity components (u,

[1] `https://www.ogs.it/it/european-multidisciplinary-seafloor-and-water-column-observatory-emso-eric`

v, w) throughout the water column. These instruments are particularly valuable for tracking the movement of water masses, including the inflow of NAdDW into the deep layers, and for detecting convection events, indicated by strong vertical downward velocities.

- An Aanderaa current meter SEAGUARD RCM, located near the bottom, is used to measure the horizontal velocity components (u, v) in the deep layer. This instrument is particularly valuable because the velocities measured by the ADCP near the bottom are noisy, and information about the velocities there is essential to clearly assess the penetration of NAdDW into the deep SAP.

- Two PPS sediment traps, placed at about 130 and 1100 dbar, are used to collect sinking particles. The upper sediment trap targets particles influenced by surface processes, while the deep sediment trap monitors the sinking of particles in the deep SAP. Both sediment traps quantify the vertical particle fluxes and provide information on the transport of organic and inorganic material, as well as the influence of water mass dynamics.

- A ProOceanus CO2-PRO CV pCO_2 sensor is installed at about 1100 dbar to monitor carbon dynamics in the deep sea. It allows assessment of carbon variability associated with deep water masses, including the inflow of NAdDW, and provides insights into processes such as carbon sequestration, remineralisation of sinking organic matter, and the overall biogeochemical cycle in the deep layers of the water column.

The mooring line instruments are retrieved at regular intervals (typically one year) during maintenance cruises, which also include conducting CTD casts and collecting water samples (fig. I-Intro.2). These activities are used to validate and assess the quality of the data recorded by the moored sensors. In addition, the CTD profiles provide observations with higher vertical resolution, enabling detailed investigation of the temporal development of the water masses in the SAP.

Work on board the ship also includes direct comparisons between the time series recorded by the recovered instruments and the CTD casts. These comparisons are important for detecting possible instrument malfunctions that could lead to greater discrepancies if the decision was made to redeploy the instrument. Whenever CTD cast measurements from the previous recovery are available, they are used to estimate the offsets and drifts of the different time series, to gain insight into the evolution of instrument performance over time and to allow comparison with previous time series.

Another important part of the validation process is the comparison of all CTDs deployed along the mooring line with a reference CTD instrument. For this purpose, the instruments are deployed together in the rosette at an intermediate depth of approximately 250 m for several hours. This arrangement allows direct assessment of the behaviour of the instruments compared to the reference CTD instrument, and ensures that any offsets can be accurately quantified. During this procedure, water samples are also collected for salinity measurements and Winkler titration, to further improve the comparison between the instruments through independent chemical analyses.

This comprehensive approach provides a robust method for detecting instruments that have accumulated offsets or drifts over time. It enables the identification of instruments that need to be recalibrated, ensuring the reliability, accuracy, and consistency of long-term time series measurements at the mooring line.

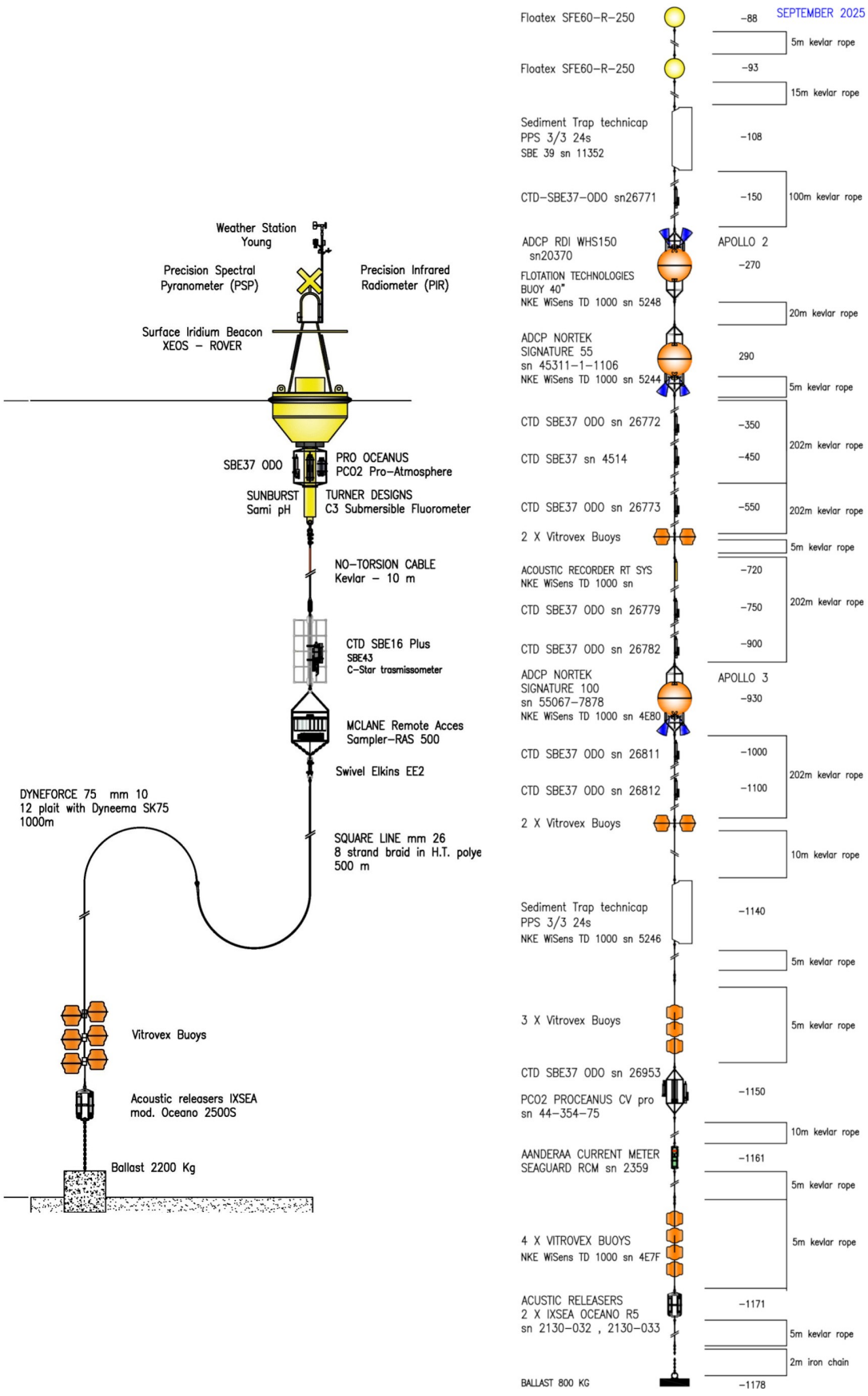

Figure I-Intro.1: E2M3A-B meteorological (left) and E2M3A-M deep (right) mooring lines.

(a) (b) (c)

Figure I-Intro.2: Work on the ship during maintenance cruises. **a**, Preparation of the mooring CTDs (on the table) before redeploying the deep mooring line. **b**, A rosette with Niskin bottles (long grey plastic cylinders) is used to collect water samples at the desired depths, together with a high-accuracy CTD SBE911 to obtain vertical profiles of the thermohaline and biogeochemical properties of the water masses along the water column. **c**, Collection of a water sample from a Niskin bottle to determine the salinity at a specific depth by chemical analysis.

Chapter 1

Quality control of EMSO-ERIC E2M3A mooring data

1.1 Statistical quality control of CTD data

To ensure reliable measurements, the data are subjected to quality control procedures such as physical range checks, despiking, and rate of change test. Physical range checks flag values outside physically realistic limits, while despiking removes isolated peaks caused by noise or interference, and rate of change test identify rapid, unrealistic fluctuations between successive measurements. These steps help to ensure that the dataset accurately reflects the physical variability of the water column.

1.1.1 Physical range

The aim of the physical range test is to identify and remove outliers in the temperature, salinity, and dissolved oxygen measurements. These thresholds are based on regional studies of water mass properties in the Adriatic Sea (Cardin et al., 2014b). To account for natural variability, two sets of thresholds are applied depending on the depth layer, as shown in tables 1.1 and 1.2:

Variable	**Minimum**	**Maximum**
Potential temperature (°C)	8	32
Salinity	36	39.5
Dissolved oxygen ($mL\,L^{-1}$)	3	9

Table 1.1: Outlier thresholds for the different variables for the upper layer (>-150 m)

Variable	Minimum	Maximum
Potential temperature (°C)	10	16
Salinity	36	39
Dissolved oxygen (mL L^{-1})	3	8

Table 1.2: Outlier thresholds for the different variables for the intermediate and deepest layers (<-150 m)

It should be noted that these thresholds may need revision in the future due to ongoing oceanographic changes in the southern Adriatic. For example, the threshold for maximum salinity in the upper layer has been adjusted to 39.5 to account for the observed increase in salinity over the past 15 years.

1.1.2 Despiking

As with the physical range tests, a distinction is also made in despiking between the upper layer (depth lower than 150 m) and the intermediate to deep layers (depth greater than 150 m). To despike the time series, test value threshold coefficients (TV) are considered for each variable to identify anomalous spikes in the data time series (tables 1.3 and 1.4).

Despiking is a crucial step in dataset quality control, as it removes isolated, non-physical anomalies - often caused by sensor malfunction, electronic noise, or transmission errors - that can significantly affect statistical analyses and lead to incorrect interpretations. In oceanographic time series, these spikes do not represent actual environmental variability and can artificially amplify gradients or introduce biases in derived parameters such as density. By identifying and removing these artefacts, despiking improves data reliability and ensures that subsequent analyses reflect actual physical oceanographic processes.

Variable	Limit
Potential temperature (°C)	6
Salinity	0.9
Dissolved oxygen (mL L^{-1})	N/A

Table 1.3: TV thresholds coefficients for the different variables for the upper layer (lower than 150 m). N/A stands fo No data Available at the present time as no dissolved oxygen sensor was present at 150 dbar during the period considered.

Variable	Limit
Potential temperature (°C)	2
Salinity	0.3
Dissolved oxygen (mL L^{-1})	0.5

Table 1.4: TV thresholds coefficients for the different variables for the intermediate and deepest layers (greater than 150 m)

The test is done considering the following equation:

$$\frac{|X(k) - (X(k-1) + X(k+1))|}{2} - \frac{|X(k+1) - X(k-1)|}{2} \geq TV(X) \tag{1.1}$$

This test detects values that deviate significantly from the local mean, adjusted over neighbouring time steps. It is particularly useful for identifying isolated spikes that do not match the natural variability of the SAP.

1.1.3 Rate of change

Temporal changes in thermohaline variables and dissolved oxygen were assessed and significant anomalies were detected using the following criterion:

$$|X_i - X_{i-1}| + |X_i - X_{i-1}| \leq \epsilon \tag{1.2}$$

where the threshold ϵ is defined as $2(2\sigma_X)$ when both X_{i-1} and X_{i+1} are available, and $2\sigma_X$ otherwise. σ_X is the standard deviation of the variable X derived over the entire time series after applying the physical range test, despiking, and the second quality control procedure, including the correction of offsets and trends (section 1.2).

This approach enables the detection of abrupt, non-physical fluctuations in the data that deviate significantly from the expected variability, thereby improving the robustness of the quality control process.

1.2 CTD casts-based quality control for offset and trend correction

An important part of the post-processing of the mooring data was based on CTD casts taken during cruises. Most of these CTDs were conducted directly at the E2M3A mooring site, while some others took place at a maximum distance of 10 km from E2M3A site. These CTD measurements were carried out in a smaller area than that proposed by Cardin et al. (2020b) to ensure maximum consistency in the correction of the different time series. The cruises included in this study are listed in table 1.5. All CTD cast measurements were subjected to a systematic correction procedure that included the following steps:

- Removal of initial readings before pump stabilisation to exclude unreliable early data
- Correction of the oxygen sensor hysteresis and response time (τ)
- Application of the "wildedit" filter to remove spikes and anomalies
- Filtering based on pressure values to exclude erroneous measurements
- Loop editing to identify and define the minimum speed during profiling
- Adjustment of CTD sensor data for consistency
- Correction for thermal mass effects of the cells
- Bin averaging to standardise the data in 1 meter intervals

The most favourable situation for correcting the time series occurs when CTD cast measurements are available both immediately after the initial recovery and redeployment of the mooring instruments, and again at the next recovery and redeployment. The CTD profiles at these two key moments provide reliable reference points to detect and correct any sensor drift, bias, or offsets that may have accumulated during the deployment period, ensuring greater consistency and accuracy in the corrected time series.

Table 1.5: List of oceanographic cruises near the E2M3A site used for the CTD casts-based quality control.

Cruise	**Station**	**Latitude**	**Longitude**	**Date**	**Distance from E2M3A (km)**
Vector AM1	AM1	41.83545	17.74458	2006-11-19	0.477
Vector AM4	AM1	41.834	17.75033	2007-09-15	0.06
SESAME IT1	A16	41.8202	17.7082	2008-02-23	3.757
IT7	16	41.9804	17.9317	2008-10-10	12.8
MSM132	864	41.78316	17.70066	2009-10-13	6.88
MSM154	654	41.56258	18.19684	2010-07-10	10.802
POS414	345	41.56682	18.08362	2011-06-04	4.53
ADREX-1	001_E2M3A	41.53279	18.08582	2013-03-23	0.22
MATIS-RITMARE-02	E2M3A_M	41.53051	18.09044	2013-11-25	At E2M3A
SIRIAD-14	E2M3A	–	–	2014-03-08	At E2M3A
FIX03-RIT03	E2M3A	41.53201	18.07332	2014-09-10	At E2M3A
ADREX-2014-SED	064_E2M3A	41.52604	18.05104	2014-10-20	At E2M3A
FIX03-RIT04	VAM1	41.55322	18.0296	2015-03-22	At E2M3A
FIX03-RIT05	VAM1_BIS	41.52516	18.06808	2015-11-02	At E2M3A
SIRIAD16	E2M3A_CTD_2	41.5225	18.0712	2016-04-06	At E2M3A
Vector AM2	AM1	41.8292	17.7435	2007-02-22	0.042
TRASF TO MESSINA	E2M3A_BUOY	41.52296	18.08462	2017-03-22	At E2M3A
Vector AM3	AM1	41.838	17.7468	2007-04-15	0.545
POS514	ST-11	41.4996	18.06722	2017-05-31	3.997
FIX03-RIT07	001_E2M3A	41.51802	18.08452	2017-07-26	At E2M3A
FIX03-RIT08	E2M3A_006	41.53364	18.05364	2018-10-08	At E2M3A
MAINTENANCE BOA MARS 2019	E2M3A_0319	41.5158	18.08428	2019-03-24	At E2M3A
FIX03-RIT09	001_MOORING_E2M3A	41.54493	18.05932	2019-10-19	At E2M3A
FIX03_EMSO11	E2M3A	41.5249	18.08076	2022-10-30	At E2M3A
FIX03-12	E2M3A	41.56312	18.06437	2023-06-27	At E2M3A
Maintenance	E2M3A	–	–	2023-12-05	At E2M3A
EMSO-SA24	VAM1_E2M3A	41.5392	18.06976	2024-10-31	At E2M3A

1.2.1 Offset correction

Malfunctions of instruments can lead to deviations from the true environmental values, introducing systematic offsets in the recorded time series. To correct these deviations, CTD cast measurements taken at a maximum distance of 10 km from the mooring site were used as a reference, as they offer higher accuracy and higher vertical resolution. These reference measurements were collected during the research cruises listed in table 1.5. In addition, long-term trends in the time series were considered to ensure that all identified offsets are consistent with the known hydrographic variability of the SAP. As an example of the methodology, the time series of salinity at 1200 dbar for the year 2014/2015 is shown below.

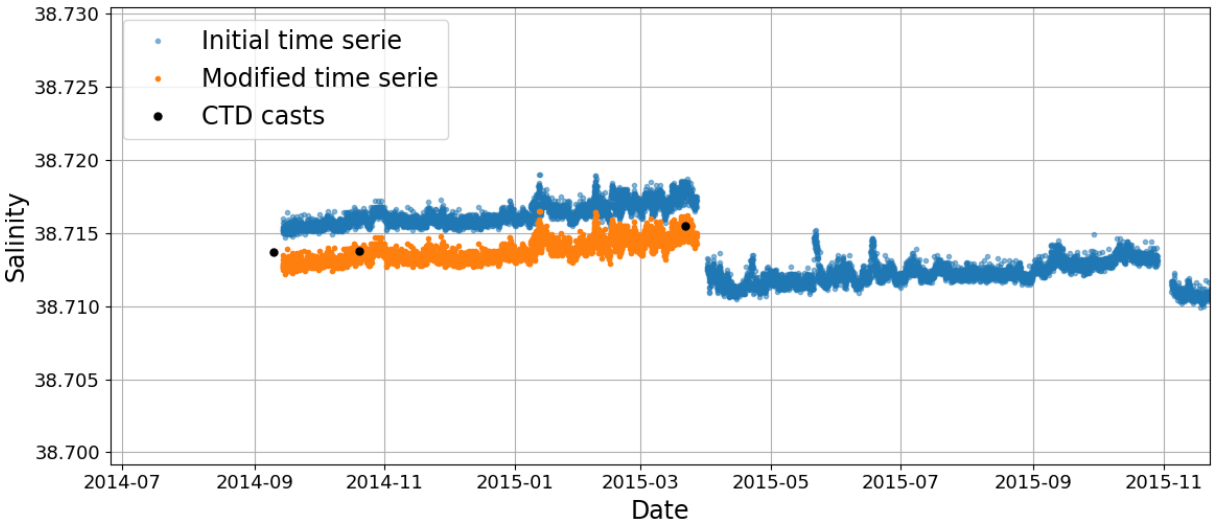

Figure 1.1: Example of offset correction - Salinity 2014/2015 at 1200 dbar

1.2.2 Trend correction

Offset correction alone is insufficient to fully correct the different time series, especially when long-term sensor drift or external influences such as biofouling or mechanical stress have affected the instruments' performance. It was therefore necessary to correct the instrumental drift while preserving the underlying environmental signal, such as the long-term increase in temperature and salinity observed in the SAP. For this purpose, high-accuracy CTD cast measurements were again used as reference points, both locally (within subsets of the time series) and globally (over the entire time series), to check and constrain the physical consistency of the applied corrections.

1.3 Correction of dissolved oxygen data

The dissolved oxygen data correction required special attention, as considerable discrepancies in the time series were found when compared with discrete dissolved oxygen measurements obtained using the Winkler titration method (differences sometimes exceeding 20 µmol L^{-1}). In particular, anomalously high values often appeared at the beginning of the time series subsets, deviating from the general trend of the subsets. In addition, as with temperature and salinity, offsets and drifts were corrected using Winkler-analysed

samples. The Winkler titration method used for the correction is a widely recognised and highly accurate technique for determining the concentration of dissolved oxygen by chemical fixation and titration, and is commonly used as a reference for validating sensor-based measurements. Winkler-analysed samples used in this thesis are presented in table 1.6.

Table 1.6: Dates and names of cruises where Winkler dissolved oxygen samples were collected

Cruise	**Date**
Medges	2013-03-23 08:11:00
Matis_24/11	2013-11-24 00:00:00
Matis_25/11	2013-11-25 00:00:00
Adrex_2014	2014-10-20 10:08:00
BADU3_2015	2015-03-26 18:05:00
Fix03-RIT07	2017-07-29 14:33:00
Fix03-RIT08	2018-10-08 04:54:46
Fix03-RIT09	2019-10-19 00:00:00
EMSOSA_24_31/10_Sample_1	2024-10-31 12:00:00
EMSOSA_24_31/10_Sample_2	2024-10-31 12:00:00
EMSOSA_24_04/11_Sample_1	2024-11-04 12:00:00
EMSOSA_24_04/11_Sample_2	2024-11-04 12:00:00
EMSOSA_24_04/11_Sample_3	2024-11-04 12:00:00

1.3.1 Adaptation time of dissolved oxygen data

The large drop observed at the beginning of the subsets of the dissolved oxygen time series corresponded to the adaptation time of the sensor, which could differ from one subset to another, as different dissolved oxygen sensors were used for the different layers of the pit investigated at E2M3A. Three methods for the correction were considered: using the standard deviation of the subset, applying a threshold to the dissolved oxygen gradient, and using an exponential decay model. The last method gave the best results. The model used is presented below:

$$\mathrm{Ox}_{\mathrm{norm}}(t) = A_1 e^{-k_1 t} + A_2 e^{-k_2 t} + C \tag{1.3}$$

where:

- t: time in seconds since the start of the observation.
- A_1, A_2: amplitudes of the exponential components.
- k_1, k_2: decay rates.
- C: offset constant (residual or asymptotic concentration).

The model is fitted to the data using nonlinear least squares, and the adaptation time associated with the faster component is given by:

$$t_{\text{adapt}} = -\frac{\ln(0.1)}{k_1} \tag{1.4}$$

This corresponds to the time at which the first exponential term decays to 10% of its initial value.

If the curve fitting fails or produces unreasonable results, the adaptation time is assigned a default value:

$$t_{\text{adapt}} = \begin{cases} \frac{86400}{2}, & \text{if fit fails} \\ \frac{86400}{2}, & \text{if } t_{\text{adapt}} > 10 \times 86400 \text{ or } t_{\text{adapt}} < 0 \\ t_{\text{adapt}}, & \text{otherwise} \end{cases} \tag{1.5}$$

An example of the result of this test is provided below:

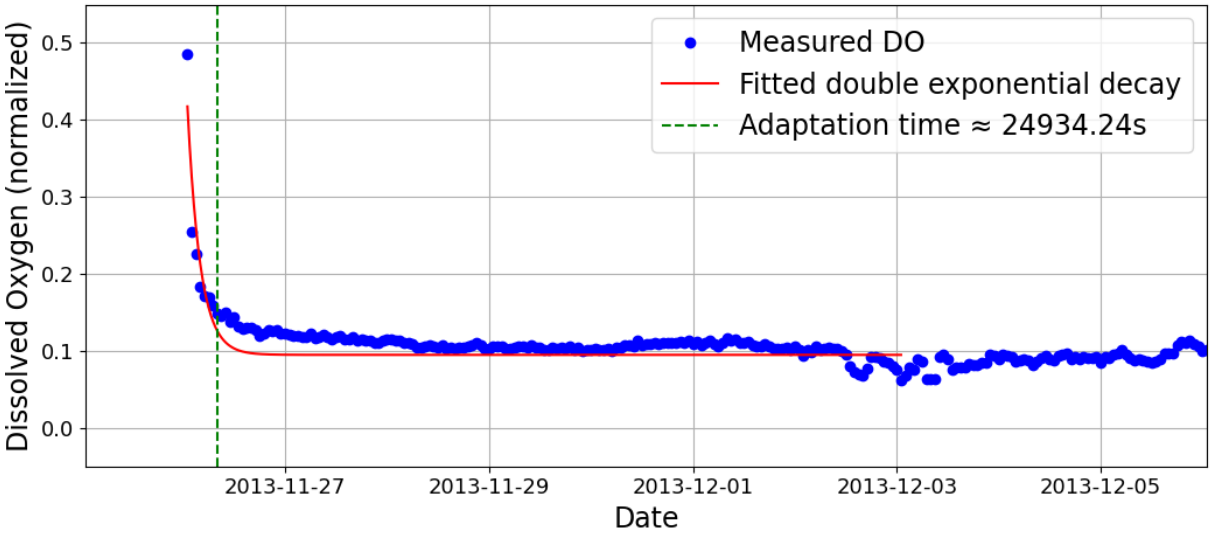

Figure 1.2: Example of adaptation time determination - 2013/2014 at 1200 dbar

1.3.2 Offset correction

The dissolved oxygen measurements were corrected for systematic offsets using a methodology similar to that used for temperature and salinity. Instead of the CTD casts, Winkler titration samples were used as a reference, as these ones provide higher accuracy for dissolved oxygen. Physical processes observed in the SAP, such as deep convection events that typically cause an abrupt increase in dissolved oxygen concentration, were also taken into account. In addition, the long-term evolution of dissolved oxygen in the deep SAP is characterised by alternating phases of rapid ventilation followed by gradual depletion (Querin et al., 2016), which was accounted for in the correction. An example of the applied offset correction is shown in fig. 1.3.

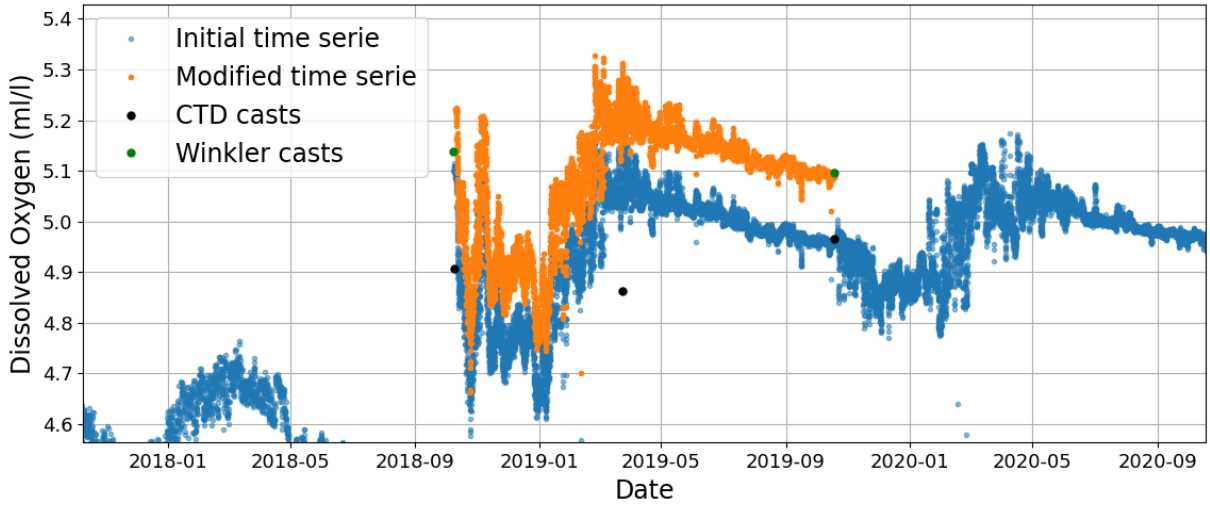

Figure 1.3: Example of offset correction for dissolved oxygen measurements - 2018/2019 at 350 dbar

1.3.3 Trend correction

The long-term sensor drift in the dissolved oxygen data was treated with a similar trend correction procedure as for temperature and salinity. In this case, Winkler titration samples were used as reference values rather than the CTD casts. This correction aims to remove instrumental drift while maintaining the natural environmental trend. An illustrative example of this correction is shown in fig. 1.4.

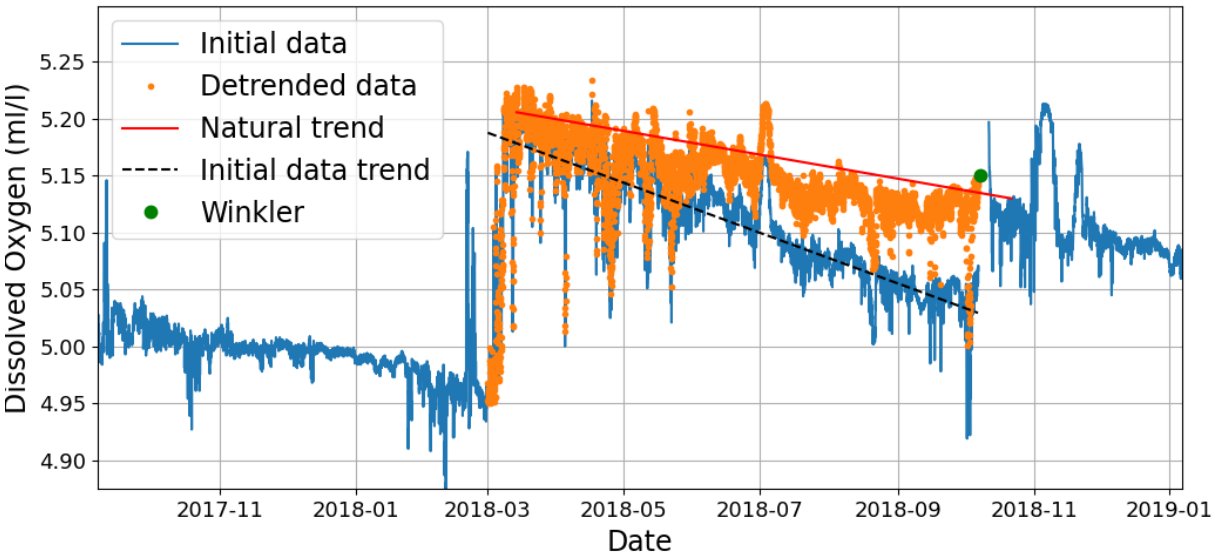

Figure 1.4: Example of trend correction - 2017/2018 at 750 dbar

1.4 Interpolation

Small gaps in the time series were filled by interpolation if this did not introduce significant bias. Only gaps of six hours or less were considered for interpolation. However, in subsets

of the time series with an original temporal resolution of three hours, no interpolation was performed, as this would have resulted in approximately 66% of the values being artificially generated, compromising the integrity of the dataset.

Part II

Climate change observation at a basin scale

Overview of the variability in the water masses of the SAP during the period 2006-2023

This introductory chapter provides an overview of the physical dynamics of the water masses in the SAP between 2006 and 2023, focusing on the identification of long-term trends and short-term fluctuations in the different layers of the water column. The analyses are based on time series of potential temperature, salinity, and dissolved oxygen recorded by the mooring (E2M3A-M). Both the qualitative review of the measurement data (see fig. II-Intro.1) and the quantitative trend analysis (see table II-Intro.1) show that these properties have increased over time at most depths during the analysed period. The only exception is for dissolved oxygen at 900 dbar, for which only three months of data were available, which coincides with a period of oxygen consumption and is therefore not representative of a long-term trend.

As shown in figs. II-Intro.1 and II-Intro.2, the potential temperature gradually decreases with depth, from a maximum of about 15.6 °C in the upper layer (150 dbar) to about 13.95 °C in the deepest layer (1200 dbar). In contrast, the potential density anomaly (PDA, defined as potential density minus 1000 $\mathrm{kg\,m^{-3}}$) increases with depth, as expected (see fig. II-Intro.3). Salinity displays a different vertical pattern: the upper layer has the highest median values (about 38.95), the intermediate to deep layers between 350 and 900 dbar are characterised by relatively similar medians (about 38.8), while the deepest layers at 1000 and 1200 dbar have the lowest medians (about 38.73). Dissolved oxygen exhibits a different distribution, with median values higher at 350 and 750 dbar than at 1200 dbar. This indicates different dynamics in the various layers. Taken together, these observations indicate that the water column in the SAP can be divided into three zones: an upper layer, an intermediate layer, and a deep layer. The first two are more directly affected by the mixing triggered by open-ocean convection (air-sea interaction) events and the influence of the ISW and the LIW, while the deepest waters are much more isolated and are not ventilated through mixing triggered by open-ocean convection events.

Layer (dbar)	Potential temperature trend ($^{\circ}C\,yr^{-1}$)	Salinity trend (yr^{-1})	Dissolved oxygen trend ($mL\,L^{-1}\,yr^{-1}$)	PDA ($kg\,m^{-3}\,yr^{-1}$)
150	0.0426	0.0298	**ND**	0.0136
350	0.0541	0.0140	0.0129	-0.0009
550	0.0526	0.0125	**ND**	-0.0017
750	0.0570	0.0129	0.0180	-0.0022
900	0.0691	0.0182	-0.1633	-0.0007
1000	0.0480	0.0081	0.0044	-0.0039
1200	0.0460	0.0077	0.0313	-0.0037

Table II-Intro.1: Trends of potential temperature, salinity, dissolved oxygen, and potential density anomaly for the considered layers at the mooring E2M3A. The values shown represent linear trends estimated over the full observation period. **ND** stands for No Data, and an orange cell indicates a trend derived from less than two years of data.

Within the three-layer structure, long-term trends vary with depth. The strongest warming occurs in the intermediate layers (350 to 750 dbar) and at 900 dbar, where trends range from 0.0526 to 0.0691 $^{\circ}C\,yr^{-1}$. Conversely, the deepest layers, at 1000 and 1200 dbar, warm more slowly, by 0.0480 and 0.0460 $^{\circ}C\,yr^{-1}$, respectively (table II-Intro.1 and fig. II-Intro.1; fig. A.1 to A.7). A similar pattern is observed for salinity, except that the upper layer shows the highest rate of increase (0.0298 yr^{-1}), exceeding that of the intermediate layers. However, the PDA trends are reversed: the deepest layers show the largest decreases, with rates ranging from -0.0037 to -0.0039 $kg\,m^{-3}\,yr^{-1}$. Taken together, these results reveal that, although a three-layer structure can be identified, the different behaviour between the upper/intermediate layers and the deepest layers is more similar to a two-layer system. This interpretation is consistent with previous studies, which indicate the deep SAP is only weakly influenced by convection, lacks direct ISW or LIW signals, and is constrained by local bathymetry (section 0.3.1; Gačić et al. (2002); Cardin et al. (2011); Bensi et al. (2014)). Trends of dissolved oxygen show that, although the deepest layers of the SAP appear isolated, this is not the case. At 1200 dbar, dissolved oxygen concentrations increase almost twice as fast as at 350 and 750 dbar. The trends at 900 and 1000 dbar remain uncertain due to limited data availability of less than 2 years. This amplified increase can be explained by three major ventilation events that occurred between 2014 and 2023, driven by the inflow of NAdDW via gravity currents (chapter 3). These inflows were strong enough to temporarily offset the declining dissolved oxygen concentrations otherwise caused by biological consumption (fig. II-Intro.1).

Figure II-Intro.1: Time series of potential temperature, salinity and dissolved oxygen at E2M3A from 2006 to 2023. The time series exhibit an overall increase in potential temperature and salinity. Shorter time-scale fluctuations are observed, linked to physical processes occurring from basin scale to microscale (such as convection (section 0.3.1), gravity currents (chapter 3), and double diffusion (chapter 4)).

Further insights are provided by Temperature/Salinity (T/S) diagrams, in which seawater temperature is plotted against salinity, and which are used to characterise water masses and their mixing based on density (fig. II-Intro.2). These results show that the dispersion of salinity values is narrowest in the deepest layers, while the interval between 150 and 750 dbar is characterised by greater variability, corresponding to the influence of ISW and LIW. The violin plots (fig. II-Intro.3) confirm this observation. In contrast, the dispersion of temperature values in the different layers appears similar, although stronger fluctuations occur in the upper and intermediate layers. This is consistent with the flank depth of the SAP, which is about 780 m, and exposes these layers to greater dynamic variability (fig. II-Intro.3 and fig. A.1 to fig. A.7). The T/S diagrams also reveal that the SAP waters have gained *"spiciness"*, a property that combines a simultaneous increase in temperature and salinity, suggesting that the SAP is dynamically active and responding to the ongoing effects of climate change.

These long-term signals are superimposed on shorter-term fluctuations related to processes occurring at different scales. At the microscale, double diffusion and salt fingering play a role (chapter 4); at the submesoscale, convection and gravity currents are important (section 0.3.1 and chapter 3); while variability at the mesoscale arises from broader circulation features. Convection events typically occur between January and March and can extend to about 900 dbar, while the inflow of NAdDW in the SAP usually occurs from March to June (chapter 3; Martellucci et al. (2024)). In 2012, 2017, 2018, and 2022, four large inflow events were identified, each generating large fluctuations associated with pulses of dense water. Their signature is visible in fig. II-Intro.3, where the trimodal distribution of salinity in the deepest layers reflects abrupt changes in thermohaline properties due to NAdDW inflows. In the upper and intermediate layers, the irregular distributions of both potential temperature and salinity confirm their stronger temporal variability.

Finally, trend calculations based on annual mean values provide additional insights (fig. A.8). At 150 dbar, the calculated trends for potential temperature, salinity, and PDA have the largest error bars, reflecting the greater variability caused by the air–sea interactions mentioned above. At greater depths, the uncertainties are more than twice as small, which is related to the fact that the deeper layers are less affected by the variability of the surface layer. For PDA, the uncertainties gradually decrease with increasing depth, illustrating the weaker influence of surface processes on the deepest layers. For dissolved oxygen, the uncertainties are around 0.01 $\mathrm{mL\,L^{-1}}$. These are explained by the alternating occurrence of ventilation events and consumption periods, which create a characteristic *"sawtooth"* pattern in the time series (Querin et al., 2016; Cardin et al., 2020a).

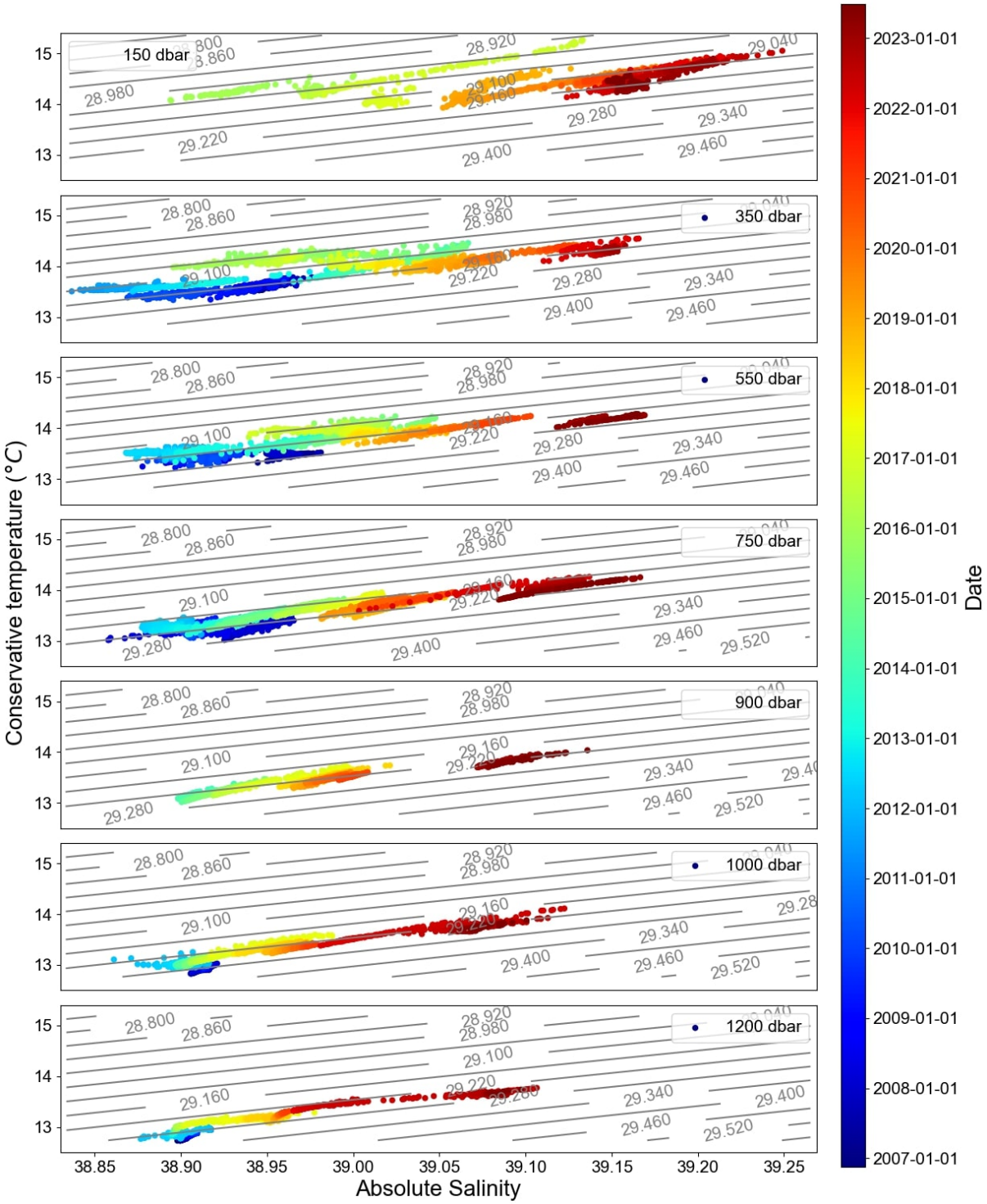

Figure II-Intro.2: T/S plots at all layers in the SAP. It can be observed that the different layers exhibits an increase in spiciness.

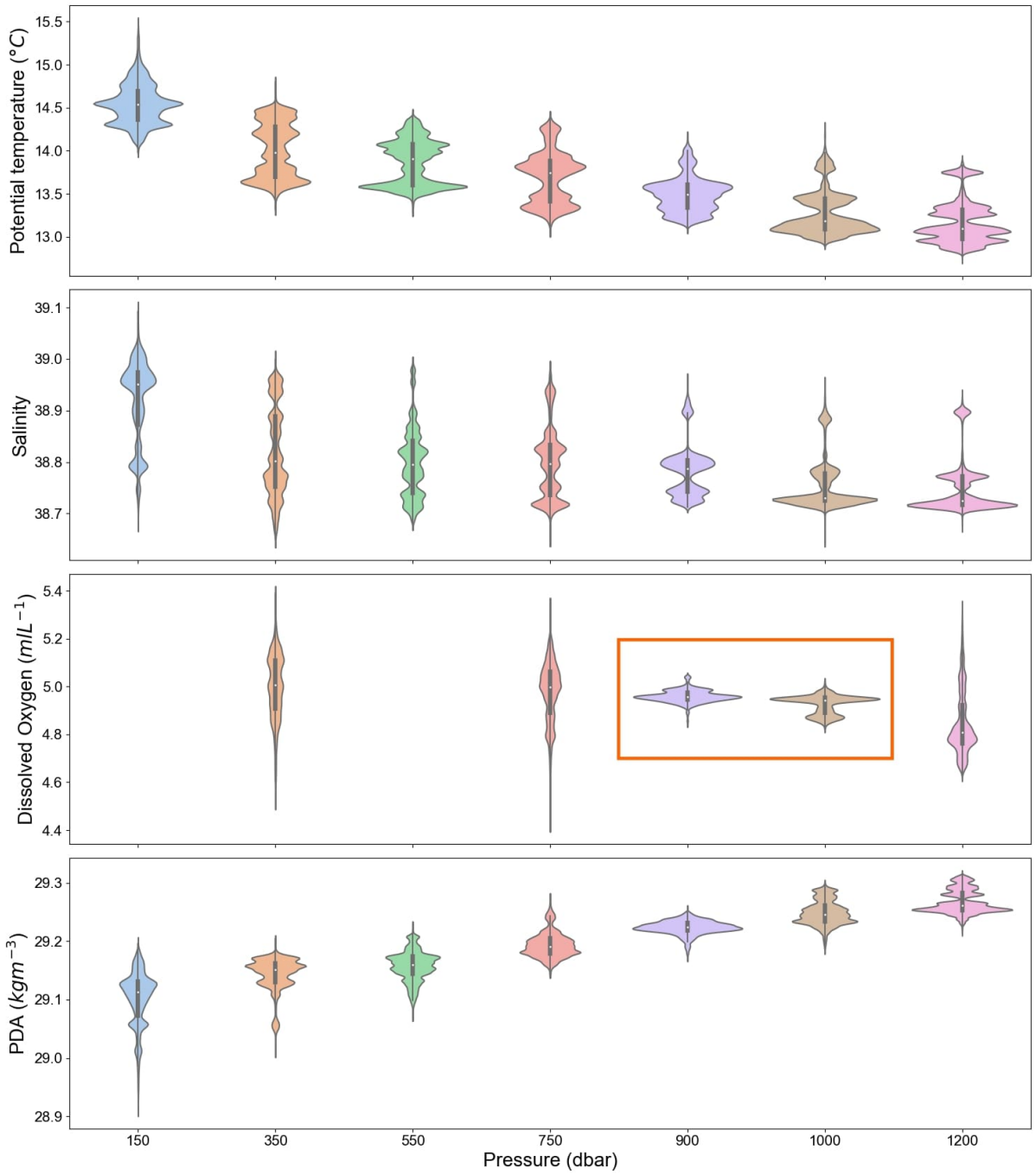

Figure II-Intro.3: Violin plots calculated for the different layers for potential temperature, salinity, dissolved oxygen, and PDA. Distributions in the orange squares represent those with less than two years of data. A system close to two layers is observed, with the first comprising upper and intermediate layers, and the second comprising deep layers.

Chapter 2

The deep Adriatic as a climate change hotspot

This section is constituted by the article published in Limnology and Oceanography Letters in 2025:

Terzić, E., Cardin, V., Le Meur, J., Dunić, N., Vodopivec, M. and Vilibić, I. (2025), Unprecedented warming and salinization observed in the deep Adriatic. Limnol. Oceanogr. Lett. https://doi.org/10.1002/lol2.70051)

Abstract: The deep Southern Adriatic is a Mediterranean region highly sensitive to climate change, influenced by dense water cascading from the northern Adriatic and heat/salt transport from the Eastern Mediterranean. Historical (since 1957) and modern (permanent and opportunistic temperature and salinity sampling, Argo floats, fixed moorings) measurements reveal a substantial change since the mid-2000s in thermohaline properties. Historically marked by steady increases in temperature, salinity, and density, with substantial saw-tooth decadal variability, the near-bottom Southern Adriatic has experienced unprecedented warming (0.8 °C) and salinization (0.2) over the past decade, accelerating in time and reversing density trends. The inflow of much more saline waters reduced stratification and altered dense water properties at its source in the northern Adriatic. This at least fivefold acceleration of the high-emission regional climate projections may have substantial effects on the Adriatic biogeochemistry and living organisms, changing sea level trends and more.

Author Contribution Statement

ET and IV co-led the entire manuscript effort and contributed equally. IV came up with the research questions and designed the study approach. VC, JLM, ND and MV collected and analyzed the E2M3A, D1200 and Vida buoy data, while ET merged these results with analysis of the Argo profiling data. ET prepared all figures, while IV wrote the initial version of the manuscript. All authors reviewed, edited and approved the manuscript.

Scientific Significance Statement

Warming of coastal and semi-enclosed basins is occurring at unprecedented levels, with some regions, such as the Mediterranean Sea, experiencing warming rates higher than the global average. In this study, we documented an additional fivefold increase in warming and a doubling in salinity trends in the deep and near-bottom waters of the Adriatic Sea (the northernmost basin of the Mediterranean) over the past 15 years. As the source region for deep Mediterranean waters, the Adriatic plays a crucial role in driving the basin-wide thermohaline circulation. The observed changes may indicate a rapid transit toward a new climate regime that may impact sea level trends, vertical mixing and transport of oxygen to the deep sea, nutrient consumption and primary production, as well as changing of the whole ecosystem towards species originating from warm and tropical seas.

Data Availability Statement

The Argo profiling float data has been taken from Euro-Argo ERIC at `https://data selection.euro-argo.eu`, ERA5 data has been downloaded from Copernicus Climate Service at `https://doi.org/10.24381/cds.adbb2d47`, while the remaining data is available at the Zenodo repository at `https://zenodo.org/records/13788664` (Terzić et al. (2024)).

2.1 Introduction

The Adriatic Sea, the northernmost Mediterranean basin, spans 800 x 200 km and features (1) a 300 km wide shelf in the North-West with depths reaching up to 80 m, (2) the middle Adriatic depressions of ca. 280 m in maximum, and (3) the 1220-meter deep Southern Adriatic Pit (SAP) in the South-East. The SAP, particularly its regions below 800 meters, is connected to the 5 200-meter deep Ionian Sea through the 800-meter deep Otranto Strait (fig. 2.1). The Adriatic Sea has been monitored for over a century (Artegiani et al., 1997; Vilibić et al., 2023) and serves as an ideal natural laboratory for studying climate change effects due to its rapid response to various forcings (Tanhua et al., 2013). From its river-exposed shelves to its mouth, through which saline Levantine waters flow, the Adriatic exhibits warming and increased salinity over centennial timescales (Lipizer et al., 2014a; Vilibić et al., 2023). However, the Adriatic-Ionian Bimodal Oscillating System (BiOS; Gačić et al. (2010); Civitarese et al. (2023)) can obscure climate change signals by introducing significant decadal variability in thermohaline properties (Mihanović et al., 2015), altering biogeochemical characteristics (Buljan, 1953; Batistić et al., 2014) and impacting fish populations and fisheries (Civitarese et al., 2023).

The BiOS and deep thermohaline circulation in the Adriatic are driven by dense water formation both on the shelf (Orlić et al., 2006; Mihanović et al., 2013) and through open-ocean convection in the SAP (Gačić et al., 2002). North Adriatic Dense Water (NAddW) is generated on the shelf, spreads over the seabed and occasionally (every few to 10 years) cascades to the near-bottom SAP layers (Querin et al., 2016; Pranić et al., 2024), strengthening the stratification and preventing open-ocean convection from reaching the bottom. Open-ocean convection in the Adriatic generates Adriatic Deep Water (AdDW), reaching depths of up to 900 meters (Cardin et al., 2011; Vilibić et al., 2023), that—combined with NAdDW outflow along the continental shelf—flows into the

Ionian Sea. Oppositely, saline Levantine Intermediate Waters (LIW) is advected into the Adriatic at intermediate depths (50-500 meters; Vilibić and Orlić (2002)). The inflow of warmer, saltier waters at these depths promotes diffusive convection and salt-fingering processes in the SAP. Along with open-ocean convection, these processes transport salt and heat toward the bottom (Amorim et al., 2024) and may contribute to changes in near-bottom SAP thermohaline properties even more than dense water cascading and open-ocean convection (Cardin et al., 2020b).

Climate change, marked by warming and salinity increases across the Mediterranean (Kassis and Korres, 2020; Skliris et al., 2025), significantly affects the Adriatic's thermohaline dynamics. Sea surface warming has been measured at 0.4 to 0.6 °C per decade since the 1970s (Reiners et al., 2024), especially in summer and coastal zones (Amos et al., 2017), though the Atlantic Multidecadal Oscillation explains half of this (Macias et al., 2013). Positive salinity trends have accelerated since 2017 (Amorim et al., 2024), influencing NAddW formation (Tojčić et al., 2023). Notably, despite temperature and salinity increases, NAddW density remained stable between 2012 and 2020 (Paladini de Mendoza et al., 2023), but LIW density has risen, reducing SAP stratification and enhancing mixing. These deep ocean changes prompt questions about whether the 'new state of the deep Adriatic' is permanent and linked to climate change or part of decadal variability. Using long-term (since 1957) multi-platform measurements in the SAP, we aim to quantify these changes and assess potential shifts in deep and near-bottom thermohaline properties.

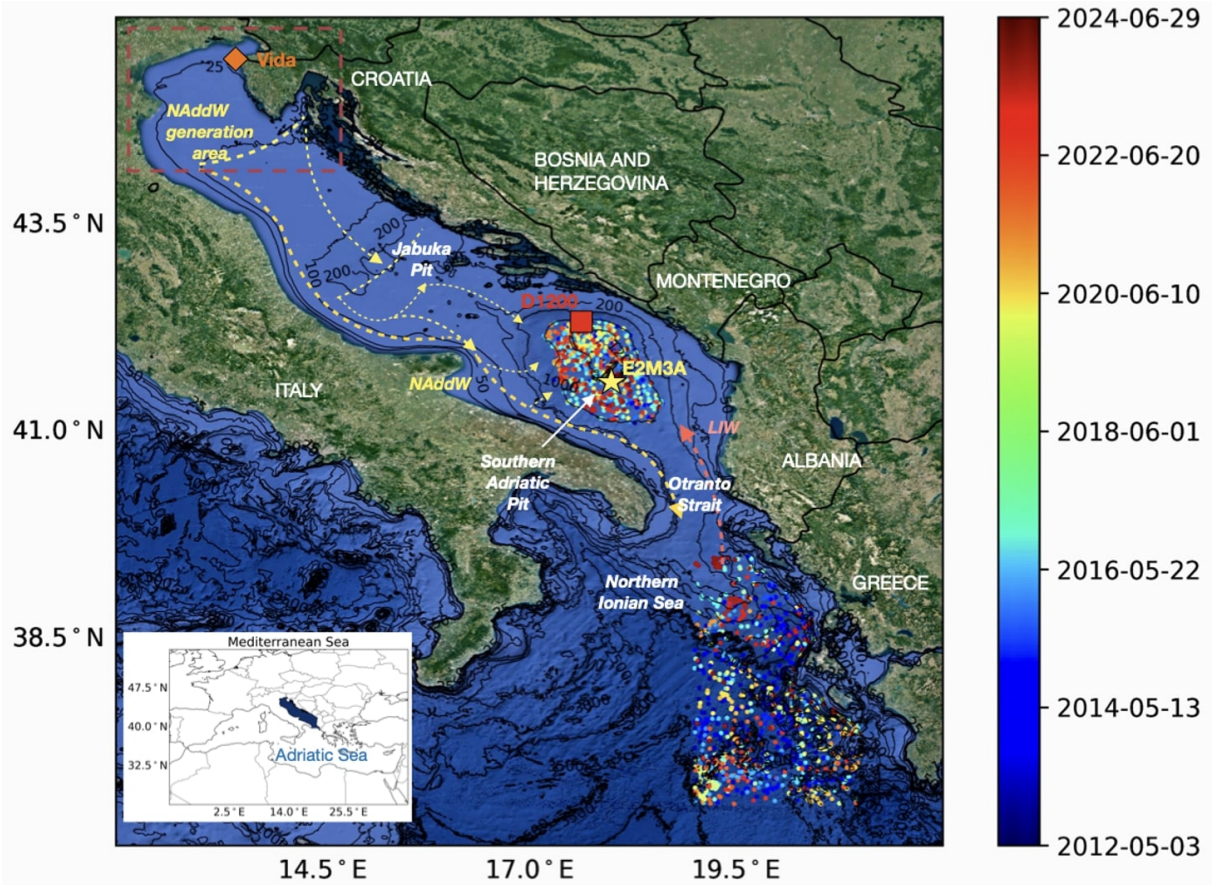

Figure 2.1: The Adriatic and northern Ionian Sea bathymetry with locations of the SAP and northeastern Ionian Sea Argo profiles (circles, time of sampling is color-coded), EMSO-E2M3A deep observatory (yellow star), station D1200 (red rectangle) and buoy Vida (orange diamond). The generation area and pathways of North Adriatic Dense Water (NAddW) are indicated. Red dashed rectangle denotes the northern Adriatic shelf over which ERA5 turbulent heat fluxes were averaged.

2.2 Materials and Methods

The temperature and salinity dataset was obtained through various Eulerian and Lagrangian platforms, as well as shipborne measurements in the Southern Adriatic (fig. 2.1). These sources include: (1) seasonal to interannual sampling at station D1200 conducted by the Institute of Oceanography and Fisheries, Croatia, since 1957 (this data is of the lowest quality and has been subjected to additional quality-check in this study; further details on sampling procedures and data accuracy can be found in Vilibić et al. (2011); here we use the data at 1000 m depth), (2) opportunistic temperature and salinity measurements, carried out by multiprobes within Italian and European projects since 1985 (more can be found in Cardin et al. (2020b)), (3) EMSO-E2M3A deep-ocean observatory (`https://emso.eu/observatories-node/south-adriatic-sea`), with (among other) deep temperature and salinity sensors located at 900, 1000 and 1200 m, with hourly resolution and being in operation since 2006 (daily averages are used in this paper), and (4) 15 Argo profiling floats (`https://www.euro-argo.eu`) that have been active in the southern Adriatic since 2010, reaching depths of at least 1000 m.

Additionally, we analyzed temperature and salinity data collected since 2004 at buoy Vida (https://www.nib.si/mbp/en/oceanographic-data-and-measurements/buoy-2) in the northern Adriatic. Sensors at buoy Vida are positioned at a depth of 2.5 m. This buoy is located within the NAddW formation area and is not affected by rivers during cold wintertime Bora outbreaks (Raicich et al., 2013). For each year, we extracted daily average of temperature and salinity during the period of NAddW formation, *i.e.*, for a day when maximum density is reached.

Potential temperature, practical salinity and potential density anomaly (PDA) were estimated from measurements using the TEOS-10 standard (https://www.teos-10.org).

To quantify year-to-year cooling changes in the NAddW formation area, we analyzed anomalies in daily latent and sensible heat fluxes from the ERA5 reanalysis (Herbasch et al., 2020), averaged over the northern Adriatic (red rectangle in fig. 2.1) for the period from December to February, during which dense water preconditioning and formation occurs (Paladini de Mendoza et al., 2023). The sum of latent and sensible heat fluxes is referred to as turbulent heat fluxes. Notably, ERA5 cooling rates are underestimated along the Bora jets (Denamiel et al., 2021), yet they exhibit the changes between years attributed to dense water formation potential.

2.3 Deep Adriatic as a climate change hot spot

The composite series from SAP observations at 1000 m (fig. 2.2) shows an overall rise in salinity and temperature, with significant decadal temperature variability before the 1990s (one should note that the oldest 1000-m temperature and salinity measured during the 1911-1914 cruises equal to ca. 12.8 °C and 38.5, respectively, Vilibić et al. (2023)). Although the historical data are with lower accuracy and reliability, our analysis follows the literature on the Adriatic thermohaline variability. For example, major cooling events in winters of 1981 (Artegiani and Salusti, 1987) and 1983 (Brankart and Pinardi, 2001) followed a large inflow of LIW (Mihanović et al., 2015), generating much cooler dense waters that cascaded into the near-bottom SAP. Less saline Western Mediterranean waters entered in the late 1980s and the early 1990s, and preconditioned by the Eastern Mediterranean Transient (EMT, Klein et al. (1999)) along with milder winter cooling (Josey, 2003; Cardin and Gačić, 2003). Both prevented dense water cascading to the near-bottom SAP between 1992 and 2000 due to its lower density (Pranić et al., 2024). Salinity rose sharply in the mid-2000s, coinciding with several NAddW formation events (in winters of 2002, 2005 and 2006; Verri et al. (2018); Pranić et al. (2024)), transporting salt to the near-bottom SAP. Since 2006, near-bottom SAP thermohaline changes clearly reflect two key processes: dense water cascading (Bignami et al., 1990; Paladini de Mendoza et al., 2023; Le Meur et al., 2025) and steady temperature and salinity increases driven by double-diffusive processes (Querin et al., 2016; Amorim et al., 2024). This *"saw-tooth"* pattern, linked to cascading events occurring every few to 10 years (Querin et al., 2016), is more evident post-2006 due to better data, however our data suggests that such pattern occurred in the 1970s-80s and 1990s-2000s. Another period without NAddW cascading to near-bottom SAP was between 2006 and 2012, again connected with anticyclonic BiOS that induced lower salinity conditions in the Adriatic.

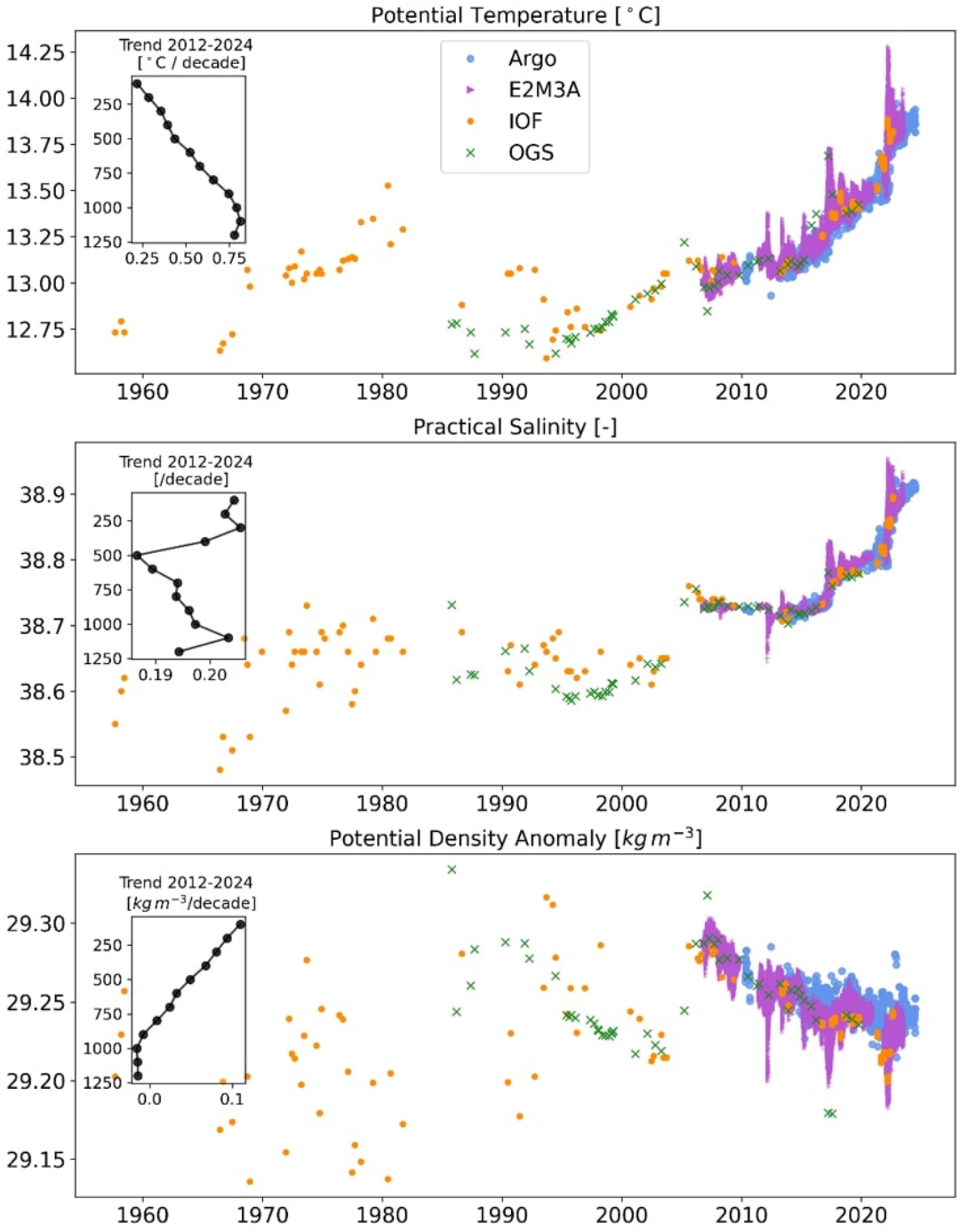

Figure 2.2: Potential temperature (up), practical salinity (middle) and potential density anomaly (PDA, bottom) obtained from all SAP observations at 1000 m since 1957 (IOR – measurements carried out by the Institute of Oceanography and Fisheries at station D1200, OGS – cruises as part of Italian and European projects, and other datasets in PANGEA Data Repository (`https://www.pangaea.de/`) and MEDATLAS Dataset (`https://nodc.inogs.it/nodc/`) in the SAP). Trends presented in insets are estimated from the Argo data in the period 2012-2024 (this period was chosen as sparse data and major data gap occurred before 2012).

From 1957 to 2024, 1000-m composite trends show significant increases in temperature

(0.088 °C), salinity (0.036), and PDA (0.0097 $\mathrm{kg\,m^{-3}}$) per decade ($p < 0.001$). Two distinct PDA regimes emerged: until the mid-2000s, PDA increased steadily, driven by salinity, while from 2006, temperature and salinity accelerated, causing PDA to decrease almost linearly (-0.03 $\mathrm{kg\,m^{-3}}$ per decade, $p < 0.001$). Between presumed or documented cascading events, temperature trends at 1000 m remained steady, around 0.38 °C, 0.35 °C, and 0.36 °C for the periods 1967–1980, 1994–2004, and 2012–2016, respectively (computed using annual averages from all measurements). Heat transport was driven by salt-fingering (Amorim et al., 2024), though no deep salinity increase was observed during the post-EMT period (1994–2004). However, the drop in temperature of the dense waters cascading into the near-bottom SAP steadily decreased from about 0.5 °C in the early 1980s, to 0.2-0.3 °C in the early 1990s, and to less than 0.2 °C in 2012, the latter being characterized by record-breaking cooling, densities and dense water generation in the northern Adriatic (Mihanović et al., 2013).

After 2017, dense water cascading events reversed the temperature shifts at 1000 m (fig. 2.2), with temperatures rising by 0.2 °C and 0.3 °C during the 2017 and 2022 events, and salinity increasing by 0.02 and 0.08, respectively. The details of the cascading events measured by bottom-mounted observatories at the western SAP slope are documented in detail in (Paladini de Mendoza et al., 2023; Le Meur et al., 2025). At the very bottom of the SAP (1200 m), temperature and salinity shifts were even larger during the 2022 event, by about 0.40 °C and 0.12 (fig. 2.3). The positive trends between cascading events have accelerated in time, with values of 0.40 °C, 0.67 °C, and 0.64 °C (temperature), and 0.062, 0.118, and 0.218 (salinity) per decade for the periods July 2012–December 2016, July 2018–December 2021, and July 2022–June 2024, respectively (estimated from Argo data at 1000 m only). Indeed, we found the entire Southern Adriatic warming and salinification (fig. 2.3), with the 14 °C isotherm deepening from 100 m in the early 2010s to near the bottom by 2024, while salinity above 38.9 was sporadically present in early 2010s but encompassed almost the entire SAP in 2024 (except at the very surface and below 1000 m).

To quantify the recent changes in stratification in the SAP, we estimated temperature, salinity and PDA differences across 100 m water layers (below the seasonal pycnocline) using Argo data (fig. 2.3). The reduction in vertical temperature gradients is particularly evident in the upper 700 meters, where the gradients decrease by more than 40% over a decade, with a maximum of 60% decrease between 500 and 600 m. The trends in salinity gradients are less pronounced, except between 300 and 500 m, where a strong decrease in vertical salinity gradient is detected, due to higher overall salinity trends at depths shallower than 400 m. Consequently, stratification below 100 m has eroded over most of the SAP, with rates of 0.010–0.015 $\mathrm{kg\,m^{-3}}$ over a decade and 100 m layers, except at the very bottom (1100–1200 m) where stratification has slightly increased. However, the latter may be attributed to much lower availability of Argo data at 1200 m depth.

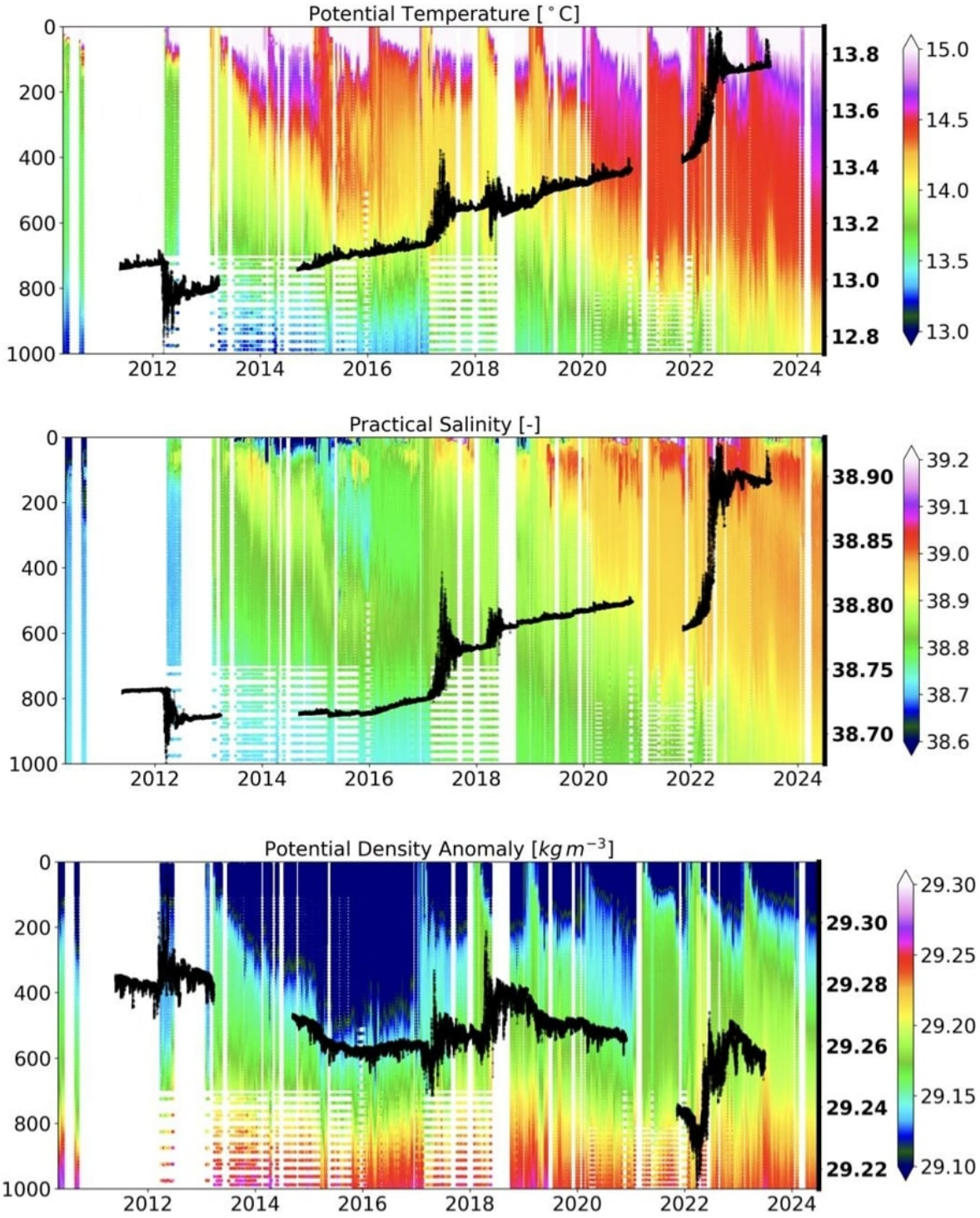

Figure 2.3: Argo-based Hovmoller diagram of the SAP potential temperature, practical salinity and PDA since 2012, with overlying EMSO-E2M3A time series (black line) measured at 1200 m.

2.4 Recent Changes in near-bottom SAP water mass source regions

Several key processes influence the near-bottom SAP: dense water generation (on the northern Adriatic shelf and through open-ocean convection in the SAP), double-diffusive processes and water exchange with the Mediterranean via the Otranto Strait. However, open-ocean convection was never recorded to reach depths below 900 m (Gačić et al., 2002; Cardin et al., 2011), which are normally occupied by the NAddW cascaded from the northern Adriatic characterized with higher thermally-driven density and slowly eroding due to heat and salt exchange with overlying waters (Querin et al., 2016; Vilibić et al., 2023).

The northern Adriatic winter turbulent heat flux anomalies over the northern Adriatic, where NAddW forms, have been predominantly higher between 2004 and 2024 than during the 1980–2010 baseline (fig. 2.4 top). Notably, the years in which major NAddW cascading events to the near-bottom SAP occurred (2012, 2017, 2018, and 2022) exhibit varying turbulent heat flux anomalies, with winters of 2018 and 2022 showing positive anomalies (the winter of 2018 was preceded by a cold autumn, Paladini de Mendoza et al. (2023)). Intuitively, despite low heat losses in 2022, haline contributions may have significantly influenced NAddW density and cascading potential to the near-bottom SAP.

To support this statement, daily averages of temperature, salinity, and PDA at the Vida buoy (northern Adriatic) during the day in a year when the PDA maximum is reached reveal significant changes in NAddW properties (fig. 2.4 middle), though the buoy was non-operational during the winters of 2007, 2008, and 2019. The buoy is located inside the northern Adriatic dense water generation area (e.g., Raicich et al. (2013)) and qualitatively reflects the wider thermohaline conditions. In 2005-06, high PDA (ca. 29.7 $\mathrm{kg\,m^{-3}}$) was driven by heat loss, while in 2004, both lower temperatures and higher salinity led to high PDA values. These waters then cascaded to the near-bottom SAP (Vilibić and Šantić, 2008), raising salinity levels in mid 2000s. In 2012, both severe cooling and high salinity produced record NAddW PDA values at its source (Mihanović et al., 2013), while in 2017 and 2018, similar conditions to 2004 were observed. In 2022, low temperature and high salinity from droughts (Bonaldo et al., 2022) resulted in the second-highest PDA value (29.82 $\mathrm{kg\,m^{-3}}$) at the Vida buoy, bringing even warmer and higher salinity waters through cascading to the near-bottom SAP (Le Meur et al., 2025).

In the northeastern Ionian Sea, Argo data from 2012 to 2024 (fig. 2.4 bottom) show much slower increases in temperature and salinity compared to the SAP (fig. 2.2 inset). Temperature trends are approximately 0.1-0.2 °C per decade (fig. 2.4 bottom), which is 2-4 times lower than observed in SAP, while salinity trends were mostly 0.05-0.10 per decade, again 2-4 times lower than observed in SAP. Overall, weak positive PDA trends exist in the northern Ionian, opposing the trends in the near-bottom SAP. This suggests that local Adriatic processes, influenced by changes in wintertime heat losses, precipitation and river discharge (Vodopivec et al., 2022; Bonaldo et al., 2022), play a larger role in shaping NAddW and consequently near-bottom SAP thermohaline properties.

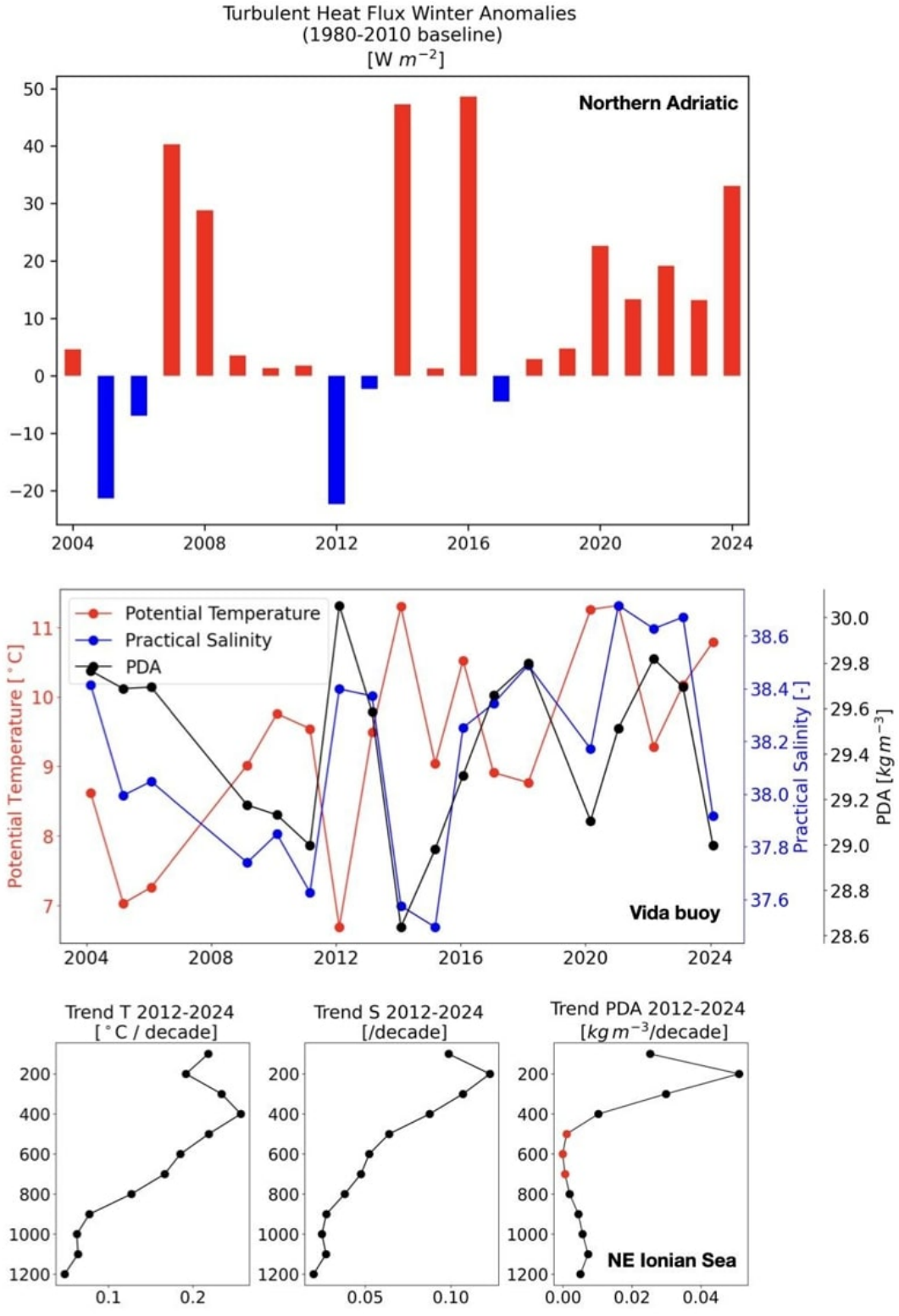

Figure 2.4: Average wintertime (DJF) ERA5 turbulent (latent+sensitive) 2004-2024 heat flux anomalies over the northern Adriatic in respect to the 1980-2010 baseline period (top), daily temperature, salinity and PDA values measured at the buoy Vida in a day of a year with maximum PDA value (middle), and 2012-2024 trends in the northeastern Ionian Sea as derived from the Argo data (bottom; red dots represent trends that are not significant at the 95% confidence level).

2.5 Discussion

The salinization and warming of the deep Mediterranean waters have been observed on a centennial scale (Vargas-Yáñez et al. (2017, 2021)), but these processes have accelerated since the 1950s (Rohling and Bryden, 1992), and even more in the last decade (García-Lafuente et al., 2021; Kubin et al., 2023). This trend is also evident in the LIW, which has exhibited temperature and salinity increases of 0.2 °C and 0.06 per decade, respectively, between 2001 and 2019 (Fedele et al., 2022). However, our analysis indicates that in the Southern Adriatic, in particular in its deepest parts, these trends have accelerated dramatically to 0.4–0.8 °C and 0.2 per decade between 2010 and 2024-two to four times higher than in the rest of the Mediterranean. Notably, the most significant temperature increases have been observed at the bottom of the SAP, where dense waters from the northern Adriatic cascade every few years, signalling a major shift in the source region of these cascading waters. Furthermore, double-diffusive transport, driven by an unprecedented influx of warm, saline waters into the Adriatic, is contributing to further warming and salinization of the Southern Adriatic and Adriatic in general.

This raises the question of whether these changes are exceptional and represent a transit in the deep Adriatic waters. Deep-water transits have been documented in the Mediterranean over the last few centuries, such as the Eastern Mediterranean Transient (EMT, Klein et al. (1999)), a unique event with possible centennial recurrence times (Incarbona et al., 2016), and the Western Mediterranean Transient, which brought waters with different temperatures and salinities to the bottom (Zunino et al., 2012). These events were driven by extraordinary wintertime forcings, as is the case here, where dense water cascading has introduced much warmer and saltier water. It is also worth considering whether such deep-water conditions will become more frequent in future climates. The state-of-the-art Med-CORDEX ensemble (Soto-Navarro et al., 2020) projects increases in surface (0–150 m) and intermediate (150–600 m, primarily LIW) temperature/salinity of 2–4 °C/0.2–1.0 and 2–3 °C/0.2–1.0, respectively, in the far future (2075–2100) under the RCP8.5 scenario. Kilometer-scale models project similar changes, e.g., approximately 0.6°C and 0.15 for temperature and salinity, respectively, for the mid-future (2031–2050) RCP8.5 scenario (Verri et al., 2024). Observations in the SAP over the last 10–15 years suggest that the projected level of centennial changes may occur in just 10–20 years, representing at least a fivefold amplification of regional climate changes projected by extreme high greenhouse emission scenarios.

The significantly higher temperature and salinity trends in the SAP, particularly in its near-bottom layers, compared to the northeastern Ionian Sea - through which the saline LIW is advected to the Adriatic - indicate that locally-driven warming of the deep Adriatic waters plays a more important role in the observed Adriatic transit than the advection of heat and salt from the Levantine Basin. These conditions resemble those observed during the positive phases of the BiOS, during which the Adriatic exhibits high-salinity conditions, facilitating the cascading of NAddW due to the higher density of saltier waters (Paladini de Mendoza et al., 2023; Pranić et al., 2024; Le Meur et al., 2025). The documented deep Adriatic changes clearly introduce the paradigm: local drying and warming may become more important for deep layers than heat and salt advection from the Ionian Sea. This interplay between processes may be perceived as a preview of future climate change (Bonaldo et al., 2022).

These observed changes in thermohaline properties are already impacting Adriatic biogeochemistry and marine life. Species residing in warmer seas are likely to benefit and

increase in abundance (Belmaker et al., 2013). In contrast, cold-water species, primarily found in the Jabuka Pit - an area known for the lowest temperatures in the Adriatic and protected as a no-take zone due to its rich biodiversity and demersal resources (Chiarini et al., 2022) - will be particularly threatened by the rapid changes in NAddW properties. All biogeochemical projections indicate that a warming Mediterranean will exhibit a decline in dissolved oxygen and nutrient availability (Reale et al., 2022), leading some species to reduce their habitat range and/or migrate northward (Palermino et al., 2024; Panzeri et al., 2024). This transient will likely exacerbate these changes, particularly for deep benthic organisms (Angeletti et al., 2015; Taviani et al., 2019), which are not adapted to such large and irreversible temperature shifts.

The shift in intermediate and deep water density trends has the potential to change sea level trends in the Adriatic. By applying a simplified methodology by Wang et al. (2017) for the whole water column, steric sea level trend between 2014 and 2024 equals 3.3 $\mathrm{mm\,yr^{-1}}$, in which thermosteric and halosteric contribution equals to 20.5 and -17.2 $\mathrm{mm\,yr^{-1}}$, respectively, the first prevailing in the upper 100 m while the second having maximum in intermediate layers. During the second half of the 20^{th} century, sea level rise trends were mitigated (compared to global trends) due to an increase in deep water density (Tsimplis and Baker, 2000). Our study indicates that deep density trends have reversed since 2006, aligning with climate projections (Soto-Navarro et al., 2020), and potentially amplifying sea level rise in coastal regions (Vecchio et al., 2023). The complexity of interactions between different drivers of thermohaline changes introduces uncertainty in determining whether these events represent decadal variability or rapid transits towards a projected warmer climate. These uncertainties, along with other observed changes in the Mediterranean, should be carefully investigated to develop appropriate mitigation and adaptation strategies, where possible.

Acknowledgements

We are grateful to all scientists, engineers, technicians and research vessel crew members that were engaged in collection of temperature and salinity data at EMSO-E2M3A observatory, Vida buoy, station D1200 and opportunistic cruises in the SAP. The Argo profiling float data were collected and made freely available by the International Argo Program and the national programs that contribute to it. This work benefited from the data produced and collected from access to the EMSO South Adriatic, an EMSO-IT and EMSO-ERIC Site, operated by OGS, CNR-ISP. Comments raised by two anonymous reviewers and editors greatly improved the quality of the manuscript. The research has been carried out with the support of Croatian Science Foundation through research projects GLOMETS (Grant IP-2022-10-306 4) and C3PO (Grant IP-2022-9139), and incoming mobility scheme for postdoctoral researchers (MOBDOL-2023-12, Elena Terzić), as well as with the support of Interreg Italy-Croatia Programme 2021-2027, project AdriaClimPlus (Grant ITHR0200333), Slovenian Research Agency (research core funding No. P1-0237), and National Recovery and Resilience project KLIMADRIA.

Part III

From basin scale to submesoscale variability in the SAP

A scale-dependent closure problem in the SAP: the role of submesoscale processes

The previous part showed that the SAP has been responding to climate change through a long-term increase in temperature and salinity over the past 60 years, with accelerated warming in the last decade. It was also noted that, following a strong inflow of saline water in January 2017, the water column in the SAP can be described as a two-layer structure (part II). Since then, no return to the previous state has been observed. Nevertheless, this basin-scale analysis lacks a complete understanding of the processes occurring at smaller scales, without which the dynamics of the Adriatic Sea cannot be fully understood. While the large-scale circulation of the Adriatic Sea provides the global framework for water mass formation and exchange, it does not fully determine the pathways through which ventilation, mixing, and transformation of water masses occur. Many of the key processes described above, DWF (section 0.3.1), gravity currents (section 0.3.2), and eddy activity (section 0.3.5), are multiscale and depend on dynamics that develop at spatial scales smaller than the basin scale.

In particular, DWF areas such as the northern Adriatic and the southern Adriatic are organised at multiple scales, beginning at the basin scale through the preconditioning induced by the interaction of water masses with different properties, especially saline LIW/ISW, and air-sea interactions driven by cooling and evaporation during Bora events (section 0.3.1). The associated vertical and lateral exchanges, however, are governed by smaller-scale processes. Convection develops through localised plumes at fine scale, while the subsequent arrest and restratification of convective patches are controlled by baroclinic instabilities that generate meanders and geostrophic eddies, mainly at the submesoscale (Marshall and Schott (1999)).

Eddies (section 0.3.5), occurring at both mesoscale and submesoscale, play a crucial role in the redistribution of heat, salt, nutrients, momentum, and potential vorticity between the air-sea interface, the mixed layer, and the ocean interior, linking vertical mixing to lateral transport (Williams and Follows, 1998; Lapeyre and Patrice, 2006; Capet et al., 2008; Lévy et al., 2012). In the South Adriatic, these eddies result from an interplay between baroclinic instabilities generated in convective patches or frontal areas, topographic control of the pit, and exchange dynamics at the Strait of Otranto, all of which make the South Adriatic a natural laboratory for the study of eddies generation across scales.

Gravity currents (section 0.3.2) transporting NAdDW evolve under the combined influence of Coriolis forces, topography, and turbulent mixing within boundary layers (Wirth, 2009). Although gravity current pathways can extend across the entire Adriatic basin,

from their generation in the northern Adriatic to the SAP, their structure and entrainment are controlled by submesoscale processes, such as shear instabilities and frictional effects, which cannot be resolved at a basin scale. The study of gravity currents in the SAP is of primary importance as they play a key role in ventilating intermediate and deep layers, transporting heat, salt, oxygen, and nutrients, or even forming new water masses through turbulent mixing.

The Adriatic Sea lacks a clear separation of scales: basin-scale circulation depends on mesoscale organisation, which in turn emerges from and is modified by submesoscale dynamics. This scale-dependent closure problem motivates a dedicated focus on submesoscale processes, which constitute the dynamical link between large-scale forcing and the effective ventilation and transformation of Adriatic water masses. In this thesis, the next chapter presents an analysis of the long-term variability of gravity currents in the deep SAP (chapter 3).

Chapter 3

Intermittent supply of dense water to the deep South Adriatic Pit: an observational study

This section is constituted by the article published in Frontiers in Marine Science in 2025:

Le Meur Julien, Wirth Achim, Paladini de Mendoza Francesco, Miserocchi Stefano, Cardin Vanessa. Intermittent supply of dense water to the deep South Adriatic Pit: an observational study. Frontiers in Marine Science, 12, 2025. doi: 10.3389/fmars.2025.1516780

Abstract: The renewal of bottom water masses in the deep South Adriatic Pit (SAP) is mainly determined by the arrival of very dense water that forms in the North Adriatic in winter (NAdDW) and which is transported into the SAP by gravity currents. To investigate the occurrence of these currents, we analyze high-frequency time series of thermohaline and velocity data at 3 moorings of the EMSO South Adriatic Sea regional facility consists of two observation areas: the South Adriatic Pit observatory (E2M3A) and the shelf and slope observatory (BB in the Bari Canyon and FF on the furrow area on the open slope), from 2012 to 2022 as well as reanalysis data from Copernicus over the same period. This analysis shows that gravity currents in the deep SAP (dSAP) only occurred in 2012, 2017, 2018 and 2022 (bottom ventilation years). The water masses were mixed differently after gravity current events, as 2012 was mainly driven by temperature, 2017 and 2022 by salinity and 2018 by both. It was also found that in 2012 and 2018 the gravity current mainly passed through FF, while in 2017 it passed through BB. An analysis of the time scale showed that the average duration of the bursts of fluctuation triggered by the arrival of the gravity current in the dSAP was a few months (3 months on average). It was also revealed that the travel time from the formation of the NAdDW to BB was around 2 months on average, and that the travel time from BB (FF) to E2M3A was around 2 weeks. A comparison between the Copernicus reanalysis and the E2M3A time series also showed consistent differences in density, both in value and variability, resulting in the detection of gravity current events being unclear for the former.

3.1 Introduction

The Adriatic Sea is a semi-enclosed basin of small size, 800 km long and 200 km wide. It is nevertheless a main driver for the eastern Mediterranean thermohaline circulation (Cushman-Roisin et al., 2001) due to the production of Adriatic deep Waters (AdDW) (Ovchinnikov et al., 1985; Artegiani et al., 1997; Gačic et al., 2001; Mantziafou and Lascaratos, 2004; Chiggiato et al., 2016; Amitai et al., 2019). The generation of dense water masses in the Adriatic are linked to the cyclonic circulation, to the strong winter cooling by cold and dry katabatic Bora winds (Supić and Orlić, 1999), and to the inflow of saline waters through the Otranto strait. These saline waters characteristics are modified by fresh water inflow, mainly through the Po river (Bensi et al., 2013). On a larger scale, it influences the Mediterranean climate (Gačić et al., 2010; Civitarese et al., 2023) and the water mass properties of the Atlantic Ocean, due to the outflow of dense waters at the Strait of Gibraltar (Bryden et al., 1994; Richardson et al., 2000; García Lafuente et al., 2007; García-Lafuente et al., 2009). More precisely, the outflow of generated dense waters through the Strait of Otranto is of great importance for both, the surface and deep layers of the Ionian Sea. It influences the BiOS mechanism, leading to the entrance of saltier (Levantine Intermediate Water, LIW) or fresher water (Atlantic Water, AW) into the Adriatic through the decadal variability between cyclonic and anticyclonic circulation of the northern Ionian gyre, (Gačić et al., 2010; Civitarese et al., 2023).

The Adriatic Sea can be divided into three sub-basins: the northern one (less than 50 m deep), the middle one with the Jakuba pit (less than 270 m deep) and the southern one with the South Adriatic Pit (1200 m deep), which is separated from the Ionian Sea by the Otranto Sill (780 m). The deep layers of the SAP are filled with the densest water masses, which can be formed locally by deep convection (see for example: (Killworth, 1983; Schott et al., 1996; Marshall and Schott, 1999; Testor et al., 2018) or remotely by gravity currents (Benjamin, 1968; Simpson, 1982; Wirth, 2009; Chiggiato et al., 2016; Rétif et al., 2024) from the northern Adriatic, the North Adriatic Dense Waters (NAdDW), where shelf convection occurs (Vilibić et al., 2023). These water masses are also modified by mesoscale and submesoscale dynamics, turbulence, and double diffusive mixing (Amorim et al., 2024).

Once the dense water is formed, it flows southward as a gravity current, following isobaths on the western side of the Adriatic Sea (Vilibić et al., 2023). It splits during its way toward the Southern Adriatic, with a part filling the Jakuba pit in the Middle Adriatic (Artegiani and Salusti, 1987), and the other part flowing towards the SAP. Topographic features play a guiding role, especially the Bari canyon (Chiggiato et al., 2016; Paladini de Mendoza et al., 2022a), leading to down-slope cascading of dense water. Some of the dense water spills over the Otranto strait into the Ionian basin (Bignami et al., 1990).

The role of gravity currents as compared to deep convection is of great importance, as the ventilation (transfer of properties such as dissolved oxygen from the surface to the interior of the ocean) of the deepest layers of the SAP is mainly caused by the former and only rarely by the latter (Gačić et al., 2002; Cardin and Gačić, 2003; Cardin et al., 2011; Bensi et al., 2014). Gravity currents flowing into the SAP do not occur every year, as this depends on the interplay between different forcing conditions mentioned above, but also on the existing stratification, which is the result of previous intermittent gravity current events and convection events on the one hand and long-term vertical diffusion on the other (Cardin et al., 2020b).

In this study, we present an analysis of occurrences of gravity currents reaching the

dSAP between 2012 and 2022 using time series data obtained from the South Adriatic EMSO regional facility (http://emso.eu/observatories-node/south-adriatic-Sea/) supplemented by data from Copernicus Marine Service. The description of methodology and data used is presented in section 2, while results and discussions are described in section 3. Conclusions are given in section 4.

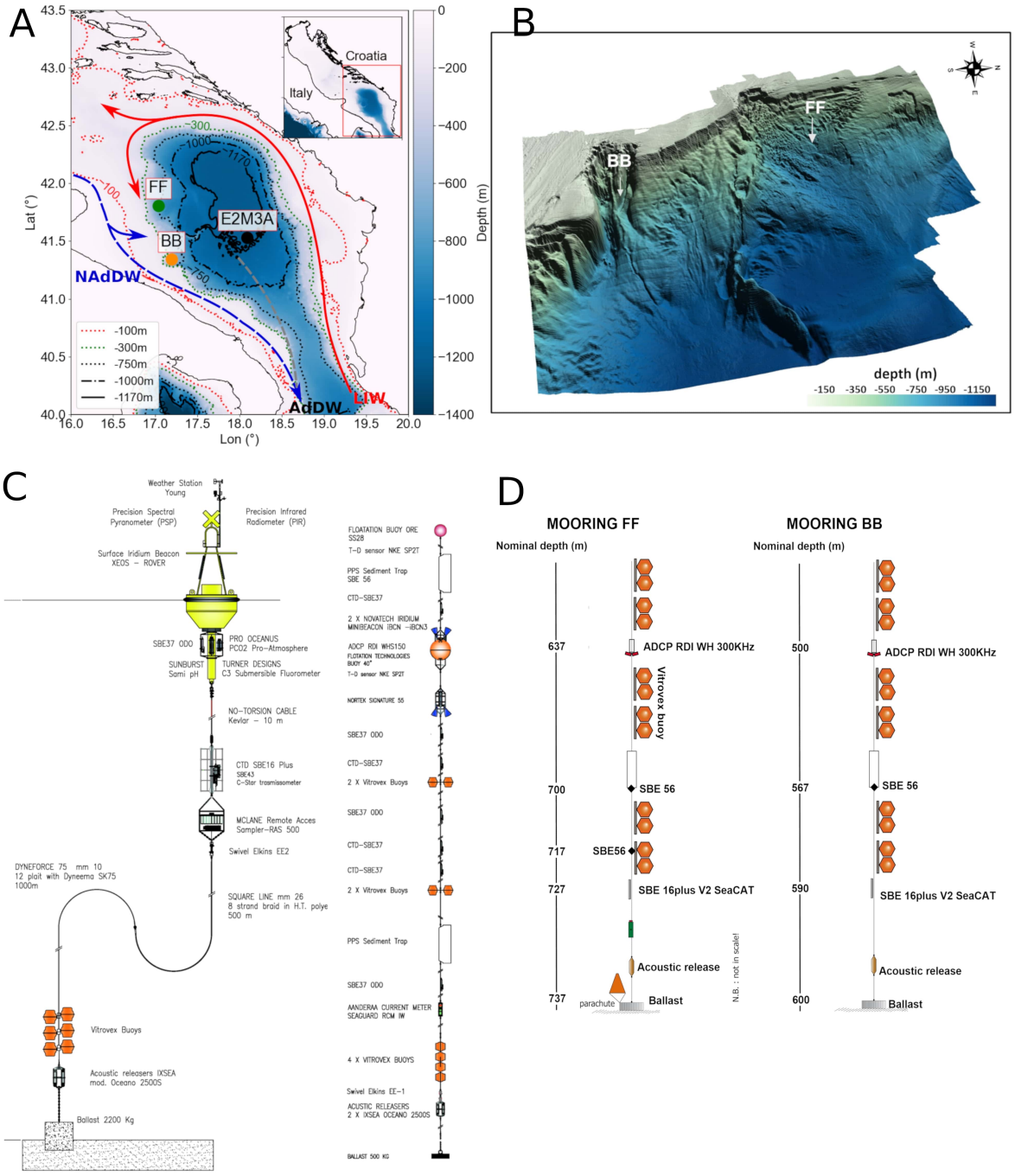

Figure 3.1: Bathymetric map of the Adriatic Sea showing the locations of moorings EMSO-E2M3A, BB, and FF, and the main water masses pathways, the Levantine Intermediate Water (LIW), the North Adriatic Dense Water (NAdDW), and the Adriatic Deep Water (AdDW). **(A)** A zoom on the area near the Bari canyon, where BB and FF moorings are located, is shown in **(B)**. Moorings of the South Adriatic regional facility, EMSO-E2M3A, EMSO-BB and EMSO-FF, are presented in (**C**, **D**) respectively.

3.2 Material and methods

3.2.1 Mooring data

The data analyzed come from the South Adriatic regional facility which is part of the EMSO-Eric observation network consisting of two sites, one of which is located in the center of the SAP (E2M3A - position: Lat 41.53 $°N$, Lon 18.06 $°E$, see fig. 3.1) and the other consisting of two moorings on the western side of the southern Adriatic continental edge (mooring BB - position Lat 41.34 $°N$, Lon 17.19 $°E$ and FF - position Lat 41.81 $°N$, Lon 17.04 $°E$, see fig. 3.1). The combination of data collected at these three moorings allows us to observe the flow of gravity currents in the SAP, after the dense water formation in the northernmost part of the Adriatic Sea. The monitoring strategy set up for the southern Adriatic observatory is based on continuous and high-frequency measurements of temperature (T), salinity (S), oxygen (O) and velocities, which are suitable for detecting both long-term changes, episodic processes over decades (Cardin et al., 2020b), and high-frequency processes (1h) such as waves and turbulence.

The E2M3A observatory, which has been in operation since 2006 (Bensi et al., 2014; Cardin et al., 2014a, 2018, 2020b,a, 2024, 2025; Amorim et al., 2024), collects hourly data of T, S and O at seven different levels of the water column (150, 350, 550, 750, 900, 1000 and 1200 dbar). In this study, we focus on the period from December 2011 to December 2022 (a period in which the availability of data is greatest for the three moorings combined) for the deepest layers of the pit.

The mooring BB is placed at 600 m depth on the main branch of the Bari Canyon system and FF on the furrow area on the open slope at 733 m depth (Paladini de Mendoza et al., 2022b, 2024a,b). The two mooring lines are 100 m long, have been in operation since 2012 and collect half-hourly T, S and current data at different levels of the water column. The Teledyne RD Workhorse 307KHz ADCP in downward-looking mode measures the currents of the last 100 m near the seafloor every 30 minutes with an accuracy of ± 0.5 $\mathrm{cm\,s^{-1}}$ and a resolution of 0.1 $\mathrm{cm\,s^{-1}}$. The ADCP is a four-beam, convex configuration with a beam angle of 20 °, the number of depth cells is set to 27 with a cell size of 4 m. A CTD probe, SBE 16plus V2 SeaCAT, is located approximately 10 m above the seafloor to record thermohaline parameters. The water conductivity data were measured with a sensor with an accuracy of 5×10^{-4} $\mathrm{S\,m^{-1}}$ and a resolution of 5×10^{-5} $\mathrm{S\,m^{-1}}$; the water temperature using a thermometer, with an accuracy of 5×10^{-3} °C and a resolution of 1×10^{-4} °C. The moorings are also equipped with a temperature sensor SBE56 (accuracy $\pm 2 \times 10^{-3}$ °C and 1×10^{-4} °C resolution), which is installed in FF at a height of 37 and 20 m from the seabed and in BB at a height of 33 m from the seabed.

In this study, we consider the potential temperature (θ) and S; θ was derived using the Gibbs Seawater GSW Oceanographic Toolbox, which contains the TEOS-10 routines (McDougall and Barker, 2011). The Python language was used in this study through several libraries: the Numpy module (Harris et al., 2020), the Pandas module (Wes McKinney, 2010), the Scipy module (Virtanen et al., 2020) and the StatsModels module (Seabold and Perktold, 2010). We used the Matplotlib module (Hunter, 2007) to display the results.

3.2.1.1 CTD instrumentation

Quality control of the E2M3A mooring data used in this study was performed in several steps according to the RITMARE Fixed Sites Network Procedures Quality Control (QC)

guide (Cardin et al., 2014b) & OceanSites QC procedures: a physical range to remove outliers, a spike test to remove large differences between sequential measurements, a change test to check the rate of change over time and an interpolation to fill gaps no longer than 6 hours. The salinity threshold of Cardin et al. (2014b) was modified, because of the increase of S in the Southern Adriatic (an increase of θ is also observed).

Additionally to the application of this standard QC, trends and offsets present in the time series were corrected with CTD casts performed at the E2M3A site, in majority realized during maintenance cruises. Trends were corrected taking into account the general trend in the area (global increase of θ and S) while offsets due to instruments errors were subtracted from the time series.

Finally, as far as BB and FF moorings are concerned, the quality of the data is ensured by regular maintenance operations during which instruments and the components of the moorings are checked to ensure their functionality, durability, and resistance during the survey period. In addition, the instruments are regularly calibrated at the factory and compared with the CTD calibrated on board, as described in Paladini de Mendoza et al. (2022a). QC of the currents and thermohaline data of the BB and FF moorings used in this study was performed in several steps according to the procedure described in the *"Data Quality Check"* paragraph of Paladini de Mendoza et al. (2022a).

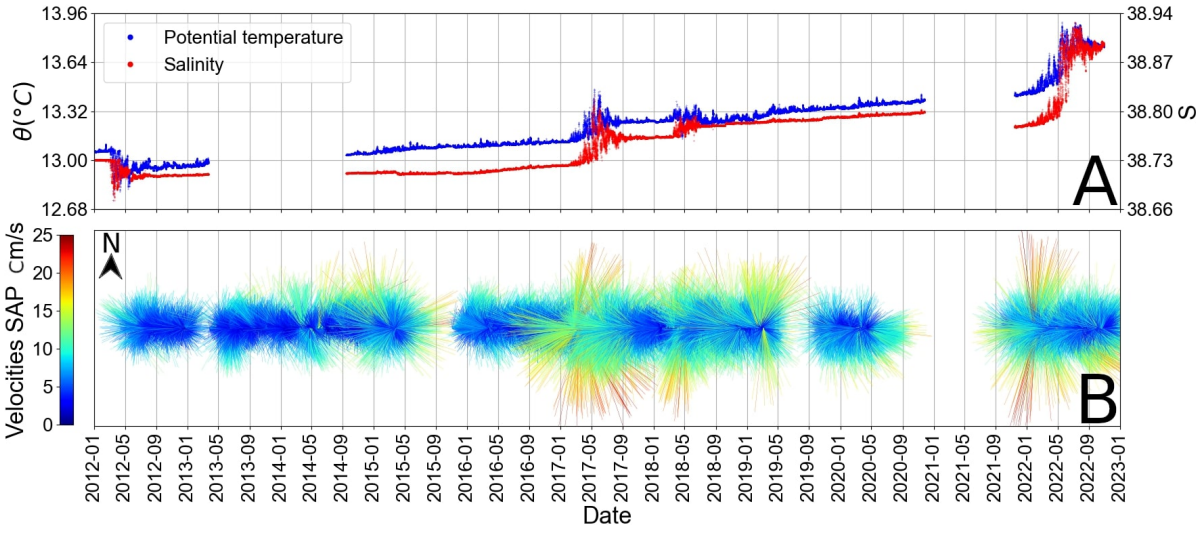

Figure 3.2: Time series of θ (**A**), S, and velocities (**B**) at E2M3A regional facility (1200m deep). Velocities are represented on a stick diagram where the sticks direction are computed according to the true North, which is oriented vertically at the top of the figure

3.2.1.2 Mixing ratio in the dSAP

The properties of the water masses in the dSAP are modified by the arrival of gravity currents. If the mixing is turbulent and the gravity current passes through BB or FF or both, with no other source, the resulting water mass (after the arrival) is formed by the weighted average of BB, FF and dSAP waters (before the arrival) at ratios R. Due to the conservation of salt and heat, we have:

$$\begin{aligned} \theta_a &= R_{BB}\theta_{BB} + R_{FF}\theta_{FF} + R_b\theta_b \\ S_a &= R_{BB}S_{BB} + R_{FF}S_{FF} + R_bS_b. \end{aligned} \tag{3.1}$$

Subscripts BB and FF stand for the properties at the two moorings, while subscripts b and a stand for the properties in the dSAP before and after the arrival of dense waters, respectively. Potential temperatures (salinities) θ_{BB}, θ_{FF} (S_{BB}, S_{FF}) are averaged over six days around the day of maximum density, while θ_b, θ_a (S_b, S_a) are averaged over two weeks, from three to one week before the arrival of the gravity current for the former and from one to three weeks after its arrival for the latter. The mixing ratios (R_{BB}, R_{FF} and R_b) are positive constants that indicate the proportion of the corresponding water mass in the resulting water mass, and their sum is therefore equal to 1. This means that the point in the θ/S diagram that represents the situation after the fluctuations must lie within the triangle formed by the water masses at BB, FF and in the dSAP before the gravity current arrives.

3.2.1.3 Velocities

In this study, we considered hourly data from an upward-looking RDI ADCP positioned at the bottom of the BB mooring and data from a point current meter Aanderaa Seaguard Recording Current Meter (RCM) positioned near-bottom layer (1166 m) of the SAP (E2M3A). The ADCP velocity data were decomposed into u and v components and represented in a coordinate system with one axis along the direction of the major variance corresponding to the canyon axis (downward flow component). The canyon axis of the main variance forms an angle of 110 ° with true north in the clockwise direction. To determine the characteristics and the number of days with gravity currents and the paths, we construct an index N_v along the downward axis, which is the number of hours in a day when the velocity in the canyon exceeds a threshold value (0.17 $\mathrm{m\,s^{-1}}$). We consider days on which $N_v > 6$. This allows us to quantify the limits of the pulse regime observed in the velocity time series. To the E2M3A speed data, a moving averaged filtered with a time window of 7 days was applied to determine the onset of gravity current. The result was then compared to the annual maximum potential density anomalies (PDA) values in the North Adriatic.

3.2.1.4 Fluctuation index

We define the temporal variability of a variable X based on a centered sliding-mean:

$$\eta_X = \langle (X(t) - \langle X(t) \rangle_{\Delta t})^2 \rangle_{\Delta t}$$

with $\Delta t = 20$ days, a period which is a compromise between smoothing the signal and keeping the relevant information for our study (the order of magnitude of the time scales we are studying is greater than 2 weeks). The normalization of a variable X is done by:

$$\widetilde{X} = \frac{X - \langle X \rangle}{\sigma(X)},$$

where $\langle X \rangle$ and $\sigma(X)$ are respectively the mean and the standard deviation of X over the whole dataset.

To identify strong fluctuation, we use 6 criteria. The first two are: $\widetilde{\eta} > 1$ for the PDA and oxygen. The third is based on the differences of the PDAs at BB and FF: if the water masses at both locations come from the same generation site, their density should be similar, i.e. $\widetilde{\Delta\rho} < 1$ with $\Delta\rho = |\langle \rho_{\mathrm{FF}} \rangle_{\Delta t} - \langle \rho_{\mathrm{BB}} \rangle_{\Delta t}|$, where ρ_{FF} and ρ_{BB} are PDA at FF and BB mooring respectively. If the water masses either at FF or BB or both are to

reach the bottom of the pit (fourth criteria), their PDA must exceed the PDA in the pit, i.e: $\rho_{\mathrm{FF}} > \rho_{\mathrm{E2M3A}}$ or $\rho_{\mathrm{BB}} > \rho_{\mathrm{E2M3A}}$ with ρ_{E2M3A} the PDA at E2M3A mooring. A fifth criteria involving the PDA of water mass generated in the North Adriatic is described in subsection 3.3.2 and a sixth one involving an analysis of mixing ratio between incoming and the already present water mass in the dSAP is presented in subsection 3.3.4. The years that satisfy all the criteria are named *"bottom ventilation years"*.

3.2.2 Copernicus reanalysis

Copernicus reanalysis data for the Mediterranean Sea and ERA-5 datasets from the Copernicus-ECMWF portal were used to assess the surface heat fluxes and the influence of salinity on the formation of dense water and the thermohaline properties of the water masses in the three sub-basins of the Adriatic Sea (North, Middle, and South).

Net surface heat fluxes were derived using hourly ERA-5 datasets of Copernicus-EMCWF (European Centre for Medium-Range Weather Forecasts, `https://doi.org/10.24381/cds.adbb2d47`) portal (Q_{tot}; (Herbasch et al., 2020; Hersbach et al., 2018)) on three different areas: North, Middle and South Adriatic. We used data from 1979 to 2022. The total surface heat flux:

$$Q_{tot} = Q_{SW} + Q_{LW} + Q_{LF} + Q_{SF}$$

is the sum of (from left to right) the short wave radiation, the long wave radiation, the latent heat flux, and the sensible heat flux. The data is sampled hourly, but in our study we use daily averages. The resolution of the grid is 0.25 °. We consider a spatial average over each of the three basins from December to March (winter period) and derive the monthly integrated surface heat flux for each month of this period.

The thermohaline properties of the water masses (S and θ) on the North Adriatic region are obtained from the Copernicus database (`https://doi.org/10.25423/CMCC/MEDSEA/_MULTIYEAR_PHY_006_004_E3R1I`) (Escudier et al., 2020; Nigam et al., 2021; Escudier et al., 2021). The data have a daily frequency and a horizontal grid resolution of 0.042 °. Salinity is averaged over the 10 upper meters of the water column (and also over the entire water column in the Material B.6) and we also consider monthly averages for salinity during the winter period. We use a dataset running from 2011 to 2022.

The PDA values are derived from daily S and θ dataset using the Gibbs Seawater (GSW) Oceanographic Toolbox, which includes the TEOS-10 routine (McDougall and Barker, 2011). We present PDA values corresponding to the mean of the PDA values in the upper 10 m of the water column.

3D velocities were also obtained from the Copernicus database (`https://doi.org/10.48670/moi-00021`) (EU Copernicus Marine Service Information, 2024). The data considered are from 2012/01/01 to 2021/06/30. They have a daily frequency and a horizontal grid resolution of 0.083 °. We consider an average of velocities at 1063 m corresponding to nodes of the model closer in latitude and longitude than 0.1 ° to the E2M3A position (4 nodes).

3.3 Results and Discussion

The water masses in the SAP area are modified by advection, convection, gravity current and/or salt fingering occurring at the basin-scale, mesoscale, submesoscale or even mi-

croscale. Historically, Lipizer et al. (2014b) has observed through a climatology analysis using all available data an increase relative to the time series in salinity and temperature of +0.18 and +0.54 °C respectively in the dSAP over the period 1911-2009, while Vilibić et al. (2023), using cruises CTD data and Argo floats, reported an acceleration of this increase during the period 2007-2022 of 0.2 and 1 °C respectively. High frequency data measured at the E2M3A also show an increase in potential temperature by +0.69 °C and in salinity by +0.17 in the period from 2012 to 2023 (fig. 3.2). In addition, a shift in salinity distribution occurred in 2017 with a sharp increase at the surface and in the intermediate layers, which reduced the stability of the vertical stratification and led to a two-layer structure with a pycnocline at 950 m (Amorim et al., 2024). In fact, Amorim et al. (2024) reported a change in regime stability after winter 2017. Gravity currents that bring dense water into the deepest part of the pit maintain this two-layer structure, increasing the density of bottom water masses.

3.3.1 Observations of gravity currents events in the dSAP

The time series of S, θ, PDA and O in the dSAP all show bursts of strong fluctuations that start in the late winter period in 2012, 2017, 2018 and 2022 and can be characterized by the fluctuation index defined in subsection 3.2.1.4 (see fig. 3.3). The strong fluctuations of oxygen during bottom ventilation years provide information about the ventilation that took place in the dSAP, as mentioned by (Gačić et al., 2002; Cardin et al., 2011; Bensi et al., 2014; Cardin et al., 2020b; Amorim et al., 2024). They cannot be the result of a deep convection event as convection, during the studied period, never reach 900 m and could then not destroy the two-layer structure which was mentioned in Amorim et al. (2024). The ventilation of the deep layer is therefore due to gravity currents. Here, we argue that the strong fluctuations are the result of gravity currents of North Adriatic origin entering the dSAP along the topography and accumulating there (Bensi et al., 2013; Mihanović et al., 2018) where it is subject to local mixing processes. The next gravity current arrives a year or a few years later.

Bursts of fluctuations of PDA at BB and FF are indicators of bottom ventilation of the SAP. If the water masses transported by these gravity currents are dense enough, they proceed to the dSAP, leading to turbulent mixing. On fig. 3.3 (and on Appendix B.1 for SBE56 fluctuations at BB or FF in 2022) we observe that in 2012, 2017, 2018 and 2022 bursts of PDA fluctuations at BB were followed by bursts of fluctuations at the E2M3A mooring. The same applies to the FF mooring. The 15-day averages of PDA at the three moorings show a saw-tooth behavior with a sudden increase in PDA, followed by a period of relaxation (fig. 3.4). This saw-tooth behavior is also discussed by Querin et al. (2016); Cardin et al. (2020b) for the SAP and by Mihanović et al. (2018) for the Jakuba pit. Querin et al. (2016) and Cardin et al. (2020b) explained this phenomena by the following: the first phase consists in a linear density decrease in the SAP, which is due to local mixing driven by flow instabilities and mesoscale turbulence generated by the large-scale cyclonic circulation of the South Adriatic sub-basin. In contrast, the second phase consists in the abrupt increase of density, which is the result of gravity currents transporting NAdDW formed during the strongest winters. The second phase effectively ventilates the dSAP which remains unventilated during the first phase. The saw-tooth behavior for oxygen observed at E2M3A was explained by Marini et al. (2006) for the Jakuba pit, where bottom water masses lose oxygen between two ventilation events due to mineralization, while nutrients increase. Martellucci et al. (2024) also observed the

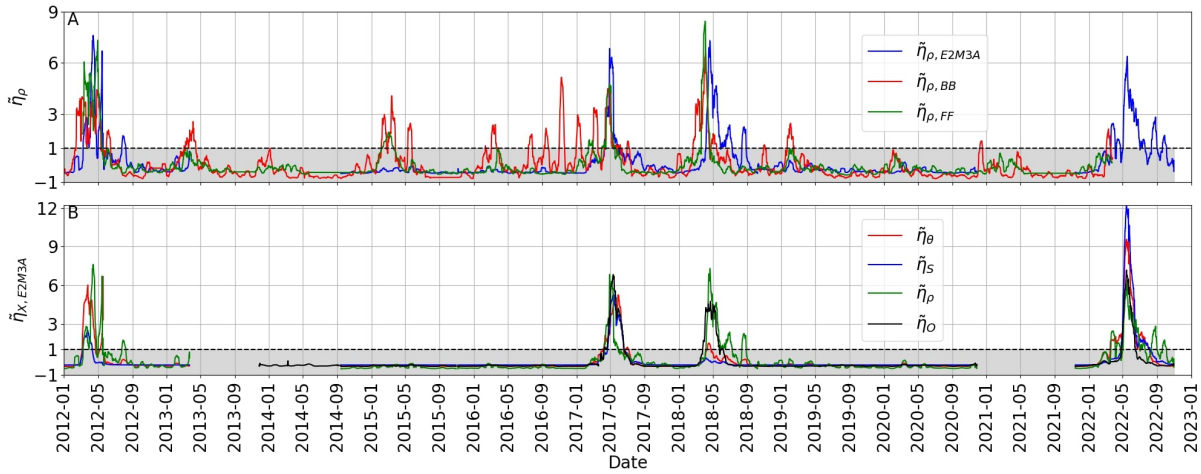

Figure 3.3: Time series of $\tilde{\eta}_\rho$ at E2M3A (blue), BB (red) and FF (green) (**A**) and time series of $\tilde{\eta}_\theta$ (red), $\tilde{\eta}_S$ (blue), $\tilde{\eta}_\rho$ (green) and $\tilde{\eta}_O$ at E2M3A (**B**). On (**A**) we observe that strong fluctuations are present in 2012, 2017, 2018 and 2022 at E2M3A, BB and FF but BB and FF also exhibits strong $\tilde{\eta}_\rho$ in 2013, 2015, 2016, 2019 and 2021. On (**B**) a consistency on the time of maximum fluctuations between the different scalar variables measured at E2M3A is observed.

same saw-tooth behavior of oxygen at the BB mooring during the 2017, 2018 and 2019 ventilation events where dissolved oxygen increased to more than 235 µmol kg^{-1}.

Table 3.1 shows that the years in which all criteria are confirmed are 2012, 2017, 2018 and 2022 (fluctuations at BB and FF for T can be seen in Appendix B.1). The occurrence of gravity currents in two consecutive years (2017/2018), as compared to a five-year period (Querin et al., 2016; Cardin et al., 2020b), possibly indicates an exceptional period of water mass changes for the south Adriatic as mentioned by (Vilibić et al., 2023; Amorim et al., 2024).

Exceptional PDA fluctuations are observed in 2015, 2016, 2019 and 2021 in BB and FF, but no remarkable fluctuations were observed in the dSAP (fig. 3.3), which is due to the fact that the water in BB and FF was not dense enough to reach the bottom (fig. 3.4). We observed nevertheless fluctuations in the upper layer (900 and 1000 dbar) (*not discussed in the article*). These waters intrude the pit at a higher level (measured at about 900 dbar, not discussed here). For instance, Martellucci et al. (2024) observe a lighter NAdDW than usual in 2015 and 2016 that filled the intermediate layer of the SAP. In 2013, strong fluctuations were also reported at BB and FF, but in the absence of data at E2M3A this year, no conclusion can be drawn about the presence of a gravity current reaching the dSAP or intruding at higher levels. As for the other years, none of the criteria are met in 2014 and 2020 (table 3.1) and no significant fluctuations are observed in neither in BB nor in FF (fig. 3.3).

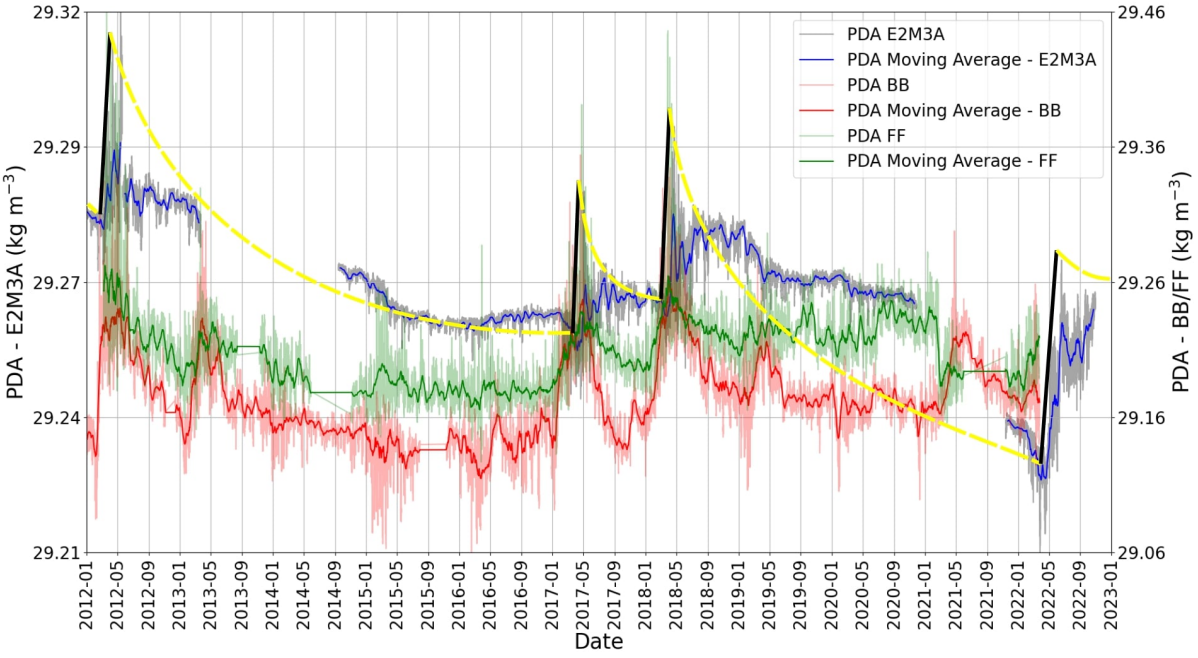

Figure 3.4: PDA time series at E2M3A (blue), BB (red) and FF (green). Bold red, blue and green lines are 15 days moving averages. The saw-tooth behavior is defined by an abrupt PDA increase (black lines) followed by a slower PDA decrease (yellow lines) . Bottom ventilation years are years when the density differences between BB and FF are small (criteria 3), where density at BB and/or FF is greater than the density at E2M3A (criteria 4).

Year	$\widetilde{\eta}_\rho > 1$	$\widetilde{\eta}_O > 1$	$\widetilde{\Delta\rho} < 1$	ρ_{FF} or $\rho_{\mathrm{BB}} > \rho_{\mathrm{E2M3A}}$	$\langle \mathrm{Max}(\rho) \rangle > 29.75\ \mathrm{kg\,m^{-3}}$	Mixing ratio
2012	✓	**ND**	✓	✓	✓	✓
2013	✗	**ND**	✓	**ND**	✓	**ND**
2014	✗	✗	✗	**ND**	✗	**ND**
2015	✗	✗	✗	✗	✗	✗
2016	✗	✗	✗	✗	✗	✗
2017	✓	✓	✓	✓	✓	✓
2018	✓	✓	✓	✓	✓	✓
2019	✗	✗	✓	✗	✗	✓
2020	✗	✗	✗	✗	✗	✗
2021	**ND**	**ND**	**ND**	**ND**	✗	**ND**
2022	✓	✓	**ND**	**ND**	✓	**ND**

Table 3.1: Fluctuations criteria (No Data at E2M3A, BB or FF is symbolized with **ND**, a non-verified criterion with ✗, and a verified one with ✓) for the 1200 dbar layer. The years meeting all the criteria from the available data are 2012, 2017, 2018, and 2022.

3.3.2 Coherence of dense water formation in the North and Middle Adriatic with fluctuations in the dSAP

Pulses of dense water in the dSAP due to gravity currents are associated with the generation of NAdDW in the North Adriatic during winter periods, as shown by Di Biagio et al. (2023), where a moderate correlation (0.68) between the high concentration of dissolved oxygen in the deeper layers of the SAP with the intermittent inflow of NAdDW was found for the period 2012-2014. Evidence for the arrival of these dense water pulses is associated with the high concentration of dissolved oxygen, as mentioned by Manca et al. (2006). To determine this arrival, we compare the annual variability of PDA maxima in the North and Middle Adriatic with the gravity current events observed in the dSAP. To do so, we used PDA derived from conservative temperature (CT) and absolute salinity (SA) (which are calculated using Copernicus T and S data, see fig. 3.5) for the entire Adriatic Sea and determined the area where the NAdDW formed and the date of the PDA maximum. We considered a two-week centered mean around this date for the North-Middle Adriatic surface waters with a threshold of

$$\langle \mathrm{Max(PDA)} \rangle_{15} > 29.75 \ \mathrm{kg\,m^{-3}} \tag{3.2}$$

minimum water PDA to be able to reach the dSAP, which is the minimum value registered at the E2M3A bottom ventilation years as will be discussed in the next paragraphs.

Results show that a gravity current event is detected in the pit when this criterion (eq. (3.2)) is verified. Several years meet this criterion: 2012, 2017, 2018 and 2022 (bottom ventilation years) and 2013. These results are consistent with Neri et al. (2022) who found NAdDW signatures with PDA values above 29.2 at bottom depth (between 40 and 60 m) at the sampling station SG05 (about 30 km from the coast near Senigalia) during the winters of 2012, 2017 and 2018. During these years, most of the water column was characterized by pools of waters with S above 38.5. In addition, Mihanović et al. (2018) reported a maximum of PDA around mid-February in 2012 along the western Adriatic shelf, a result consistent with table 3.2.

Nevertheless, the reduction in the density of the NAdDW due to mixing on the way south also plays an important role in the cascading of gravity currents in the dSAP. Therefore, an estimate of this reduction was made for bottom ventilation years (table 3.2 and fig. 3.4), which in 2012 amounted to 1.18 $\mathrm{kg\,m^{-3}}$, 0.83 $\mathrm{kg\,m^{-3}}$ in 2017, 0.56 $\mathrm{kg\,m^{-3}}$ (minimum value) in 2018 and 0.76 $\mathrm{kg\,m^{-3}}$ in 2022. Looking at the moving centered average of the speed with a window of 7 days (not shown here) at the current meter at E2M3A (fig. 3.2), it can be seen that the highest values correspond to years with bottom ventilation, with the minimum at 13.89 $\mathrm{cm\,s^{-1}}$, which corresponds to the value for the minimum density reduction found in 2018. Other bottom ventilated years depict higher velocities, such as 17.98 $\mathrm{cm\,s^{-1}}$ in 2017 and 15.65 $\mathrm{cm\,s^{-1}}$ in 2022. This indicates that the higher the turbulence level and mixing, the higher the speed in the dSAP.

The dense water formed during the bottom ventilation years also varies in its physical properties (table 3.2). While in 2012 a rather low θ value (5.80 °C) and a high S value (38.68) defined the water mass at the time and place of maximum PDA formation, in 2017 and 2022 salinity played a more important role (38.65 and 38.83 respectively and θ around 9 °C). In 2018, the situation between the two parameters as driving factors is more balanced. Potential temperature of 7.11 °C is between the values of 2012 and 2017/2022 with the lowest S value among the 4 bottom ventilation years (38.12). This observation agrees with Supić and Vilibić (2006) who stated that some years are dominated by either

low T or high S values, but there are also years when the situation is more complicated and both parameters contribute.

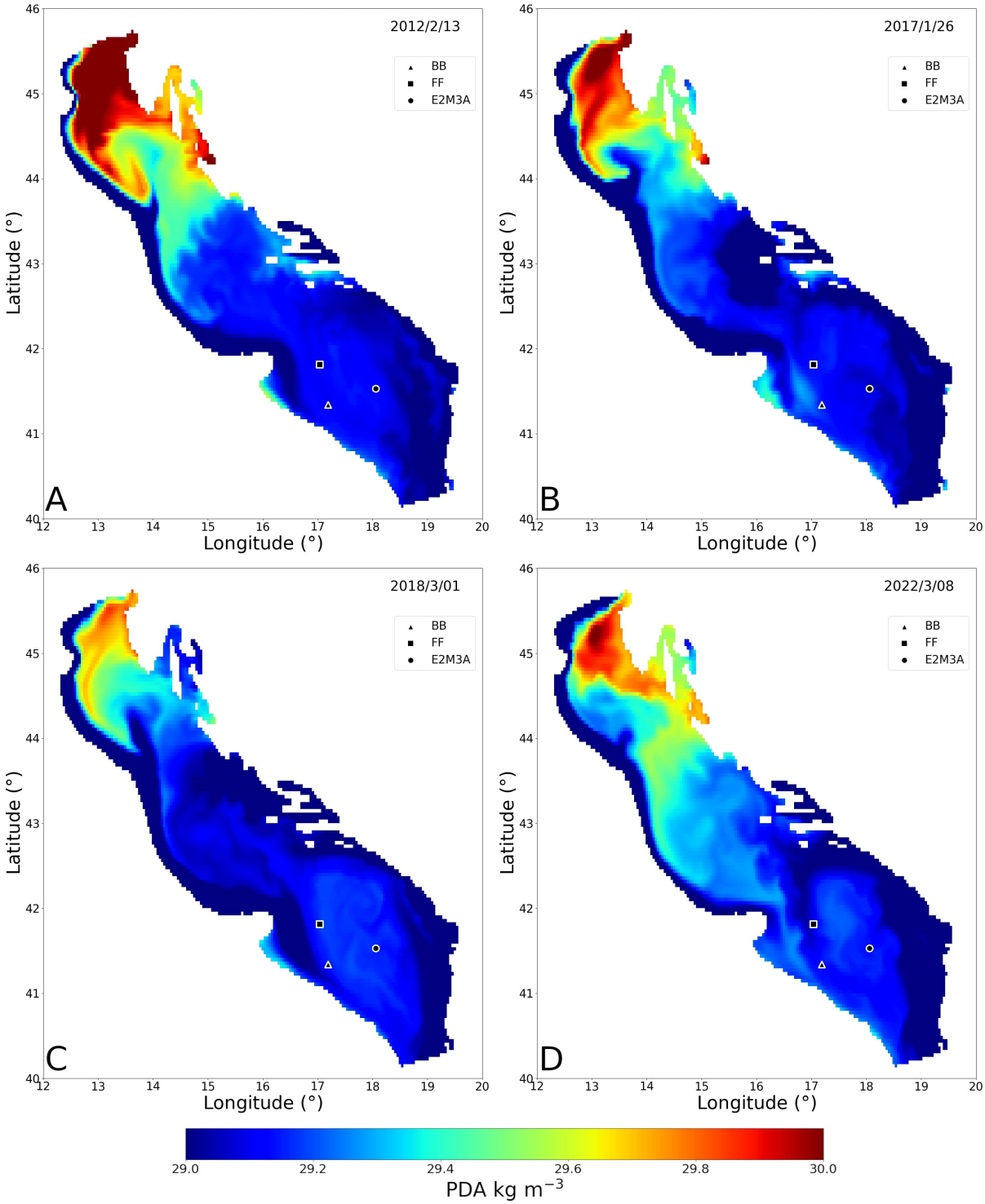

Figure 3.5: PDA map for dates when PDA is maximum in North and Middle Adriatic, for the bottom ventilation years: 2012 (**A**), 2017 (**B**), 2018 (**C**) and 2022 (**D**). We observe PDA values up to 30 kg m^{-3} and a tendency of the highest PDA to be located in the northernmost part of the Adriatic Sea. Due to the cyclonic circulation, dense water at the surface moves southward on the western side.

Winter	Date of Max	Max θ (°C)	Max S	Max PDA ($\mathrm{kg\,m^{-3}}$)	$\langle \mathrm{Max(PDA)} \rangle_{15}$
2011/2012	13/02/2012	5.80	38.68	30.50	30.41
2012/2013	23/03/2013	9.95	38.91	30.02	29.90
2013/2014	16/01/2014	12.90	38.51	29.14	29.08
2014/2015	08/03/2015	9.97	38.21	29.47	29.44
2015/2016	02/02/2016	10.74	38.45	29.524	29.50
2016/2017	26/01/2017	9.25	38.65	30.11	30.04
2017/2018	01/03/2018	7.11	38.12	29.86	29.75
2018/2019	26/02/2019	9.89	38.42	29.65	29.61
2019/2020	29/02/2020	11.93	38.78	29.55	29.52
2020/2021	16/02/2021	9.18	38.41	29.76	29.70
2021/2022	08/03/2022	9.40	38.83	30.05	30.03

Table 3.2: Maximum of densities in the North / Middle Adriatic for the different winters, with the corresponding salinities and potential temperatures. Bottom ventilation years are highlighted in green. The averaged daily maximum of PDA over 15 days centered on the maximum of PDA for the winter period.

Dense water formation is driven by heat loss and the preconditioning phase of the water column. We investigate the influence of these factors on the formation of NAdDW, firstly calculating the monthly average values of the integrated surface heat fluxes for the North, Middle, and South Adriatic fig. 3.6 and 3.7 (delimitation of these three regions is shown in the Appendixes B.2, B.3 and B.4). In the following, we determine the annual variability of spatially and monthly integrated surface heat fluxes by normalizing it, taking into account all available data sets (1979-2022) from ERA-5 (Hersbach et al., 2018; Herbasch et al., 2020). We define $\langle Q_m \rangle$ the average over all the years of the surface heat flux for the month m:

$$\widetilde{Q}_m = -\frac{Q_m - \langle Q_m \rangle}{\langle Q_m \rangle}. \tag{3.3}$$

Secondly, monthly average values of salinity values integrated over the upper 10 m (fig. 3.7) and over the whole water column (B.6) are also derived for the North Adriatic.

The analysis of the time series show that in 2012 strong heat losses occur ($-5 \cdot 10^8$ $\mathrm{W\,m^{-2}}$) (fig. 3.6) in February as compared to other years of our dataset (fig. 3.7). At the same time, high saline waters fill the surface layer in the North Adriatic especially in January and February (37.9 and 37.8 respectively) (fig. 3.7) leading to the formation of very dense waters with a maximum observed on the 13/02/2012 (table 3.2). Mihanović et al. (2013) and Janeković et al. (2014) showed that the increase of 0.3 in S during the preconditioning of the water column in the North Adriatic (summer-autumn 2011) was one of the main factor that trigger the 2012 event.

In 2017 and after, the oceanographic condition of the Adriatic changed due to an overall

increase of S as mentioned in Amorim et al. (2024). Regarding the North Adriatic, that year's strongest integrated heat loss with a value of $-6 \cdot 10^8$ W m^{-2} took place in January (fig. 3.6) and exhibits the maximum value among all Januaries of the period considered (fig. 3.7). Salinity values are also among the highest (with a mean value greater than 38.3 on the whole water column in January (B.6) and nearly 37.9 for the upper 10m (fig. 3.7)). These results explain the high PDA values we observe in January 2017 in table 3.2 with a maximum on the 26/01/2017 in the Northern Adriatic of 30.11 kg m^{-3}.

In 2018, as already mentioned, the situation is more balanced. We observe relatively low S values in the North Adriatic compared to the other years (fig. 3.7). As for the winter period, the beginning was characterized by strong heat losses ($-4 \cdot 10^8$ W m^{-2}, fig. 3.6) in December, no significant losses in January and a subsequent strong loss ($-3.7 \cdot 10^8$ W m^{-2}, fig. 3.6) in February. The latter destabilized the water column, which was already less stable due to the intrusion of high saline water in early 2017, as shown by Amorim et al. (2024). The combination of these conditions could explain that the high density water (table 3.2) triggered the gravity current observed this year in the deepest part of the pit, where the highest density value was observed at the end of April (fig. 3.4).

Winter 2022 can be considered a very mild winter for the North Adriatic, as there are no strong losses compared to the other years (positive normalized values, fig. 3.7) (fig. 3.6). However, in contrast to the other years analyzed above, very strong heat losses events occurred in December and January in the Middle Adriatic ($-5.9 \cdot 10^8$ W m^{-2} and $-4.8 \cdot 10^8$ W m^{-2} respectively, fig. 3.6). In terms of salinity, the winter months in the north have the highest value for the entire water column compared to all years, with a mean value around 38.45 (B.6). This high amount of salt in the water column leads to PDA = 30.03 kg m^{-3}, which is among the highest observed during the bottom ventilation years (table 3.2). The strong heat losses in the Middle rather than in the Northern Adriatic could explain the observation of gravity currents in the pit earlier than in the other years (19/02/2022).

Figure 3.6: Q_{tot} monthly integrated for the winter period (from December to March) in the North (**A**), Middle (**B**) and South (**C**) Adriatic from winter 2011/2012 to winter 2021/2022. Strong heat losses will be present during strong winters (January 2017 for example) and may induce generation for very dense waters. Strong heat losses at the beginning of the winter period will allow a strong preconditioning of the water mass.

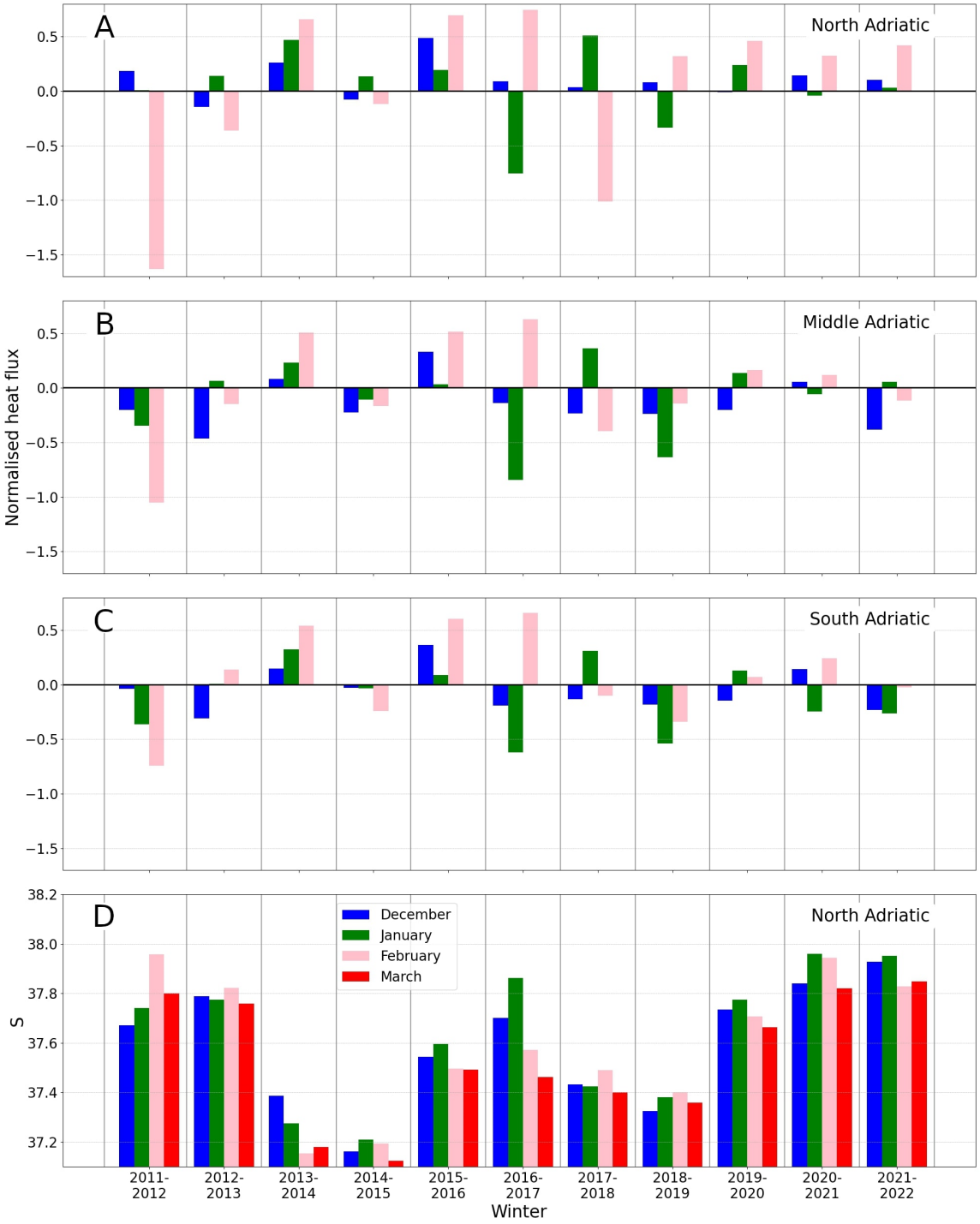

Figure 3.7: Total surface heat flux monthly normalized for the winter period (December to February) in the North (**A**), Middle (**B**) and South (**C**) Adriatic from winter 2011/2012 to winter 2021/2022 and salinity monthly average for winter period (December to March) in the North Adriatic from winter 2011/2012 to winter 2021/2022 (**D**). The normalization for (**A**), (**B**) and (**C**) is done monthly with eq. (3.3) considering the period 1979/2022. Strong negative values in February 2012 as well as in January 2017 and February 2018, mean that, considering all the Januaries of Februaries from 1979 to 2022, these were particularly strong. For (**D**) salinity is average over the 10 upper meters of the water column. High values of S, as during winter 2021/2022, may favor the formation of very dense water.

3.3.3 Time scale analysis

In this section, we first consider the typical time scales of the duration of the gravity current event at BB and at E2M3A. Secondly, we estimate the travel time and speed of the gravity current from the generation site in the North Adriatic to BB/FF and from BB/FF to E2M3A. Results are presented in table 3.3.

To determine the duration of the gravity current event, we use the ADCP data at BB. A gravity current is present when the observed speed V is greater than 0.17 $\mathrm{m\,s^{-1}}$, which corresponds to the average speed plus one standard deviation. We further consider speeds greater than 0.17 $\mathrm{m\,s^{-1}}$ along the down-slope axis (V_c). This threshold can be justified considering the study of Paladini de Mendoza et al. (2022a) where it was observed that the passage of gravity currents in FF or BB are marked by a decrease of water temperature and/or high salinity values which is more important for velocities greater than 0.17 $\mathrm{m\,s^{-1}}$. The beginning of bursts of fluctuations in the dSAP was defined as the time when η_ρ exceeds two times σ_s, the standard deviation of fluctuations during non-bottom ventilation years.

The speeds recorded at BB along the down-slope axis (fig. 3.8 **B**, **C**, **D** and **E**) exhibit regimes formed by a series of pulses or consisting of isolated points, which are in the following neglected, (section 3.2.1.3) to determine the beginning and the end of the pulse regime in the speed time series (fig. 3.8 and table 3.3). The results show that pulses end earlier in 2018 and 2022 (mid-May) than in 2012 and 2017 (beginning of June) (table 3.3) which lead to an average duration of the pulses of 106 days during the bottom ventilation years (table 3.3). Moreover, we determined the average travel time between BB (FF) and E2M3A, using bursts of fluctuations of PDA, of 15.5 days (14 days) (table 3.3). These results show, firstly, that the mean velocity of the gravity current from BB (FF) to the dSAP is on average of 0.057 $\mathrm{m\,s^{-1}}$ (0.078 $\mathrm{m\,s^{-1}}$) (table 3.3). Secondly, they show that the end of the cascading of gravity currents in the dSAP (and so the beginning of the relaxation period) ends no later than 29/06 in 2012, 20/06 in 2017, 01/06 in 2018 and 02/06 in 2022. Considering the average time travel observed between BB and E2M3A, these values are consistent with those of Martellucci et al. (2024), who mentions an outflow of NAdDW from the Bari canyon toward the SAP usually in spring from March to June. These values indicate then that the duration time of bursts of fluctuations in the dSAP varies from 58 days in 2018 to 111 days in 2012 (table 3.3) which is also consistent with the fact that among bottom ventilation years, 2018 is the year when the less dense water was formed in the North (table 3.2). We observe that in 2017 and 2018 the duration of pulses at BB is greater than the duration of bursts of fluctuations in the dSAP (table 3.3). The opposite was true in 2022, which is explained by water passing though FF played a greater role in the renewal of the dSAP water mass (Appendix B.1) and pulses began earlier there (10/02, not shown here).

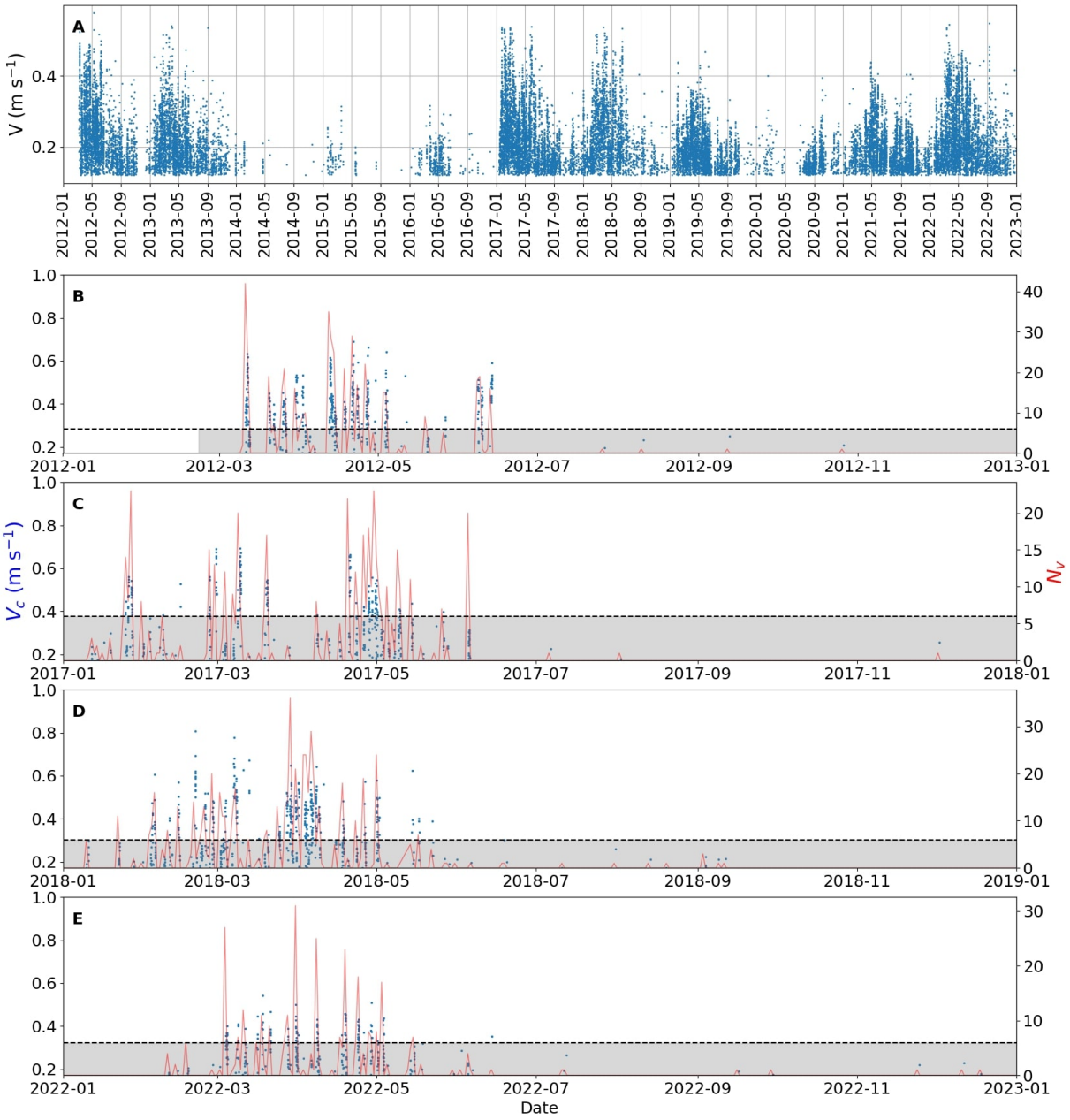

Figure 3.8: (**A**) Speed at BB mooring, only considering values above the threshold of 0.17 m s^{-1}. Down-slope velocities above 0.17 m s^{-1} for (**B**) 2012, (**C**) 2017, (**D**) 2018, and (**E**) 2022 (bottom ventilation years) are shown in blue. For (**B**), (**C**), (**D**), and (**E**) the daily number of speed greater than 0.17 m s^{-1} is shown in red (section 3.2.1.3). We consider days when the number of values N_v is greater than 6 for the detection of the beginning and the end of the gravity current event.

During bottom ventilation years, the minimum travel time from the formation site in the North Adriatic to the dSAP (interval between the date of the PDA maximum in the North Adriatic and the date of the start of the bursts of fluctuations at E2M3A) ranges from 25 days to 73 days, see table 3.2 and 3.3. However, in 2022, we obtain a negative value indicating that the start of the bursts of fluctuations in the dSAP is due to either dense water that formed well before 08/03/2022 (date of the PDA maximum, table 3.2) or dense water formed in the Middle Adriatic (see section 3.3.2 above). Assuming that the

maximum of the PDA at the formation site in the North Adriatic generates the maximum of the PDA in the dSAP, a more accurate travel time ranges from 52 days in 2018 to 99 days in 2017 (table 3.3) which is consistent with the order of magnitude of 2–4 months for the travel time from the North to the Southern Adriatic mentioned in the literature (Vilibić and Orlić, 2001, 2002; Rubino et al., 2012; Benetazzo et al., 2014). These travel times, lead to the velocity of the dense water masses (table 3.3) ranging from 0.083 $\mathrm{m\,s^{-1}}$ in 2012 to 0.16 $\mathrm{m\,s^{-1}}$ in 2018.

	2012	2017	2018	2022
Arrival time at BB	ND before March	24/01/2017	22/01/2018	05/03/2022
End of pulses in BB	13/06/2012	05/06/2017	17/05/2018	15/05/2022
Pulses duration at BB (days)	ND before March	132	115	71
Beginning - E2M3A	09/03/2012	09/04/2017	04/04/2018	19/02/2022
Fluctuations in E2M3A (days)	111	72	58	102
Date of maxima of PDA North	13/02/2012	26/01/2017	01/03/2018	08/03/2022
Date of maxima of PDA BB	03/05/2012	20/04/2017	07/04/2018	ND
Time travel North-BB (days)	80	84	37	ND
Speed North-BB ($\mathrm{m\,s^{-1}}$)	0.093	0.089	0.206	ND
Date of maxima of PDA (SAP)	12/05/2012	09/05/2017	19/04/2018	19/06/2022
Time travel BB - E2M3A (days)	16	15	15	16
Time travel FF - E2M3A (days)	12	12	16	16
Speed BB - E2M3A ($\mathrm{m\,s^{-1}}$)	0.055	0.059	0.059	0.055
Speed FF - E2M3A ($\mathrm{m\,s^{-1}}$)	0.089	0.089	0.066	0.066
Minimal time travel North - E2M3A (days)	25	73	34	-18
Time travel North - E2M3A (BB/FF) (days)	96/92	99/96	52/53	ND

Table 3.3: Duration time of bursts at E2M3A and BB, travel times from the dense water generation site in the North to BB and from BB to E2M3A, as well as associated velocities.

Year	North ($m\,s^{-1}$)	Middle ($m\,s^{-1}$)	South ($m\,s^{-1}$)
2012	-0.016	-0.015	-0.031
2017	-0.015	-0.023	-0.035
2018	-0.032	-0.034	-0.038

Table 3.4: Mean value of projected northward velocities along the Adriatic axis (V') in the near bottom (15-25 cm above the bottom) for areas on the western side of the North, Middle, and South Adriatic in 2012, 2017, and 2018. These values represent the ambient velocities to which the gravity current is submitted. They were determined for the period corresponding to the gravity current event (from the time of maximum PDA in the North to the time of maximum in BB) in 2012, 2017, and 2018. 2018 appears to be the year with the highest southward velocities.

In the literature, Vilibić and Orlić (2001) mentioned a time of two months for the arrival of the NAdDW near Bari, which means a velocity of $7-8$ $cm\,s^{-1}$ (a value also mentioned by Hendershott and Rizzoli (1976)). However, as showed by Vilibić (2003) in his study around the Palagruza Sill, the NAdDW current can be very variable and reach velocities of up to 20 $cm\,s^{-1}$ in the southeast. This variability in NAdDW velocity was also mentioned by Benetazzo et al. (2014), who found a NAdDW velocity in the order of 30 $cm\,s^{-1}$ when leaving the northern basin in the early stage of formation and 9 $cm\,s^{-1}$ on average after this early stage. Another hypothesis for the short time travel in 2018 is a higher ambient velocity of the water masses, to which the gravity currents is submitted on its way southward. To investigate this feature, maps of the difference in 7-day mean projected meridional velocity along the Adriatic axis in the near bottom ($15-25$ m above the bottom) (V') between 2018 and the other bottom ventilation years (not shown here, see Appendix B.8 for the difference between 2018 and 2017). We observed higher V' values southward in 2018 explaining the higher dense water velocity observed. This result is confirmed by table 3.4 and Appendix B.7, which take into account the three areas on the western part of the Adriatic Sea sub-basins for 2012, 2017 and 2018 in the near-bottom region, and which depict higher ambient velocities in each basin in 2018 as compared to the other years.

3.3.4 Mixing ratio

The water masses in the dSAP after a bottom ventilation event are a mixture of intruding waters, mainly through BB and FF, and the water present before the event (see section 3.2.1.2). If the mixing is due to turbulent motion of water parcels, the difference in the molecular diffusion coefficients does not matter and the mixing ratios of eq. (3.1) apply. The different water masses are presented in θ/S diagrams (fig. 3.9), and can be distinguished based on their thermohaline properties (see section 3.2.1.2). A mixing of water masses shown in this diagram leads to a new water mass consisting of the weighed combination of all water masses involved. Therefore, in our case, the water mass after the bottom ventilation event must lie within the triangle represented by the water mass at E2M3A before the fluctuation and the water masses at BB and FF (see section 3.2.1.2). In terms of eq. (3.1), this means that all ratios (R) lie in the interval $[0, 1]$ and their sum equals unity. This condition is satisfied by the thermohaline properties for all the bottom

ventilation years considered, i.e. 2012, 2017 and 2018 (no thermohaline data is present for 2022 at BB/FF) (fig. 3.9). This finding presents criteria 6, further indicating that a gravity current event is responsible for bottom ventilation.

In addition, it is interesting to note that for all the three years the θ/S properties differ. Indeed, the percentage of water mass originating from BB or FF involved in changing the properties of the deepest water mass at E2M3A differs between the different bottom ventilation events (fig. 3.9) with values ranging from 10% to 23% for BB in 2012 and 2017, respectively and from 12% to 48% for FF in 2018 and 2012, respectively. This means that in 2012 and 2018, the water mass involved in the change of the deepest waters of the dSAP passed mainly through FF, while in 2017 it passed mainly through BB. In 2022, in Appendix B.1, fluctuations seem to occur mainly at FF mooring, indicating that the water flowing into the pit came mainly from FF in that year.

In all three bottom ventilation years, we observe an increase in density due to gravity currents (fig. 3.9). This increase is 1×10^{-2} kg m^{-3} in 2012, 5×10^{-3} kg m^{-3} in 2017 and 1.2×10^{-2} kg m^{-3} in 2018. Considering the period studied, for which the density has a variability of -0.1 kg m^{-3}, this means that the density changes are of 10%, 5% and 12% of the total variability in 2012, 2017 and 2018 respectively, and they are opposing the general trend (increasing in density, fig. 3.3). These changes are non-negligible, because in order to reach the bottom, the density of the water mass transported by the gravity current has only to be slightly superior to the water mass in place. The information about potential temperature and salinity shows which variable was the driver for the gravity current. In 2012, we observed a decrease in S and θ by almost 2.5×10^{-2} and 0.13 °C, respectively, suggesting that temperature was the driver of the gravity current. In contrast, 2017 shows an increase in both S and θ by almost 4×10^{-2} and 0.14 °C, respectively, suggesting that salinity is the driver. In 2018, we observed both a decrease in θ by about 1×10^{-2} °C and an increase in S by about 1.5×10^{-2} °C (fig. 3.9). This year, the change in water mass properties is almost perpendicular to the isopycnals, which leads to a significant increase in density. In 2012 and 2017, the change was mostly along the isopycnals, the former exhibiting a decrease and the latter an increase in spiciness.

The intrusion of the water transported by the gravity current into the dSAP is mainly turbulent, since no replacement of the previous water mass was found. This is evidence by the substantial value of R_b for all three bottom ventilation events. Furthermore, for the different bottom ventilation years, the change vector at 1200 dbar at E2M3A before and after the fluctuations is close to the vector at 1000 dbar at E2M3A and almost perpendicular to the vector defined by the difference of these two water masses before the fluctuations (fig. 3.9). This means that the mixing between the water masses at 1000 dbar and at 1200 dbar, which would lead to a variation along the initial water masses differences, is small.

A θ/S diagram also provides information that helps to exclude convection being responsible for the change of water mass properties in the dSAP as seen on fig. 3.9, where the point corresponding to the water mass after the bottom ventilation at 1000 dbar has a lower density than the point corresponding to the same situation at 1200 dbar for all three years. This means that convection, which homogenizes the water masses in the vertical, is not involved here and that the dSAP is ventilated by gravity currents.

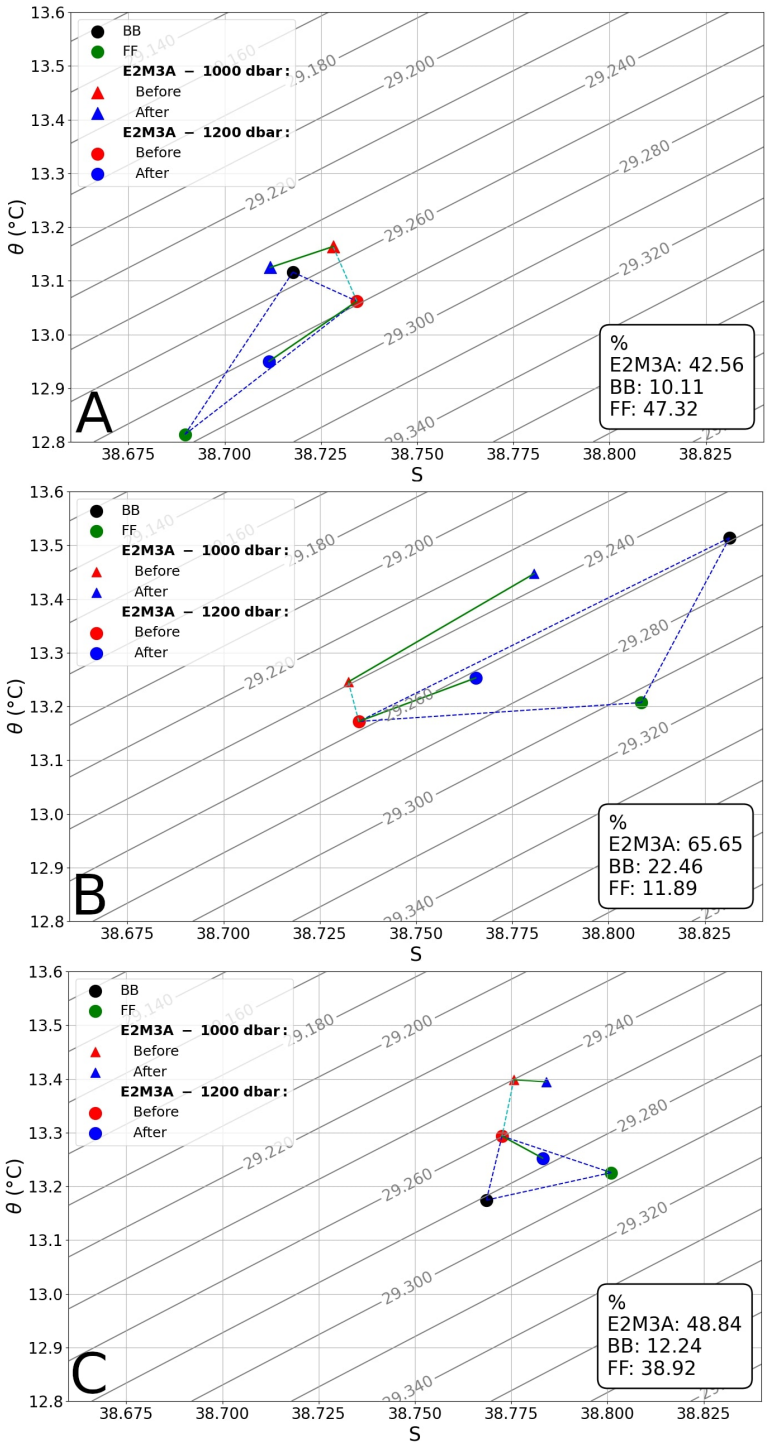

Figure 3.9: θ/S diagrams at E2M3A, at 1000 and 1200 dbar, for the bottom ventilation years recorded: 2012 (**A**), 2017 (**B**) and 2018 (**C**). Isopycnals are represented by the contour lines. The point representing the situation at 1200 dbar after the fluctuation (blue point) is within the triangle defined by the water mass coming from BB (black point), the water mass coming from FF (green point) and the water mass before the fluctuation (red point) for the different bottom ventilation years. The difference between the two depths (1000 and 1200 dbar) is almost perpendicular to their respective changes in water-mass properties.

3.3.5 Detection of gravity currents using Copernicus reanalysis

The observation of gravity currents through the Copernicus reanalysis is subject to the performance of the model to detect mesoscale processes. To compare E2M3A Lagrangian observations and Copernicus Eulerian results, we derive 15 point average of Copernicus PDA around E2M3A position (fig. 3.10). Results show that bursts of fluctuations are not well represented in the Copernicus reanalysis as no significant event is reported during bottom ventilation years by the fluctuation index (fig. 3.10). Furthermore, the correlation coefficient between the two time series is equal to 0.24 (and 0.13 for a weekly average) which indicates that this model does not have a vertical resolution high enough to detect gravity currents cascading to the dSAP, see Laanaia et al. (2010). During bottom ventilation years, we can observe fluctuations on the Copernicus reanalysis, but, considering the whole time series, they are not significant in terms of the fluctuation index (see fig. 3.10 a). Nevertheless, as presented in fig. 3.11, potential temperature and salinity of the Copernicus reanalysis follow the general trend of E2M3A time series. For the horizontal velocities, the amplitudes in the Copernicus reanalysis are typically 5 times smaller and gravity currents are not discernible. The reanalysis poor results depicted in fig. 3.10 are due to a next to compensation of the influence of potential temperature and salinity when density is considered and a deficiency of the Copernicus data to capture high frequency (weekly) changes. Today's fine resolution numerical models of the Adriatic do not allow sufficient resolution to represent the topographic features important for the dynamics of a gravity current and its non-linear dynamics.

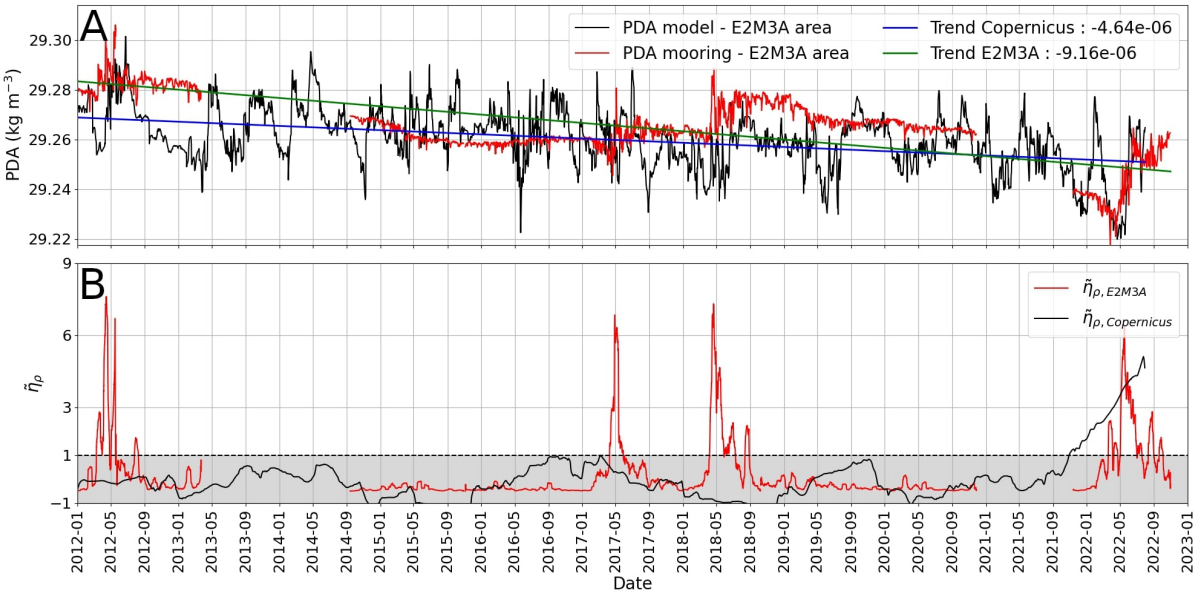

Figure 3.10: Comparison of the daily averaged between the Copernicus reanalysis and E2M3A mooring of the PDA time series (**A**) and the comparison of the fluctuation index (**B**).

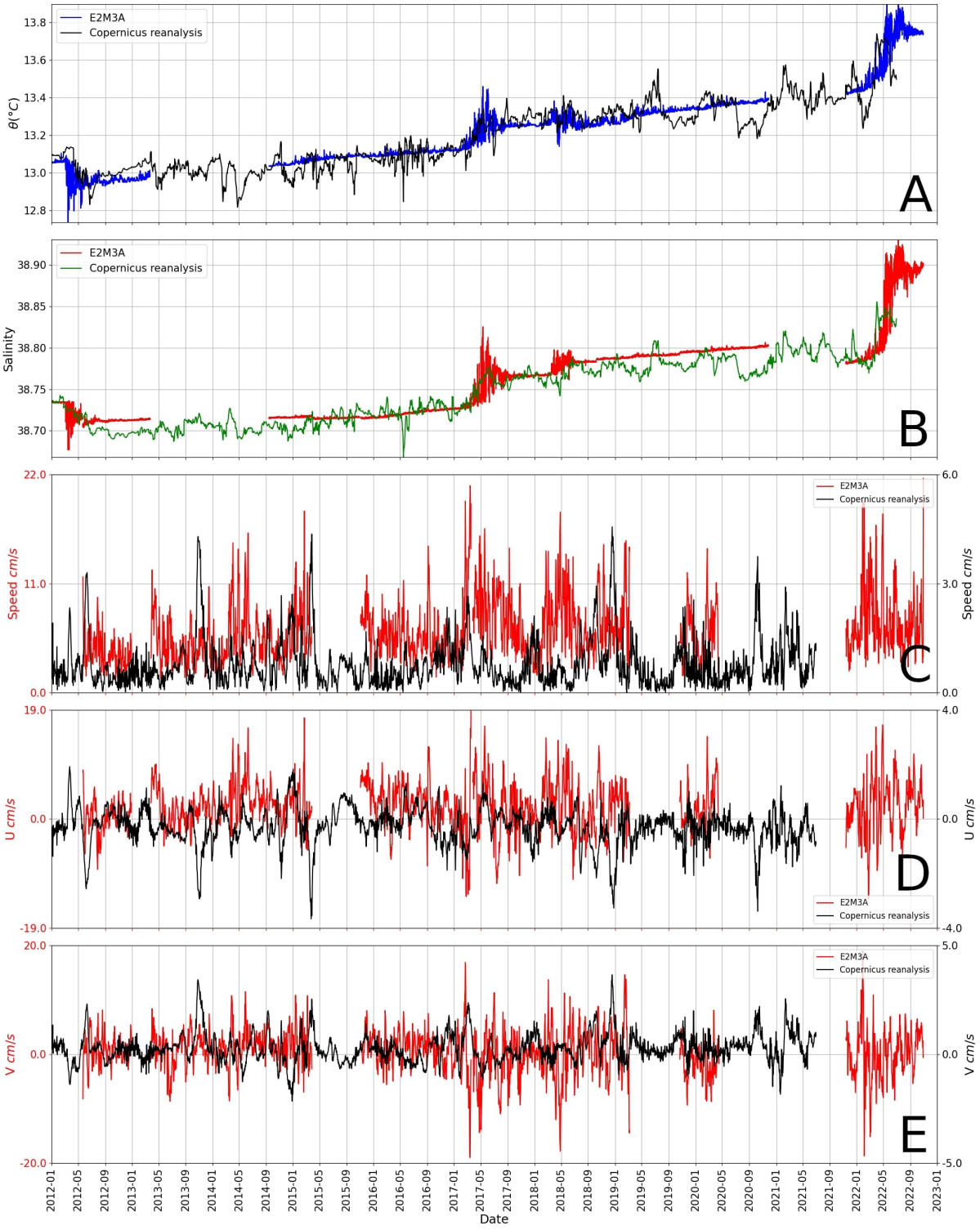

Figure 3.11: Comparison of θ (**A**), S (**B**), Speed (**C**), zonal component of velocity u (**D**) and meridional component of velocity (**E**) for E2M3A and the Copernicus reanalysis. For θ and S the general trend is well captured by the reanalysis. Differences appear for the speed and the components of velocity, where strong fluctuations observed on Copernicus reanalysis time series are absent from E2M3A observations

3.4 Conclusion

We presented a comparison of three moorings (E2M3A, BB and FF) CTD and velocity data as well as reanalysis from Copernicus to determine that gravity currents reached the dSAP in 2012, 2017, 2018 and 2022. This result is based on six criteria (see table 3.1) applied during the period 2012-2022. We found an almost perfect concordance of all criteria, as only during bottom ventilation years all criteria are satisfied for all available data (see table 3.1).

The definition of the fluctuation index ($\tilde{\eta}$), which determines the time interval during which the significant fluctuations occur, made it possible to show a consistency between, firstly, the detection at the three moorings, since events reported in BB/FF are followed by events at E2M3A, and secondly, the different criteria based on data studied when considering only the dSAP. The latter have linked bursts of fluctuations in density ($\tilde{\eta}_\rho > 1$, first criteria) and oxygen ($\tilde{\eta}_O > 1$, second criteria), proving that ventilation has taken place. Apart from the fact that the fluctuation index for moorings BB and FF must be satisfied, the normalized density difference should be significantly small (less than 1) to assume that the observed bursts of fluctuation are the result of the passage of a gravity current from the same source region. We observed that the years that meet the fluctuation index all meet this condition (third criteria). The dense water that flowed in BB or FF did not necessarily lead to bursts of fluctuations in the dSAP, even if their density difference was small, but rather in the upper layers of the pit (900 dbar and 1000 dbar) or even not at all. This means that the water transported by the gravity currents must be denser than the water already present in the dSAP (fourth criteria). The definition of the density threshold of 29.75 $\mathrm{kg\,m^{-3}}$ using the Copernicus reanalysis on the North Adriatic (fifth criteria) represents the minimum density of the NAdDW to reach the dSAP. Furthermore, the analysis of θ/S diagrams provides valuable information on the mixing ratio between the water masses of the three moorings. The thermohaline properties of the water masses in the dSAP after the bursts of fluctuations show to be differently mixed among bottom ventilation years, with different contributions from BB and FF. The θ/S diagram shows that 2012 was mainly driven by potential temperature, while 2017 was mainly driven by salinity. The year 2018 seems to be influenced by both salinity and potential temperature. It was also found that in 2012 and 2022 the gravity current was mainly passing though FF, on the open slope North of the Bari canyon. Furthermore, we found that the water transported by the gravity current is mainly turbulent since no replacement of water masses took place in the dSAP and that convection cannot be responsible for the change in water mass properties in the dSAP, as the bottom density is greater than density at 1000 dbar after the bottom ventilation.

The combination of all criteria was only met for the bottom ventilation years (2012, 2017, 2018 and 2022), but among other years some are characterized by a gravity current event when the water density was not high enough to reach the dSAP (2015, 2016, 2019 and 2021). It was also found that 2013 also satisfied the fifth criteria. Furthermore, in 2013 and 2019 the criteria on the difference in density between BB and FF is satisfied, but this can also be achieved without a gravity current.

NAdDW formed during bottom ventilation years and with PDAs greater than 30 $\mathrm{kg\,m^{-3}}$ were generated by the same forcing that drive gravity current in the dSAP. In 2012, potential temperature was the main driver of NAdDW formation, while in 2017 and 2022 it was salinity. In 2018 both potential temperature and salinity were involved in the NAdDW formation. The bottom ventilation years were also characterized by strong integrated

heat losses that triggered the formation of this water (fig. 3.7).

The time scale analysis, taking into account both the ADCP and PDA time series (2012-2022), revealed firstly that the duration of speed pulses in BB is a few months (from late January to May), leading to an average duration of bursts of fluctuations in the dSAP of a few months (from March to June) for all the bottom ventilation years. Second, the time travel from the generation of NAdDW to BB was found to be 80, 84, and 37 days in 2012, 2017, and 2018, respectively, implying that the speed of the gravity current varies from year to year. A tentative explanation for the short travel time in 2018 is the higher south-eastward ambient velocity on the west coast of the Adriatic as compared to the other bottom ventilation years (on average 0.04 $\mathrm{m\,s^{-1}}$ in 2018 and 0.02 $\mathrm{m\,s^{-1}}$ in 2012 and in 2017). After reaching BB (FF), the travel time to the dSAP is around two weeks, which corresponds to an average speed of 0.06 $\mathrm{m\,s^{-1}}$ (0.08 $\mathrm{m\,s^{-1}}$).

Finally, the comparison between the Copernicus reanalysis and the E2M3A PDAs time series for the dSAP show consistent differences in both value and variability. The former does not clearly detect gravity current events during bottom ventilation years (fig. 3.10), which is certainly due to a low vertical resolution of the numerical model employed. Nevertheless, temperature and salinity time series of both datasets are similar and show the same trend, suggesting that the density compensation, emphasizing small differences in T and S between observations and the reanalysis, leads to significant differences in the PDAs.

Our results show that the stratification and ventilation of the dSAP are determined by the competition between small-scale mixing, which has a homogenizing effect, and intermittent gravity currents, which have a restratifying and ventilating effect (see also (Querin et al., 2016; Cardin et al., 2020b)). Both processes are strongly influenced by small-scale turbulent dynamics. While the former is continuous and local, the latter is intermittent, almost singular in space and time and also strongly dependent on small-scale topographic features and remote forcings. Parameterization exist to represent the former in digital twins or avatars of the ocean, while the latter is more difficult to capture. The dSAP is thus an example of a long-term, large-scale climatic evolution that depends on small-scale short-term processes that need to be investigated using high-frequency long term observational data.

This study highlights how high frequency measurements of physical and biogeochemical parameters of the South Adriatic EMSO regional facility are necessary in the perspective of observing mesoscale and submesoscale processes that affect the circulation of the Adriatic Sea and in term the general Mediterranean overturning circulation.

Acknowledgments

This work benefited from data produced and collected by the OGS- EMSO South Adriatic Site, an EMSO IT Joint Research Unit and the EMSO-ERIC Site. The authors would like to thank the PHYS group, the TEC group and the CTMO of the OGS and the CNR-ISP for their valuable support and work in maintaining the EMSO-SA site regional facility and their valuable help in realizing this work. The results contain modified Copernicus Climate Change Service information 2020. Neither the European Commission nor ECMWF is responsible for any use that may be made of the Copernicus information or data it contains. This study has been conducted using EU Copernicus Marine Service Information and DOI links to data used in this study.

Funding

The author(s) declare that financial support was received for the research and/or publication of this article. This work was carried out within the framework of the cooperation agreement between EMSO-Italy and OGS/CNR-ISP to financially support the operation of the South Adriatic Regional Facility. Funding support was also given by the National Recovery and Resilience Plan of Italian Ministry of University and Research funded by EU – Next Generation EU Mission 4 "Education and Research" – Component 2: Project IR0000032 – ITINERIS, so as by a grant from the Ufficio Supporto alla Ricerca e Grant of CNR-Italy (CNR-USRG). OGS and CNR provided the ship-time to maintain the sites

Conflict of Interest Statement

The authors declare that the research was conducted in the absence of any commercial or financial relationships that could be construed as a potential conflict of interest.

Author Contributions

JM: Conceptualization, Data curation, Formal analysis, Investigation, Methodology, Software, Visualization, Writing – original draft, Writing – review & editing. AW: Writing – original draft, Writing – review & editing, Conceptualization, Investigation, Methodology, Supervision, Formal analysis. FM: Writing – original draft, Writing – review & editing. SM: Writing – original draft, Writing – review & editing. VC: Writing – original draft, Writing – review & editing, Conceptualization, Funding acquisition, Investigation, Methodology, Resources, Supervision, Formal analysis.

Data Availability Statement

The datasets presented in this study can be found in online repositories. The names of the repository/repositories and accession number(s) can be found in the article/Supplementary Material. Further inquiries can be directed to the corresponding author/s. Data are available at the National Oceanographic Data Center – NODC (`https://nodc.ogs.it`), at

the ISP ERDDAP Server (`https://bo.isp.cnr.it/erddap/index.html`), on the Copernicus marine data store (`https://data.marine.copernicus.eu/products`) and on the Copernicus climate data store (`https://cds.climate.copernicus.eu/datasets`).

Part IV

Microscale variability in the SAP in the context of a climate change

Extension of the closure problem to microscale dynamics

The analyses presented in the previous parts demonstrate how the dynamics governing the SAP operate across multiple scales. Basin-scale circulation determines the long-term trends of thermohaline and biogeochemical properties (part II), while mesoscale and submesoscale processes, such as convection, eddies, and gravity currents, organise ventilation, lateral exchange, and restratification (part III). However, although these scales describe the organisation of the flow, they do not close the system, as the mechanisms by which water masses are actually mixed and transformed operate at smaller scales.

For gravity currents, basin-scale dynamics determine their pathways from the northern Adriatic towards the SAP, while submesoscale dynamics shape their structure and interaction with the ambient flow. The exchange of heat and salt between the current and the surrounding water occurs at smaller scales, within shear-driven turbulence and boundary layers developing along the current interface and the topography. These processes control entrainment, diapycnal mixing, and, consequently, the impact of gravity currents on deep-water ventilation (Legg et al., 2009) (section 0.3.2).

Similarly, in areas where convection occurs, vertical exchange operates through fine-scale convective plumes, while the effective mixing of heat and salt depends on turbulence and molecular diffusion at the microscale (Marshall and Schott, 1999). Mesoscale, submesoscale, and fine-scale processes structure the circulation, while microscale mechanisms govern the transformation of water masses (section 0.3.1).

Among these microscale mechanisms, double-diffusive instabilities arise from the large difference in the molecular diffusivities of heat and salt and develop at the microscale (Stern, 1960; Marshall and Schott, 1999; Talley et al., 2011). In a water column stable with respect to mean density, such processes can sustain microscale convective motions, such as salt fingering, that enhance vertical exchange. Over time, this microscale mixing affects stratification, diapycnal fluxes, and water mass properties, thereby influencing the long-term thermohaline structure and ventilation of the SAP (chapter 4).

The changes observed in the SAP since 2017 suggest that the response of the system cannot be fully understood without considering microscale mixing processes. While basin-scale observations reveal a persistent decoupling between deep and upper layers (part II), and submesoscale analyses show the role of gravity currents (part III), modifications in the water column temperature and salinity gradients affect the dominant double-diffusive regime in the SAP. A shift in the double-diffusive regime would imply changes in microscale mixing efficiency, with consequences for stratification and long-term thermohaline evolution. This motivates a dedicated analysis of microscale processes in the following chapter, focusing on double-diffusive regimes.

Chapter 4

Tipping of the double-diffusive regime in the southern adriatic pit in 2017 in connection with record high-salinity values

This section is constituted by the article published in Ocean science in 2024:

F. L. L. Amorim, J. Le Meur, A. Wirth, and V. Cardin. Tipping of the double-diffusive regime in the southern adriatic pit in 2017 in connection with record high-salinity values. Ocean Science, 20(2):463–474, 2024. doi: 10.5194/os-20-463-2024.

Abstract: In double-diffusive mixing, whenever salinity and temperature decrease with depth, the water column is either unstable or predisposed to a state called salt fingering (SF), which exhibits increased vertical mixing. Analysis of a high-frequency time series of thermohaline data measured at the EMSO-E2M3A regional facility in the southern Adriatic Pit (SAP) from 2014 to 2019 reveals that in the south Adriatic, SF is the dominant regime. The same time series shows the presence of a very saline core of the Levantine Intermediate Water that penetrated with unprecedented strength during the winter of 2016/17 at around 550 dbar and even higher-salinity water above. The effect of strong heat loss at the surface during that winter allowed deep convection to transport this high-salinity water from the intermediate to the deep layers within the pit. This resulted in an increased predisposition to SF throughout the water column. In the subsurface layer (350 to 550 dbar) the increase is from 27% to 72% of observations. We observe an alteration of vertical stratification throughout the water column during the winter of 2016/17 from a stratified water column to an almost homogeneous water column down to 700 dbar , with no return in the following years.

4.1 Introduction

The southern Adriatic Pit (SAP) is an important deep-water formation region. The formed dense waters in the area enter the eastern Mediterranean bringing oxygenated cold water to deeper layers. The stratification is altered by convection, gravity currents,

lateral intrusions from neighbouring basins and double-diffusive mixing. The first two are intermittent strong events, while the last one is continuous with varying magnitude. During winter, vertical convection can occur, destroying density barriers throughout the water column. These combined processes allow efficient mixing and exchange of properties between the upper, intermediate and sometimes also the deep layers, resulting in changes in the properties and stability of water characteristics (Leaman and Schott, 1991; Leaman, 1994; Mertens and Schott, 1998; Vilibić and Orlić, 2002; Cardin and Gačić, 2003; Cardin et al., 2011). Intermittent gravity currents bring cold water masses from the northern Adriatic to the deep parts of the SAP, a process that is affected by topographic canyons and which restores the bottom-to-surface density difference (Chiggiato et al., 2016). The water mass characteristics in the southern Adriatic lead to a predisposition to the double-diffusive salt finger process (SF; the temperature stratification is stable, while the haline stratification is unstable) because of the warm and salty Levantine Intermediate Water (LIW) overlying the colder and fresher deep Adriatic water (AdDW). Indeed, double-diffusive convection occurs in the ocean when either the temperature or salinity-induced stratification is statically unstable, while the overall density stratification is statically stable (Stern, 1960). The potential energy bound in the un stable component is released by molecular diffusion, which is 100 times faster for heat than for salt (Stern, 1960; Schmitt, 1994; McDougall et al., 1988) describe the vertical stratification in terms of the following stability regimes: SF, diffusive convective (the temperature stratification is unstable, while the haline stratification is stable), doubly stable and statically unstable. According to You (2002), large areas of the world's oceans are favorable to double diffusion, including the Mediterranean and the Adriatic seas. Specifically, SFs have been observed in the Mediterranean Sea (Schmitt, 1994; Meccia et al., 2016; Menna et al., 2021), the Tyrrhenian Sea (Tait and Howe, 1968; Durante et al., 2019) and the Adriatic Sea (Carniel et al., 2008). Double-diffusion studies in the oceans typically use CTD profile transects acquired at high frequency (hours) but over a short period (days to weeks). They also provide a fine vertical resolution but are not able to depict a continuous evolution of double diffusion over several years. Durante et al. (2019) used a longer time series of CTD casts, and Menna et al. (2021) analyzed years of Argo data profiles in the Tyrrhenian and Ionian/Levantine seas, respectively, with the temporal resolution of the analyzed data ranging from weeks to months. Taillandier et al. (2020) used a combination of about 700 CTD and Argo float profiles collected from 2013 to 2017 to study thermohaline stair cases related to double diffusion in the western Mediterranean Sea. In this work, we examine high-frequency, long time data from the EMSO-E2M3A regional facility (`http://emso.eu/observatories-node/south-adriatic-sea/`, last access: 18 March 2024) that allow us to assess the temporal evolution of double diffusion over long timescales at high frequency (hours) but only at a coarse vertical resolution at a fixed horizontal location. Fine-scale double-diffusive stair cases typically extending $O(10\ \mathrm{m})$ vertically cannot be directly observed with our data, but vertical temperature and salt stratification leading to double diffusion can be observed. In the SAP, the saltier Levantine Intermediate Water (LIW) forms intrusive features (Vilibić and Orlić, 2001; Vilibić and Supić, 2005; Gačić et al., 2010). Double-diffusive mixing processes acting at the interfaces of these intrusions alter heat and salt transport, but turbulence levels must be sufficiently low for double diffusion to act (Lee et al., 2014). Cardin et al. (2020b) estimated a high vertical bulk diffusivity coefficient in the deep SAP (below the sill depth of 780 m) of $5 \times 10^4\ \mathrm{m^2\,s^{-1}}$ based on two types of data, i.e., 13-year time series of observational data (2006–2019) of temperature from the EMSO-E2M3A observatory and available vertical profiles (1985–2019) in the area. The

differences in the molecular diffusivity of temperature and salinity can enhance vertical mixing through double diffusion, resulting in effective large-scale (bulk) diffusivities on the order of 10^4 $m^2\,s^{-1}$ (Radko, 2013; Bryden et al., 1994). Even though this pro cess happens on molecular scales, it can affect larger spatial extents by mixing water mass properties. Double diffusion is particularly widespread in the main thermocline (Radko, 2013) and contributes to the vertical transport of heat, affecting the global climate due to the air–sea fluxes occurring in the sea surface. The prevalence of double diffusion in the upper ocean can enhance the mixing of nutrients, which directly controls biological productivity (Radko, 2013; Meccia et al., 2016). Despite their potentially important contribution to vertical mixing, there is no quantitative work that has investigated the evolution of double-diffusion regimes using continuous long-term datasets (multi-year) with a high frequency (hours to days). In this study, we describe the changes in double-diffusion regimes using time series data obtained from the EMSO-E2M3A in the SAP. A description of the observational data and applied methodology is provided in the following section while the analysis and discussion are presented in section 4.3. Conclusions are given in section 4.4.

4.2 Data and methods

The data used in this study were obtained from the EMSO south Adriatic deep observatory that is one of the regional infrastructures established at *"key environmental sites"* in European seas within the framework of the EMSO ERIC (European Multidisciplinary Seafloor and water column Observatory – European Research Infrastructure Consortium) network. The observatory consists of two sites: the first located in the center of the south Adriatic Pit, at depths of around 1200 dbar (E2M3A, 4.1), and the second on the western side of the escarpment (BB and FF). The data collected at the E2M3A site enable the monitoring of changes that can be linked to variations in the submesoscale, mesoscale and general circulation of the eastern Mediterranean Sea or, on a larger timescale, to the climate variability in the area, demonstrating the importance of high-frequency measurements to resolving events and rapid processes (Cardin et al., 2020b) as well as their long-term occurrence and modulation.

In recent years, the observatory has allowed monitoring of convective processes and the formation and arrival of dense water (crucial for oxygenation in the deep sea). The EMSO-E2M3A site (position 41.53 °N, 18.06 °E) has operated almost continuously since 2006 (Bensi et al. (2014); Cardin et al. (2015, 2018, 2020a); `http://emso.eu/observatories-node/south-adriatic-sea/`, last access: 18 March 2020). The EMSO-E2M3A dataset used in this study consists of potential temperature (θ) and salinity (S) data collected hourly at seven vertical levels (150, 350, 550, 750, 900, 1000 and 1200 dbar) ranging from November 2014 to October 2019; these dates were chosen to consider the longest period available between two maintenance cruises with calibration of instruments.

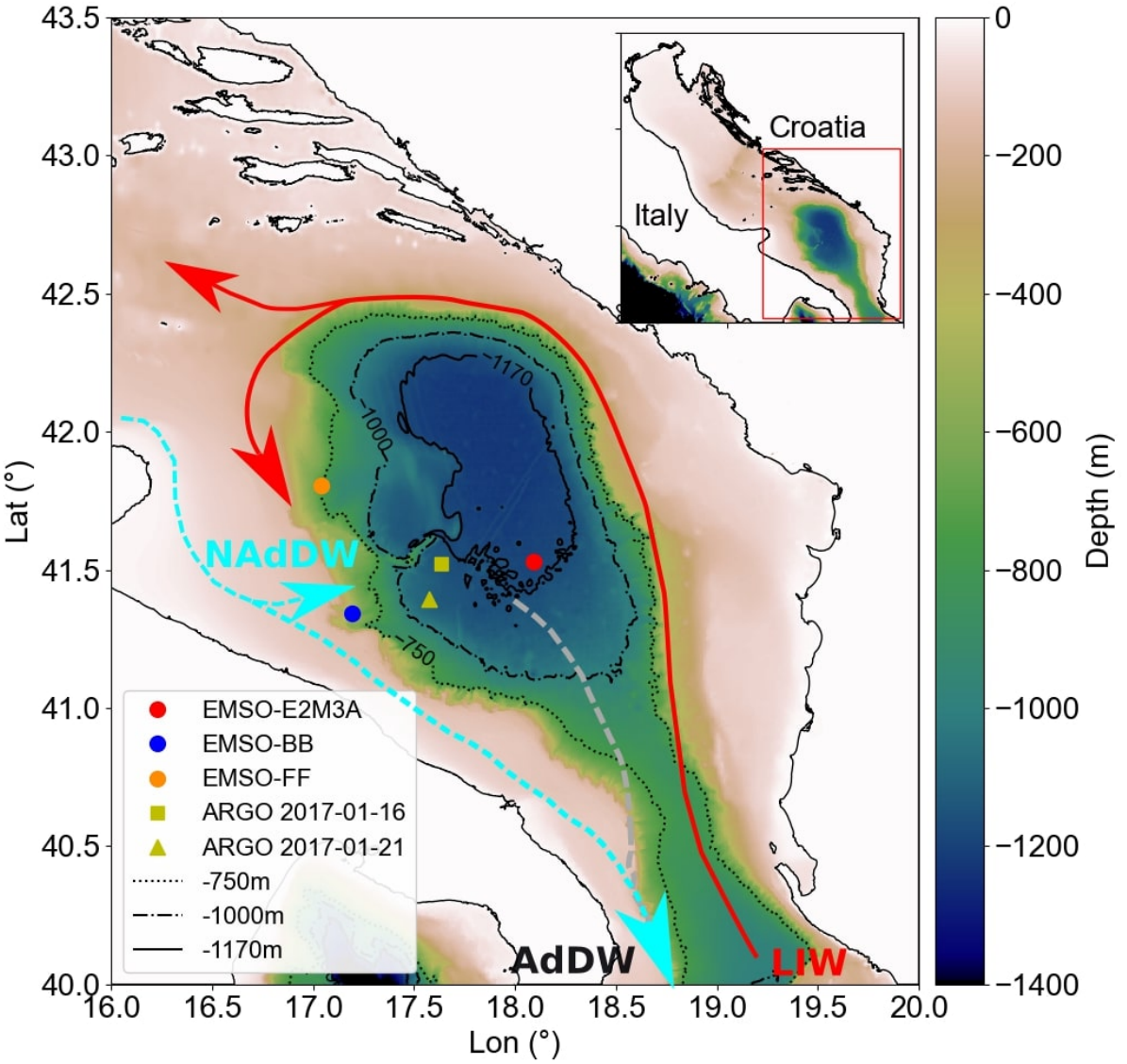

Figure 4.1: EMSO-E2M3A mooring location (red dot) in the South Adriatic Pit (SAP) at a depth of about 1200 dbar and Argo floats positions (yellow square and triangle), with the main water mass routes: Adriatic Deep Water (AdDW), Levantine Intermediate Water (LIW) and North Adriatic Dense Water (NAdDW). Other components of the EMSO ERIC South Adriatic Facility: moorings BB (blue dot) and FF (orange dot).

Derived parameters such as θ, Turner angle and squared buoyancy frequency (hereafter referred as Tu and N^2, respectively) were calculated using the Gibbs Seawater (GSW) Oceanographic Toolbox containing the TEOS-10 routines (McDougall and Barker, 2011). Calculations were achieved using the NumPy module (Harris et al., 2020), the pandas module (Wes McKinney, 2010) and the SciPy module (Virtanen et al., 2020) from Python. The different figures presented here were obtained thanks to the Matplotlib module (Hunter, 2007), again from Python. The squared buoyancy frequency (N^2) values are calculated considering 33h filtered conservative temperature (CT) and 33h filtered absolute salinity (SA) (McDougall and Barker, 2014) and are centreds at the mean pressure between two of the mooring time series, i.e., at 450, 650, 825, 950 and 1100 dbar (we re-

moved the 150 dbar layer as important gaps in this time series are present). Interpolation is then performed to obtain a visualization of N^2 on the whole water column. In order to explore if the water column was favorable to double-diffusive regimes and its related possible local stability condition we estimated the Turner angle (Tu) defined following 4.1 (Ruddick, 1983):

$$Tu = \arctan(\alpha\frac{\partial\theta}{\partial z} - \beta\frac{\partial S}{\partial z}, \alpha\frac{\partial\theta}{\partial z} + \beta\frac{\partial S}{\partial z}) \tag{4.1}$$

where arctan is the arctangent of the fourth quadrant; α is the coefficient of thermal expansion; β is the equivalent coefficient for the addition of salinity, sometimes called the *"coefficient of salt contraction"*; θ is the potential temperature; and S is the salinity. The Turner angle, Tu, compares the density stratification due to the temperature gradient with that due to the salinity gradient (van der Boog et al., 2022). The types of instability are determined by the signs of the potential density and salinity gradients rather than by their absolute values (Meccia et al., 2016).

When Tu is between -45 ° and -90 °, diffusive–convective double diffusion is possible; for Tu between -45 ° and 45 °, the water column is doubly stable, meaning that the water column is stably stratified with respect to both temperature and salinity, and for Tu between 45 ° and 90 °, SF double diffusion is expected (You, 2002). To calculate Tu, only data periods that covered all available vertical levels were used to achieve the best discretization of the vertical gradient by using the values of two consecutive levels. Therefore, we considered for this purpose the time series at the seven levels ranging from November 2014 to October 2019. To evaluate further the water mass properties in the vertical, we calculated the vector length (VL) defined following 4.2:

$$VL = \sqrt{(\alpha\frac{d\theta}{dz})^2 + (\beta\frac{dS}{dz})^2} \tag{4.2}$$

To the best of our knowledge, the VL has not been discussed in connection with stratification and the Tu. A higher VL indicates an increased change in water mass properties and therefore emphasizes the importance of Tu. On the other hand, when the VL is small the water column is essentially unstratified and changes in the Tu are insignificant. A water mass is characterized by θ and S, its potential temperature and salinity. The variables Tu and VL are simply the polar coordinates in (θ, S) space. It is Tu that determines the stability regime and VL the significance.

Complementing the time series data of T and S, we used the two Argo float number 6903197 profiles (`https://www.euro-argo.eu/Argo-Data-access`, last access: 19 February 2024), daily ERA5 net surface heat fluxes (Q_{tot}; Hersbach et al. (2018); Herbasch et al. (2020)) from the European Centre for Medium-Range Weather Forecasts (ECMWF) and mixed layer depth (MLD), provided by the Copernicus Marine Service at the nearest grid point to EMSO-E2M3A. The winter period is considered to run from December to February. Heat flux variations were determined by averaging Q_{tot} over an area containing points 0.3 ° from E2M3A; this yields an average of four points. The MLD was calculated using its maximum in an area closer than 0.1 ° from the mooring location.

Surface relative vorticity is defined following 4.3:

$$RV = \frac{\partial v}{\partial x} - \frac{\partial u}{\partial y} \tag{4.3}$$

where u and v are surface geostrophic velocities ($SEALEVEL\ EUR\ PHY\ L4\ MY$ 008 068

product; Copernicus Marine Service) in an area limited by the isobath of 1150 dbar. The RV is the average of 18 grid points around the mooring position with 0.125° spatial resolution. It is important to note that the EMSO-E2M3A deep mooring is very close to the center of the SAP, where the relative vorticity has a smaller variance than at the edges on the 1000 m isobath.

The two Argo float (no. 6903197) profiles used here are profile 81 (16 January 2017) and profile 82 (21 January 2017), which are located about 38 and 46 km (at 41.52 °N, 17.64 °E and 41.40 °N, 17.57 °E, respectively) from the mooring (fig. 4.1)). The Argo profiles of potential temperature and salinity were first linearly interpolated to 1 dbar vertical resolution, and the Turner angle was calculated using the 20-point moving-average profiles to avoid excessive noise in the results.

4.3 Analysis and discussion

4.3.1 Thermohaline variability in the area

The Hovmöller diagrams, based on time series of potential temperature and salinity measured at SAP (fig. 4.2), show a clear change in the characteristics before and after 2017. Looking at the 5-year dataset used for this work (November 2014–October 2019), the water column from the end of 2014 to the end of 2016 shows a clear signature of LIW occurrence restricted to the layer between 400 and 600 m, with a core value of 38.84. Unfortunately, the lack of data from the 150 dbar time series prevents defining the characteristics of the upper layer between November 2014 and November 2015. However, there is an indication of an intrusion of less saline water into the LIW horizon, which seems to be the cause of the deepening of the LIW core to around 550 m by mid-2015, also reducing its thickness. In October 2016, exceptionally, the surface layer was filled to about 300 dbar by very salty and warm waters, presumably an intrusion of LSW (Levantine Surface Water), with values above 38.90 (since no data were available above 150 m, the value could not be accurately determined). These two cores with high salinity were also observed by Mihanović et al. (2021) based on Argo float data in the same area.

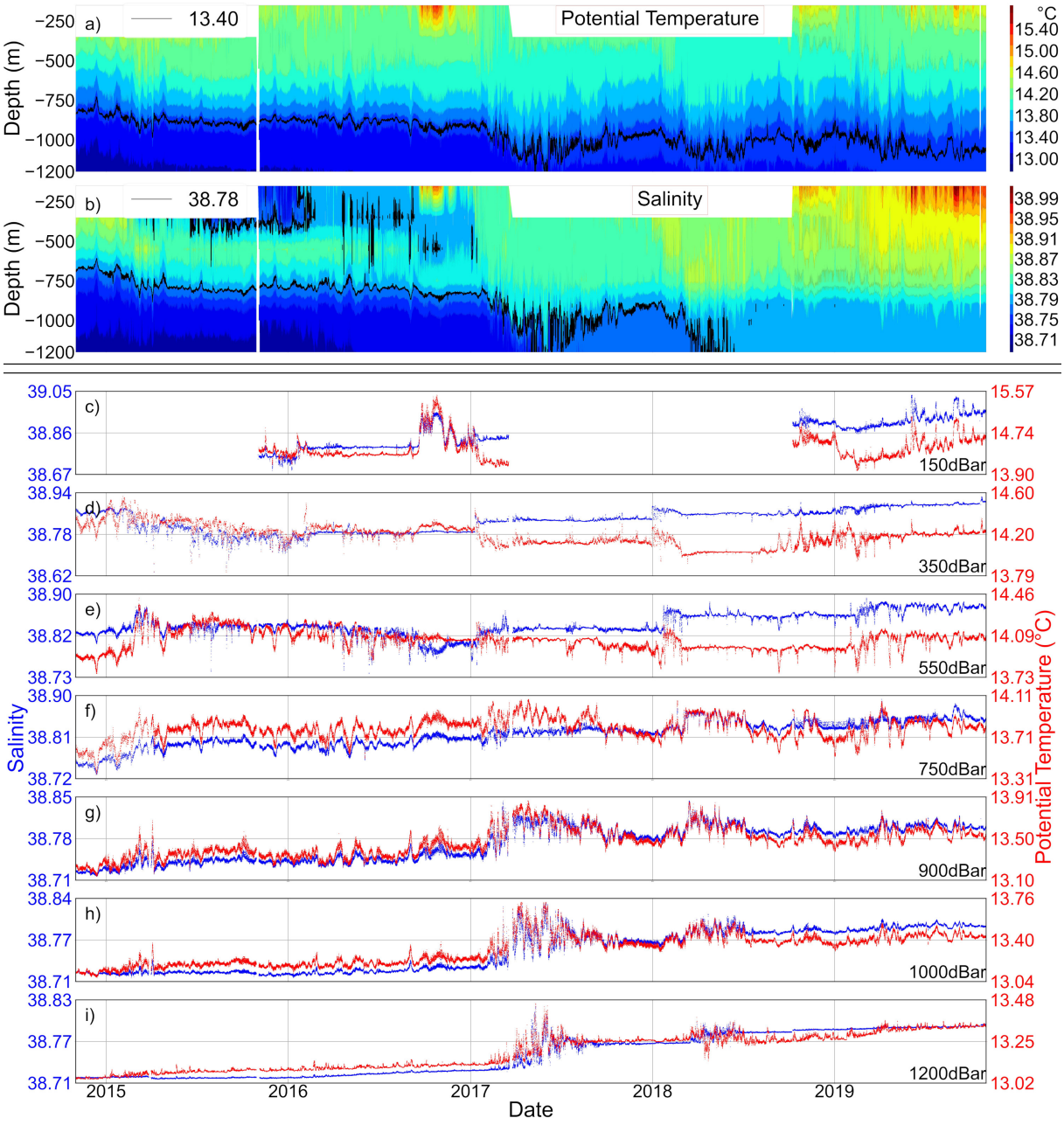

Figure 4.2: Hovmöller diagrams **(a, b)** and time series **(c–i)** of potential temperature (°C; red) and salinity (blue) from the E2M3A mooring in the SAP. The isotherm of 13.4 °C and the isohaline of 38.78 (black solid line) show the mentioned strong oscillations after the winter of 2016/17 in the Hovmöller diagrams of and S, respectively.

By December 2016, the deep salinity maxima mixed with surrounding waters and deepened to about 800 dbar with a reduced value of around 38.82. In early 2017, the salinity at the surface and in the inter mediate layer changed radically. The most important feature is the intrusion of high salinity into the intermediate layers contributing to a strong convection event in early winter, which is confirmed by the pool of homogenized water to a depth of about 700 dbar in the pit (fig. 4.3b). Indeed, strong heat losses occurred in January (620 W m^2; Table 1) (fig. 4.3a), which, together with the contribution of salt in the water column, facilitated the erosion of the stratification (fig. 4.3b, table 4.1). Mihanović et al. (2021) reported very high-salinity values (above 38.9) in the

upper 100 dbar in the southern Adriatic as early as mid-March from Argo data, which increased to an exceptional salinity and temperature maximum at and near the surface by summer. Throughout the year, salinity in the water column remained exceptionally high, confirming the same trend observed by Mihanović et al. (2021) along the Palagruža transect during summer and autumn. Moreover, temperature and salinity observations are higher than the values/data reported in previous climatologies for the Adriatic and in the literature (Buljan and Zore-Armanda, 1976; Artegiani et al., 1997; Lipizer et al., 2014a). In 2017 the water column showed a two-layer structure divided by the isohaline value of 38.83, with high-salinity waters occupying the surface and intermediate layers (down to about 800-850 dbar) and less saline waters (about 38.78) filling the deeper part of the pit. Water temperature in the latter, usually lower than 13 °C, increased to ≈13.2 °C. The strong oscillations (fig. 4.2) occurring during this period below 750 dbar are not directly related to salt fingering predisposition and will be discussed in chapter 3.

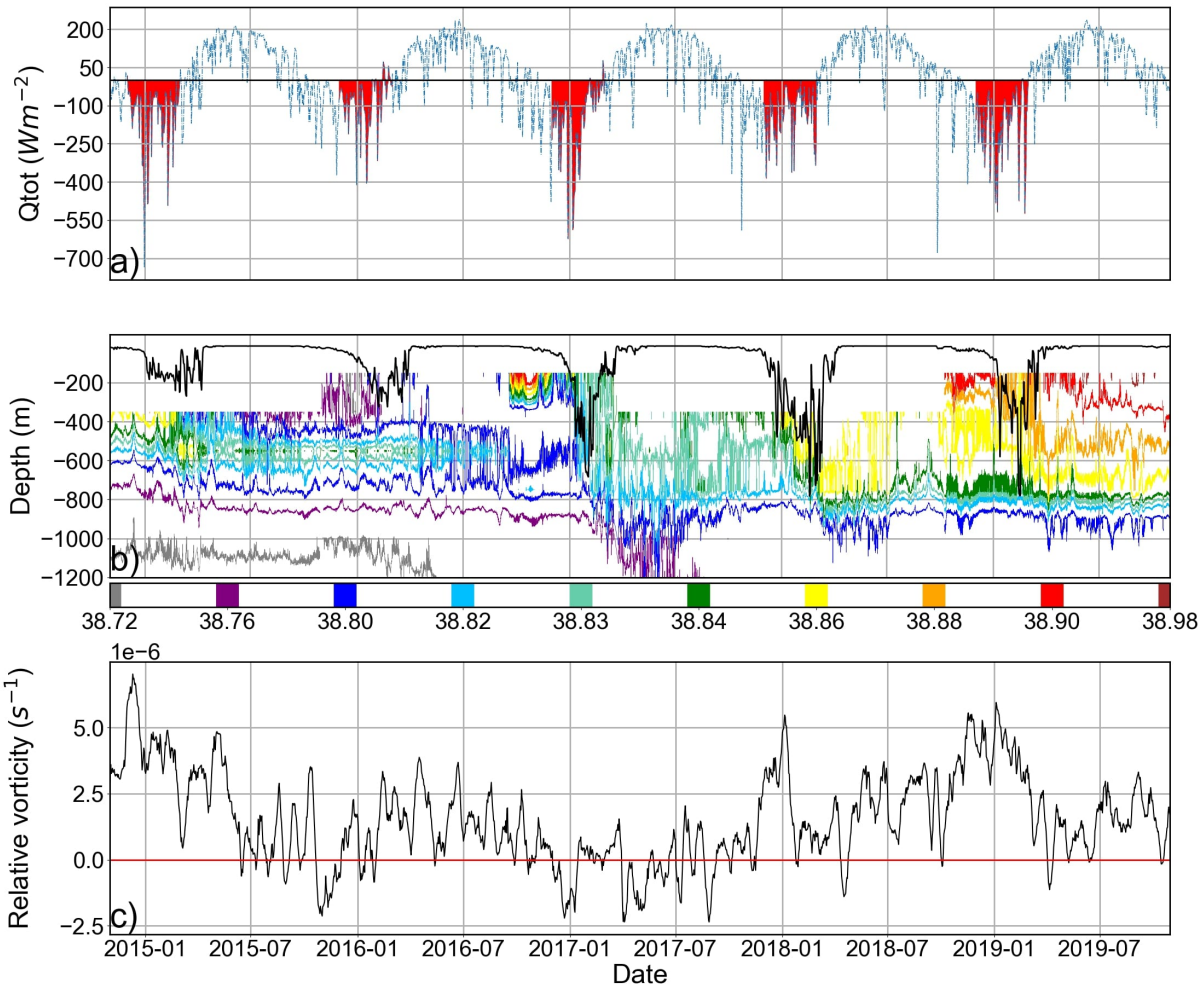

Figure 4.3: The evolution of the three forcings connected to the changes in buoyancy. (a) Net surface heat flux (Qtot ($\mathrm{W\,m^2}$; blue line) emphasizing the periods of winter negative surface heat flux (areas in red), (b) Salinity with mixed layer depth (MLD (m); solid black line) and (c) Relative vorticity (RV ($\mathrm{s^{-1}}$; solid black line). Surface salinity in the southern Adriatic peaked between August and October 2017, as indicated by data from two floats in the southern Adriatic (not shown). In early 2018, another sharp increase in salinity and temperature was observed in the surface and intermediate layers, reaching values of 38.89 and 14.25 °C, respectively, predisposing the water column to convection. Integrated surface heat loss for the winter period (table 4.1) showed that despite less severe heat losses in the winter of 2018/19 (but very frequent weak losses in February and March), the new contribution of salt triggered again the convective mixing of the water column to about 850 dbar (fig. 4.3b).

The water column maintained its *"two-layer structure"* in terms of salinity, with a halocline with values between 38.82 and 38.80 separating the surface layer from the deep layer. The deep layer (1000-1200 dbar) also experienced a sharp increase in salinity with values between 38.76 and 38.78 (fig. 4.2 and fig. 4.3b), which had never been observed in the last decade. The fluctuations observed in the deepest layers in the previous year were present also after March 2018. Inflow of high-salinity and warm waters into the pit was registered closer to the surface in summer, which slowly deepened its horizon in the winter of 2018/19 and completely filled the surface and intermediate layers with values of

around 38.88 during the winter period (end of February– beginning of March 2019). As a result, the amount of salt present in the water column triggered a convective mixing similar to that observed in the winter of 2017/18. No substantial changes were observed in the deep layer, which maintained the same characteristics as in late 2018 throughout 2019 and until the end of the study period. The above discussion indicates that saltier waters overlying less salty waters are a recurrent feature over the whole water column in the SAP. This leads to a predisposition to SF or convection.

Winter	Integrated fluxes ($\mathrm{J\,s^{-1}}$)	Maximum heat loss ($\mathrm{W\,m^{-2}}$)	Mixed layer depth (dbar)
2014-2015	-1.14×10^9	-736	270
2015-2016	-6.75×10^8	-411	325
2016-2017	-1.22×10^9	-623	684
2017-2018	-1.01×10^9	-385	782
2018-2019	-1.35×10^9	-523	781

Table 4.1: Integrated heat fluxes for the winter period (December February; area in red, fig. 4.3a), maximum heat loss and the depth reached by the mixed layer during the convection.

4.3.2 Abrupt squared buoyancy frequency changes

The Hovmöller plot of Brunt–Väisälä frequency N^2 (fig. 4.4) shows a change in the stability structure of the water column in the SAP before and after the beginning of 2017. In winter 2015/16, the water column had high stability at about 450 dbar and 800 dbar, which prevented convection despite high integrated heat losses. The barrier of high stability at about 450 dbar was eroded in 2016 due to saline intrusions in the upper layer. During winter 2016/17, the water column stability weakened further due to strong surface cooling, also pushing the core of the stable middle layer, which was around 800 dbar, down to about 950 dbar. After the winter of 2016/17, the N^2 structure did not return to the state of previous years. Three forcings favored the change in the N^2 structure in 2017 (as shown in fig. 4.3): first, strong heat loss at the surface during the winter of 2016/17, with the high salinity below the surface (150 to 350 dbar) pushing the intrusion of the LIW core downward; second, the departure of the less saline water above the LIW (fig. 4.2); and third, the change in relative vorticity. The last one shifted from cyclonic (1.7×10^{-6} $\mathrm{s^{-1}}$), favoring preconditioning, to anticyclonic (-2.3×10^{-6} $\mathrm{s^{-1}}$), possibly leading to upward Ekman pumping that brought more saline water to the surface, followed by a sharp jump back to cyclonic due to sinking of the dense waters. These three factors contributed to the observed low Brunt–Väisälä frequency N^2 (fig. 4.4) and the SF-favorable scenario.

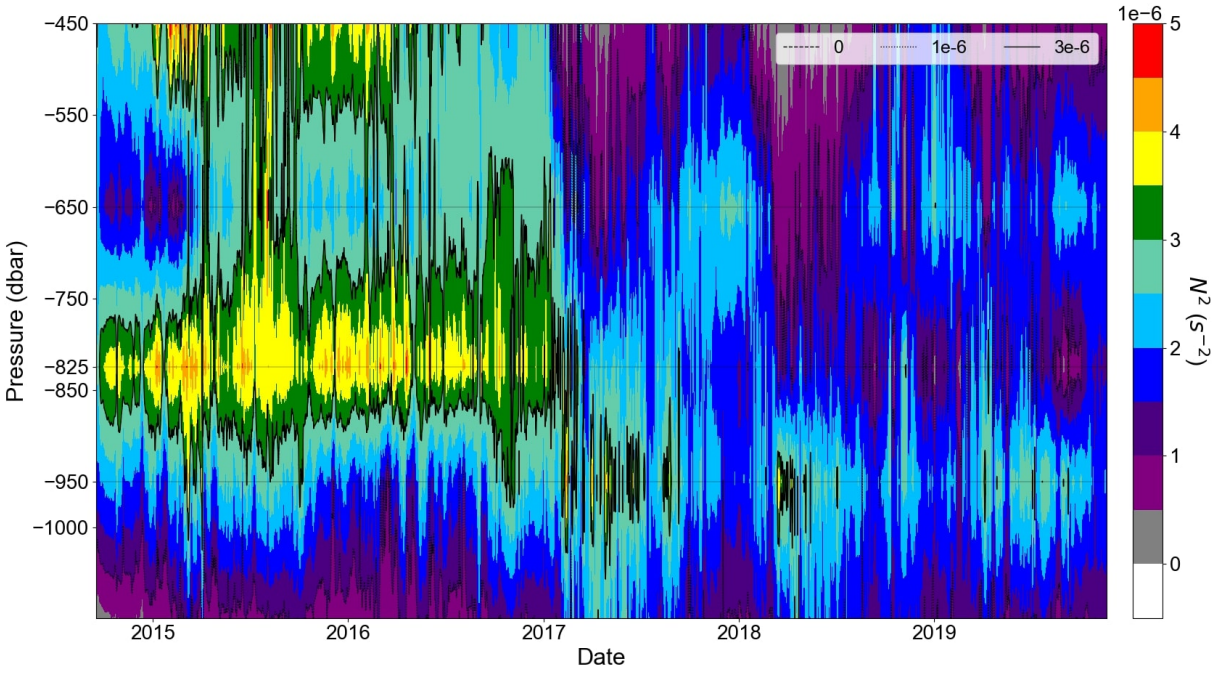

Figure 4.4: Hovmöller diagram of squared buoyancy frequency (N^2; s^{-2} . The layers with data (at mid-pressure between two observation depths) are marked with thin solid lines (450, 650, 825, 950 and 1100 dbar). A clear change in N^2 after the winter of 2016/17 is noticed.

4.3.3 Double diffusion and its evolution

Ocean stratification is subject to abrupt changes due to intermittent events such as gravity currents, horizontal intrusions and convection, as discussed in the previous subsection. These events not only overlap the continuous double-diffusive mixing but also interact with each other. In this section, we emphasize the effect of changes due to the convective process on the double-diffusive regime. We characterize the double diffusion by the Turner angle, Tu, and vector length, VL, introduced in section 4.2. During the 5-year period, the Tu time series (4.5a–e) showed variability ranging mainly from SF to doubly stable regimes, with the SF regime (blue line in 4.5a–e) dominating below a depth of 550 dbar.

The uppermost layer (350|550 dbar) is favourable to SF at the end of 2014 due to low salinity at 550 dbar. With the decrease in salinity at 350 dbar and an increase at 550 dbar (fig. 4.2d, e), the uppermost layer turns to doubly stable conditions from late winter 2014/15 throughout 2016. At the same time, the potential temperature at 550 dbar increases and the stratification in both variables decreases, as can also be seen in VL in fig. 4.6a. The stable stratification leads to low values of double-diffusion vertical mixing in the upper layer (350|550 dbar), and the underlying layers evolve more independently. Due to an increase in salinity at 350 dbar in early 2017, the uppermost layer showed peaks of strong conditions of SF and high VL. Subsequently, convection occurred causing the sharp decrease in VL and the occurrence of an unstable regime described by the Turner angle. The upper layer is homogenizing. This scenario of increased salinity in the upper part of the layer, leading to a favorable SF regime, convection and consequently a decrease in VL, also occurs with a time lag in the adjacent lower layer (550|750 dbar) and is repeated in 2018 in the same period. A further increase in salinity in 2018 and 2019 leads to a

strong SF condition but at low VL values, which is only sporadically interrupted by an increase in temperature at 350 dbar.

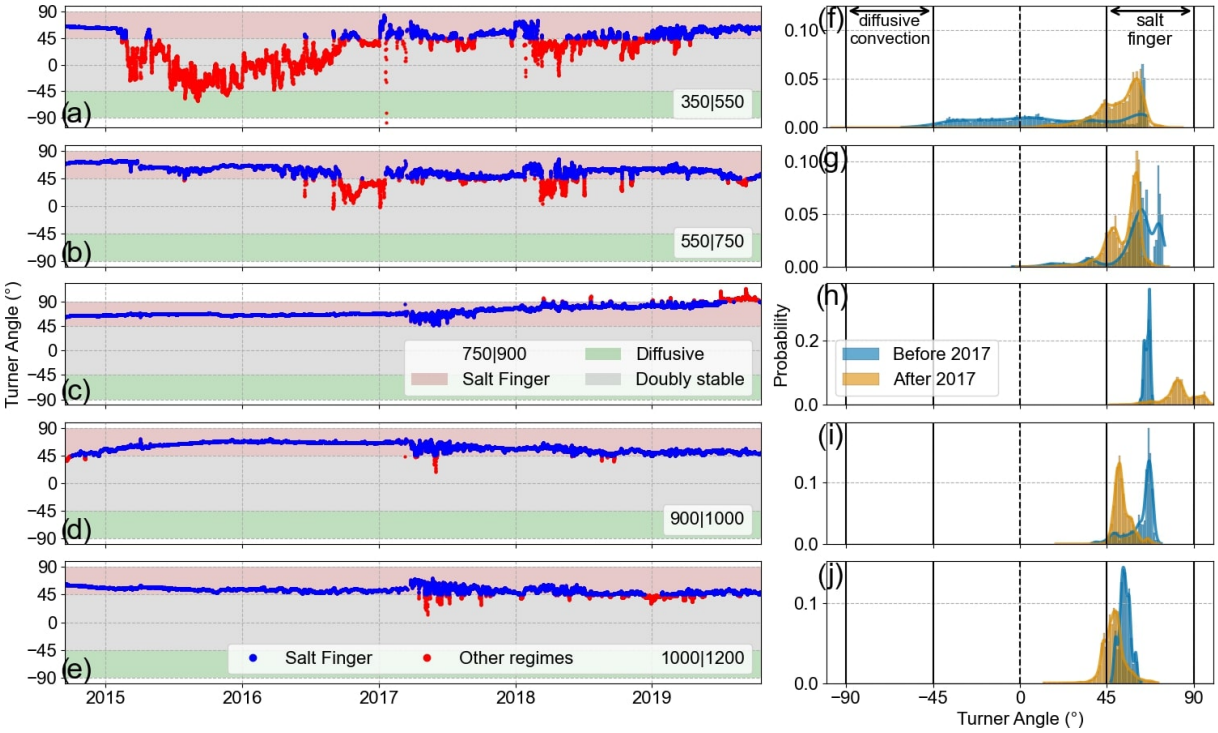

Figure 4.5: Turner angle time series using vertical potential temperature and salinity gradients and (f–j) the related PDFs calculated before (blue) and after (orange) 2017. The numbers in the legend represent the pressure levels that define the layer, and blue markers are periods of SF regime (pink background).

The second layer (550|750 dbar, 4.5b and 4.6b) is in a SF regime, interrupted only in late 2016 and spring 2018. In the first period, a reduction in salinity at 550 *dbar* leads to stabilization. This reduction is not observed in the adjacent layers and results from the deepening of the LIW layer, which also reduces the stability of the upper layer. In the second period, the stabilization is due to a sudden increase in salinity at 750 dbar, which is observed to varying magnitude throughout the water column. Since the stabilization strongly reduces the VL down to 900 dbar, it is due to convective (winter convection) mixing.

The third layer (750–900 dbar, 4.5c and 4.6c) shows a continuous increase in Tu from SF to unstable by the end of 2019 due to a continuous increase in salinity at 750 dbar. There is a sudden decrease in VL due to the 2017 event, caused by an increase in salinity at 900 dbar.

In the two deepest layers (900–1000 and 1000–1200 dbar, 4.5d, e and 4.6d, e), there is a shift towards reduced predisposition of SF strength after the 2017 event, which is also seen by increased variability in VL. Analysis of VL shows an eradication of stratification in early 2017 from 350 dbar down to 900 dbar, which persists until the end of the data record. The prominent peaks in Tu and VL in the first layer (350|550 dbar) in early 2017 are due to the arrival of warm, salty water at 350 dbar that possibly triggered strong SF (see also 4.7 and the discussion of the Argo data below). The stabilization of the water column in early spring 2017 in the two lower layers, seen by a jump and fluctuations in

the VL, is due to gravity currents (see 3)

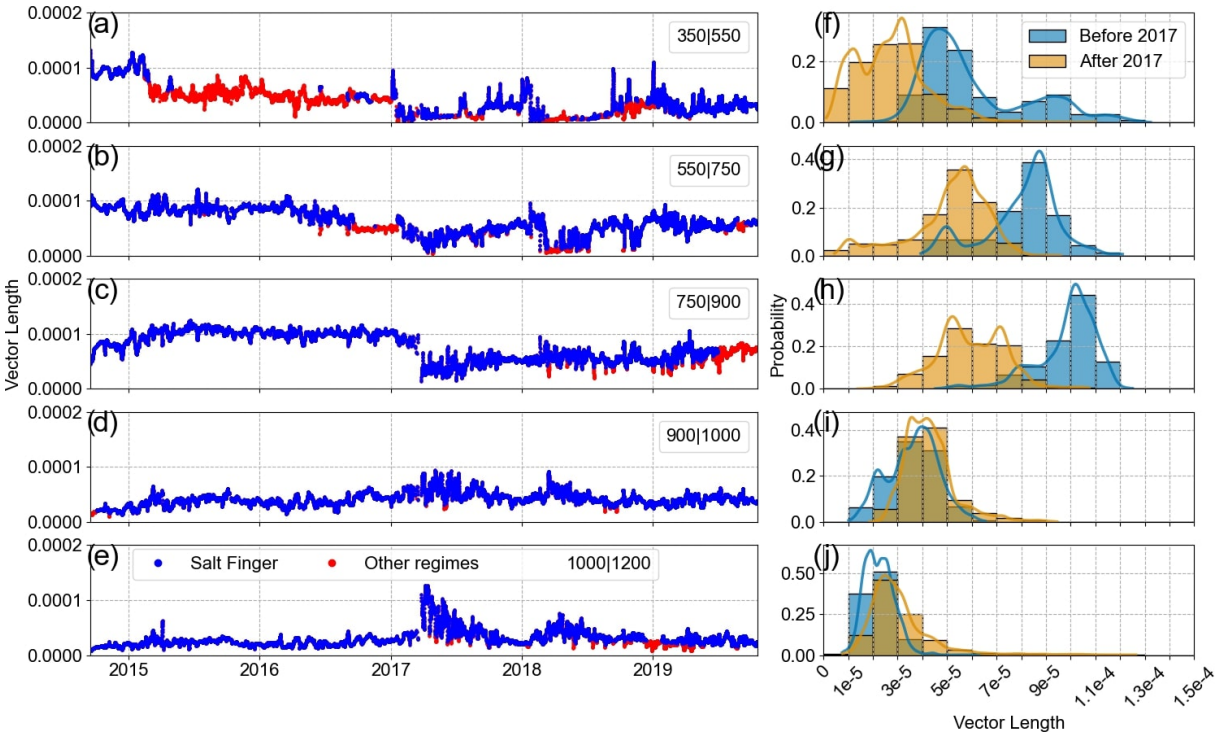

Figure 4.6: Vector length (1 m^{-1}) time series and (f–j) the related PDFs.

We also plotted the probability density functions (PDFs) of Tu and VL through the end of 2016 and from 2017 through the end of the observation period (4.5f–j and 4.6f–j). All PDFs from Tu show dominance of the SF regime except in the uppermost layer due to the period from early 2015 to the end of 2016. The regime change in 2017 is indicated by an increase in Tu in the 750|900 dbar layer and a decrease in the 900|1000 dbar layer. In these two layers, the peaks of the PDFs are well separated, indicating a regime change. In the deepest layer (1000|1200 dbar), an oscillatory pattern from 2017 is observed, moving from SF to a doubly stable regime, spreading the PDF in the second period but keeping the peaks close. The Tu shows a notable tendency in SF in the 750|900 dbar layer after 2017 and a stabilizing trend in the layer below due to the convective event in 2017.

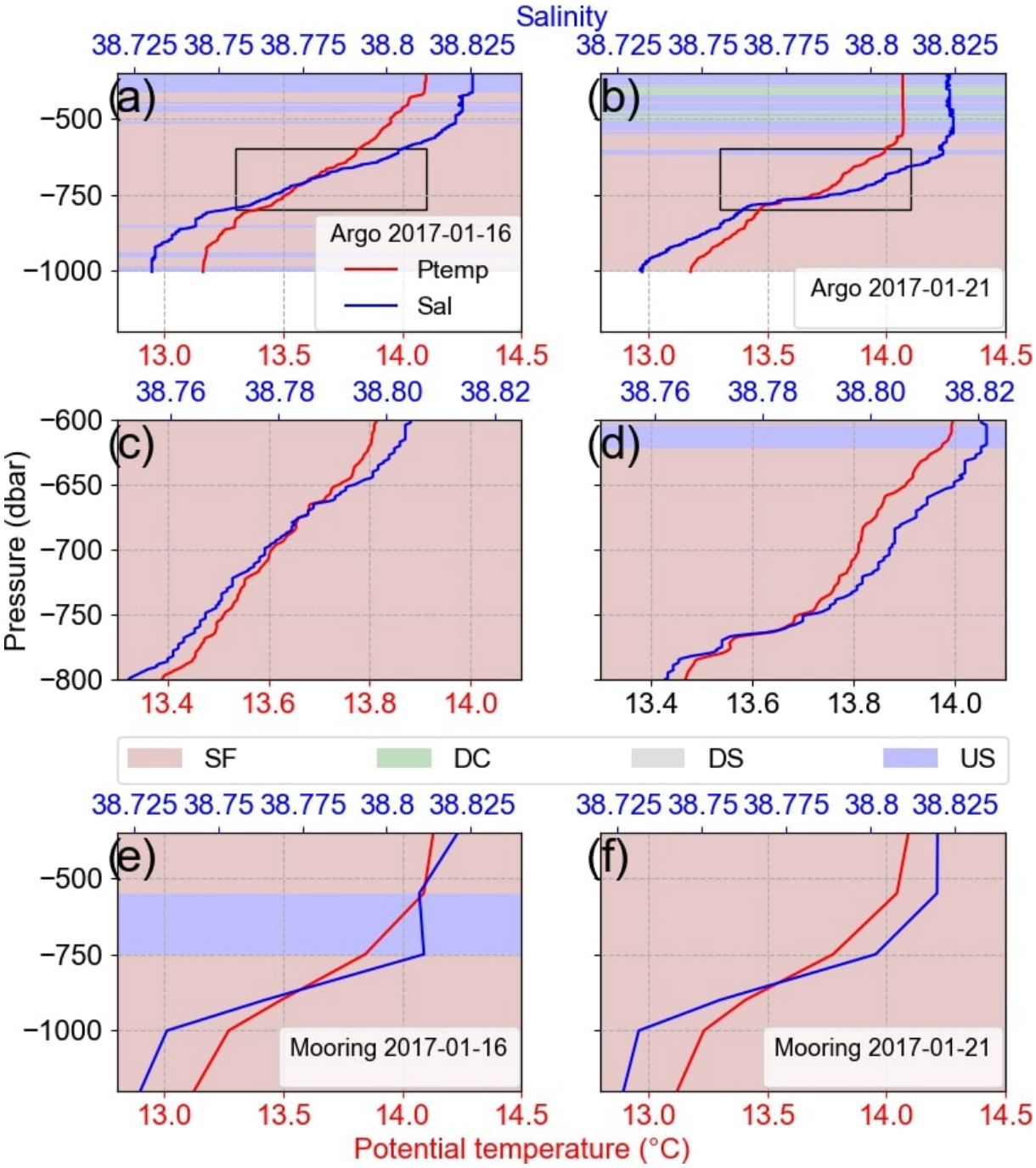

Figure 4.7: Argo float and S profiles on 16 and 21 January 2017, with rectangles defining the area to be zoomed. (c–d) Zoom of Argo profiles between 600 and 800 dbar showing staircase features below convection depth in the SF regime. (e–f) Mooring data collected on 16 and 21 January 2017 showing good coherence with Argo data. Potential temperature (Ptemp; red lines) and salinity (Sal; blue lines). The background colors represent the Turner angle regimes: SF– salt finger; DC – diffusive convection; DS – doubly stable; US – unstable.

The PDFs of VL show a significant decrease above 900 dbar, indicating the eradication of stratification, decreasing salinity gradients; the PDFs are well separated for the two layers between 550 and 900 dbar. Interestingly, the 750|900 dbar layer is characterized

by a clear positive trend in SF regime after 2017, but the VL decreased notably. As already mentioned, we assume that the conditions are still favourable to SF, but with the decreased vertical gradients in salinity, the favourable associated vertical mixing is weaker.

The SF occurrence was 83% of all measurements. The most relevant change in SF occurrence is for the uppermost layer (350|550 dbar), changing from 27% to 72% for measurements before and after 2017, respectively, indicating the significant increase in SFs (4.5a, blue dots). Our observational data show a shift in the vertical double-diffusion regimes in the SAP during the winter of 2016/17 in all layers (4.5) in the Tu and VL variables. During this period our data from EMSO-E2M3A show the dominance of SF conditions from 350 dbar to the bottom (4.7e and f) at a VL which is significantly non-vanishing (4.6a–e). These results are confirmed by the Argo float section (4.7a–d). The Argo floats have a fine vertical resolution and clearly show the existence of staircases (4.7c and d) (van der Boog et al., 2022). The staircase structure of SF has thin interfaces separating thicker, well-mixed layers. Salt flux from the upper high-salinity layer to the low-salinity layer below continuously mixes the water, and the convective turbulence of the layers limits the length of the fingers (Schmitt, 1988, 2003; Carniel et al., 2008; Durante et al., 2021).

The increase in near-surface salinity by horizontal advection through the Strait of Otranto (Kokkini et al., 2020; Mihanović et al., 2021) favors SF, followed by convection down to 500 dbar on 21 January 2017. We go further and hypothesize that the high salinity at the surface of the SAP could influence the observed change in relative vorticity through a salt lens of warm waters, explaining the anticyclonic tendency (see, i.e., Tokos and Rossby (1991), for subsurface salt-lens dynamics) during the preconditioning phase in the winter of 2016/17. The strong wintertime cooling then leads to convection and the sinking of the salt lens, which increases the relative vorticity. Below the convection depth the SF strength persists. In contrast with the results of Meccia et al. (2016), we observed an increased predisposition of SF occurrence in the SAP due to the increase in salinity, and this could enhance salt finger double diffusion in the subsurface layer of 350|550 dbar. The results of Carniel et al. (2008)) showed that the northern part of the Adriatic works differently than the SAP because of the Po River plume influence, which brings fresh water to the surface and allows the presence of diffusive–convective double diffusion, not significantly observed in the SAP in the analysed data. Still, the same order of magnitude for the diffusivity coefficient was estimated ($O(10^{-4}\ \mathrm{m^2\,s^{-1}})$).

4.4 Conclusion

SF is the dominant regime at the EMSO-E2M3A facility. From 2014 to the end of 2016 strong stratification above 400 dbar and at 800 dbar reduced the double-diffusive favourable mixing between the upper ocean and the deep SAP. After the winter of 2014/15, the upper layer passes from SF to doubly stably stratified, further reducing the possibility of having active salt fingering and consequently double-diffusion vertical mixing. A shift in the SF characteristics is observed in the winter of 2016/17 throughout the water column due to the arrival of high-salinity waters that favored a convective event penetrating to about 750 dbar. This extreme event increases the conditions for SF above 900 dbar and homogenizes the water column above. No return to the previous state is seen in the observation period. This might possibly happen on a decadal timescale, as it was determined in (Cardin et al., 2020b) that the characteristic timescale of the deep SAP is

around 7 years. Continued observations are necessary to draw conclusions on a return to the previous state. Salt fingering is shown to be a consequence and a possible driver of the density structure in the SAP: it is governed by salt intrusions through the Strait of Otranto and increases the vertical mixing. Salt intrusions from the Ionian Sea favor SF and convection and homogenize the water column in the SAP. Dense gravity currents originating from the northern Adriatic have the potential to enhance the stratification by increasing the density in the SAP. The vertical exchange is performed by enhanced mixing due to SF and convection. How the competition between sporadically extreme and continuous processes changes the structure of the water column and how it acts on the thermohaline circulation of the Mediterranean will be a subject of future studies.

To the best of our knowledge, it is the first time that a high-frequency multi-year time series from different water depths is used to determine the Turner angle and the double-diffusive regimes. The supplementary analysis of vector length to verify the significance of Turner angle results was a novelty introduced in this study and, analysed together with the squared buoyancy frequency, allowed us to discuss the stability structure changes. The increase in SF observations after the winter of 2016/17 cannot be ignored because it can modify the thermohaline circulation in the region (Zhang and Schmitt, 2000), affecting the water exchange between the Adriatic and Mediterranean.

The high vertical diffusivity coefficient of 5 $m^2\,s^{-1}$ found in Cardin et al. (2020b) is here explained by the dominant SF double-diffusion regime below 750 dbar, and the probability of SF occurring in the whole water column increased after the winter of 2016/17.

All documented events occurred during a period of unprecedented high-salinity transport from the Ionian to Adriatic seas. The North Ionian Gyre (NIG) vorticity (not shown) decreased in the period from 2015 to 2018, and the system turned anticyclonic in 2017 (Mihanović et al., 2021; Civitarese et al., 2023). After 2018, the vorticity started to increase again and turned cyclonic in 2019. The eastward extension of the NIG between 2015 and 2019 was not enough to prevent the flow toward the Adriatic along the eastern Ionian seaboard, conveying a large input of salt into the SAP (4.2).

Measurements at the EMSO-E2M3A facility have demonstrated the Eulerian or fixed-point observatories' importance as an essential component of the global ocean observing system. They allow the detection of extreme events that occur rarely during the multi-year observation period, such as the strong convection events that homogenize the water column leading to long-term alterations of the density structure. They also offer several unique features not found in other systems and therefore complement them (Cristini et al., 2016), and they provide a unique opportunity for multidisciplinary and interdisciplinary work combining a variety of observations on a large range of timescales.

Code availability

Code is available at `https://doi.org/10.5281/zenodo.10863275` (Amorim, 2024).

Data availability

The original contributions presented in the study are included in the article and Supplement, and further inquiries can be directed to the corresponding author/s. Data are available at the National Oceanographic Data Center – NODC (`https://doi.org/10.6092/F8E6D18EF877-4AA5-A983-A03B06CCB987`, Cardin et al. (2015); `https:`

//doi.org/10.6092/238B5903-A173-4FC3-AC5F-5FEDF1064A39, Cardin et al. (2018); https://doi.org/10.6092/d0d50095-bd30-4ff7-8d0a-a12121e72f78, Cardin et al. (2020a)), the Copernicus Marine Service (mixed layer depth, https://doi.org/10.48670/moi-00141, Escudier et al. (2020); surface geostrophic velocities, https://doi.org/10.25423/CMCC/MEDSEA_MULTIYEAR_PHY_006_004_E3R1, Nigam et al. (2021)) and the Copernicus Data Climate Store (surface heat flux, https://doi.org/10.24381/cds.adbb2d47, Hersbach et al. (2018)).

Supplement

The supplement related to this article is available on chapter C and online at: https://doi.org/10.5194/os-20-463-2024-supplement.

Author contribution

All the authors contributed to the conceptualization, writing the original draft, and review and editing. VC provided the funding acquisition.

Competing interests

The contact author has declared that none of the authors has any competing interests.

Disclaimer

Publisher's note: Copernicus Publications remains neutral with regard to jurisdictional claims made in the text, published maps, institutional affiliations, or any other geographical representation in this paper. While Copernicus Publications makes every effort to include appropriate place names, the final responsibility lies with the authors.

Special issue statement

This article is part of the special issue "Extremes in the marine environment: analysis of multi-temporal and multi-scale dynamics using observations, models, and machine learning techniques". It is not associated with a conference.

Acknowledgements

The authors thank the reviewers for the helpful comments that substantially improved the final version of this work. We are also grateful to the OGS PHYS and TECDEV groups and the captain and crew of the RV OGS Explora and RV Laura Bassi for the valuable support and work during the maintenance of the EMSO-E2M3A regional facility. The Argo data used in this work were collected and made freely available by the International Argo Program and the national programs that contribute to it (https://argo.ucsd.edu, last access: 18 March 2024; https://www.ocean-ops.org, last access: 18 March 2024). The results contain modified Copernicus Climate Change Service information

2020. Neither the European Commission nor ECMWF is responsible for any use that may be made of the Copernicus information or data it contains. This study has been conducted using EU Copernicus Marine Service Information and DOI links to data used in this study.

Financial support

This study has been developed in the framework of the project "CIR01_00030 - InSEA - Iniziative in Supporto al consolidamento e potenziamento dell'infrastruttura EMSO e delle sue attività – Rafforzamento del capitale umano", financed by the Ministry of University and Research – Development and Cohesion Fund (FSC) under the "PNIR – Programma Nazionale Infrastrutture di Ricerca" – DD 2595 24/12/2019 – Rafforzamento del capitale umano delle Infrastrutture di Ricerca.

Conclusion & Perspectives

The aim of this thesis was to understand how the different physical processes in the SAP work at their respective scale and what effects they have on the dynamics of the SAP. These issues were explored through the following questions:

1 - How does the SAP react to the effects of global warming and the increasing salinisation of the Adriatic Sea?

Over the past 20 years, the SAP has experienced warming and salinisation throughout the water column, resulting in increased spiciness at all layers. However, the layers do not evolve in the same way. The strongest warming and salinisation occur in the intermediate to deep layers (350 to 900 dbar) compared to the deepest layers (1000 to 1200 dbar). In contrast, the upper layer (150 dbar) exhibits more moderate warming but stronger salinisation than the intermediate layers. These trends reflect the diverse dynamics of the SAP, influenced by topography, air-sea fluxes, advection, and the interaction of different water masses (part II). Analysis of measurements since 1957 (chapter 2) also shows persistent warming and salinisation of the deep SAP, which has intensified in the last decade (an increase of 0.2 and 0.4 to 0.8 °C), two to four times higher than in the rest of the Mediterranean Sea. These observations indicate that changes projected for a centennial timescale in the Mediterranean Sea could occur within just 10 to 20 years in the Adriatic Sea.

Over the past two decades, the SAP has also recorded negative PDA trends, with the largest values in the deepest layers (-0.0037 to -0.0039 $\mathrm{kg\,m^{-3}}$), accompanied by less temporal variability than in the other layers. This supports the view that the current SAP is a two-layered system, particularly after the significant salt input to the Adriatic Sea in January 2017, when higher stability was observed in the deepest layers compared to the rest of the water column (chapter 4). Higher temperature trends were observed compared to the north-eastern Ionian Sea, emphasising the importance of locally driven processes. Despite these observations, the complexity of interactions between the drivers of thermohaline changes leads to uncertainty as to whether the observed changes represent a climate trend or reflect decadal variability.

2 - The deep SAP water masses being mainly renewed by the North Adriatic Dense Water (NAdDW), have there been changes in the drivers, periodicity or timescales of the associated gravity currents?

The stratification and ventilation of the deep SAP are determined by the competition between firstly small-scale mixing, which continuously contributes to the homogenisation of the water column, and secondly intermittent gravity currents, which cause restratification and ventilation. Gravity currents are spatially and temporally intermittent, and their occurrence strongly depends on fine-scale topographic features and remote forcing. In the SAP, four gravity currents were observed reaching the bottom between 2007 and 2023, specifically in 2012, 2017, 2018, and 2022. To identify these events, six independent criteria were developed using data from three moorings, all located along the path of the gravity currents: EMSO-E2M3A (E2M3A, in the centre of the SAP), EMSO-BB (BB, in the Bari canyon), and EMSO-FF (FF, on the open slope north of the Bari canyon). All criteria were met for the aforementioned years for the available data.

Firstly, bursts of PDA and dissolved oxygen fluctuations at three moorings were quantified using the fluctuation index ($\tilde{\eta}$), which measures the duration of significant variability (chapter 3). A significant $\tilde{\eta}$ in both PDA and dissolved oxygen defined the *first and second* criteria and indicated ventilation at the bottom of the SAP. Secondly, the normalised

density difference between BB and FF had to be significantly small to attribute the observed fluctuations to gravity currents (*third criterion*). Although four events reached the bottom of the SAP, this was not the case for several others (2015, 2016, 2019, and 2021), which intruded at shallower depths as the cascading waters were not denser than those at the bottom of the SAP. This implied a criterion for the density of the cascading water (*fourth criterion*). Thirdly, the literature indicates that the densest water driving the southward gravity currents is formed in the northern Adriatic Sea. To identify the years and areas where the highest density water masses form, a density threshold of 29.75 $\mathrm{kg\,m^{-3}}$ was applied to the Copernicus reanalysis (*fifth criterion*). Finally, T/S diagrams (chapter 3) confirmed that the water mass observed after significant fluctuations was a mixture of the resident E2M3A water mass and the inflowing water masses from BB and FF (mixing ratio, *sixth criterion*).

The T/S diagrams indicate that the thermohaline properties of the water masses formed in the deep SAP after a gravity current event varied between bottom ventilation years, reflecting different mixing ratios of water from BB and FF. Specifically, deep SAP ventilation was dominated by inflowing water from FF in 2012, 2018, and 2022, and from BB in 2017. Furthermore, the relative importance of temperature compared to salinity has changed over time. In 2012, the gravity current was mainly driven by potential temperature; in 2017 and 2022, by salinity; and in 2018, by both. This is explained by the large salt inflow into the Adriatic Sea in January 2017 (chapters 3 and 4). These results suggest that both the relative contribution of the drivers and the preferred path of gravity currents have changed over the observed events (chapter 3).

An analysis of the time scale showed that NAdDW pulses typically occur within a few months, from late January to May, and produce bursts of fluctuations in the deep SAP lasting a few months from March to June. The travel time between BB (FF) and E2M3A was estimated at about two weeks, corresponding to an average speed of 0.06 $\mathrm{m\,s^{-1}}$ (0.08 $\mathrm{m\,s^{-1}}$). In addition, variability was found in the travel time between the NAdDW formation area and BB: 80, 84, and 37 days in 2012, 2017, and 2018, respectively. The shorter travel time in 2018 was attributed to the stronger south-easterly ambient velocity on the west coast of the Adriatic Sea compared to the other bottom ventilation events.

3 - What are the mechanisms and consequences for the recent changes in the double diffusive regime in the SAP?

Salt fingering is a continuous process that has been shown to be both a consequence and a possible driver of density structure in the SAP. It is also the dominant regime at E2M3A (chapter 4). This regime is controlled by the intrusion of salt from the Ionian Sea through the Strait of Otranto, which homogenises the water column and promotes convection. The vertical exchange in the SAP is therefore influenced by mixing caused by salt fingering and convection events. This vertical exchange competes with gravity currents (chapter 3), which, unlike salt fingering, tend to reinforce stratification.

Between 2014 and the end of 2016, it was found that strong stratification above 400 dbar and at 800 dbar reduced the double-diffusive favourable mixing between the upper layer and the deep SAP. It was also observed that the upper layer shifted from a regime of salt fingering to a doubly stably stratified regime after the winter of 2014/2015, reducing the potential for active salt fingering and consequently double-diffusive vertical mixing. In January 2017, a major shift occurred when very salty water from the Ionian Sea entered the Adriatic Sea and triggered a convective event down to 750 dbar. This favoured salt fingering above 900 dbar and homogenised the water column, and no return to the previ-

ous state has been observed to date. The increase in the salt fingering regime after this extreme event is of great importance, as it can change the entire thermohaline circulation of the region. In particular, it was found that the high vertical diffusivity coefficient of 5 $m^2\,s^{-1}$ reported by (Cardin et al., 2020b) can be explained by the predominance of the salt fingering double-diffusion regime below 750 dbar, with the probability of salt fingering occurring throughout the water column increasing after January 2017.

Analysing the physical oceanography of the SAP from the basin scale to the microscale reveals the associated scale dependant closure problem and the interactions between processes across scales. The thermohaline changes observed at the basin scale (part II) influenced the stability of the SAP water column, the properties of the gravity current cascading into the SAP (chapter 3), and the prevailing double diffusive regime (chapter 4). After 2017, gravity currents exhibited a stronger influence of salinity, with the upper to intermediate layers maintaining their predisposition to salt fingering, while the deepest layers displayed a more variable mixing regime. Conversely, gravity currents transport heat and salt into the deep SAP, increasing its stability and further decoupling it from the upper water column. The more variable mixing regime observed in the deepest layers after 2017 can therefore be attributed to the interplay between the penetration of gravity currents and variability at the basin scale.

Overall, the relative decoupling between the deep layers and the rest of the water column results from a combination of basin scale processes, such as the intrusion of high salinity, the stabilising effect of gravity currents at depth, and the contrasting variability of mixing regimes in the water column, which together determine stability and transport throughout the water column.

In this study, we obtained significant and original results:

- We analysed the physical processes occurring at basin scale, submesoscale, and microscale, as well as their interactions, using observational and modelled data in a dynamic area, the SAP.
- We found that the Adriatic Sea, already known to produce the densest water mass in the Mediterranean, acts as a hotspot for climate change, demonstrating the importance of marginal seas for global thermohaline circulation. The results show that processes previously thought to occur on centennial timescales may take place within decades, emphasising the sensitivity of the SAP to regional and large-scale climate drivers.
- We documented the extraordinary event of 2017, driven by a strong salt inflow into the Adriatic Sea, across multiple scales and at high temporal resolution, providing unique insights into the rapid restructuring of the SAP water column.
- We observed changes in the characteristics of gravity currents cascading to the SAP bottom in terms of drivers, timescales, and paths. In particular, 2017 appeared to be a turning point after which salinity played a greater role.
- We used, for the first time, a high-frequency, multi-year time series at different water depths to determine the Turner angle and the double diffusive regimes. This allows an accurate description of how these regimes evolve in response to changing conditions.

Based on the results of this thesis, several perspectives and future directions can be considered.

This study, and more broadly the study of water masses in the SAP, could benefit from models with finer resolution. As discussed in section 3.3.5, the Copernicus reanalysis with a horizontal resolution of ≈ 4 km is not able to clearly detect every gravity current events. This limitation is understandable given the complex bathymetry of the Bari canyon, which is only 6 km long. Modelling the salt fingering shift observed at the mooring is an even greater challenge, as this process occurs on even smaller spatial scales. However, the use of finer models also comes with disadvantages: higher computational cost, rapidly increasing output size with resolution, and greater sensitivity to numerical noise and boundary conditions. A possible solution, especially for investigating gravity currents, is the development of a finer resolution model focusing on the Bari canyon region. In addition to numerical modelling, laboratory experiments could also provide important insights. The use of a 3D representation of the Bari canyon area (as done by Tassigny et al. (2024) for the Strait of Gibraltar) would make it possible to investigate the displacement of dense water masses within the canyon.

Further studies should aim to understand, first, the dynamics of boundary currents in the SAP and, second, the generation mechanisms of mesoscale and submesoscale eddies from these boundary currents. Boundary currents are potentially important for the downwelling of water masses (Spall, 2004) in the South Adriatic basin. Boundary currents, especially the EAC and the WAC, play a central role in redistributing water masses and in exchanges between coastal and open-sea regions. Mesoscale and submesoscale eddies are of major importance for lateral mixing, vertical transport, and the variability of water-mass properties. Increasing our knowledge of these features requires both high temporal resolution observations and numerical models capable of resolving their temporal and spatial variability. Such a study would quantify the exchange pathways within the basin and assess their influence on large-scale circulation and water-mass formation processes.

Another perspective could focus on improving the mooring line. However, it already provides a wide range of valuable data, and any changes should have a clear, realistic purpose rather than being made for their own sake. Installing CTD sensors every 100 m would be scientifically exceptional but unrealistic given the associated costs (instrumentation and calibration) and logistical constraints. Nevertheless, some potential improvements have been identified. Firstly, the ADCP Nortek Signature 100 at 900 dbar installed in September 2025 will allow for the measurement of vertical velocities over a greater range, enabling clear detection of the entrance of dense NAdDW into the deepest layer of the SAP. These velocity measurements in the deep SAP will allow for the derivation of turbulence, shear, and Reynolds stresses. Secondly, installing an ADV between the two already mounted ADCPs at 300 dbar could fill the gap in velocity measurements and provide an even more complete picture of water mass movements in the SAP. Thirdly, and already planned, is the installation of an inductive cable to facilitate data retrieval without recovering the entire mooring. This modification will be a significant improvement, making data collection more efficient and dynamic. Finally, additional sensors could be considered: a Photosynthetically Active Radiation (PAR) sensor on the buoy line near the surface, planned to be mounted during the next oceanographic cruise, to study the biogeochemistry of the surface layer; and a turbidimeter at about 750 dbar on the deep mooring line to detect high-frequency particle fluxes. This would allow the detection of short-term pulses associated with gravity currents that cannot be resolved by the current

sediment traps.

In addition to the mooring, deploying a series of drifting buoys could complement the Eulerian measurements by revealing the presence of submesoscale processes in the SAP and characterising their scales, lifetimes, and effects on transport and mixing.

Bibliography

Allen, J. R. L. (1971). Mixing at turbidity current heads, and its geological implications. Journal of Sedimentary Research, volume 41(1):97–113. ISSN 1527-1404. doi:10.1306/74D721F8-2B21-11D7-8648000102C1865D.

Amitai, Y., Ashkenazy, Y., and Gildor, H. (2019). The effect of wind-stress over the eastern mediterranean on deep-water formation in the adriatic sea. Deep Sea Research Part II: Topical Studies in Oceanography, volume 164:5–13. ISSN 0967-0645. doi:10.1016/j.dsr2.2018.11.015.

Amorim, F. L. L., Le Meur, J., Wirth, A., and Cardin, V. (2024). Tipping of the double-diffusive regime in the southern adriatic pit in 2017 in connection with record high-salinity values. Ocean Science, volume 20(2):463–474. doi:10.5194/os-20-463-2024.

Amos, C. L., Umgiesser, G., Ghezzo, M., Kassem, H., and Ferrarin, C. (2017). Sea Surface Temperature Trends in Venice Lagoon and the Adjacent Waters. Journal of Coastal Research, volume 33(2):385 – 395. doi:10.2112/JCOASTRES-D-16-00017.1.

Angeletti, L., Canese, S., Franchi, F., Montagna, P., Reitner, J., Walliser, E., and Taviani, M. (2015). The "chimney forest" of the deep Montenegrin margin, south-eastern Adriatic Sea. Marine and Petroleum Geology, volume 66:542–554. ISSN 0264-8172. doi:10.1016/j.marpetgeo.2015.04.001. Carbonate conduits linked to hydrocarbon-enriched fluid escape.

Artale, V., Calmanti, S., and Sutera, A. (2002). Thermohaline circulation sensitivity to intermediate-level anomalies. Tellus A: Dynamic Meteorology and Oceanography. doi:10.3402/tellusa.v54i2.12130.

Artegiani, A., Paschini, E., Russo, A., Bregant, D., Raicich, F., and Pinardi, N. (1997). The adriatic sea general circulation. part 1: Air–sea interactions and water mass structure. Journal of Physical Oceanography, volume 27(8):1492 – 1514. doi:10.1175/1520-0485(1997)027<1492:TASGCP>2.0.CO;2. Available at: "https://archimer.ifremer.fr/doc/00108/21891/.

Artegiani, A. and Salusti, E. (1987). Field observations of the flow of dense water on the bottom of the adriatic sea during the winter of 1981. Oceanologica Acta, volume 10(4):387–391.

Batistić, M., Garić, R., and Molinero, J. C. (2014). Interannual variations in adriatic sea zooplankton mirror shifts in circulation regimes in the ionian sea. Climate Research, volume 61:231–240. doi:10.3354/cr01248.

Belmaker, J., Parravicini, V., and Kulbicki, M. (2013). Ecological traits and environmental affinity explain red sea fish introduction into the mediterranean. Global Change Biology, volume 19(5):1373–1382. doi:10.1111/gcb.12132.

Benetazzo, A., Bergamasco, A., Bonaldo, D., Falcieri, F., Sclavo, M., Langone, L., and Carniel, S. (2014). Response of the adriatic sea to an intense cold air outbreak: Dense water dynamics and wave-induced transport. Progress in Oceanography, volume 128:115–138. ISSN 0079-6611. doi:10.1016/j.pocean.2014.08.015.

Benjamin, T. B. (1968). Gravity currents and related phenomena. Journal of Fluid Mechanics, volume 31(2):209–248. doi:10.1017/S0022112068000133.

Bensi, M., Cardin, V., and Rubino, A. (2014). Thermohaline Variability and Mesoscale Dynamics Observed at the Deep-Ocean Observatory E2M3A in the Southern Adriatic Sea, chapter 9, pages 139–155. American Geophysical Union (AGU). ISBN 9781118847572. doi:10.1002/9781118847572.ch9.

Bensi, M., Cardin, V., Rubino, A., Notarstefano, G., and Poulain, P. M. (2013). Effects of winter convection on the deep layer of the southern adriatic sea in 2012. Journal of Geophysical Research: Oceans, volume 118(11):6064–6075. doi:10.1002/2013JC009432.

Bethoux, J., Gentili, B., Morin, P., Nicolas, E., Pierre, C., and Ruiz-Pino, D. (1999). The mediterranean sea: a miniature ocean for climatic and environmental studies and a key for the climatic functioning of the north atlantic. Progress in Oceanography, volume 44(1):131–146. ISSN 0079-6611. doi:10.1016/S0079-6611(99)00023-3.

Bignami, F., Salusti, E., and Schiarini, S. (1990). Observations on a bottom vein of dense water in the southern adriatic and ionian seas. Journal of Geophysical Research: Oceans, volume 95(C5):7249–7259. doi:10.1029/JC095iC05p07249.

Bindoff, N., Cheung, W., Kairo, J., Arístegui, J., Guinder, V., Hallberg, R., Hilmi, N., Jiao, N., Karim, M., Levin, L., O'Donoghue, S., Cuicapusa, S. P., Rinkevich, B., Suga, T., Tagliabue, A., and Williamson, P. (2019). Changing ocean, marine ecosystems, and dependent communities. In Pörtner, H.-O., Roberts, D., Masson-Delmotte, V., Zhai, P., Tignor, M., Poloczanska, E., Mintenbeck, K., Alegría, A., Nicolai, M., Okem, A., Petzold, J., Rama, B., and Weyer, N., editors, IPCC Special Report on the Ocean and Cryosphere in a Changing Climate, pages 447–587. Cambridge University Press, Cambridge, UK and New York, NY, USA. doi:10.1017/9781009157964.007.

Bonaldo, D., Bellafiore, D., Ferrarin, C., Ferretti, R., Ricchi, A., Sangelantoni, L., and Vitelletti, M. L. (2022). The summer 2022 drought: a taste of future climate for the po valley (italy)? Regional Environmental Change, volume 23(1):1. ISSN 1436-378X. doi:10.1007/s10113-022-02004-z.

Brankart, J.-M. and Pinardi, N. (2001). Abrupt cooling of the mediterranean levantine intermediate water at the beginning of the 1980s: Observational evidence and model simulation. Journal of Physical Oceanography, volume 31(8):2307–2320. doi:10.1175/1520-0485(2001)031<2307:ACOTML>2.0.CO;2.

Bryden, H. L., Candela, J., and Kinder, T. H. (1994). Exchange through the strait of gibraltar. Progress in Oceanography, volume 33(3):201–248. ISSN 0079-6611. doi:10.1016/0079-6611(94)90028-0.

Buljan, M. (1953). Fluctuation of salinity in the adriatic. Acta Adriatica, volume 2(2):1–64. Izvještaj Republičke Ribarstveno-biološke ekspedicije 'Hvar' 1948–1949.

Buljan, M. and Zore-Armanda, M. (1976). Oceanographical properties of the adriatic sea. Marine Biology Annual review, volume 14:11–98.

Capet, X., McWilliams, J. C., Molemaker, M. J., and Shchepetkin, A. F. (2008). Mesoscale to submesoscale transition in the california current system. part iii: Energy balance and flux. Journal of Physical Oceanography, volume 38(10):2256 – 2269. doi:10.1175/2008JPO3810.1.

Cardin, V., Bensi, M., and Pacciaroni, M. (2011). Variability of water mass properties in the last two decades in the south adriatic sea with emphasis on the period 2006–2009. Continental Shelf Research, volume 31(9):951–965. ISSN 0278-4343. doi:10.1016/j.csr.2011.03.002.

[Dataset] Cardin, V., Bensi, M., Siena, G., and Ursella, L. (2014a). E2m3a-2011-2013-time-series-southadriatic. doi:10.6092/84CB588D-97E5-4C64-91BB-BA6109DFA530.

[Dataset] Cardin, V., Bensi, M., Ursella, L., and Siena, G. (2015). E2m3a-2013-2015-time-series south adriatic. doi:10.6092/F8E6D18E-F877-4AA5-A983-A03B06CCB987.

[Dataset] Cardin, V., Bensi, M., Ursella, L., and Siena, G. (2018). E2m3a-2015-2017-time series-south adriatic. doi:10.6092/238B5903-A173-4FC3-AC5F-5FEDF1064A39.

Cardin, V. and Gačić, M. (2003). Long-term heat flux variability and winter convection in the adriatic sea. Journal of Geophysical Research: Oceans, volume 108(C9). doi:10.1029/2002JC001645.

[Dataset] Cardin, V., Siena, G., Brunetti, F., , and Kuchler, S. (2020a). E2m3a-2017-2019-ctd-time-series southadriatic. doi:10.6092/d0d50095-bd30-4ff7-8d0a-a12121e72f78.

Cardin, V., Siena, G., Giorgetti, A., Ursella, L., Brosich, A., and Partescano, E. (2014b). The ritmare fixed sites network procedures for real-time data quality control. doi:10.13140/RG.2.2.31100.44166.

[Dataset] Cardin, V., Ursella, L., Le Meur, J., Siena, G., Mansutti, P., Fabio, B., and Elena, P. (2024). E2m3a-2019-2020-water-column-time-series- southadriatic. doi:10.13120/QAC0-1S48.

[Dataset] Cardin, V., Ursella, L., Le Meur, J., Siena, G., Mansutti, P., Fabio, B., and Elena, P. (2025). E2m3a-2021-2022-water-column-time-series- south adriatic. doi:10.13120/S046-JA62.

Cardin, V., Wirth, A., Khosravi, M., and Gačić, M. (2020b). South adriatic recipes: Estimating the vertical mixing in the deep pit. Frontiers in Marine Science, volume 7. ISSN 2296-7745. doi:10.3389/fmars.2020.565982.

Carniel, S., Sclavo, M., Kantha, L., and Prandke, H. (2008). Double-diffusive layers in the adriatic sea. Geophysical Research Letters, volume 35(2). doi:10.1029/2007GL032389.

Chiarini, M., Guicciardi, S., Angelini, S., Tuck, I. D., Grilli, F., Penna, P., Domenichetti, F., Canduci, G., Belardinelli, A., Santojanni, A., Arneri, E., Milone, N., Medvešek, D., Isajlović, I., Vrgoč, N., and Martinelli, M. (2022). Accounting for environmental and fishery management factors when standardizing cpue data from a scientific survey: A case study for nephrops norvegicus in the pomo pits area (central adriatic sea). PLOS ONE, volume 17(7):1–30. doi:10.1371/journal.pone.0270703.

Chiggiato, J., Artale, V., Durrieu de Madron, X., Schroeder, K., Taupier-Letage, I., Velaoras, D., and Vargas-Yáñez, M. (2023). Chapter 9 - recent changes in the Mediterranean Sea. In Schroeder, K. and Chiggiato, J., editors, Oceanography of the Mediterranean Sea, pages 289–334. Elsevier. ISBN 978-0-12-823692-5. doi: 10.1016/B978-0-12-823692-5.00008-X.

Chiggiato, J., Bergamasco, A., Borghini, M., Falcieri, F. M., Falco, P., Langone, L., and et al. (2016). Dense-water bottom currents in the southern adriatic sea in spring 2012. Marine Geology, volume 375:134–145. ISSN 0025-3227. doi:10.1016/j.margeo.2015.09.005.

Civitarese, G., Gačić, M., Batistić, M., Bensi, M., Cardin, V., Dulčić, J., and et al. (2023). The bios mechanism: History, theory, implications. Progress in Oceanography, volume 216:103056. ISSN 0079-6611. doi:10.1016/j.pocean.2023.103056.

Cristini, L., Lampitt, R. S., Cardin, V., Delory, E., Haugan, P., O'Neill, N., Petihakis, G., and Ruhl, H. A. (2016). Cost and value of multidisciplinary fixed-point ocean observatories. Marine Policy, volume 71:138–146. ISSN 0308-597X. doi:10.1016/j.marpol.2016.05.029.

Cushman-Roisin, B. and Beckers, J.-M. (2011). Introduction to Geophysical Fluid Dynamics: Physical and Numerical Aspects. Academic Press, 2nd edition. ISBN 9780120887590.

Cushman-Roisin, B., Gacic, M., Poulain, P.-M., and Artegiani, A. (2001). Physical Oceanography of the Adriatic Sea: Past, Present and Future. Dordrecht: Springer. ISBN 978-90-481-5921-5. doi:10.1007/978-94-015-9819-4.

Cushman-Roisin, B., Korotenko, K. A., Galos, C. E., and Dietrich, D. E. (2007). Simulation and characterization of the adriatic sea mesoscale variability. Journal of Geophysical Research: Oceans, volume 112(C3). doi:10.1029/2006JC003515.

de Pascual-Collar, A., G. Sotillo, M., Levier, B., Aznar, R., Lorente, P., Amo-Baladrón, A., and Álvarez-Fanjul, E. (2019). Regional circulation patterns of mediterranean outflow water near the iberian and african continental slopes. Ocean Science, volume 15(3):565–582. doi:10.5194/os-15-565-2019.

Denamiel, C., Tojčić, I., and Vilibić, I. (2021). Balancing accuracy and efficiency of atmospheric models in the northern adriatic during severe bora events. Journal of Geophysical Research: Atmospheres, volume 126(5):e2020JD033516. doi:10.1029/2020JD033516. E2020JD033516 2020JD033516.

Di Biagio, V., Martellucci, R., Menna, M., Teruzzi, A., Amadio, C., Mauri, E., and Cossarini, G. (2023). Dissolved oxygen as an indicator of multiple drivers of the marine

ecosystem: the southern adriatic sea case study. State of the Planet, volume 1-osr7:10. doi:10.5194/sp-1-osr7-10-2023.

dos Santos Nogueira, H. I. (2014). Experimental characterization of unsteady gravity currents developing over smooth and rough beds. Phd thesis, University of Coimbra. Tese de doutoramento.

Durante, S., Oliveri, P., Nair, R., and Sparnocchia, S. (2021). Mixing in the tyrrhenian interior due to thermohaline staircases. Frontiers in Marine Science, volume 8. ISSN 2296-7745. doi:10.3389/fmars.2021.672437.

Durante, S., Schroeder, K., Mazzei, L., Pierini, S., Borghini, M., and Sparnocchia, S. (2019). Permanent thermohaline staircases in the Tyrrhenian Sea. Geophysical Research Letters, volume 46(3):1562–1570. doi:10.1029/2018GL081747.

Early, J. J., Samelson, R. M., and Chelton, D. B. (2011). The evolution and propagation of quasigeostrophic ocean eddies*. Journal of Physical Oceanography, volume 41(8):1535 – 1555. doi:10.1175/2011JPO4601.1.

Escudier, R., Clementi, E., Cipollone, A., Pistoia, J., Drudi, M., Grandi, A., Lyubartsev, V., Lecci, R., Aydogdu, A., Delrosso, D., Omar, M., Masina, S., G., C., and Pinardi, N. (2021). A high resolution reanalysis for the mediterranean sea. Frontiers in Earth Science, volume 9. doi:10.3389/feart.2021.702285.

[Dataset] Escudier, R., Clementi, E., Omar, M., Cipollone, A., Pistoia, J., Aydogdu, A., Drudi, M., Grandi, A., Lyubartsev, V., Lecci, R., Cretí, S., Masina, S., Coppini, G., and Pinardi, N. (2020). Mediterranean sea physical reanalysis (cmems med-currents) (version 1). doi:10.25423/CMCC/MEDSEA_MULTIYEAR_PHY_006_004_E3R1.

[Dataset] EU Copernicus Marine Service Information, C. (2024). Global Ocean Physics Reanalysis. doi:10.48670/moi-00021.

Fedele, G., Mauri, E., Notarstefano, G., and Poulain, P. M. (2022). Characterization of the atlantic water and levantine intermediate water in the mediterranean sea using 20 years of argo data. Ocean Science, volume 18(1):129–142. doi:10.5194/os-18-129-2022.

García-Lafuente, J., Delgado, J., Sánchez Román, A., Soto, J., Carracedo, L., and Díaz del Río, G. (2009). Interannual variability of the Mediterranean outflow observed in espartel sill, western Strait of Gibraltar. Journal of Geophysical Research: Oceans, volume 114(C10). doi:10.1029/2009JC005496.

García-Lafuente, J., Sammartino, S., Huertas, I. E., Flecha, S., Sánchez-Leal, R. F., Naranjo, C., Nadal, I., and Bellanco, M. J. (2021). Hotter and weaker mediterranean outflow as a response to basin-wide alterations. Frontiers in Marine Science, volume Volume 8 - 2021. ISSN 2296-7745. doi:10.3389/fmars.2021.613444.

García Lafuente, J., Sánchez Román, A., Díaz del Río, G., Sannino, G., and Sánchez Garrido, J. C. (2007). Recent observations of seasonal variability of the mediterranean outflow in the strait of gibraltar. Journal of Geophysical Research: Oceans, volume 112(C10). doi:10.1029/2006JC003992.

Gačic, M., Lascaratos, A., Manca, B., and Mantziafou, A. (2001). Adriatic Deep Water and Interaction with the Eastern Mediterranean Sea. Dordrecht: Springer. ISBN 978-90-481-5921-5. doi:10.1007/978-94-015-9819-4_4.

Gačić, M., Borzelli, G. L. E., Civitarese, G., Cardin, V., and Yari, S. (2010). Can internal processes sustain reversals of the ocean upper circulation? The Ionian Sea example. Geophysical Research Letters, volume 37(9). doi:10.1029/2010GL043216.

Gačić, M., Civitarese, G., Miserocchi, S., Cardin, V., Crise, A., and Mauri, E. (2002). The open-ocean convection in the southern adriatic: a controlling mechanism of the spring phytoplankton bloom. Continental Shelf Research, volume 22(14):1897–1908. ISSN 0278-4343. doi:10.1016/S0278-4343(02)00050-X.

Giorgi, F. (2006). Climate change hot-spots. Geophysical Research Letters, volume 33(8). doi:10.1029/2006GL025734.

Hariri, S. (2020). Near-surface transport properties and lagrangian statistics during two contrasting years in the adriatic sea. Journal of Marine Science and Engineering, volume 8(9). ISSN 2077-1312. doi:10.3390/jmse8090681.

Harris, C. R., Millman, K. J., van der Walt, S. J., Gommers, R., Virtanen, P., Cournapeau, D., Wieser, E., Taylor, J., Berg, S., Smith, N. J., Kern, R., Picus, M., Hoyer, S., van Kerkwijk, M. H., Brett, M., Haldane, A., del Río, J. F., Wiebe, M., Peterson, P., Gérard-Marchant, P., Sheppard, K., Reddy, T., Weckesser, W., Abbasi, H., Gohlke, C., and Oliphant, T. E. (2020). Array programming with numpy. Nature, volume 585(7825):357–362. ISSN 1476-4687. doi:10.1038/s41586-020-2649-2.

Hendershott, M. C. and Rizzoli, P. (1976). The winter circulation of the adriatic sea. Deep Sea Research and Oceanographic Abstracts, volume 23(5):353–370. ISSN 0011-7471. doi:10.1016/0011-7471(76)90834-2.

Herbasch, H., Bell, B., Berrisford, P., Hirahara, S., Horányi, A., Muñoz-Sabater, J., Nicolas, J., and et al. (2020). The ERA5 global reanalysis. Quarterly Journal of the Royal Meteorological Society 146, volume 146:1999–2049. doi:10.1002/qj.3803.

Hersbach, H., Bell, B., Berrisford, P., Biavati, G., Horányi, A., Muñoz Sabater, J., Nicolas, J., Peubey, C., Radu, R., Rozum, I., Schepers, D., Simmons, A., Soci, C., Dee, D., and Thépaut, J.-N. (2018). ERA5 hourly data on single levels from 1940 to present. Copernicus Climate Change Service (C3S) Climate Data Store (CDS), pages 357–362. doi:10.24381/cds.adbb2d47.

Hinkel, J., Lincke, D., Vafeidis, A. T., Perrette, M., Nicholls, R. J., Tol, R. S. J., Marzeion, B., Fettweis, X., Ionescu, C., and Levermann, A. (2014). Coastal flood damage and adaptation costs under 21st century sea-level rise. Proceedings of the National Academy of Sciences, volume 111(9):3292–3297. doi:10.1073/pnas.1222469111.

Hopkins, T., Artegiani, A., Kinder, C., and Pariante, R. (1999). A discussion of the northern adriatic circulation and flushing as determined from the elna hydrography 2 3. The Adriatic Sea, Ecosystem Research Report No. 32, 1999, EUR 18834, European Commission, Brussels, volume 32.

Hunter, J. D. (2007). Matplotlib: A 2D Graphics Environment. Computing in Science and Engineering, volume 9(3):90–95. doi:10.1109/MCSE.2007.55.

Huppert, H. E. (1982). The propagation of two-dimensional and axisymmetric viscous gravity currents over a rigid horizontal surface. Journal of Fluid Mechanics, volume 121:43–58. doi:10.1017/S0022112082001797.

Huppert, H. E. (2006). Gravity currents: a personal perspective. Journal of Fluid Mechanics, volume 554:299–322. doi:10.1017/S002211200600930X.

Huppert, H. E. and Simpson, J. E. (1980). The slumping of gravity currents. Journal of Fluid Mechanics, volume 99(4):785–799. doi:10.1017/S0022112080000894.

Incarbona, A., Martrat, B., Mortyn, P. G., Sprovieri, M., Ziveri, P., Gogou, A., Jordà, G., Xoplaki, E., Luterbacher, J., Langone, L., Marino, G., Rodríguez-Sanz, L., Triantaphyllou, M., Di Stefano, E., Grimalt, J. O., Tranchida, G., Sprovieri, R., and Mazzola, S. (2016). Mediterranean circulation perturbations over the last five centuries: Relevance to past eastern mediterranean transient-type events. Scientific Reports, volume 6(1):29623. ISSN 2045-2322. doi:10.1038/srep29623.

IPCC, I. P. o. C. C. (2022). The Ocean and Cryosphere in a Changing Climate: Special Report of the Intergovernmental Panel on Climate Change. Cambridge University Press.

Ivanovic, R. F., Valdes, P. J., Flecker, R., and Gutjahr, M. (2014). Modelling global-scale climate impacts of the late miocene messinian salinity crisis. Climate of the Past, volume 10(2):607–622. doi:10.5194/cp-10-607-2014.

Janeković, I., Mihanović, H., Vilibić, I., and Tudor, M. (2014). Extreme cooling and dense water formation estimates in open and coastal regions of the adriatic sea during the winter of 2012. Journal of Geophysical Research: Oceans, volume 119(5):3200–3218. doi:10.1002/2014JC009865.

Josey, S. A. (2003). Changes in the heat and freshwater forcing of the eastern mediterranean and their influence on deep water formation. Journal of Geophysical Research: Oceans, volume 108(C7). doi:10.1029/2003JC001778.

Kassis, D. and Korres, G. (2020). Hydrography of the eastern mediterranean basin derived from argo floats profile data. Deep Sea Research Part II: Topical Studies in Oceanography, volume 171:104712. ISSN 0967-0645. doi:10.1016/j.dsr2.2019.104712. Revisiting the Eastern Mediterranean: Recent knowledge on the physical, biogeochemical and ecosystemic states and trends (Volume II).

Killworth, P. D. (1983). Deep convection in the world ocean. Reviews of Geophysics, volume 21(1):1–26. doi:10.1029/RG021i001p00001.

Klein, B., Roether, W., Manca, B. B., Bregant, D., Beitzel, V., Kovacevic, V., and Luchetta, A. (1999). The large deep water transient in the eastern mediterranean. Deep Sea Research Part I: Oceanographic Research Papers, volume 46(3):371–414. ISSN 0967-0637. doi:10.1016/S0967-0637(98)00075-2.

Kokkini, Z., Mauri, E., Gerin, R., Poulain, P., Simoncelli, S., and Notarstefano, G. (2020). On the salinity structure in the south adriatic as derived from float and glider observations in 2013–2016. Deep Sea Research Part II: Topical Studies in Oceanography, volume 171:104625. ISSN 0967-0645. doi:10.1016/j.dsr2.2019.07.013.

Korotenko, K. A. (2007). Modeling the mesoscale variability in the adriatic sea. Oceanology, volume 47(3):313–324. ISSN 1531-8508. doi:10.1134/S0001437007030034.

Kubin, E., Menna, M., Mauri, E., Notarstefano, G., Mieruch, S., and Poulain, P.-M. (2023). Heat content and temperature trends in the mediterranean sea as derived from argo float data. Frontiers in Marine Science, volume Volume 10 - 2023. ISSN 2296-7745. doi:10.3389/fmars.2023.1271638.

Laanaia, N., Wirth, A., Molines, J. M., Barnier, B., and Verron, J. (2010). On the numerical resolution of the bottom layer in simulations of oceanic gravity currents. Ocean Science, volume 6(2):563–572. doi:10.5194/os-6-563-2010.

Lapeyre, G., Klein, P., and Hua, B. L. (2006). Oceanic restratification forced by surface frontogenesis. Journal of Physical Oceanography, volume 36(8):1577 – 1590. doi:10.1175/JPO2923.1.

Lapeyre, G. and Patrice, K. (2006). Impact of the small-scale elongated filaments on the oceanic vertical pump. Journal of Marine Research (0022-2402) (Yale University), 2006-11 , Vol. 64 , N. 6 , P. 835-851, volume 64. doi:10.1357/002224006779698369.

Le Meur, J., Wirth, A., Paladini de Mendoza, F., Miserocchi, S., and Cardin, V. (2025). Intermittent supply of dense water to the deep South Adriatic Pit: an observational study. Frontiers in Marine Science, volume Volume 12 - 2025. ISSN 2296-7745. doi:10.3389/fmars.2025.1516780.

Leaman, K. D. (1994). The Formation of Western Mediterranean Deep Water, chapter 12, pages 227–248. American Geophysical Union (AGU). ISBN 9781118665039. doi:10.1029/CE046p0227.

Leaman, K. D. and Schott, F. A. (1991). Hydrographic structure of the convection regime in the Gulf of Lions: Winter 1987. Journal of Physical Oceanography, volume 21(4):575 – 598. doi:10.1175/1520-0485(1991)021<0575:HSOTCR>2.0.CO;2.

Lee, C. (2010). Frontal instability of lock-exchange gravity currents. Modern Physics Letters B, volume 24:1369–1372. doi:10.1142/S0217984910023645.

Lee, C., Chang, K.-I., Lee, J. H., and Richards, K. J. (2014). Vertical mixing due to double diffusion in the tropical western pacific. Geophysical Research Letters, volume 41(22):7964–7970. doi:10.1002/2014GL061698.

Legg, S., Briegleb, B., Chang, Y., Chassignet, E. P., Danabasoglu, G., Ezer, T., Gordon, A. L., Griffies, S., Hallberg, R., Jackson, L., Large, W., Özgökmen, T. M., Peters, H., Price, J., Riemenschneider, U., Wu, W., Xu, X., and Yang, J. (2009). Improving oceanic overflow representation in climate models: The gravity current entrainment climate process team. Bulletin of the American Meteorological Society, volume 90(5):657 – 670. doi:10.1175/2008BAMS2667.1.

Lejeusne, C., Chevaldonné, P., Pergent-Martini, C., Boudouresque, C., and Pérez, T. (2010). Climate change effects on a miniature ocean: The highly diverse, highly impacted mediterranean sea. Trends in Ecology and Evolution, volume 25:250–260. doi: 10.1016/j.tree.2009.10.009.

Li, P. and Tanhua, T. (2020). Recent changes in deep ventilation of the Mediterranean Sea; evidence from long-term transient tracer observations. Frontiers in Marine Science, volume Volume 7 - 2020. ISSN 2296-7745. doi:10.3389/fmars.2020.00594.

Li, X., Rowley, R. J., Kostelnick, J. C., Braaten, D., Meisel, J. J., and Hulbutta, K. (2009). Gis analysis of global impacts from sea level rise. Photogrammetric Engineering and Remote Sensing, volume 75:807–818.

Lipizer, M., Partescano, E., Rabitti, A., Giorgetti, A., and Crise, A. (2014a). Qualified temperature, salinity and dissolved oxygen climatologies in a changing adriatic sea. Ocean Science, volume 10(5):771–797. doi:10.5194/os-10-771-2014.

Lipizer, M., Partescano, E., Rabitti, A., Giorgetti, A., and Crise, A. (2014b). Qualified temperature, salinity and dissolved oxygen climatologies in a changing adriatic sea. Ocean Science, volume 10(5):771–797. doi:10.5194/os-10-771-2014.

Lévy, M., Ferrari, R., Franks, P. J. S., Martin, A. P., and Rivière, P. (2012). Bringing physics to life at the submesoscale. Geophysical Research Letters, volume 39(14). doi: 10.1029/2012GL052756.

Macias, D., Garcia-Gorriz, E., and Stips, A. (2013). Understanding the causes of recent warming of mediterranean waters. how much could be attributed to climate change? PLOS ONE, volume 8(11):1–6. doi:10.1371/journal.pone.0081591.

Manca, B., Ibello, V., Pacciaroni, M., Scarazzato, P., and Giorgetti, A. (2006). Ventilation of deep waters in the adriatic and ionian seas following changes in thermohaline circulation of the eastern mediterranean. Climate Research - CLIMATE RES, volume 31:239–256. doi:10.3354/cr031239.

Mantziafou, A. and Lascaratos, A. (2004). An eddy resolving numerical study of the general circulation and deep-water formation in the adriatic sea. Deep Sea Research Part I: Oceanographic Research Papers, volume 51(7):921–952. ISSN 0967-0637. doi: 10.1016/j.dsr.2004.03.006.

Marini, M., Russo, A., Paschini, E., Grilli, F., and Campanelli, A. (2006). Short-term physical and chemical variations in the bottom water of middle adriatic depressions. Climate Research, volume 31(2/3):227–237. ISSN 0936577X, 16161572. doi:10.3354/cr 031227.

Marshall, J. and Schott, F. (1999). Open-ocean convection: Observations, theory, and models. Reviews of Geophysics, volume 37(1):1–64. doi:10.1029/98RG02739.

Martellucci, R., Menna, M., Mauri, E., Pirro, A., Gerin, R., Paladini de Mendoza, F., Garić, R., Batistić, M., di Biagio, V., Giordano, P., Langone, L., Miserocchi, S., Gallo, A., Notarstefano, G., Savonitto, G., Bussani, A., Pacciaroni, M., Zuppelli, P., and Poulain, P.-M. (2024). Recent changes of the dissolved oxygen distribution in the deep convection cell of the southern adriatic sea. Journal of Marine Systems, volume 245:103988. ISSN 0924-7963. doi:/10.1016/j.jmarsys.2024.103988.

Maxworthy, T. and Narimousa, S. (1994). Unsteady, turbulent convection into a homogeneous, rotating fluid,with oceanographic applications. Journal of Physical Oceanography, volume 24(5):865 – 887. doi:10.1175/1520-0485(1994)024<0865:UTCIAH>2.0.CO;2.

McDougall, T. J. and Barker, P. M. (2011). Getting started with TEOS-10 and TS26 the Gibbs Seawater (GSW) Oceanographic Toolbox. SCOR/IAPSO WG127, volume 127:1–28.

McDougall, T. J. and Barker, P. M. (2014). Comment on "buoyancy frequency profiles and internal semidiurnal tide turning depths in the oceans" by b. king et al. Journal of Geophysical Research: Oceans, volume 119(12):9026–9032. doi:10.1002/2014JC010066.

McDougall, T. J., Thorpe, S. A., and Gibson, C. H. (1988). Small-scale turbulence and mixing in the ocean: A glossary. In Nihoul, J. and Jamart, B., editors, Small-Scale Turbulence and Mixing in the Ocean, volume 46 of Elsevier Oceanography Series, pages 3–9. Elsevier. doi:10.1016/S0422-9894(08)70533-6.

Meccia, V. L., Simoncelli, S., and Sparnocchia, S. (2016). Decadal variability of the turner angle in the mediterranean sea and its implications for double diffusion. Deep Sea Research Part I: Oceanographic Research Papers, volume 114:64–77. ISSN 0967-0637. doi:10.1016/j.dsr.2016.04.001.

Menna, M., Gerin, R., Notarstefano, G., Mauri, E., Bussani, A., Pacciaroni, M., and et al. (2021). On the circulation and thermohaline properties of the eastern mediterranean sea. Frontiers in Marine Science, volume 8. ISSN 2296-7745. doi:10.3389/fmars.2021.671469.

Mertens, C. and Schott, F. (1998). Interannual variability of deep-water formation in the northwestern mediterranean. Journal of Physical Oceanography, volume 28(7):1410 – 1424. doi:10.1175/1520-0485(1998)028<1410:IVODWF>2.0.CO;2.

Middleton, G. V. (1993). Sediment deposition from turbidity currents. Annual Review of Earth and Planetary Sciences, volume 21(Volume 21, 1993):89–114. ISSN 1545-4495. doi:10.1146/annurev.ea.21.050193.000513.

Mihanović, H., Janeković, I., Vilibić, I., Kovačević, V., and Bensi, M. (2018). Modelling interannual changes in dense water formation on the northern adriatic shelf. Pure and Applied Geophysics, volume 175(11):4065–4081. ISSN 1420-9136. doi:10.1007/s00024-018-1935-5.

Mihanović, H., Vilibić, I., Carniel, S., Tudor, M., Russo, A., Bergamasco, A., and et al. (2013). Exceptional dense water formation on the adriatic shelf in the winter of 2012. Ocean Science, volume 9(3):561–572. doi:10.5194/os-9-561-2013.

Mihanović, H., Vilibić, I., Dunić, N., and Šepić, J. (2015). Mapping of decadal middle adriatic oceanographic variability and its relation to the bios regime. Journal of Geophysical Research: Oceans, volume 120(8):5615–5630. doi:10.1002/2015JC010725.

Mihanović, H., Vilibić, I., Šepić, J., Matić, F., Ljubešić, Z., Mauri, E., Gerin, R., Notarstefano, G., and Poulain, P.-M. (2021). Observation, preconditioning and recurrence of exceptionally high salinities in the adriatic sea. Frontiers in Marine Science, volume 8. ISSN 2296-7745. doi:10.3389/fmars.2021.672210.

Munk, W. H. (1950). On the wind-driven ocean circulation. Journal of Meteorology, volume 7(2):79–93. doi:10.1175/1520-0469(1950)007<0079:OTWDOC>2.0.CO;2.

Negretti, M. E., Tucciarone, F. L., and Wirth, A. (2021). Intruding gravity currents and re-circulation in a rotating frame: Laboratory experiments. Physics of Fluids, volume 33(9):096607. ISSN 1070-6631. doi:10.1063/5.0058629.

Neri, F., Romagnoli, T., Accoroni, S., Campanelli, A., Marini, M., Grilli, F., and et al. (2022). Phytoplankton and environmental drivers at a long-term offshore station in the northern adriatic sea (1988–2018). Continental Shelf Research, volume 242:104746. doi:10.1016/j.csr.2022.104746.

[Dataset] Nigam, T., Escudier, R., Pistoia, J., Aydogdu, A., Omar, M., Clementi, E., Cipollone, A., Drudi, M., Grandi, A., Mariani, A., Lyubartsev, V., Lecci, R., Cretí, S., Masina, S., Coppini, G., and Pinardi, N. (2021). Mediterranean Sea Physical Reanalysis INTERIM (CMEMS MED-Currents, E3R1i system) (Version 1). doi:10.25423/CMCC/MEDSEA_MULTIYEAR_PHY_006_004_E3R1.

Orlić, M., Dadić, V., Grbec, B., Leder, N., Marki, A., Matić, F., Mihanović, H., Beg Paklar, G., Pasarić, M., Pasarić, Z., and Vilibić, I. (2006). Wintertime buoyancy forcing, changing seawater properties, and two different circulation systems produced in the Adriatic. Journal of Geophysical Research: Oceans, volume 111(C3). doi:10.1029/2005JC003271.

Ouzani, R. and Khelladi, S. (2023). Numerical study of salt fingers dynamics: Effects of the density inversion. Thermal Science and Engineering Progress, volume 40:101770. ISSN 2451-9049. doi:10.1016/j.tsep.2023.101770.

Ovchinnikov, I. M., Zats, V. I., Krivosheia, V. G., and Udodov, A. I. (1985). Formation of deep eastern Mediterranean waters in the Adriatic Sea. Oceanology, volume 25:704–707.

Ozer, T., Gertman, I., Kress, N., Silverman, J., and Herut, B. (2017). Interannual thermohaline (1979–2014) and nutrient (2002–2014) dynamics in the Levantine surface and intermediate water masses, SE Mediterranean Sea. Global and Planetary Change, volume 151:60–67. ISSN 0921-8181. doi:10.1016/j.gloplacha.2016.04.001. Climate Variability and Change in the Mediterranean Region.

[Dataset] Paladini de Mendoza, F., Miserocchi, S., Langone, L., Giordano, P., Schroeder, K., Borghini, M., and Verrazzo, G. (2024a). Moored ADCP measurements in the Southern Adriatic Sea at mooring site BB and FF, June 2020 - April 2023. doi:10.5281/zenodo.10604970.

[Dataset] Paladini de Mendoza, F., Miserocchi, S., Langone, L., Giordano, P., Schroeder, K., Borghini, M., and Verrazzo, G. (2024b). Moored CTD measurements in the Southern Adriatic Sea at mooring site BB and FF, June 2020 - March 2022. doi:10.5281/zenodo.14576897.

Paladini de Mendoza, F., Schroeder, K., Langone, L., Chiggiato, J., Borghini, M., Giordano, P., and et al. (2022a). Deep-water hydrodynamic observations of two moorings sites on the continental slope of the southern Adriatic Sea (Mediterranean Sea). Earth System Science Data, volume 14(12):5617–5635. doi:10.5194/essd-14-5617-2022.

Paladini de Mendoza, F., Schroeder, K., Langone, L., Chiggiato, J., Borghini, M., Giordano, P., and Miserocchi, S. (2023). Deep-water dynamics along the 2012–2020 observations on the continental margin of the southern adriatic sea (mediterranean sea). Journal of Marine Science and Engineering, volume 11(7). ISSN 2077-1312. doi: 10.3390/jmse11071364.

[Dataset] Paladini de Mendoza, F., Schroeder, K., Langone, L., Chiggiato, J., Borghini, M., Giordano, P., Verazzo, G., and Miserocchi, S. (2022b). Moored current and temperature measurements in the Southern Adriatic Sea at mooring site BB and FF, March 2012-June 2020. doi:10.5281/zenodo.7311090.

Palermino, A., De Felice, A., Canduci, G., Biagiotti, I., Costantini, I., Centurelli, M., Menicucci, S., Gašparević, D., Tičina, V., and Leonori, I. (2024). Modeling of the habitat suitability of european sprat (sprattus sprattus, l.) in the adriatic sea under several climate change scenarios. Frontiers in Marine Science, volume Volume 11 - 2024. ISSN 2296-7745. doi:10.3389/fmars.2024.1383063.

Panzeri, D., Reale, M., Cossarini, G., Salon, S., Carlucci, R., Spedicato, M. T., Zupa, W., Vrgoč, N., and Libralato, S. (2024). Future distribution of demersal species in a warming mediterranean sub-basin. Frontiers in Marine Science, volume Volume 11 - 2024. ISSN 2296-7745. doi:10.3389/fmars.2024.1308325.

Pedlosky, J. (1996). Ocean Circulation Theory. Springer. ISBN 9780387943619. doi: 10.1007/978-3-662-03203-6.

Pisano, A., Marullo, S., Artale, V., Falcini, F., Yang, C., Leonelli, F. E., Santoleri, R., and Buongiorno Nardelli, B. (2020). New evidence of mediterranean climate change and variability from sea surface temperature observations. Remote Sensing, volume 12(1). ISSN 2072-4292. doi:10.3390/rs12010132.

Pranić, P., Denamiel, C., and Vilibić, I. (2024). Kilometer-scale assessment of the adriatic dense water multi-decadal dynamics. Journal of Geophysical Research: Oceans, volume 129(10):e2024JC021182. doi:10.1029/2024JC021182. E2024JC021182 2024JC021182.

Princevac, M., Fernando, H., and Whiteman, C. (2005). Turbulent entrainment into natural gravity-driven flows. Journal of Fluid Mechanics, volume 533:259–268. doi: 10.1017/S0022112005004441.

Querin, S., Bensi, M., Cardin, V., Solidoro, C., Bacer, S., Mariotti, L., Stel, F., and Malačič, V. (2016). Saw-tooth modulation of the deep-water thermohaline properties in the southern adriatic sea. Journal of Geophysical Research: Oceans, volume 121(7):4585–4600. doi:10.1002/2015JC011522.

Radko, T. (2013). Double-Diffusive Convection. Cambridge University Press.

Rahmstorf, S. (1998). Influence of mediterranean outflow on climate. Eos, Transactions American Geophysical Union, volume 79(24):281–282. doi:10.1029/98EO00208.

Raicich, F., Malačič, V., Celio, M., Giaiotti, D., Cantoni, C., Colucci, R. R., Čermelj, B., and Pucillo, A. (2013). Extreme air-sea interactions in the gulf of trieste (north adriatic) during the strong bora event in winter 2012. Journal of Geophysical Research: Oceans, volume 118(10):5238–5250. doi:10.1002/jgrc.20398.

Reale, M., Cossarini, G., Lazzari, P., Lovato, T., Bolzon, G., Masina, S., Solidoro, C., and Salon, S. (2022). Acidification, deoxygenation, and nutrient and biomass declines in a warming mediterranean sea. Biogeosciences, volume 19(17):4035–4065. doi:10.5194/bg-19-4035-2022.

Reiners, P., Obrecht, L., Dietz, A., Holzwarth, S., and Kuenzer, C. (2024). First Analyses of the TIMELINE AVHRR SST Product: Long-Term Trends of Sea Surface Temperature at 1 km Resolution across European Coastal Zones. Remote Sensing, volume 16(11). ISSN 2072-4292. doi:10.3390/rs16111932.

Rétif, S., Negretti, M. E., and Wirth, A. (2024). Predicting the vertical density structure of oceanic gravity current intrusions. Scientific Reports, volume 14(1):10274. ISSN 2045-2322. doi:10.1038/s41598-024-60878-x.

Richardson, P., Bower, A., and Zenk, W. (2000). A census of meddies tracked by floats. Progress in Oceanography, volume 45(2):209–250. ISSN 0079-6611. doi:10.1016/S0079-6611(99)00053-1.

Rivetti, I., Boero, F., Fraschetti, S., Zambianchi, E., and Lionello, P. (2017). Anomalies of the upper water column in the mediterranean sea. Global and Planetary Change, volume 151:68–79. ISSN 0921-8181. doi:10.1016/j.gloplacha.2016.03.001. Climate Variability and Change in the Mediterranean Region.

Robinson, A. R. and Golnaraghi, M. (1994). The physical and dynamical oceanography of the Mediterranean Sea. In Malanotte-Rizzoli, P. and Robinson, A. R., editors, Ocean Processes in Climate Dynamics: Global and Mediterranean Examples, pages 255–306. Springer Netherlands, Dordrecht. ISBN 978-94-011-0870-6. doi:10.1007/978-94-011-0870-6_12.

Rohling, E. J. and Bryden, H. L. (1992). Man-induced salinity and temperature increases in western mediterranean deep water. Journal of Geophysical Research: Oceans, volume 97(C7):11191–11198. doi:10.1029/92JC00767.

Romanou, A., Tselioudis, G., Zerefos, C. S., Clayson, C.-A., Curry, J. A., and Andersson, A. (2010). Evaporation–precipitation variability over the mediterranean and the black seas from satellite and reanalysis estimates. Journal of Climate, volume 23(19):5268 – 5287. doi:10.1175/2010JCLI3525.1.

Rubino, A., Romanenkov, D., Zanchettin, D., Cardin, V., Hainbucher, D., Bensi, M., and et al. (2012). On the descent of dense water on a complex canyon system in the southern Adriatic basin. Continental Shelf Research, volume 44:20–29. doi:10.1016/j.csr.2010.11.009.

Ruddick, B. (1983). A practical indicator of the stability of the water column to double-diffusive activity. Deep Sea Research Part A. Oceanographic Research Papers, volume 30(10):1105–1107. ISSN 0198-0149. doi:10.1016/0198-0149(83)90063-8.

Schmitt, R. (1988). Mixing in a thermohaline staircase. In Nihoul, J. and Jamart, B., editors, Small-Scale Turbulence and Mixing in the Ocean, volume 46 of Elsevier Oceanography Series, pages 435–452. Elsevier. doi:10.1016/S0422-9894(08)70563-4.

Schmitt, R. (2003). Observational and laboratory insights into salt finger convection. Progress in Oceanography, volume 56(3):419–433. ISSN 0079-6611. doi:10.1016/S0079-6611(03)00033-8. Double-Diffusion in Oceanography.

Schmitt, R. W. (1994). Double diffusion in oceanography. Annual Review of Fluid Mechanics, volume 26(Volume 26, 1994):255–285. ISSN 1545-4479. doi:10.1146/annurev.fl.26.010194.001351.

Schott, F. and Leaman, K. D. (1991). Observations with moored acoustic doppler current profilers in the convection regime in the Gulf of Lions. Journal of Physical Oceanography, volume 21(4):558–574.

Schott, F., Visbeck, M., Send, U., Fischer, J., Stramma, L., and Desaubies, Y. (1996). Observations of deep convection in the Gulf of Lions, northern Mediterranean, during the winter of 1991/92. Journal of Physical Oceanography, volume 26(4):505 – 524. doi:10.1175/1520-0485(1996)026<0505:OODCIT>2.0.CO;2.

Schroeder, K., Cozzi, S., Belgacem, M., Borghini, M., Cantoni, C., Durante, S., Petrizzo, A., Poiana, A., and Chiggiato, J. (2020). Along-path evolution of biogeochemical and carbonate system properties in the intermediate water of the western Mediterranean. Frontiers in Marine Science, volume Volume 7 - 2020. ISSN 2296-7745. doi:10.3389/fmars.2020.00375.

Seabold, S. and Perktold, J. (2010). Statsmodels: Econometric and Statistical Modeling with Python, volume 2010. S. van der Walt and J. Millman. doi:10.25080/Majora-92bf1922-011.

Shapiro, G. I. and Hill, A. E. (1997). Dynamics of dense water cascades at the shelf edge. Journal of Physical Oceanography, volume 27(11):2381 – 2394. doi:10.1175/1520-0485(1997)027<2381:DODWCA>2.0.CO;2.

Simpson, J. E. (1982). Gravity currents in the laboratory, atmosphere, and ocean. Annual Review of Fluid Mechanics, volume 14:213–234. doi:10.1146/annurev.fl.14.010182.001241.

Simpson, J. E. (1997). Gravity Currents in the Environment and the Laboratory. Cambridge University Press, Cambridge, UK, 2nd edition. ISBN 9780521664011.

Skliris, N., Marsh, R., Breedon, M., and Josey, S. A. (2025). Accelerated warming and salinification of the Mediterranean Sea: Implications for dense water formation. Journal of Marine Science and Engineering, volume 13(1). ISSN 2077-1312. doi:10.3390/jmse13010025.

Skliris, N., Sofianos, S., Gkanasos, A., Mantziafou, A., Vervatis, V., Axaopoulos, P., and Lascaratos, A. (2012). Decadal scale variability of sea surface temperature in the Mediterranean Sea in relation to atmospheric variability. Ocean Dynamics, volume 62(1):13–30. ISSN 1616-7228. doi:10.1007/s10236-011-0493-5.

Skliris, N., Zika, J. D., Herold, L., Josey, S. A., and Marsh, R. (2018). Mediterranean sea water budget long-term trend inferred from salinity observations. Climate Dynamics, volume 51(7):2857–2876. ISSN 1432-0894. doi:10.1007/s00382-017-4053-7.

Soto-Navarro, J., Jordá, G., Amores, A., Cabos, W., Somot, S., Sevault, F., Macías, D., Djurdjevic, V., Sannino, G., Li, L., and Sein, D. (2020). Evolution of Mediterranean Sea water properties under climate change scenarios in the Med-CORDEX ensemble. Climate Dynamics, volume 54(3):2135–2165. ISSN 1432-0894. doi:10.1007/s00382-019-05105-4.

Spall, M. A. (2004). Boundary currents and watermass transformation in marginal seas. Journal of Physical Oceanography, volume 34(5):1197 – 1213. doi:10.1175/1520-0485(2004)034<1197:BCAWTI>2.0.CO;2.

Spall, M. A. and Price, J. F. (1998). Mesoscale variability in Denmark Strait: The PV outflow hypothesis. Journal of Physical Oceanography, volume 28(8):1598 – 1623. doi:10.1175/1520-0485(1998)028<1598:MVIDST>2.0.CO;2.

Stern, M. E. (1960). The "salt-fountain" and thermohaline convection. Tellus, volume 12:172–175.

Stommel, H. (1948). The westward intensification of wind-driven ocean currents. Transactions, American Geophysical Union, volume 29(2):202–206. doi:10.1029/TR029i002p00202.

Supić, N. and Orlić, M. (1999). Seasonal and interannual variability of the northern Adriatic surface fluxes. Journal of Marine Systems, volume 20(1):205–229. ISSN 0924-7963. doi:10.1016/S0924-7963(98)00083-9.

Supić, N. and Vilibić, I. (2006). Dense water characteristics in the northern Adriatic in the 1967–2000 interval with respect to surface fluxes and Po river discharge rates. Estuarine, Coastal and Shelf Science, volume 66(3):580–593. ISSN 0272-7714. doi:10.1016/j.ecss.2005.11.003.

Taillandier, V., Prieur, L., D'Ortenzio, F., Ribera d'Alcalà, M., and Pulido-Villena, E. (2020). Profiling float observation of thermohaline staircases in the western Mediterranean Sea and impact on nutrient fluxes. Biogeosciences, volume 17(13):3343–3366. doi:10.5194/bg-17-3343-2020.

Tait, R. and Howe, M. (1968). Some observations of thermo-haline stratification in the deep ocean. Deep Sea Research and Oceanographic Abstracts, volume 15(3):275–280. ISSN 0011-7471. doi:10.1016/0011-7471(68)90005-3.

Talley, L. D., Pickard, G. L., Emery, W. J., and Swift, J. H. (2011). Descriptive Physical Oceanography: An Introduction. Academic Press, Amsterdam, 6th edition. ISBN 9780123855303.

Tanhua, T., Hainbucher, D., Schroeder, K., Cardin, V., Álvarez, M., and Civitarese, G. (2013). The Mediterranean Sea system: a review and an introduction to the special issue. Ocean Science, volume 9(5):789–803. doi:10.5194/os-9-789-2013.

Tassigny, A., Negretti, M., and Wirth, A. (2024). Dynamics of intrusion in downslope gravity currents in a rotating frame. Physical Review Fluids, volume 9(7):074605. doi:10.1103/PhysRevFluids.9.074605.

Taviani, M., Angeletti, L., Foglini, F., Corselli, C., Nasto, I., Pons-Branchu, E., and Montagna, P. (2019). U/Th dating records of cold-water coral colonization in submarine canyons and adjacent sectors of the southern Adriatic Sea since the last glacial maximum. Progress in Oceanography, volume 175:300–308. ISSN 0079-6611. doi: 10.1016/j.pocean.2019.04.011.

Taylor, J. R. and Thompson, A. F. (2023). Submesoscale dynamics in the upper ocean. Annual Review of Fluid Mechanics, volume 55(Volume 55, 2023):103–127. ISSN 1545-4479. doi:10.1146/annurev-fluid-031422-095147.

[Dataset] Terzić, E., Cardin, V., Le Meur, J., Dunić, N., Vodopivec, M., and Vilibić, I. (2024). The deep adriatic transient dataset [dataset]. doi:10.5281/zenodo.13788664.

Terzić, E., Cardin, V., Le Meur, J., Dunić, N., Vodopivec, M., and Vilibić, I. (2025). Unprecedented warming and salinization observed in the deep Adriatic. Limnology and Oceanography Letters. doi:10.1002/lol2.70051.

Testor, P., Bosse, A., Houpert, L., Margirier, F., Mortier, L., Legoff, H., and et al. (2018). Multiscale observations of deep convection in the northwestern Mediterranean Sea during winter 2012–2013 using multiple platforms. Journal of Geophysical Research: Oceans, volume 123(3):1745–1776. doi:10.1002/2016JC012671.

Tojčić, I., Denamiel, C., and Vilibić, I. (2023). Kilometer-scale trends and variability of the Adriatic present climate (1987–2017). Climate Dynamics, volume 61(5):2521–2545. ISSN 1432-0894. doi:10.1007/s00382-023-06700-2.

Tokos, K. S. and Rossby, T. (1991). Kinematics and dynamics of a Mediterranean salt lens. Journal of Physical Oceanography, volume 21(6):879 – 892. doi:10.1175/1520-0485(1991)021<0879:KADOAM>2.0.CO;2.

Trotta, F., Pinardi, N., Fenu, E., Grandi, A., and Lyubartsev, V. (2017). Multi-nest high-resolution model of submesoscale circulation features in the Gulf of Taranto. Ocean Dynamics, volume 67(12):1609–1625. ISSN 1616-7228. doi:10.1007/s10236-017-1110-z.

Tsimplis, M. N. and Baker, T. F. (2000). Sea level drop in the Mediterranean Sea: An indicator of deep water salinity and temperature changes? Geophysical Research Letters, volume 27(12):1731–1734. doi:10.1029/1999GL007004.

Ungarish, M. (2022). On the spinup and spreadout of a cartesian gravity current on a slope in a rotating system. Journal of Fluid Mechanics, volume 943:A31. doi:10.1017/jfm.2022.447.

Ursella, L., Kovačević, V., and Gačić, M. (2011). Footprints of mesoscale eddy passages in the Strait of Otranto (Adriatic Sea). Journal of Geophysical Research: Oceans, volume 116(C4). doi:10.1029/2010JC006633.

Valle-Levinson, A. (2022). Introduction and classification. In Introduction to Estuarine Hydrodynamics, page 1–7. Cambridge University Press.

Vallis, G. K. (2017). Atmospheric and Oceanic Fluid Dynamics: Fundamentals and Large-Scale Circulation. Cambridge University Press, 2nd edition. ISBN 9781107065505. doi:10.1017/9781107588417.

van der Boog, C. G., Dijkstra, H. A., Pietrzak, J. D., and Katsman, C. A. (2022). Spatial variations of Antarctic Intermediate Water in the Caribbean Sea due to vertical mixing along its path. Geophysical Research Letters, volume 49(3):e2021GL095977. doi:10.1029/2021GL095977.

Vargas-Yáñez, M., García-Martínez, M., Moya, F., Balbín, R., López-Jurado, J., Serra, M., Zunino, P., Pascual, J., and Salat, J. (2017). Updating temperature and salinity mean values and trends in the western Mediterranean: The RADMED project. Progress in Oceanography, volume 157:27–46. ISSN 0079-6611. doi:10.1016/j.pocean.2017.09.004.

Vargas-Yáñez, M., Juza, M., García-Martínez, M. C., Moya, F., Balbín, R., Ballesteros, E., Muñoz, M., Tel, E., Pascual, J., Vélez-Belchí, P., and Salat, J. (2021). Long-term changes in the water mass properties in the Balearic channels over the period 1996–2019. Frontiers in Marine Science, volume Volume 8 - 2021. ISSN 2296-7745. doi:10.3389/fmars.2021.640535.

Vecchio, A., Anzidei, M., and Serpelloni, E. (2023). Sea level rise projections up to 2150 in the northern Mediterranean coasts. Environmental Research Letters, volume 19(1):014050. doi:10.1088/1748-9326/ad127e.

Veronis, G. (1965). On finite amplitude instability in thermohaline convection. Journal of Marine Research, volume 23:1–17.

Verri, G., Furnari, L., Gunduz, M., Senatore, A., Santos da Costa, V., De Lorenzis, A., Fedele, G., Manco, I., Mentaschi, L., Clementi, E., Coppini, G., Mercogliano, P., Mendicino, G., and Pinardi, N. (2024). Climate projections of the Adriatic Sea: role of river release. Frontiers in Climate, volume Volume 6 - 2024. ISSN 2624-9553. doi:10.3389/fclim.2024.1368413.

Verri, G., Pinardi, N., Oddo, P., Ciliberti, S. A., and Coppini, G. (2018). River runoff influences on the central Mediterranean overturning circulation. Climate Dynamics, volume 50(5):1675–1703. ISSN 1432-0894. doi:10.1007/s00382-017-3715-9.

Vilibić, I. and Šantić, D. (2008). Deep water ventilation traced by synechococcus cyanobacteria. Ocean Dynamics, volume 58(2):119–125. ISSN 1616-7228. doi:10.1007/s10236-008-0135-8.

Vilibić, I. and Supić, N. (2005). Dense water generation on a shelf: the case of the Adriatic Sea. Ocean Dynamics, volume 55(5):403–415. ISSN 1616-7228. doi:10.1007/s10236-005-0030-5.

Vilibić, I. (2003). An analysis of dense water production on the North Adriatic shelf. Estuarine, Coastal and Shelf Science, volume 56(3):697–707. ISSN 0272-7714. doi:10.1016/S0272-7714(02)00277-9.

Vilibić, I., Mihanović, H., Šepić, J., and Matijević, S. (2011). Using self-organising maps to investigate long-term changes in deep Adriatic water patterns. Continental Shelf Research, volume 31(6):695–711. ISSN 0278-4343. doi:10.1016/j.csr.2011.01.007.

Vilibić, I. and Orlić, M. (2001). Least-squares tracer analysis of water masses in the South Adriatic (1967–1990). Deep Sea Research Part I: Oceanographic Research Papers, volume 48(10):2297–2330. ISSN 0967-0637. doi:10.1016/S0967-0637(01)00014-0.

Vilibić, I. and Orlić, M. (2002). Adriatic water masses, their rates of formation and transport through the Otranto Strait. Deep Sea Research Part I: Oceanographic Research Papers, volume 49(8):1321–1340. ISSN 0967-0637. doi:10.1016/S0967-0637(02)00028-6.

Vilibić, I., Pranić, P., and Denamiel, C. (2023). North Adriatic dense water: lessons learned since the pioneering work of Mira Zore-Armanda 60 years ago. Acta Adriatica, pages 53–78. . doi:10.32582/aa.64.1.11.

Virtanen, P., Gommers, R., Oliphant, T. E., Haberland, M., Reddy, T., Cournapeau, D., Burovski, E., Peterson, P., Weckesser, W., Bright, J., van der Walt, S. J., Brett, M., Wilson, J., Millman, K. J., Mayorov, N., Nelson, A. R. J., Jones, E., Kern, R., Larson, E., Carey, C. J., Polat, I., Feng, Y., Moore, VanderPlas, J., Laxalde, D., Perktold, J., Cimrman, R., Henriksen, I., Quintero, E. A., Harris, C. R., Archibald, A. M., Ribeiro, A. H., Pedregosa, F., van Mulbregt, P., and Contributors, S. . (2020). Scipy 1.0: Fundamental algorithms for scientific computing in python. Nature Methods, volume 17(3):261–272. ISSN 1548-7105. doi:10.1038/s41592-019-0686-2.

Vodopivec, M., Zaimi, K., and Peliz, A. J. (2022). The freshwater balance of the Adriatic Sea: A sensitivity study. Journal of Geophysical Research: Oceans, volume 127(11):e2022JC018870. doi:10.1029/2022JC018870. E2022JC018870 2022JC018870.

Wåhlin, A. K. and Walin, G. (2001). Downward migration of dense bottom currents. Environmental Fluid Mechanics, volume 1(2):257–279. ISSN 1573-1510. doi:10.1023/A:1011520432200.

Wang, G., Cheng, L., Boyer, T., and Li, C. (2017). Halosteric sea level changes during the Argo era. Water, volume 9(7). ISSN 2073-4441. doi:10.3390/w9070484.

Wes McKinney (2010). Data Structures for Statistical Computing in Python. In Stéfan van der Walt and Jarrod Millman, editors, Proceedings of the 9th Python in Science Conference, pages 56 – 61. doi:10.25080/Majora-92bf1922-00a.

Williams, R. G. and Follows, M. J. (1998). Eddies make ocean deserts bloom. Nature, volume 394(6690):228–229. ISSN 1476-4687. doi:10.1038/28285.

Wirth, A. (2009). On the basic structure of oceanic gravity currents. Ocean Dynamics, volume 59(4):551–563. ISSN 1616-7228. doi:10.1007/s10236-009-0202-9.

Yano, J. (2023). Double-diffusion convection. In Geophysical Convection Dynamics, volume 5 of Developments in Weather and Climate Science, chapter 6. Royal Meteorological Society /Elsevier, Toulouse, France /Amsterdam. ISBN 9780323912136.

You, Y. (2002). A global ocean climatological atlas of the Turner angle: implications for double-diffusion and water-mass structure. Deep Sea Research Part I: Oceanographic Research Papers, volume 49(11):2075–2093. ISSN 0967-0637. doi:10.1016/S0967-0637(02)00099-7.

Zhang, J. and Schmitt, R. W. (2000). The impact of salt fingering on the thermohaline circulation under mixed boundary conditions. Journal of Physical Oceanography, volume 30(6):1223 – 1231. doi:10.1175/1520-0485(2000)030<1223:TIOSFO>2.0.CO;2.

Zunino, P., Schroeder, K., Vargas-Yáñez, M., Gasparini, G., Coppola, L., García-Martínez, M., and Moya-Ruiz, F. (2012). Effects of the western Mediterranean transition on the resident water masses: Pure warming, pure freshening and pure heaving. Journal of Marine Systems, volume 96-97:15–23. ISSN 0924-7963. doi: 10.1016/j.jmarsys.2012.01.011.

Appendices

Appendix A

Variability of water masses properties in the SAP

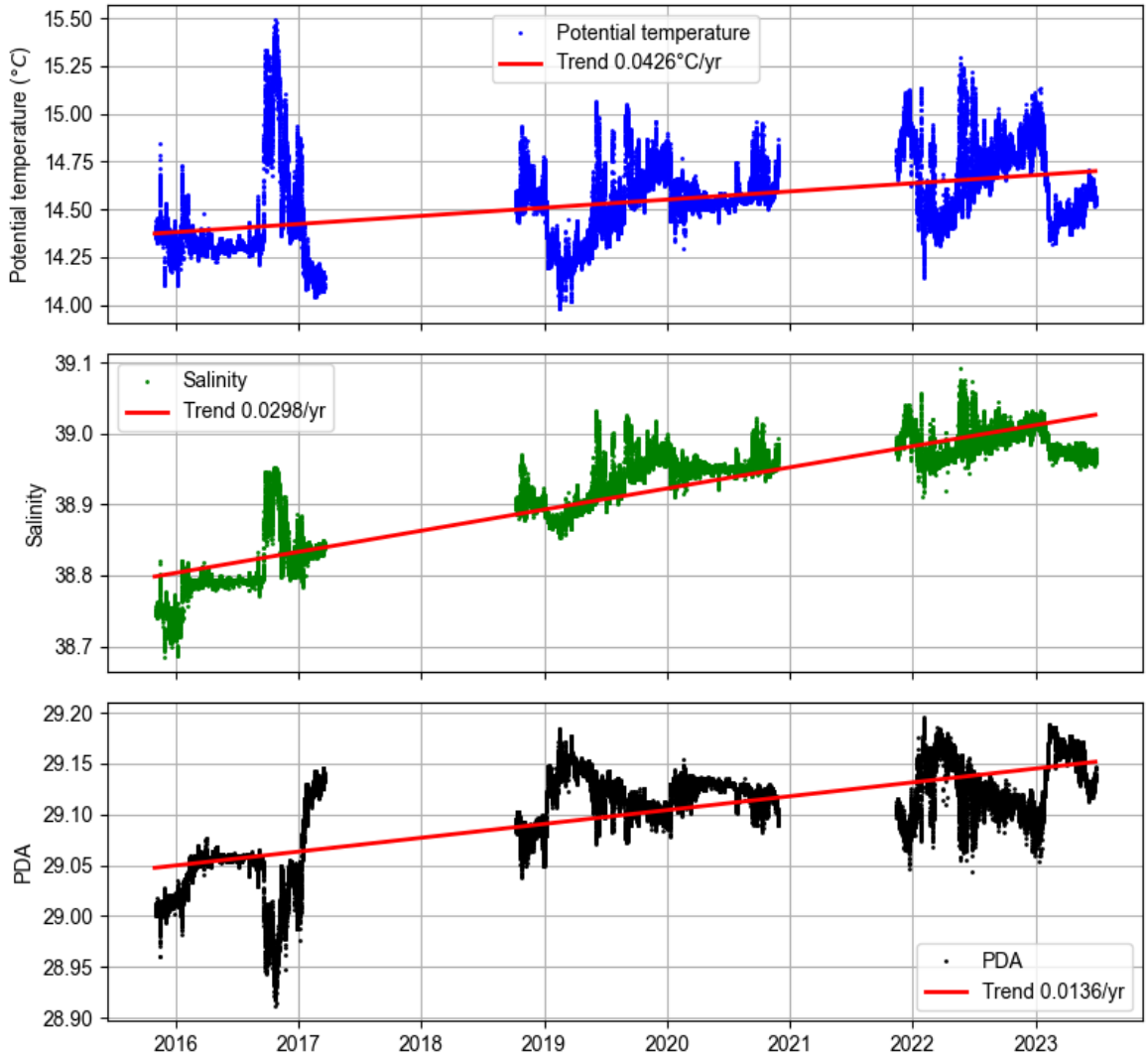

Figure A.1: Trends of potential temperature, salinity and potential density anomaly at 150 dbar

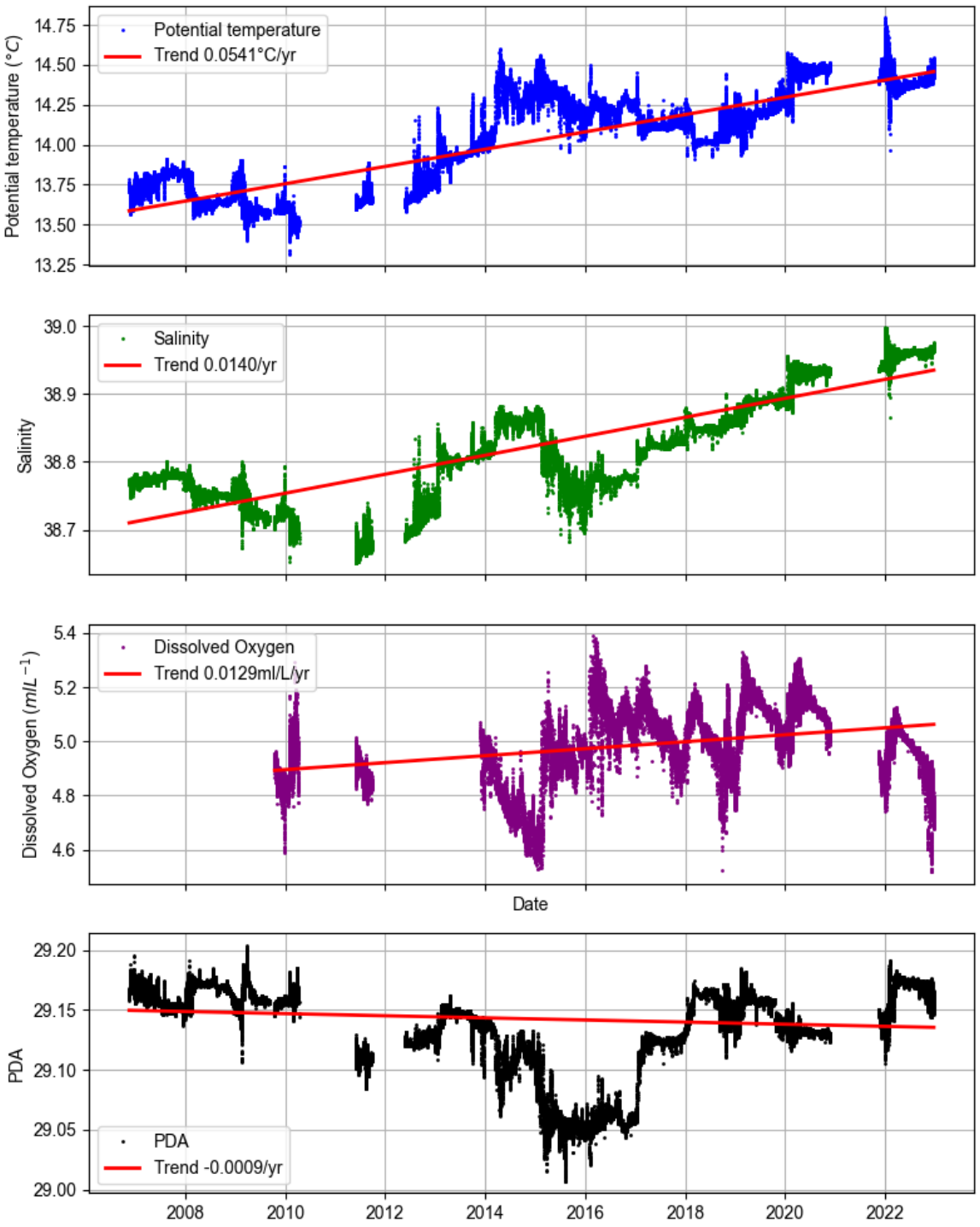

Figure A.2: Trends of potential temperature, salinity, dissolved oxygen and potential density anomaly at 350 dbar

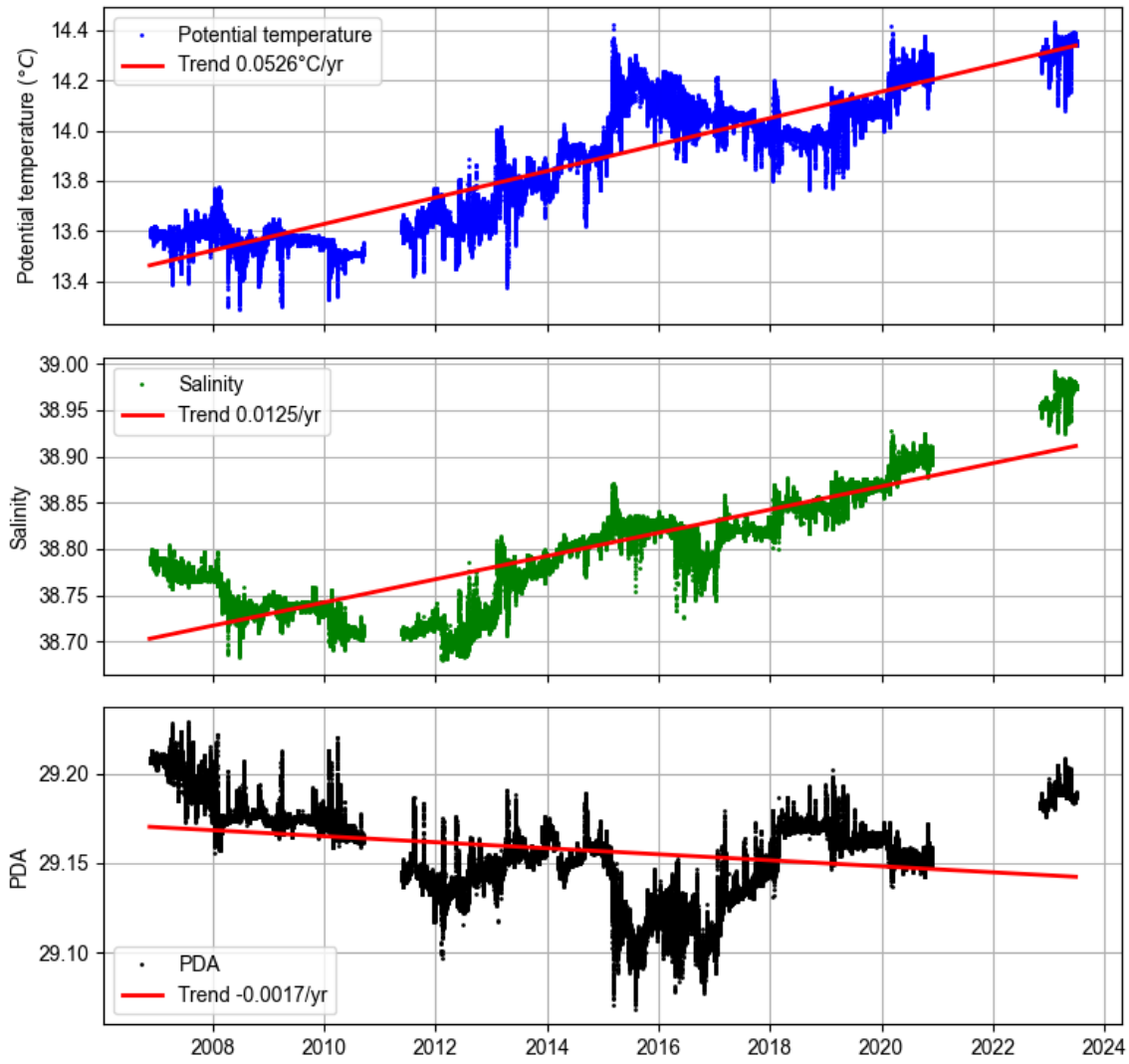

Figure A.3: Trends of potential temperature, salinity and potential density anomaly at 550 dbar

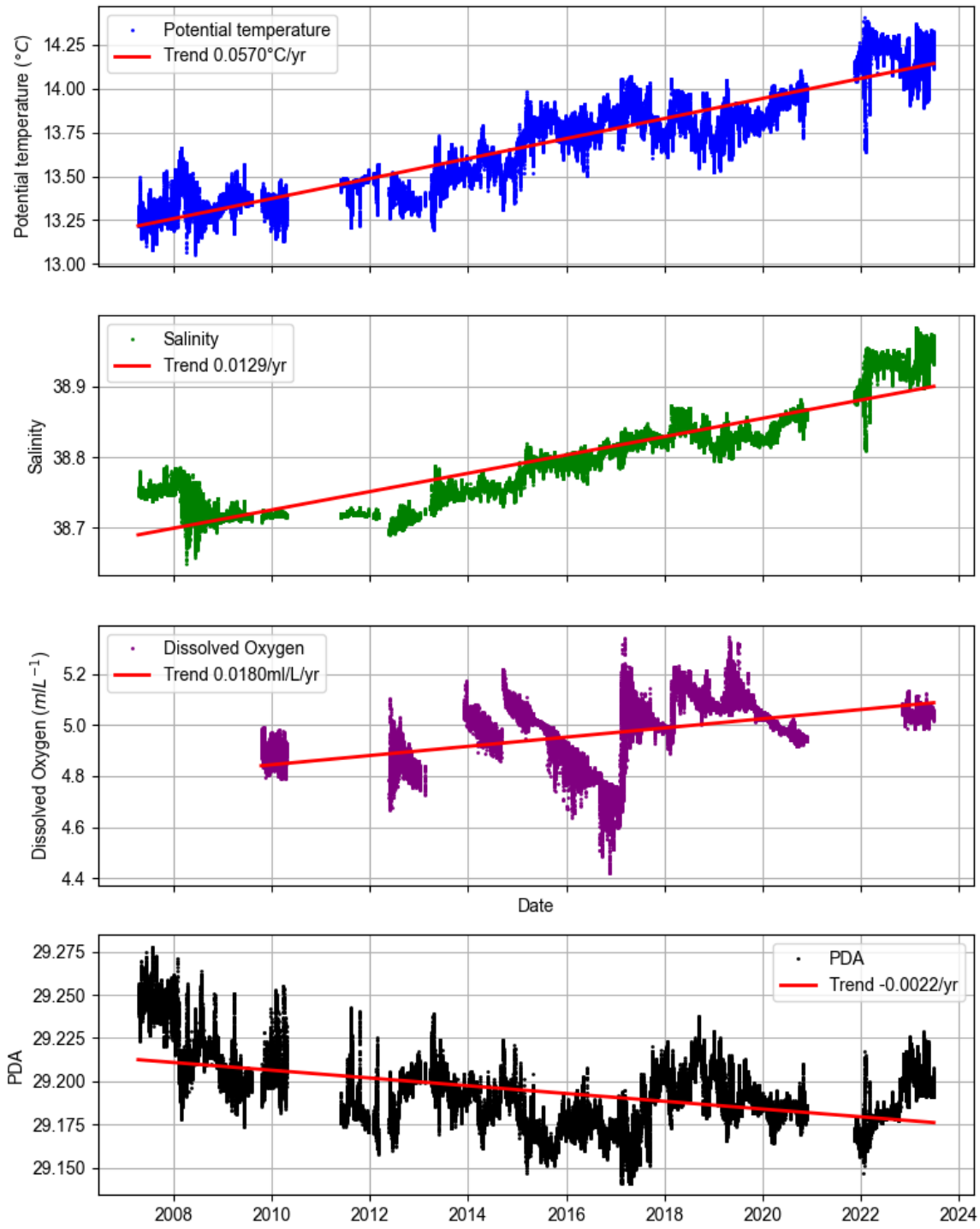

Figure A.4: Trends of potential temperature, salinity, dissolved oxygen and potential density anomaly at 750 dbar

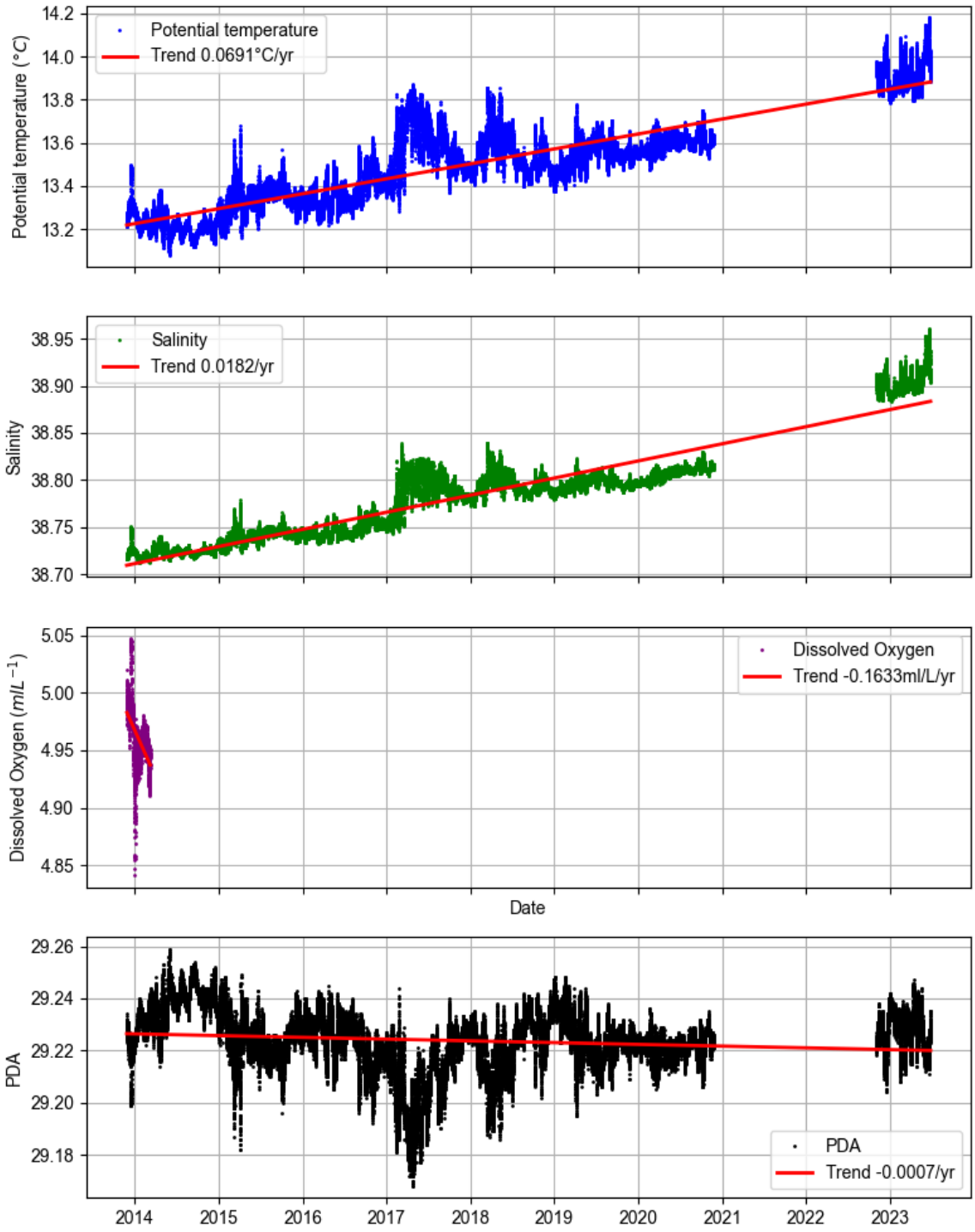

Figure A.5: Trends of potential temperature, salinity, dissolved oxygen and potential density anomaly at 900 dbar

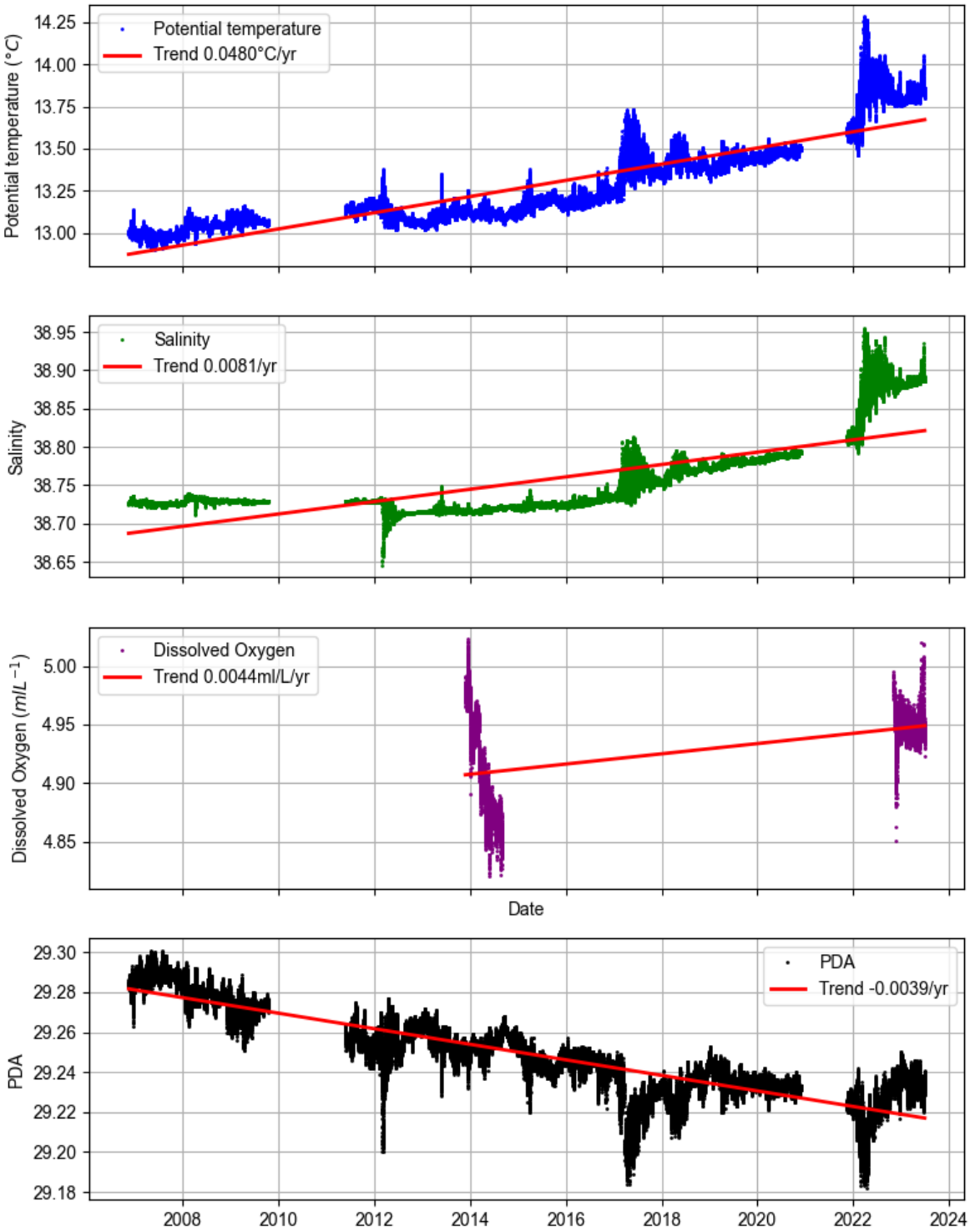

Figure A.6: Trends of potential temperature, salinity, dissolved oxygen and potential density anomaly at 1000 dbar

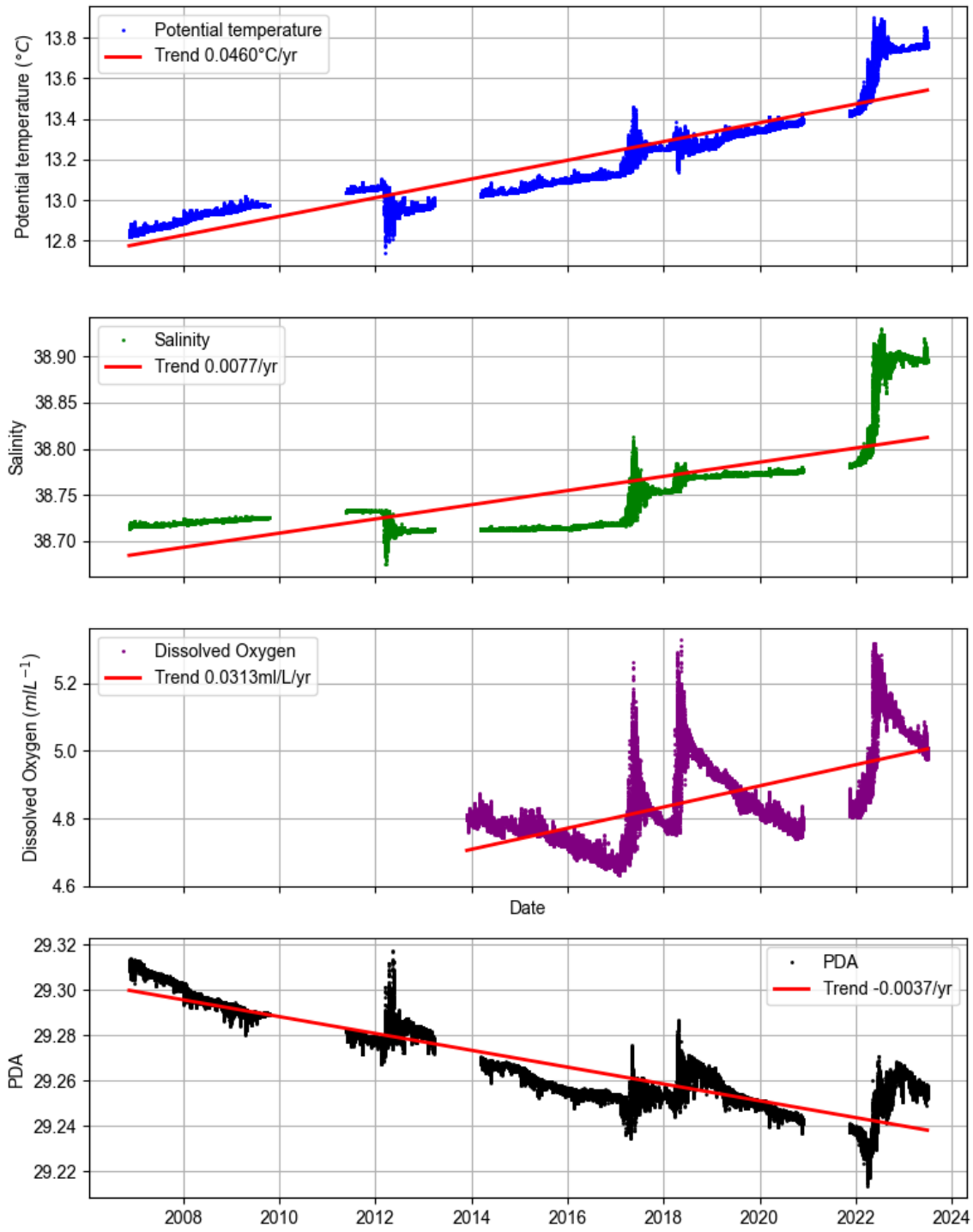

Figure A.7: Trends of potential temperature, salinity, dissolved oxygen and potential density anomaly at 1200 dbar

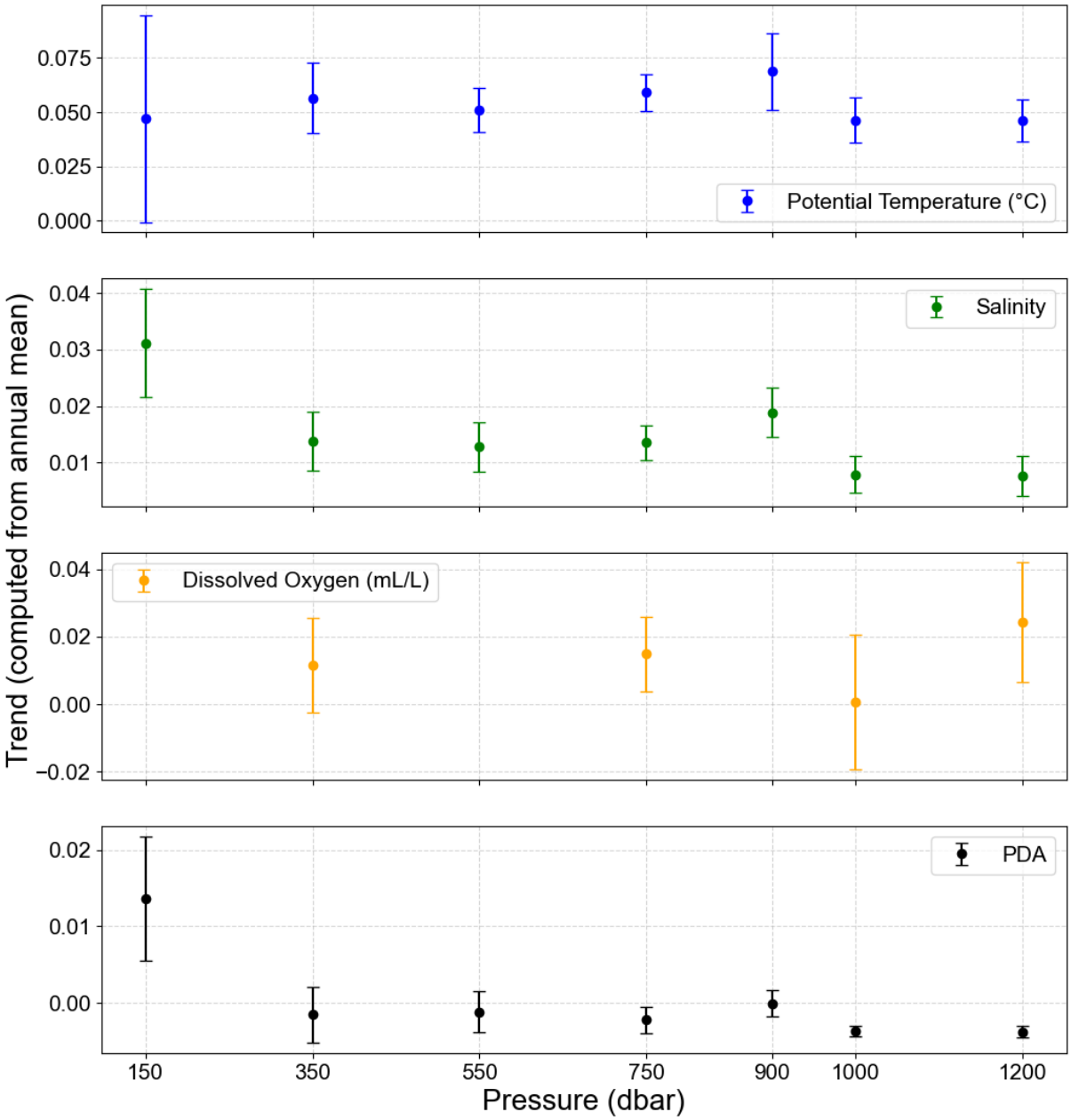

Figure A.8: Trends and errors bars of potential temperature, salinity, dissolved oxygen and potential density anomaly for the different layers computed with annual mean of the different variables.

Appendix B

Analysis of bottom ventilation years in the SAP

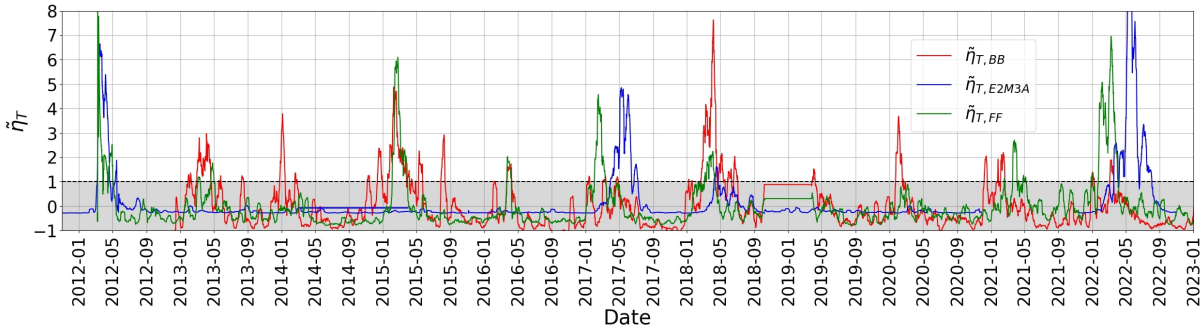

Figure B.1: Time series of $\tilde{\eta}_T$ at E2M3A (blue), BB (red) and FF (green). Temperature data used here at BB and FF were obtained with CTD SBE56 placed at around 40 m above the bottom of the two respective mooring lines. In 2022, bursts of fluctuations observed at E2M3A are mainly due to bursts of fluctuations observed in FF.

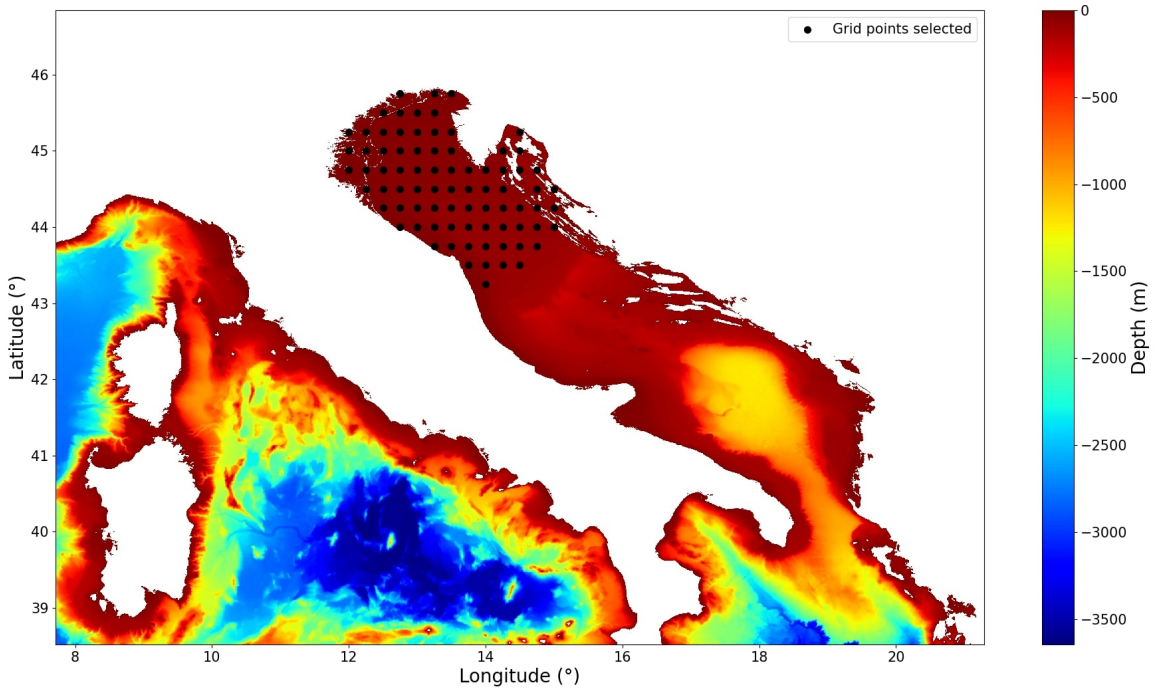

Figure B.2: Map of the points selected for the derivation of Q_{tot} in the North Adriatic

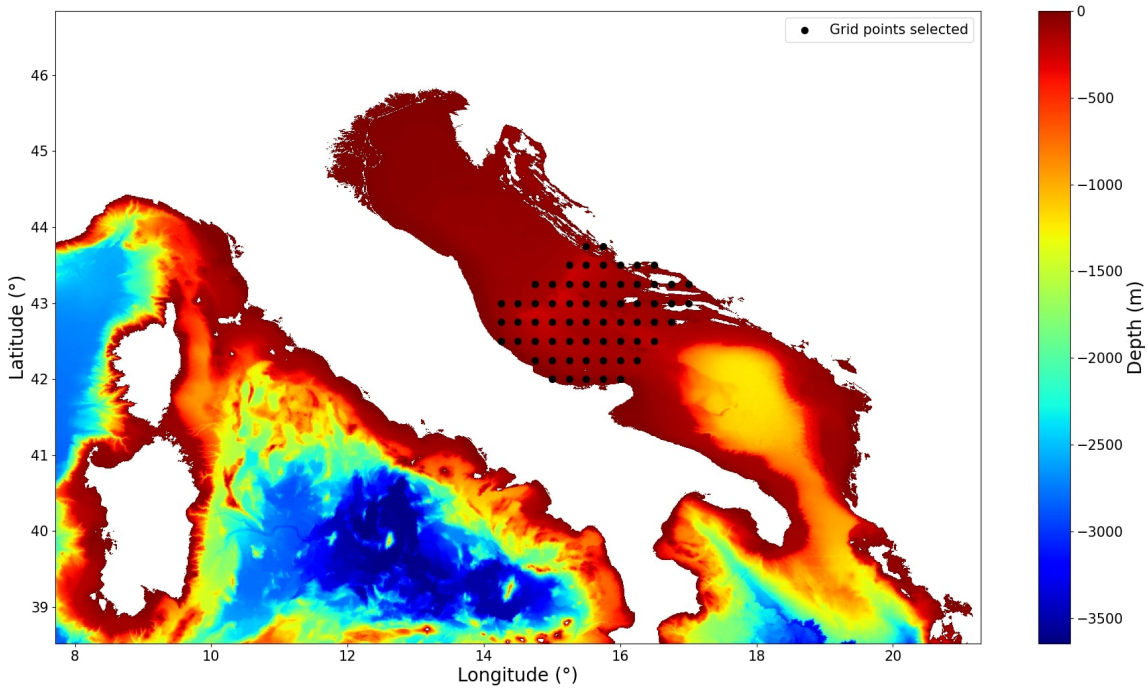

Figure B.3: Map of the points selected for the derivation of Q_{tot} in the Middle Adriatic

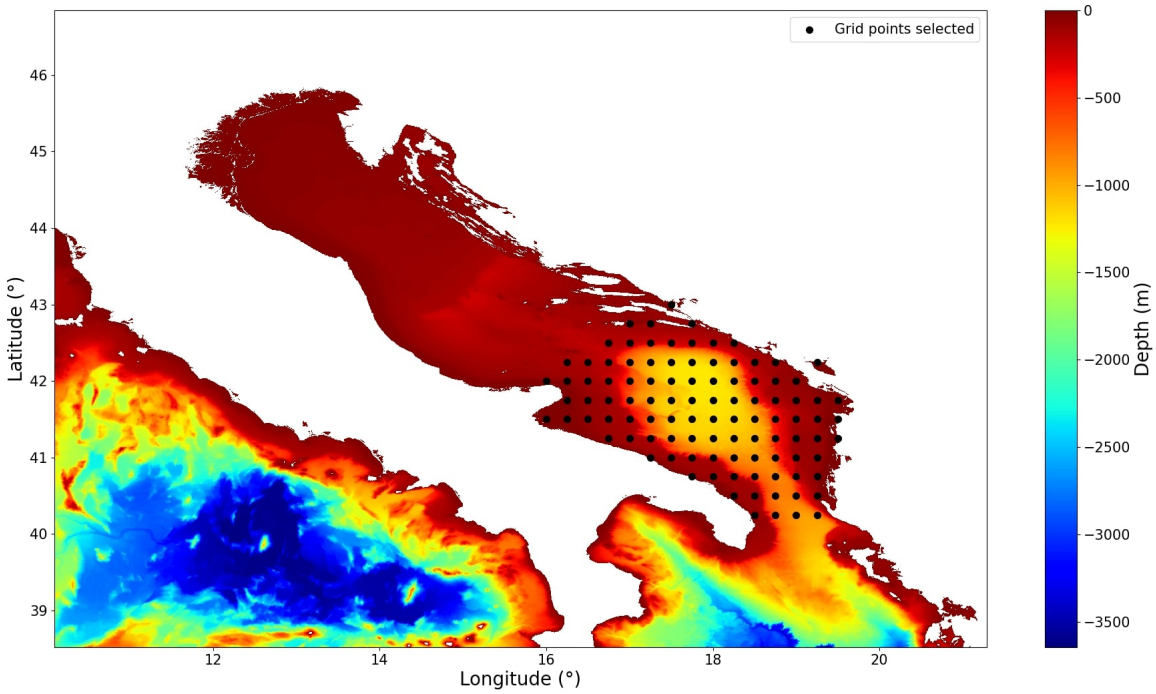

Figure B.4: Map of the points selected for the derivation of Q_{tot} in the South Adriatic

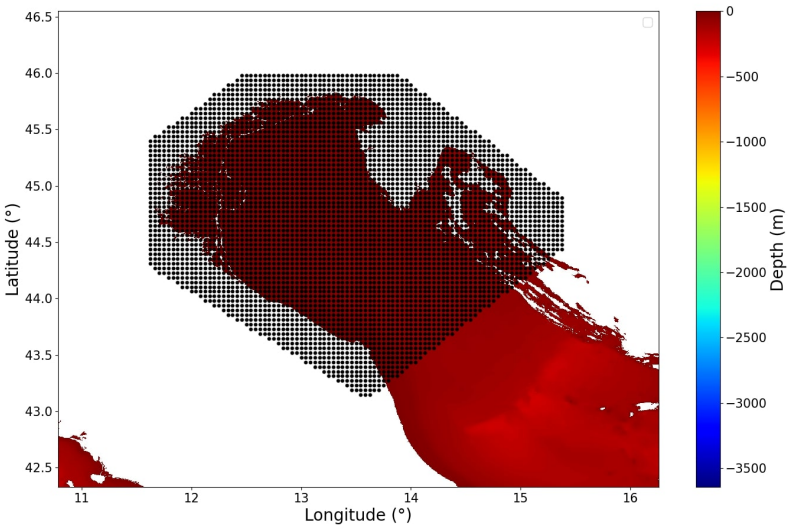

Figure B.5: Points considered for the derival of monthly salinity in the North Adriatic (for both the 10m average and the whole water column average)

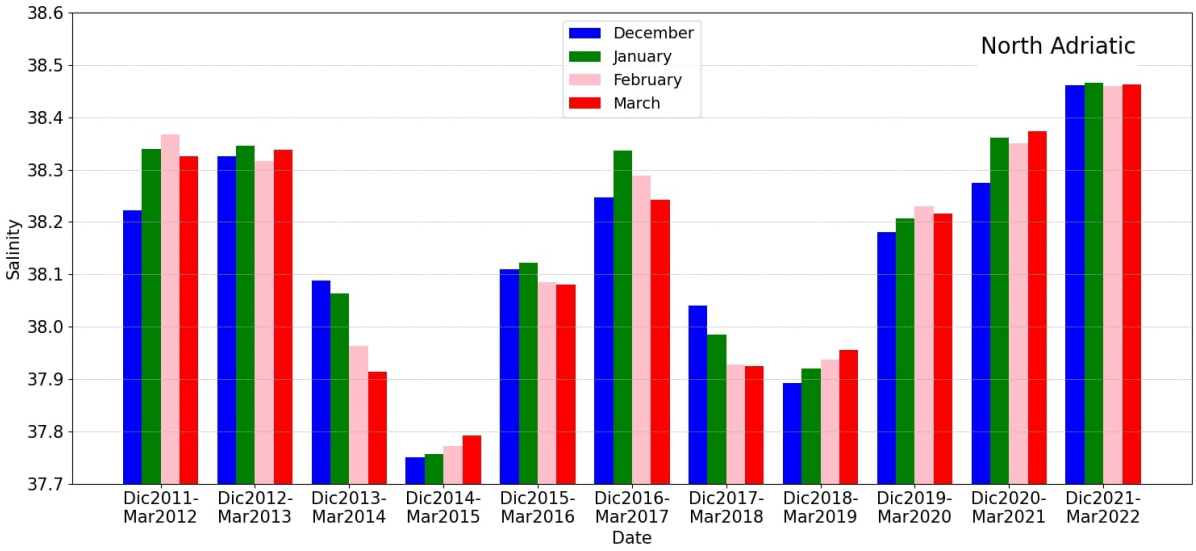

Figure B.6: Salinity monthly average on the whole water column for winter period (December to March) in the North Adriatic from winter 2011/2012 to winter 2021/2022. High values of S, as during winter 2021/2022, may favor the formation of very dense water.

Figure B.7: Time series of velocities at the near bottom (15/25 m above the bottom) in the North, Middle, and South Adriatic for 2012, 2017, and 2018. These velocities are the result of averages on areas near the eastern coast of Italy. The black vertical lines represent the date of maximum of density in the northern Adriatic while the yellow lines represent the date of maximum of density at BB.

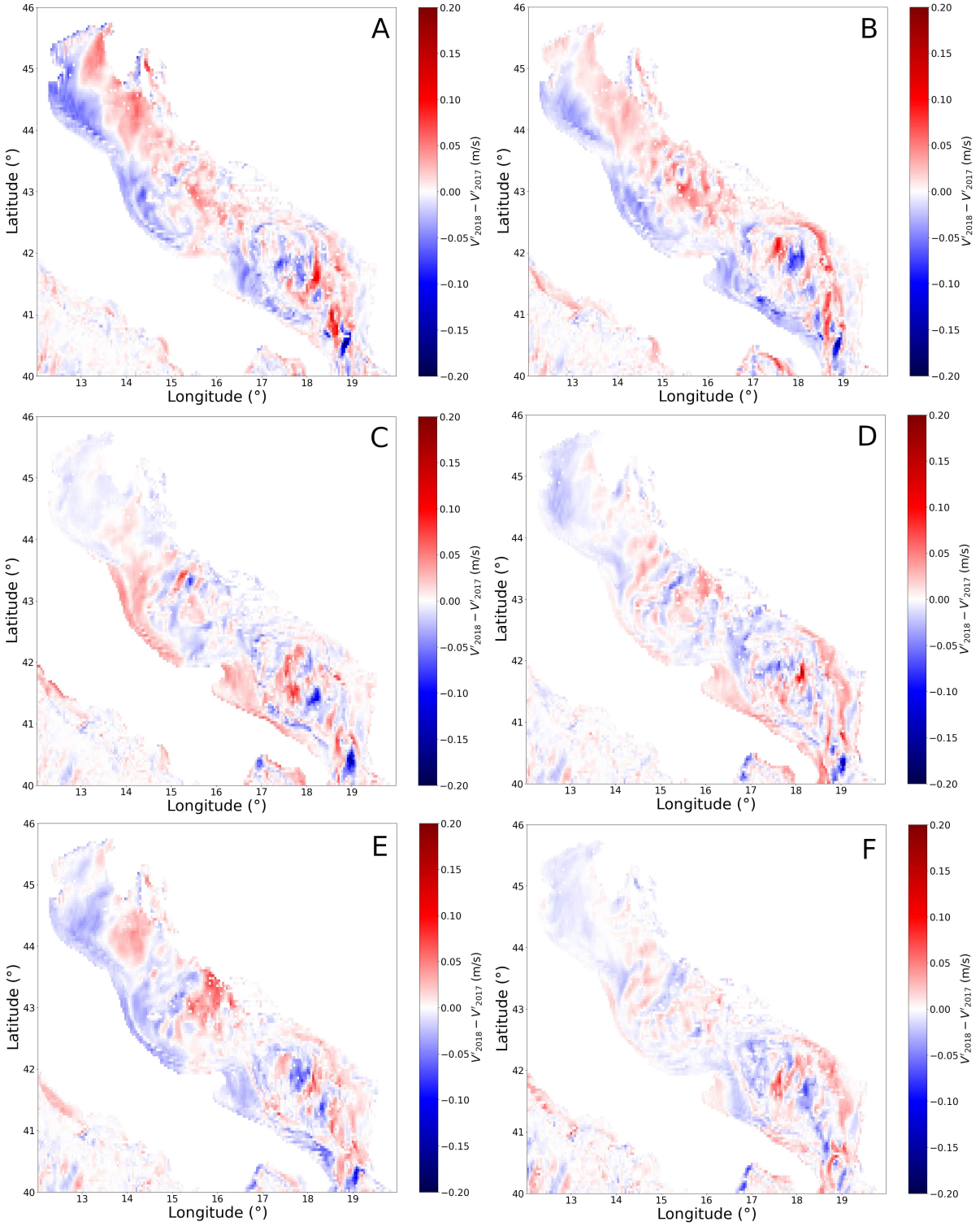

Figure B.8: 7 day averages of the projected Northward velocity (V') from week 19/02-25/02 to the week 26/03-01/04 in 2018 (left column) and differences between 2018 and 2017 for the same quantity (right column). Velocities were derived with SSH maps from Copernicus reanalysis and are projected along the Adriatic Sea axis. A negative value means that, along the western coast of the Adriatic Sea, we observe a higher southward ambient velocity in 2018.

Appendix C

Double-diffusive regime analysis: grid for calculation of relative vorticity and MLD

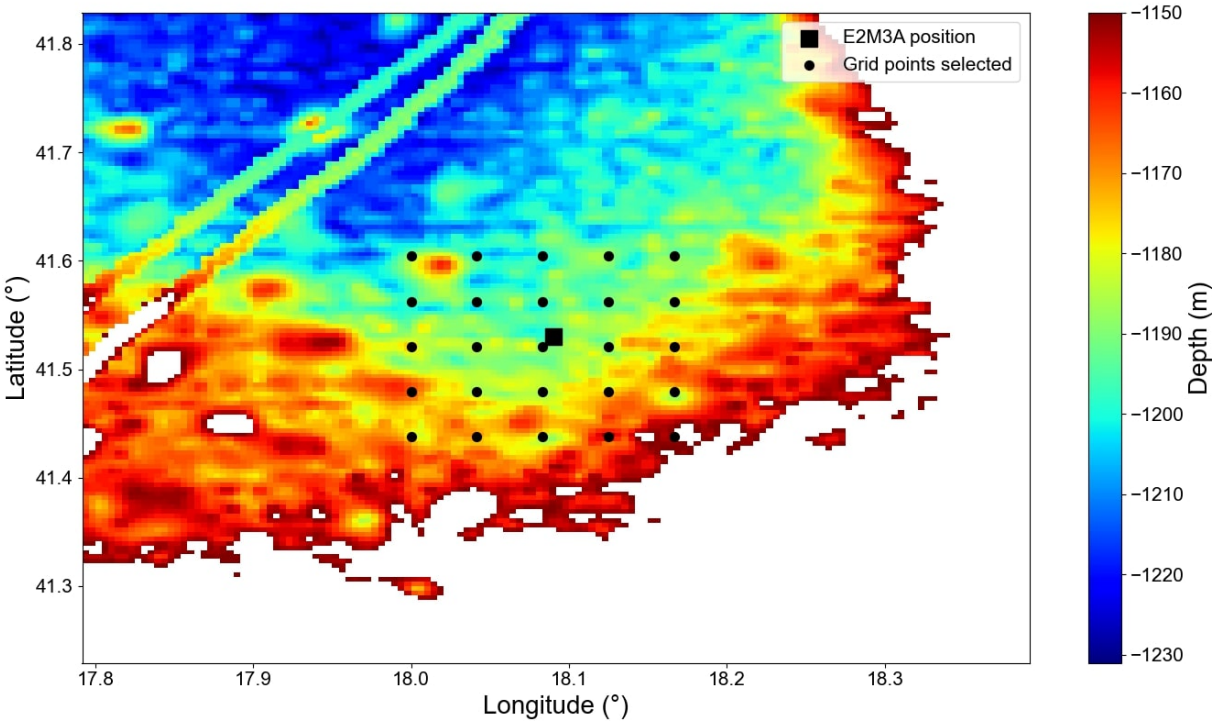

Figure C.1: Selected grid points near the E2M3A position used to calculate the maximum depth of the mixed layer for the entire study period.

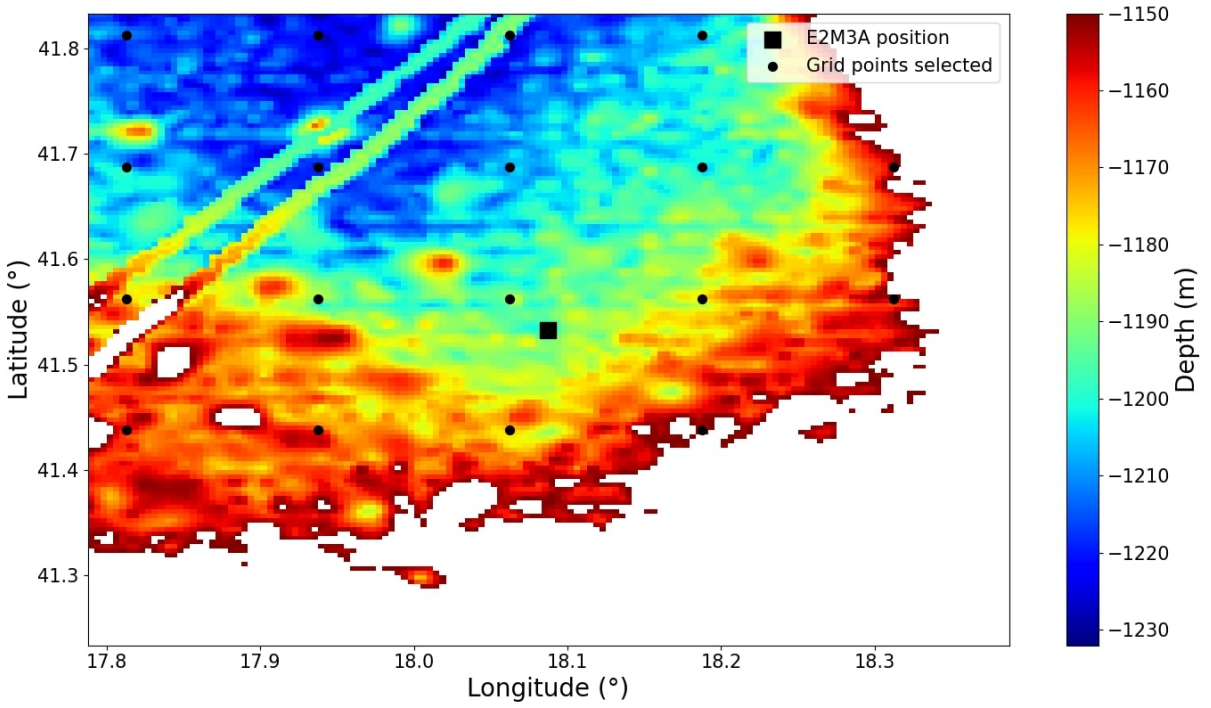

Figure C.2: Selected grid points near the E2M3A position used to calculate the average relative vorticity for the entire study period.

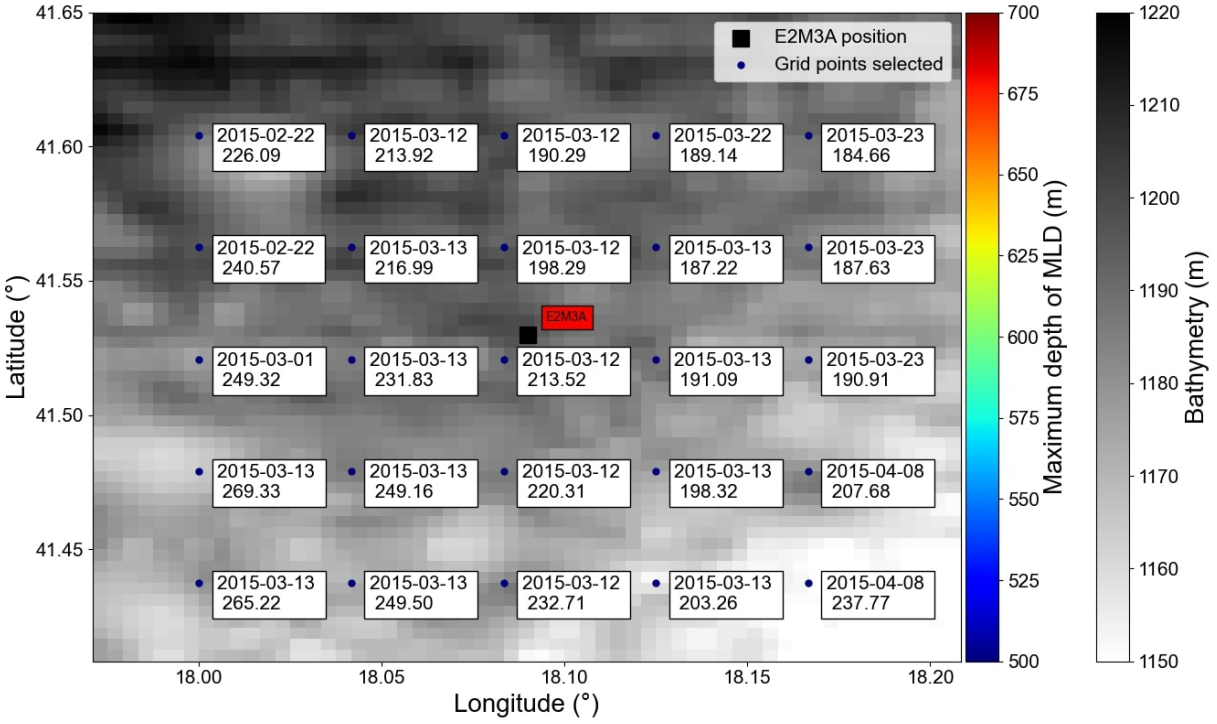

Figure C.3: Selected grid points near E2M3A location used to determine the maximum depth of the mixed layer in winter 2015, as indicated in table 4.1.

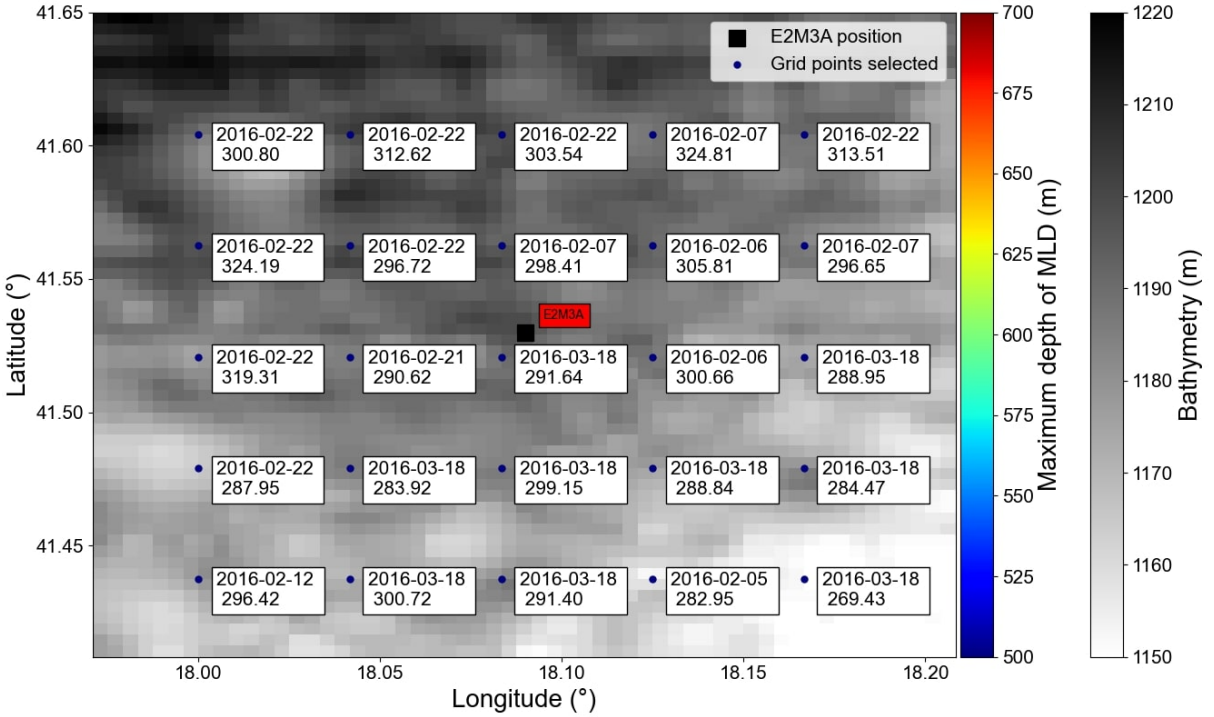

Figure C.4: Selected grid points near E2M3A location used to determine the maximum depth of the mixed layer in winter 2016, as indicated in table 4.1.

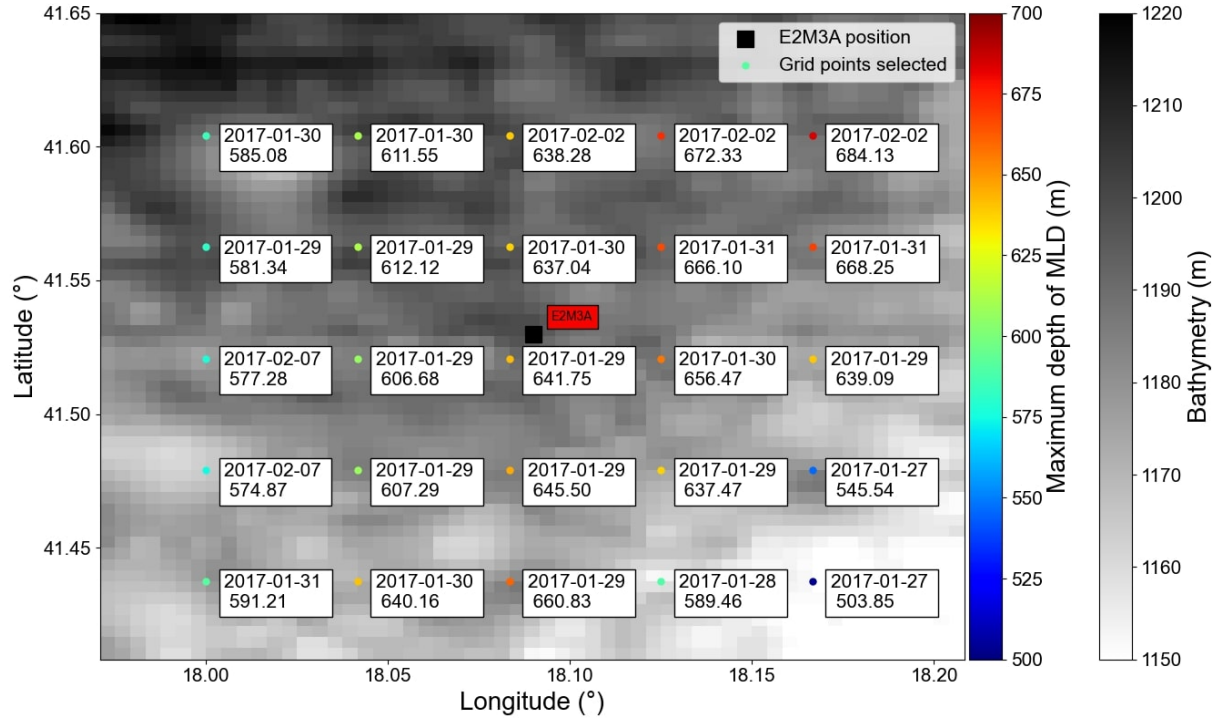

Figure C.5: Selected grid points near E2M3A location used to determine the maximum depth of the mixed layer in winter 2017, as indicated in table 4.1.

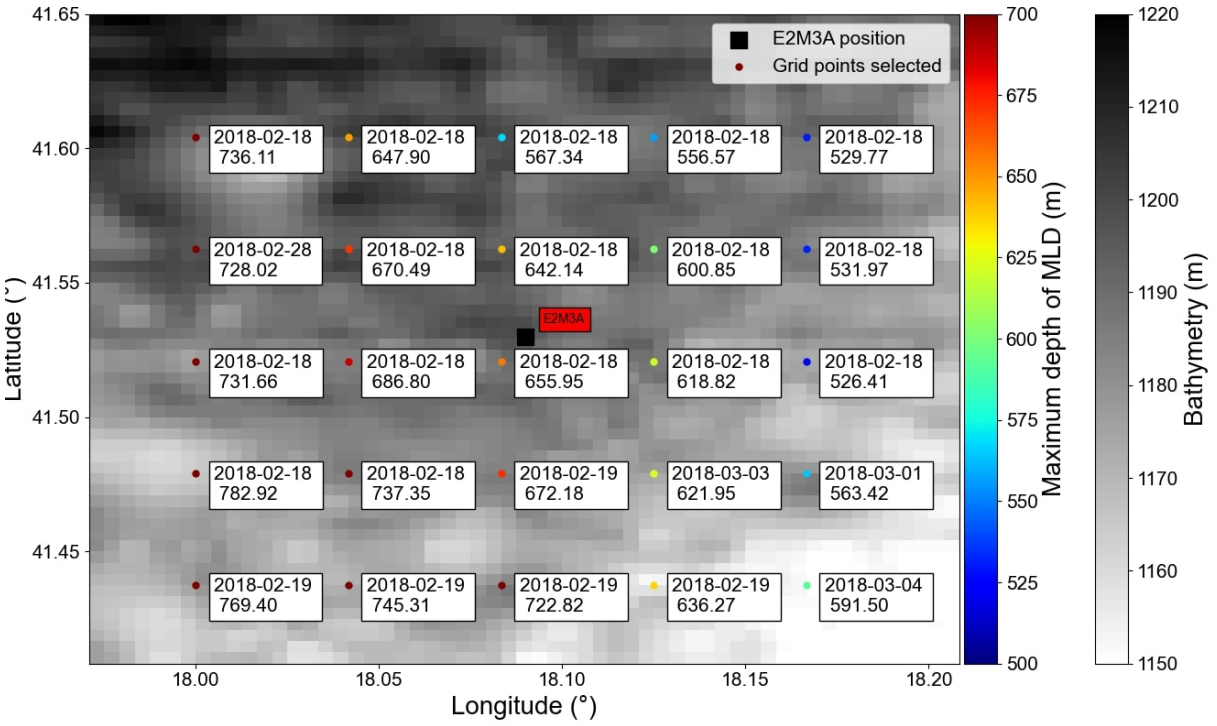

Figure C.6: Selected grid points near E2M3A location used to determine the maximum depth of the mixed layer in winter 2018, as indicated in table 4.1.

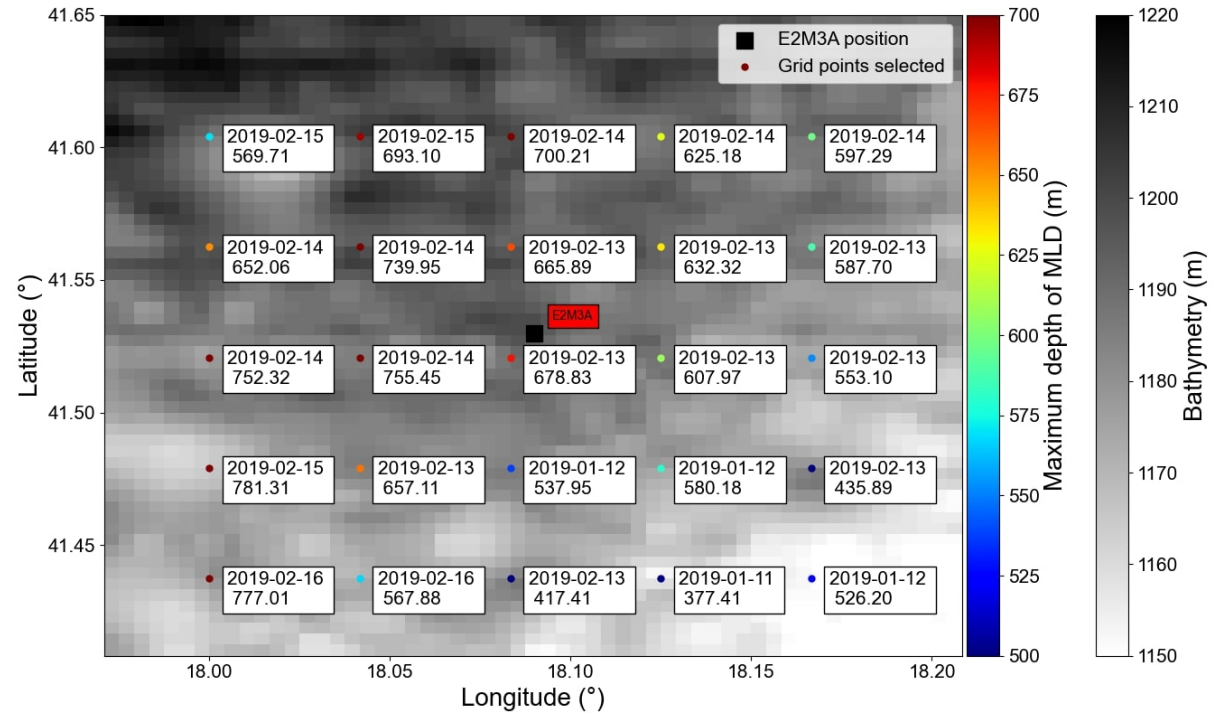

Figure C.7: Selected grid points near E2M3A location used to determine the maximum depth of the mixed layer in winter 2019, as indicated in table 4.1.